IntechOpen

Advances in Nanofibers

Edited by Russell Maguire

ADVANCES IN NANOFIBERS

Edited by **Russell Maguire**

Advances in Nanofibers
http://dx.doi.org/10.5772/45983
Edited by Russell Maguire

Contributors

Samuel Chigome, Nelson Torto, Tianyan You, Jianshe Huang, Wutian Wu, Kai Wei, Ick-Soo Kim, Shinsuke Ifuku, Y. L. Mo, Jorge J. Santiago-Aviles, Andy Alubaidy, Bo Tan, Krishnan Venkatakrishnan

Notice

First published in Croatia, 2013 by INTECH d.o.o.
eBook (PDF) Published by IN TECH d.o.o.
Place and year of publication of eBook (PDF): Rijeka, 2019.
IntechOpen is the global imprint of IN TECH d.o.o.
Printed in Croatia

Legal deposit, Croatia: National and University Library in Zagreb

Additional hard and PDF copies can be obtained from orders@intechopen.com

Advances in Nanofibers
Edited by Russell Maguire
p. cm.
ISBN 978-953-51-1209-9
eBook (PDF) ISBN 978-953-51-5726-7

Meet the editor

Russ Maguire is a founder and President at Global Nanocomposites, LLC. He was a Boeing Fellow in the Research & Technology (BR&T) organization specializing in composite materials. He was a leader in BR&T for external technology collaborations in new M&P, and responsible for new technology discovery, evaluation, acquisition and implementation to meet next generation commercial aircraft goals and requirements; specifically on developing collaborations in Saudi Arabia, Singapore, Canada, China and Italy. He was a BR&T nanotechnology focal and member of the Boeing Advanced Concept Center. Russ has been an invited keynote/plenary speaker at international composite conferences in US, Europe and Asia, and was a member of the Nanotechnology/Aerospace Industry Liaison group to the White House. He has been an invited reviewer for AFWAL and NASA ACEE composites, an advisory member of the Princeton TRI, and invited to the Gordon Conference on Composites.

Contents

Preface

Book "Advances in Nanofibers" is a research publication that covers original research on developments within the Nanofibers field of study. The book is a collection of reviewed scholarly contributions written by different authors. Each scholarly contribution represents a chapter and each chapter is complete in itself but related to the major topics and objectives. The chapters included in the book are: Electrospun Nanofiber Based Solid Phase Extraction, Electrospun Nanofibers: From Rational Design, Fabrication to Electrochemical Sensing Applications, Chitin Nanofibers, Preparations and Applications, Fabrication of Nanofibrous Scaffolds by Electrospinning, Carbon Nanofiber Concrete for Damage Detection of Infrastructure, Materials and Processes for Ion Permeable Separating Membranes by Electro-Spinning, Nanofibers Reinforced Polymer Composite Microstructures, Use of Self-Assembly Nanofibre Biomaterials for Neural Repair After Injury. The target audience comprises scholars and specialists in the field.

Dr. Russell Maguire
Boeing Technical Fellow,
President, Global Nanocomposites LLC
Bellevue WA, USA

Chapter 1

Electrospun Nanofiber Based Solid Phase Extraction

Samuel Chigome and Nelson Torto

Additional information is available at the end of the chapter

http://dx.doi.org/10.5772/57100

1. Introduction

The objectives of a sample preparation technique in Analytical Chemistry are twofold; transformation of a sample into a form that is suitable for instrumental analysis and to ensure that the sample is at the detection level for the instrument of choice. Solid phase extraction (SPE) is a popular sample preparation technique for liquid samples with subsequent chromatographic analysis [1]. SPE is employed with the aim of either reducing interferences or achieving analyte preconcentration in order to enhance instrumental detection. Although SPE can be described as a physical extraction process involving a liquid phase and a solid phase (that can be packed or free flowing sorbent), the increased use of packed sorbent formats seems to have led to a bias towards packed sorbent SPE devices [2]. One of the first applications of packed sorbent SPE was reported in 1951, when Braus and co-workers packed 1.2-1.5 kg of granular activated carbon into an iron cylinder for the isolation of organic compounds [3]. Since then, there has been significant progress in SPE technology, as evidenced by reports on new formats and sorbents covering a wide range of morphologies and chemistries [1].

SPE research and developments have progressed with a focus on SPE device fabrication or SPE method development. In principle, the heart of the SPE technique is the sorbent material as it has a direct influence on the selectivity, sorptive capacity and the format or the configuration of the resultant SPE device (s).

To predict and optimize extraction, it is important to be aware of the nature of the sorbent used with respect to physicochemical characteristics. The most important physicochemical characteristics for optimal extraction are porosity, specific surface area and surface chemistry.

Given that there will always be a need for new sorbent materials, it is imperative to focus research efforts on versatile sorbent fabrication techniques that could address current and anticipated challenges. Electrospinning is seen as having great potential as a sorbent fabrication technique, given its versatility [4].

The objective of the chapter is to equip the readers with sufficient knowledge that would enable them to fabricate and employ electrospun nanofibers as sorbents not only for SPE but for a wide range of applications. A discussion of the fundamental principles of SPE, the challenges associated with further research efforts and the unlimited potential that lies in electrospinning to address SPE will be presented. The use of electrospun nanofibers for SPE is an area that is still at its infancy (Scifinder scholar search of the words *"Electrospinning" and "Solid Phase Extraction"* showed 34 hits which consisted of 30 papers, 2 review articles, 2 patents and 0 books/book chapters) thus the chapter will be presented mostly in a postulative manner on the basis of the experiments conducted in the authors' research lab as well as literature reports.

2. Fundamental principles of sorbent extraction

Sorption can be defined as a process by which a substance (*sorbate*) is sorbed (*adsorbed* or *absorbed*) on or into another substance (*sorbent*) [5]. In the sample preparation context, the term sorbent refers to the solid extracting phase, including solid-supported liquid phases upon which an analyte is retained. Schwarzenbach and co-workers [6] made a distinction between absorption meaning into a three dimensional matrix, and adsorption as meaning onto two dimensional surface. Figure.1. shows a schematic representation of analyte adsorption (analyte accumulation onto the sorbent surface) and absorption (analyte accumulation into the bulk of the sorbent) type extraction mechanisms.

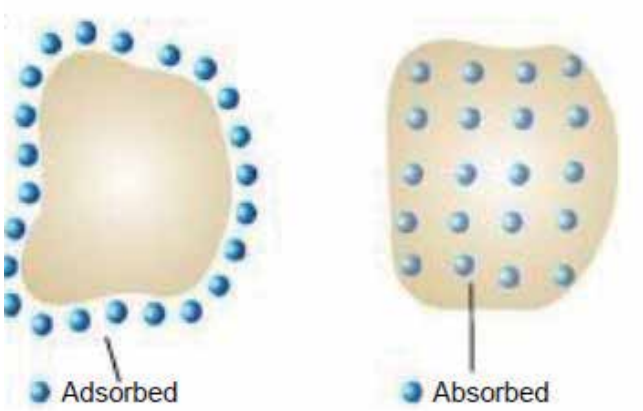

Figure 1. Schematic representation of (a) absorptive and (b) adsorptive extraction processes [7].

Although sorbent based extraction techniques could be classified on the basis of either adsorption or absorption, the two processes are not completely separable as they occur concurrently. In principle, what differs is the extent of contribution of the predominant extraction mechanism as that is solely dependent on the nature of the extraction phase. Consequently, it may be difficult to distinguish between the two processes experimentally [8].

thus the general term *sorption* is often used to refer to a combination of these processes. Despite the uncertainty of the extent of contribution of adsorption or absorption mechanisms in extraction, fundamentally, all sorbent based extraction techniques are guided by the thermodynamic partition or distribution coefficient K, which is usually expressed as the ratio of analyte concentration in the sorbent phase, $C_{sorbent}$ to that in the sample phase, C_{sample};

$$K = \frac{C_{sorbent}}{C_{sample}} \tag{1}$$

For adsorption, surface structure (porosity and surface area governing the available sites for analyte retention) is the more important sorbent characteristic compared to chemical composition. While the chemical composition (governing the diffusion coefficient of the analyte into the sorbent) of the liquid phase is the more important for absorption.

Sorption from the sample phase is essentially a dynamic process in a heterogeneous system in which transport of the analytes between the sorbent and the sample phase is achieved. The process proceeds by a decrease in free energy until it reaches the minimum value (that is equilibrium). The mechanism of analyte adsorption or absorption is governed by the characteristics of interactions between the analyte and active sites of the sorbent. Therefore, sorbent selection is based on the binding mechanisms between the sorbent and analyte of interest. Table.1. shows different interaction mechanisms with their corresponding energies.

Interaction mechanism	Energy (kJ/mol)
Van der Waals	1-5
Dipole-induced dipole	2-7
Dipole-dipole	5-10
Hydrogen bonding	5-10
Ionic	50-200
Covalent	100-1000

Table 1. Energies of interaction mechanisms [9].

The process of analyte sorption can be assumed to consist of multiple steps. Any of the steps may become rate limiting in controlling sorption of an analyte. The analyte may interact with a sorbent in at least four ways:

1. Through absorption, the analyte may interact with the sorbent by penetrating its three dimensional structure. Three dimensional penetration into the sorbent is a particularly dominating process for solid supported liquid phases. In the absorption process, analytes do not compete for sites; therefore, absorbents can have a high capacity for the analyte.
2. The analyte may interact two dimensionally with the sorbent surface through adsorption due to intermolecular forces [10]. Surface interactions may result in displacement of water

or other solvent molecules by the analyte. In the adsorption process, analytes may compete for sites; therefore, adsorbents have limited capacity. Three steps occur during the adsorption process on porous sorbents; (a) *film diffusion* (when the analyte passes through a surface film to the solid phase surface), (b) *pore diffusion* (when the analyte passes through the pores of the solid phase), and (c) *adsorptive reaction* (when the analyte *binds*, *associates* or *interacts* with the sorbent surface) [11].

3. If the analyte is ionisable in aqueous solution, there may be an electrostatic attraction between the analyte and the charged sites on the sorbent surface. Sorbents specifically designed to exploit these types of ionic interactions are referred to as *ion-exchange* (either anion or cation exchange).

4. It is possible that the analyte and the sorbent may be chemically reactive toward each other such that the analyte becomes covalently bonded to the sorbent. This type of sorption is generally detrimental to analytical recovery and may lead to slow or reduced recovery [6, 11].

For porous sorbents, most of the surface area is inside the nanopores of the sorbent (see Fig. 2.). Nanopores of the sorbent are classified into three as; *micropores* (diameters smaller than 2 nm), *mesopores* (2 to 50 nm), and *macropores* (greater than 50 nm) [12]. Most of the surface area is derived from the small diameter micropores and the medium diameter mesopores. Porous sorbents vary in pore size, shape, tortuosity and are characterized by properties such as particle diameter, pore diameter, pore volume, specific surface area and particle distribution.

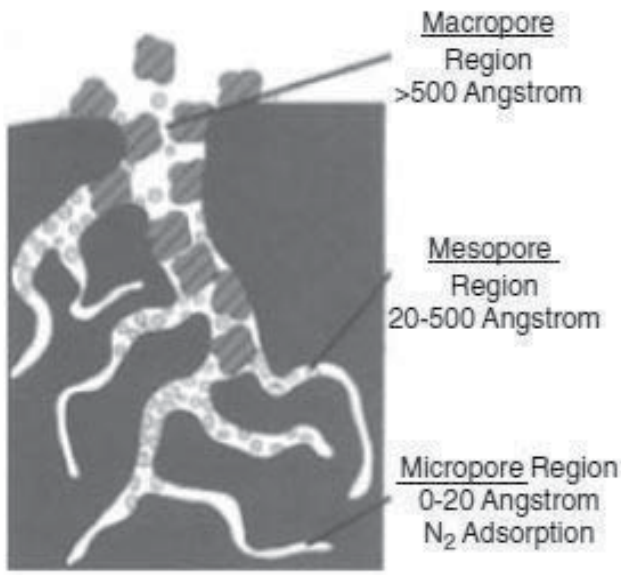

Figure 2. Schematic representation of porous regions of a sorbent [13].

2.1. Solid phase extraction process

Classically, batch mode liquid solid extractions were used in which the liquid sample was placed in contact with the bulk free flowing solid extracting phase. Equilibrium between the two phases was allowed to occur, followed by physical separation (decanting or filtering). Advancements of liquid solid extractions could be said to have taken two approaches; the first being solid phase microextraction (SPME) which consists of a two-step process in which the sorbent or solid supported sorbent is allowed to reach equilibrium before analyte desorption [14-17]. Figure.3. shows the most widely used version of SPME which is based on an organic polymer coated fused silica fiber operated in a syringe format. The syringe is designed to move the fiber in and out of the needle, which allows exposure of the fiber during extraction and desorption [18].

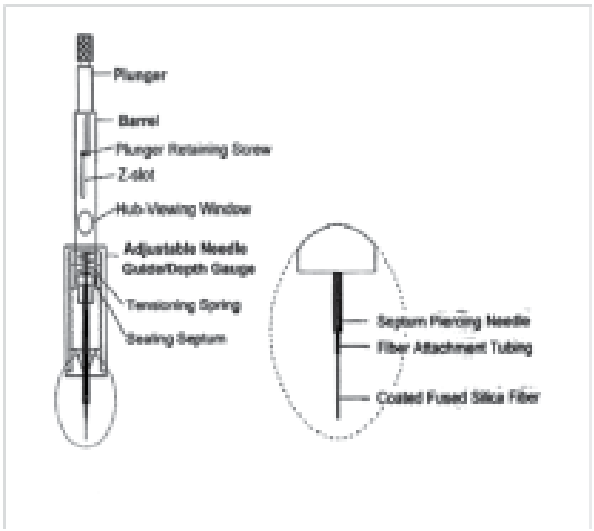

Figure 3. Schematic representation of the components of a commercially available SPME device [18].

While packed sorbent format SPE generally involves four steps;

Conditioning: functions to activate or "wet" the sorbent to prepare for its interaction with the analyte. This is especially necessary for hydrophobic sorbents that would not be activated by an aqueous sample. If the sorbent is not adequately conditioned, poor analyte retention may be achieved. If pH is critical for retention, then the conditioning solvent has to be matched to that of the sample to prepare for maximum analyte retention during the loading step.

Loading: when the liquid sample is added to the sorbent, sufficient residence time should be allowed for maximum analyte-sorbent interaction. This is especially critical when employing ion exchange to provide for adequate residence time of the sample solution in the sorbent since the analyte has to achieve an appropriate orientation for electrostatic retention with the sorbent functional groups.

Washing: this serves to remove interferences retained on the sorbent leaving behind the analytes of interest. In some cases, it could be used to wash-off the analyte of interest while retaining the interferences. In mechanisms employing ion exchange, the pH of the wash solvent should be sufficient enough to disrupt the charged sites of interferences but not affect the analyte.

Elution: the elution solvent should be strong enough to disrupt all analyte-sorbent interactions in order to obtain the highest recoveries. However, there is a limit to the strength as harsh solvents would not only desorb analytes from the sorbent, but also strip strongly retained interferences.

Figure.4. shows schematic representations of the four approaches typically taken in practical SPE applications. Figure.4. (a) shows a three step SPE process in which; (1) the sorbent is conditioned after which the sample is loaded and finally (2) the analyte is eluted with the interferences being retained (clean up) or the analyte is simply eluted into a smaller sample volume (preconcentration).

Figure.4. (b) shows a four step SPE process in which; (1) the sorbent is conditioned after which the sample is loaded, (2) the interferences eluted and finally (3) the analyte is eluted (clean up) or the analyte is simply eluted into a smaller sample volume (preconcentration).

Figure.4. (c) shows a five step SPE process in which; (1) the sorbent is conditioned after which the sample is loaded, (2) the interferences eluted, (3) a fraction of analyte is selectively eluted and finally (4) the second fraction of analytes is eluted.

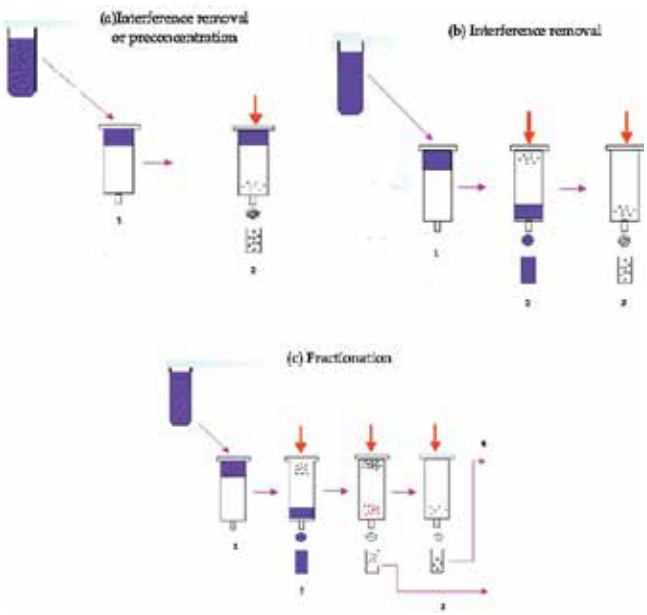

Figure 4. Schematic representation of practical SPE operations

http://dx.doi.org/10.5772/57100

3. Nanofiber based sorbents

Sorbent selection for SPE is normally guided by the ability of a material to retain analytes selectively as well as facilitate rapid and complete elution. The sorption process must be reversible [19, 20]. In addition to reversible sorption, SPE sorbents should possess a large specific surface area as well as exhibit stability in the sample matrix and elution solvents. Lastly, a sorbent material with a good surface contact with the sample solution would be most preferred.

Poole and co-workers [21] categorized SPE sorbents into three as; (i) general purpose, (ii) class specific and (iii) analyte specific. The most common retention mechanisms in SPE are based on van der Waals forces, π-π interactions, hydrogen bonding, dipole-dipole interactions and ion exchange interactions. As a result, sorbents can be classified on the basis of retention mechanisms as; (i) reversed phase (ii) normal phase and (iii) ion exchange. From the materials perspective, sorbents are classified into three as; (i) carbon based (ii) inorganic based and (iii) polymer based.

The SPE sorbent fabrication technique of choice could be viewed as one that produces a material that exhibits chemical and morphological properties that can be easily modified. Similarly, an optimal SPE sorbent material combines the following benefits: (i) small diameter, (ii) large specific surface area, (iii) simplified fabrication/synthesis, (iv) ability to be modified in order to incorporate all sorbent chemistries/functionalities, (v) ability to be modified in order to incorporate all sorbent morphologies (vi) a material that can be packed in the lower (less than 10) mg range without presenting a backpressure limitation or low analyte recoveries.

The advent of nanotechnology has been a major leap forward in the research area of sorbent based sample preparation techniques as it opened up possibilities for a new class of materials that could be used in SPE applications. The main benefit of nanostructured materials is their large specific surface area that facilitates the miniaturization of SPE allowing for the use of a reduced sorbent bed mass that achieves high extraction efficiency.

Although nanoparticles offer improved performance as sorbent material [22], they inherently exhibit some limitations. One of the main challenges is associated with their handling in packed SPE formats.

Given the fact that nanoparticles have shown excellent properties as sorbent material, it would seem prudent to focus developmental efforts on nanostructured material with the aim to address the challenges of nanoparticles. This brings about a need for an alternative fabrication approach that carries with it the benefits of nanoparticles at the same time addressing some (if not all) of their limitations. From our research group's perspective, the use of electrospun nanofibers as sorbent material is seen as a possible way of carrying along the benefits of nanoparticles, whilst addressing their limitations and increasing the possibilities for modifying sorbent morphology and functionality. It is upon this background that the section has been compiled to present and discuss relevant examples that demonstrate the potential of electrospinning as an alternative fabrication technique.

3.1. Range of sorbent materials

For it to be a good alternative, it should be able to fabricate a wide range of materials on the basis of type (inorganic, organic, inorganic/organic hybrid and biological), stability (mechanical and chemical) and morphology (pore structure and surface area).

3.1.1. Carbon based

Commercial polyacrylonitrile (PAN) based carbon fibers account for nearly 90% of the total carbon fiber output worldwide due to the high carbon yield and easy carbonization process. Therefore, PAN is mostly chosen as the precursor polymer for the preparation of electrospun carbon nanofibers (CNFs) [23].

Porous carbon nanofibers fabricated by thermal activation of electrospun PAN based CNFs have improved sorptive properties due to their large specific surface area. In a report by Oh and co-workers, a study was carried out to determine the toluene adsorption capacity for PAN-based steam activated carbon nanofibers (ACNFs) [24]. The CNFs were activated between 800°C and 1000°C in order to evaluate the effect of activation temperature on fiber porosity. A relatively large adsorption capacity (65 g toluene/100 g ACNFs) was achieved by ACNFs (activated at 1000°C) with a specific surface area of 1403 m^2g^{-1} as compared to (40 g toluene/100 g ACNFs) that was achieved for ACNFs (activated at 800°C) with a lower specific surface area of 853 m^2/g. The results obtained in the study clearly demonstrated the great potential of steam activation as a post electrospinning modification approach for the fabrication of carbon nanofibers with a large sorptive capacity that could be used as sorbent material for SPE.

Shim and co-workers, compared the adsorption properties of electrospun steam activated carbon nanofibers and commercially available activated carbon fibers (CFs) [25]. Although there was a significant attenuation in the average fiber diameter from 20 μm (CFs) to 250 nm (ACNFs), the change in specific surface area was not significant (1015 m^2/g for CFs to 1193 m^2/g for ACNFs). Nevertheless, ACNFs exhibited a much larger adsorption capacity and faster adsorption/desorption kinetics due to their large number of shallow micropores and a more homogeneous surface, all these properties brought about by their nanoscale size. As demonstrated by the results obtained in the study, it was interesting to note that, besides the specific surface area, the pore structure and surface homogeneity also plays a significant role in improving sorptive capacity.

Bui and co-workers explored an alternative approach for fabricating porous carbon nanofibers in which PAN/pitch blends were electrospun with subsequent steam activation [26]. The specific surface area of the fabricated ACNFs increased from 723 m^2/g (activation temperature 700°C) to 1877 m^2/g (activation temperature 900°C). This was attributed to an increase in the mesopore fraction as the micropore fraction decreased. Given the fact that a specific surface area of 1877 m^2/g is among the highest ever reported for nanostructured materials, it is expected that carbon nanofibers fabricated in the study would exhibit an excellent sorptive capacity.

3.1.2. Silica based

Over the years, silica microparticles have been used widely as a sorbent for solid phase extraction. Recently, the focus has shifted to the use of silica nanoparticles due to their large specific surface area and intrinsic surface reactivity [27]. However, the use of silica nanoparticles for packed sorbent SPE still remains a challenge chiefly because of high back pressure, which explains why to date the smallest microparticle that has been used for packed sorbent SPE has a diameter of 8 μm [28]. Due to the fact that the simplest electrospinning set-up allows the collection of nanofibers in the form of a porous nonwoven mesh, it follows that porous electrospun nanofiber based SPE sorbent formats could be easily fabricated. Therefore, it is anticipated that electrospun silica nanofibers would be used for packed sorbent SPE, thus overcoming the high back pressure limitation associated with silica nanoparticles.

The fabrication of inorganic nanofibers typically involves the electrospinning of a polymer/sol composite and subsequent calcination of the electrospun fibers. In 2002, Shao and co-workers were the first to report the fabrication of silica nanofibers [29]. The experimental approach involved first, the preparation of a silica sol from tetraethyl orthosilicate (TEOS), H_3PO_4, H_2O followed by electrospinning of a PVA/silica sol. The PVA/ silica fibers were calcined to remove PVA resulting in amorphous silica fibers.

In 2003, Choi and co-workers reported a simplified approach in which silica nanofibers were fabricated directly from a silica sol [30]. Their fabrication method involved the preparation of a silica sol from TEOS, distilled water, ethanol and HCL with subsequent electrospinning. An interesting aspect of the fabrication approach was the fact that unlike in the first report by Shao and co-workers [29], TEOS did not contain a polymer to help spinnability, thus there was no need for the calcination step. Spectroscopic characterizationof the silica nanofibers confirmed the extensive hydrolysis of the TEOS suggesting the availability of a substantial amount of silanol groups for silylation [30].

A way of improving the adsorption capacity of silica nanofibers is to increase the specific surface area as a function of the pore volume. Wei and co-workers fabricated porous silica nanofibers containing catalytic silver nanoparticles [31]. TEOS, poly [3- (trimethoxysily) propylmethacrylate] (PMCM) and $AgNO_3$ were used as precursors for the production of silica/ polymer hybrid nanofibers. On heat treatment of the electrospun fibers, degradation of the PMCM polymer resulted in pores that led to the increase in specific surface area from 11 m^2/g to 600 m^2/g. The porous fibers exhibited an improved catalytic activity due to the increased surface area. Therefore it is expected that a similar approach could be used to improve the adsorptive capacity of silica fibers in SPE applications.

3.1.3. Polymer based

Synthetic polymers are the most popular class of materials that have been electrospun for SPE applications. Some of these polymers include polystyrene or polystyrene copolymers,[32-41] Nylon 6,[42-44] and poly (ethylene terepthalate) [45]. Other reports have appeared in the Chinese database, unfortunately the polymeric material was not described in English [46-48]. It is expected that synthetic polymers will continue to be the most popular class of electrospun

materials for use as SPE sorbents. This is due to the fact that, of all the materials that have been electrospun, polymers show the greatest potential for tuning of the sorptive chemistries.

Sorptive capacity of polymer nanofibers could be improved by increasing the pore volume. There are several methods that have been reported for introducing porous structures in nanofibers which include electrospinning of polymer blends, [49] controlled humidity, [50] the salt induced process [51] and silica nanotemplating [52]. Silica nanotemplating is a relatively simple process compared to the other methods as they require handling of complicated interactions between the polymer matrix and pore generator. In addition, porosity and pore size of the resultant porous nanofibers may be controlled easily by adjusting the content and size of silica nanoparticles.

Shi and co-workers fabricated porous nylon 6 nanofibers using silica nanoparticles as the nanotemplate [52]. The experimental approach involved the fabrication of nylon 6/silica nanofiber composites, followed by removal of the silica nanoparticles through treatment with hydrofluoric acid. After the removal of the silica nanoparticles, the specific surface area and pore volume increased from 4.68 m^2/g to 8.31 m^2/g and 0.0133 cm^3/g to 0.0250 cm^3/g respectively. The increase in specific surface area demonstrated that the approach could be used to improve the sorptive capacity of nylon nanofibers for SPE applications.

3.2. Control of selectivity

Selectivity of sorbent material is a parameter of great concern in current SPE applications. Over the years, various sorbent modification strategies have been employed to impart selectivity based on basicity, acidity, polarity, size and more recently molecular recognition [53-55]. For it to be a good alternative, electrospinning should be able to allow the incorporation of an unlimited range of functionalities in order to target a broad spectrum of analytes.

3.2.1. Polarity based

Besides the conventional small functional groups like sulphonates and carboxylic acids, macromolecules can be incorporated into polymer nanofibers to improve their selectivity as SPE sorbents. Wan and co-workers reported the fabrication of porphyrinated nanofibers by copolymerization and electrospinning [56]. The fabrication approach involved solution copolymerization of acrylonitrile with vinyl porphyrins (see Scheme.1) and subsequent electrospinning of the resulting porphyrin copolymers.

3.2.2. Ion exchange based

At the beginning of 2008, Kang and co-workers reported a comparative study of the performances of poly (styrene-co-methacrylic), poly (styrene-co-*p*-sodium styrene sulphonate) and polystyrene nanofibers for the extraction of steroidal compounds [35]. Of the three kinds of nanofibers, those of poly (styrene-co-*p*-sodium styrene) exhibited the highest extraction efficiencies, while those of polystyrene were the least efficient. The trend was attributed to the fact that the polar model analytes favored the polar sorbent. With respect to applications, the study provided a platform for different chemistries that may introduce selectivity based on

http://dx.doi.org/10.5772/57100

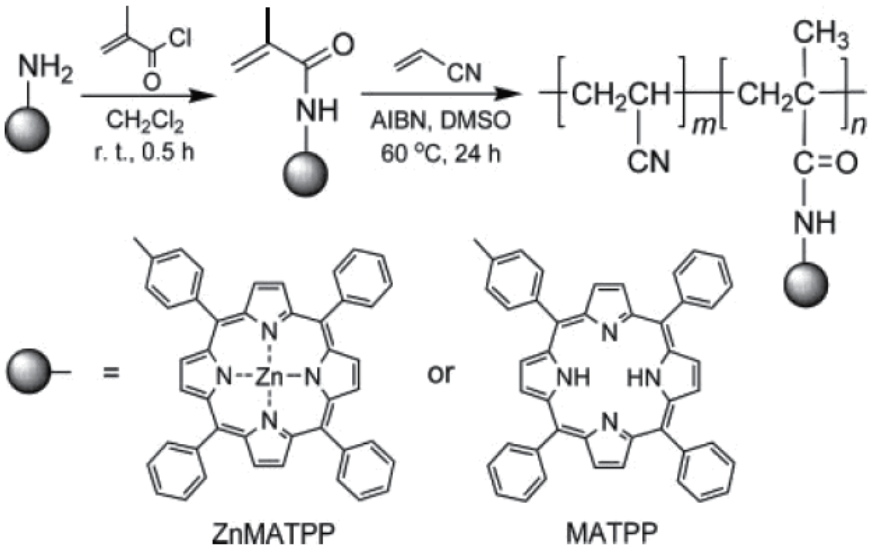

Scheme 1. Schematic representation of synthesis and molecular structure of the porphyrin copolymers [56].

hydrophobicity (polystyrene nanofibers) for non polar analytes, strong cation exchange properties (poly (styrene-co-*p*-sodium styrene sulphonate) nanofibers) for basic and neutral analytes and weak cation exchange properties (poly (styrene-co-methacrylic) nanofibers for strongly basic analytes. Due to the ease of spinnability of polystyrene copolymers and the demonstrated performance of the resultant fibers as SPE sorbents, a wide range of functionalities can be introduced on the polystyrene backbone by an experimental approach that involves copolymerization and electrospinning. It is expected that in the near future, SPE sorbents based on electrospun polystyrene copolymers will increase as there is a wide range of vinylic monomers that can be copolymerized with styrene.

3.2.3. Molecular imprinting based

Of all SPE sorbent materials that have been reported to date, those fabricated via the molecular imprinting technology have shown the best selectivity after immunosorbents [57].

Through electrospinning it is possible to incorporate the selectivity of MIPs either by encapsulating MIP nanoparticles into electrospun nanofibers or by imprinting the electrospun fibers.

Yoshimatsu and co-workers encapsulated molecularly imprinted nanoparticles into poly (ethylene terephthalate) (PET) nanofibers through electrospinning [45]. The composite nanofibers (Fig.5.) were used as a sorbent material for batch solid phase extraction of propanolol. As confirmed by radio ligand binding analysis, the specific binding sites in the composite nanofibers remained easily accessible and were chiral-selective. Furthermore, it was demonstrated that without the electrospun nanofiber based solid phase extraction step, the existence of propranolol residues in water could not be confirmed even with the sensitivity of HPLC–MS/MS analysis [45].

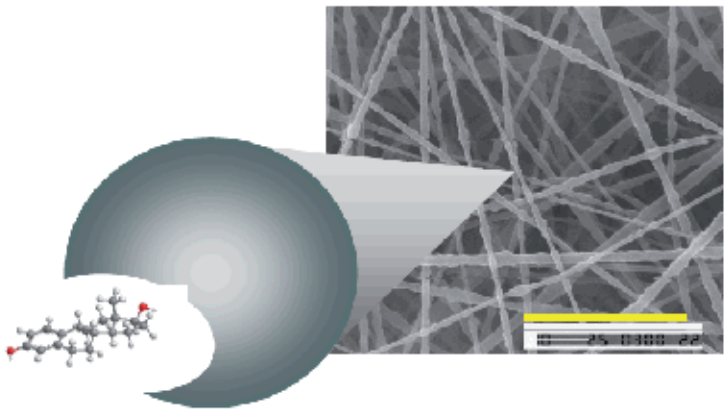

Figure 5. SEM image of electrospun nanofiber composite membrane containing molecular imprinted nanoparticles [45].

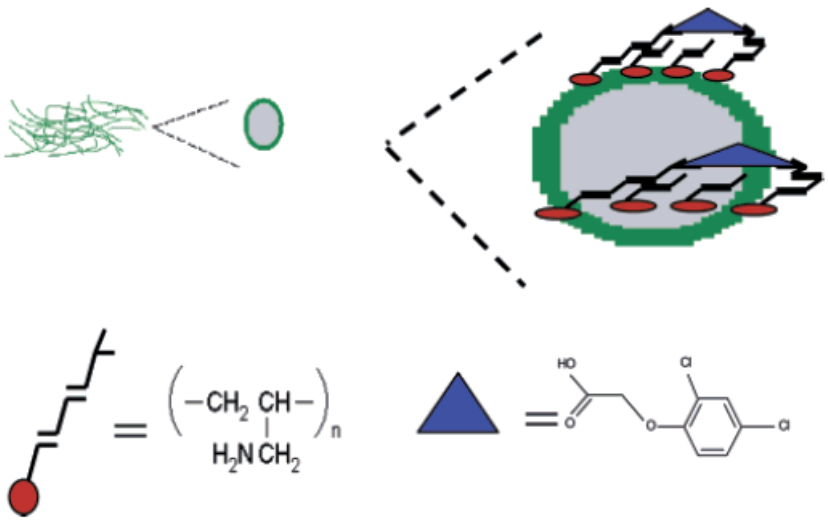

Figure 6. Schematic representation of molecularly imprinted nanofibers with binding sites specific for 2,4-D template molecules [58].

Chronakis and co-workers reported a simplified approach that allowed the generation of template defined sites directly during electrospinning [58]. The electrospun nanofibers were prepared from a solution mixture of PET and polyallylamine in the presence of a template molecule, 2,4-dichlorophenoxyacetic acid (2,4-D). Polyallylamine was used to provide functional groups that interacted with the template during the electrospinning process, and PET was used as the supporting matrix to ensure easy fiber formation and to minimize the conformational change of the polymers when the nanofibers were subjected to different

solvent treatments. Figure.6. shows a schematic representation of a possible binding site model for the reported 2,4-D imprinted nanofibers.

4. Nanofiber based SPE method development

What is the starting point in electrospun nanofiber based SPE method development? The questions can be classified into four as;

i. *Nature of the analyte*: What are the functional groups on the analyte? What is the logP of the analyte? What is the pKa of the analyte? What is the solubility of the analyte?

ii. *Nature of the electrospun fibers*: How does one introduce a functionality of the target analyte onto the surface of electrospun fibers? Which polymer (s) or spinnable precursor (s) material should be employed? Which electrospinning protocol should be adopted (electrospinning conditions and electrospinning set-up)? Is there a need to modify the morphology of the fibers, if there is, how could it be done? What diameter of the fibers should be fabricated?

iii. *Nature of the SPE device*: What is the best way of handling the fibers (that is what sort of SPE device (s) should be fabricated)? What is the best way of packing the nanofibers (that is what shape or format)? How much sorbent should be packed?

iv. *SPE operation*: What sample volume, analyte concentration, volume of SPE solvents and at what flow rate?

Of all these, the most important aspect is to come up with a feasible electrospun nanofiber based SPE device as that serves as a platform for a optimal SPE method development.

To date, fabricated SPE devices that employ electrospun nanofibers as a sorbent bed have been based on polystyrene or nylon polymers. This has resulted in a classification of electrospun nanofiber based SPE devices into two as: polystyrene type (polymer fibers of a relatively low mechanical strength); and, nylon type (polymer fibers of a relatively high mechanical strength) [59].

4.1. Polystyrene type SPE devices

In 2007, Kang and co-workers were the first to report the use of electrospun polymer nanofibers for packed sorbent SPE [60]. They manually packed 1 mg of polystyrene nanofibers into a 200 μl micro pipette tip to form a micro column as shown in Fig.7. (a) and (b) as published in their 2009 article. Solvents were pushed through the electrospun nanofiber based SPE device manually by the pressure of air forced by a gas tight plastic syringe (2 mL) (Fig.7 (c)). The device demonstrated a leap forward regarding the use electrospun nanofibers for miniaturized SPE devices. Although the packing process involved the use of simple homemade tools, it seems the packing operation is not that simple as reproducibility relies very much on operator experience. Nevertheless, the study created a platform for further research as it clearly demonstrated that nanofibers allowed the miniaturization of SPE devices without compro-

mising the extraction efficiency. The packing procedure took advantage of the ease of rolling polystyrene nanofibers into nanofiber clews. Several reports followed where either polystyrene or polystyrene copolymer nanofibers were employed as the sorbent bed packed in micro column format [61-66].

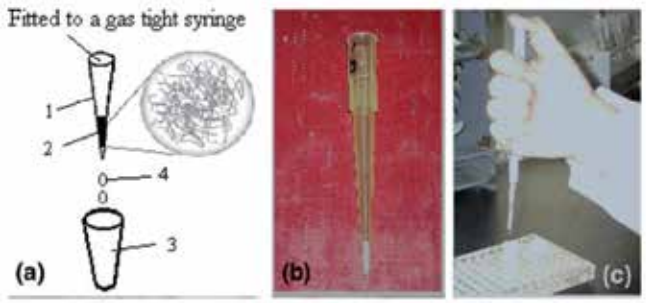

Figure 7. Micro column packed with polystyrene nanofibers and designed setup: (a) Schematic representation of packed fiber solid phase extraction device: (1) Pipette tip, (2) nanofibers packed, (3) eppendorf certrifuge tube, (4) desorption solution; and (b) Photograph of the micro-column; and (c) Photograph of a manual device [63].

All reports seem to have focused mainly on demonstrating the feasibility of using electrospun nanofibers as a SPE sorbent material since the experiments were biased towards obtaining maximum recovery.

For a better understanding of the use of electrospun nanofibers as a sorbent bed, it would be necessary to determine the mechanical strength, packing density and retention characteristics of the sorbent bed. In an effort to determine the mechanical strength of electrospun polystyrene fibers as a function of the effect of the force applied in the manual packing process, in our research group we viewed the top side of the micro column sorbent bed under scanning electron microscopy (SEM) (see Fig.8. (b-c)). The SEM morphology confirmed that the force applied did not induce any breakup or significant flattening of the electrospun polystyrene fibers.

One of the main drawbacks of the micro column packing procedure is consistency as it relies very much on the experience of the researcher. The main challenge is the rolling up of a uniform size of fiber clews. Without precise control of the size of fiber clews as well as the force applied, it would be difficult to maintain a uniform packing density and sorbent bed height, thus inconsistency of flow characteristics. Since electrospun nanofibers are applicable as a HPLC stationary phase, adopting this packing method for HPLC columns would be a challenge. This is in light of the fact that, without precise control of the packing procedure, band broadening could result due to multiple flow paths as a function of non uniform fiber orientation. Despite all these challenges, the development of the micro column packing procedure was invaluable to electrospun nanofiber based SPE sorbent research as it was used as a platform for evaluating the feasibility of using electrospun nanofibers as a sorbent bed.

Two important aspects in the development of SPE technology are simplicity of sorbent fabrication and miniaturization of devices. It is a fact that electrospun fibers could be packed

http://dx.doi.org/10.5772/57100

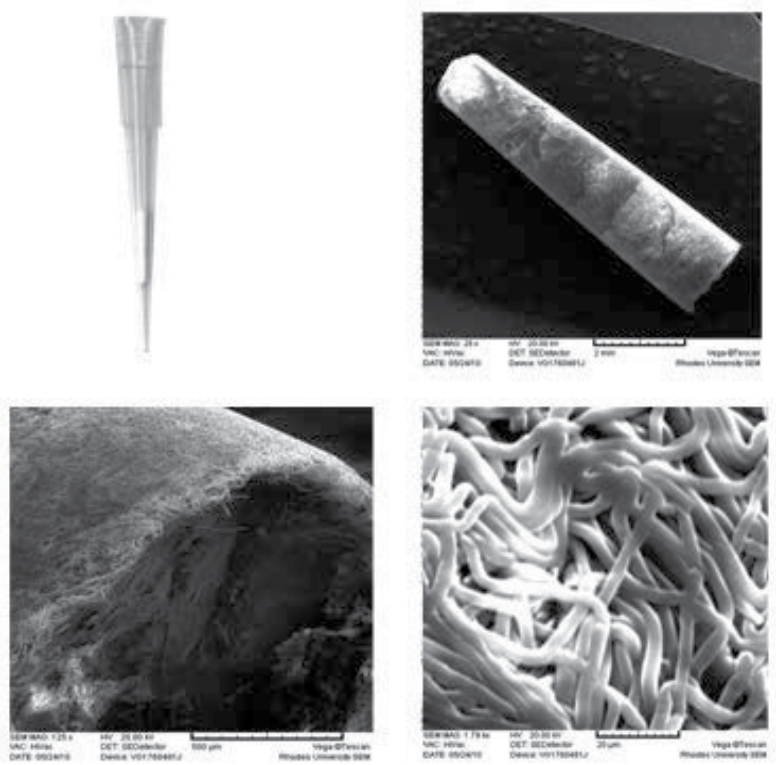

Figure 8. (a) Photograph of micro column SPE device, SEM images of (b) sorbent bed (c) magnification of top edge (d) zoomed in top surface.

in all existing formats and configurations for both SPE and SPME [4]. Furthermore, the use of electrospun fibers introduces an aspect of simplicity and miniaturization to the fabrication of SPE devices.

To date, methods of SPE disk fabrication involve a complicated multi step process in which microparticles are tightly held together within an inert fiber matrix, such as polytetrafluoroethylene [67]. This has limited the range of disk sorbent chemistries that are available. Two possible ways of simplifying the disk sorbent fabrication process would be; (i) to incorporate nanoparticles into nanofibers and pack the fibers in disk format or (ii) to fabricate nanofibers of the material with the chemistry of interest and pack them in disk format.

In 2010, our group reported an alternative polystyrene fiber based SPE device fabrication procedure [68]. The experimental approach consisted of copolymerization with subsequent electrospinning of the resultant polymer. 10 mg of electrospun polystyrene fibers were packed in a disk format (5 mm × 1 mm) (Fig.9.). The study clearly demonstrated how the use of electrospun fibers can simplify SPE disk fabrication as the sorbent material was packed using simple homemade tools. It is expected that in the near future, a wide range of chemistries will

be introduced on disk SPE devices fabricated using a similar approach that will ultimately lead to a routine disk fabrication technology.

Although the procedure involved a manual compression stage, it was presumably simplified as it did not involve the rolling up of fiber clews. Unlike the micro column SPE device where some degree of flattening was observed, for this device, flattening was not observed as viewed under SEM (see Fig.9. b-c). This suggested that the force applied in the packing process was lower compared to that applied for the micro column SPE device. A possible explanation could be that the wire (0.5 mm diameter) employed in the micro column SPE device fabrication procedure by virtue of having a smaller contact surface compared to the glass rod (5 mm diameter) employed in the disk SPE device fabrication procedure resulted in increased pressure.

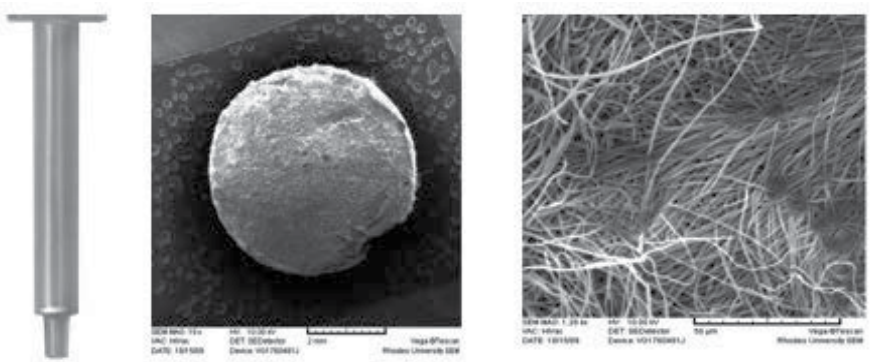

Figure 9. (a) Photograph of disk (I) SPE device, images of (b) sorbent bed (c) zoomed in top surface [68].

Despite the observed slight flattening of the electrospun polystyrene fibers in the micro column packing format, percolation of the solvents was not hindered which suggested that the packing procedure was adequate for fundamental experiments. To date, it seems, the only way of fabricating SPE devices that use electrospun nanofibers of a relatively low mechanical strength (as represented by polystyrene) would be via a mechanical compression stage. A possible way of improving on consistency could be to automate the mechanical compression stage.

4.3. Nylon type SPE devices

In 2009, Xu and co-workers were the first to report the fabrication of SPE devices that rely on relatively mechanically strong electrospun nanofibers as the sorbent bed [69]. Nylon 6 nanofiber sorbent beds were "packed" by cutting out circular portions (1.5 cm × 120-150 μm × 1.5 mg) of the nanofiber sheet (see Fig.10.).

There have been several other reports on the use of nylon 6 nanofibers packed in the same format [70-74]. Similar to the first report by Xu and co-workers [69], all these reports seem to have focussed on demonstrating the feasibility of using electrospun nylon 6 nanofibers as a SPE sorbent material.

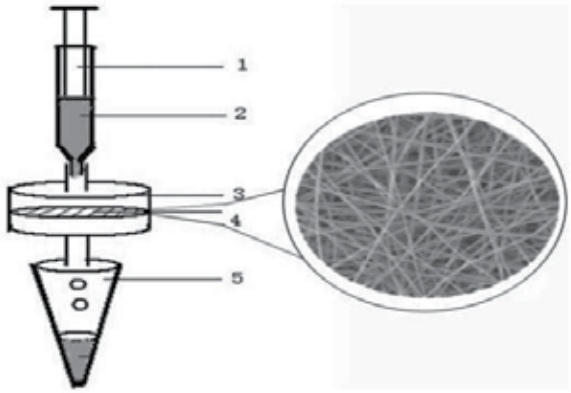

Figure 10. The fiber-filter solid phase extraction (SPE) device: gas tight syringe (1); sample solution (2); filter (3); electrospun mat using nylon 6 nanofibers (4); and, collecting tube (5) [70].

In 2011, Bagheri and co-workers reported an alternative fabrication procedure for a nylon type SPE device in which a polypyrrole-nylon 6 blend was employed as a sorbent bed [75]. Similar to the nylon 6 disk sorbent fabrication procedure, a nanofiber sheet (1× 1 cm) was cut out directly from the aluminium foil (see Fig.11.). However, the extraction procedure was not a flow through process as the sorbent bed was held by a wire and dipped into a sample solution. Although they referred to their device as micro SPE, it could be regarded as a SPME device as it was equilibrium based. Nevertheless, it is presented in this context as the fabrication procedure takes advantage of the mechanical strength of nylon nanofibers to illustrate the dependence of electrospun nanofiber evice fabrication on nanofiber mechanical stability.

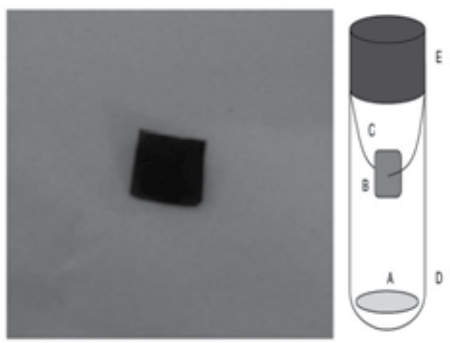

Figure 11. (a) Image of the polypyrrole-polyamide nanofiber sheet used for micro-solid phase extraction (μ-SPE). (b) Sample extraction: (A) magnetic bar; (B) nanofiber sheet; (C) thin holding wire; (D) vial; and, (E) vial cap [75].

The only report of electrospun nanofiber based micro extraction in a packed syringe (MEPS) was by Bagheri and co-workers [76]. Their packing procedure involved the manual compression of 8.1 mg of polyrrole/nylon 6 nanofiber blend into a 1 mL insulin injection syringe. The electrospun nanofiber sorbent bed was laid flat at the bottom of the syringe barrel between

two SPE frits. It is quite unfortunate that the authors did not publish the resultant SPE device otherwise it would have contributed towards a better understanding of the behaviour of the sorbent bed under compression. Similar to conventional MEPS [77] (see Fig.12.) procedure that proceeds via a draw eject cycle, a variable speed stirring motor was employed to drive solvents through the electrospun nanofiber MEPS device. Despite the fact that the authors did not publish their fabricated device, their contribution was invaluable as they were the first to demonstrate an electrospun nanofiber based MEPS device.

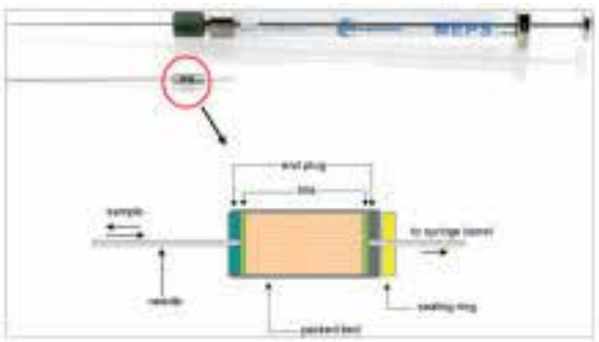

Figure 12. Representation of a MEPS syringe from SGE Analytical Science [77]

In our group, we fabricated a miniaturised version of an electrospun nylon 6 nanofiber based disk SPE device (Fig.13.a). The device was fabricated by cutting out circular portions of 5 mm diameter from the nanofiber sheet (Figure.13.b) and stacking them up to an optimal sorbent mass of 4.6 mg (5× 350 μm disks).

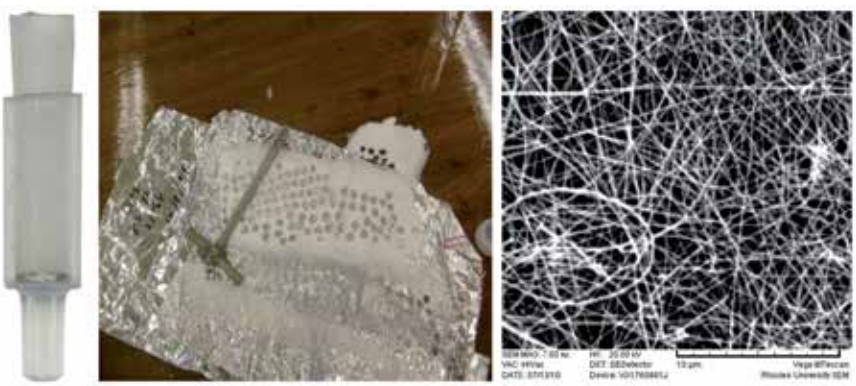

Figure 13. (a) Photograph of disk (II) SPE device, (b) photograph of an electrospun nylon 6 nanofiber mat showing regions from which disks were cut and (c) SEM image of sorbent bed zoomed in top surface [59].

Operationally, solvents have been driven through the SPE sorbent bed manually by a micro-pipette, syringe or by a vacuum manifold. All these approaches seem to be tedious particularly

at the stage of determining the breakthrough volume. Simplification of the electrospun nanofiber based SPE process has been achieved in our group by employing a syringe pump for semi automation.

Figure 14. Syringe pump driven semi automated systems (a) micro column SPE device (b) modified disk (I) and disk (II) SPE device (s) (c) syringe pump (d) polypropylene syringe (e) PVC tubing (f) polypropylene adaptor (g) glass adaptor.

It is expected that in future, further simplification of electrospun nanofiber based SPE operation may be achieved employing robotic solid phase extraction systems. Despite the fact that robotic SPE systems like the Hamilton Micro Lab 2200 [20] and the Zymark Py Technology II® [21] achieved minimal success contrary to expectation, the knowledge gained could be useful as a step towards a new direction in automated electrospun nanofiber based SPE.

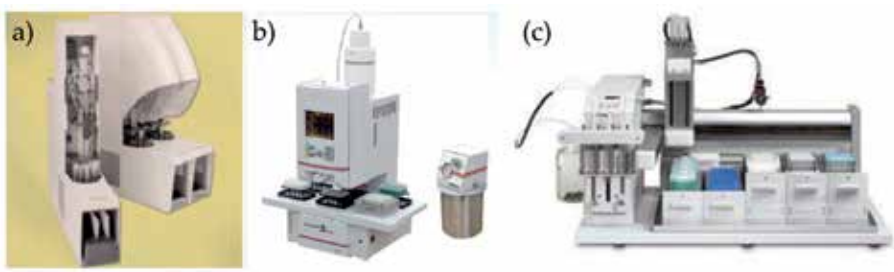

Figure 15. Most common robots for automated SPE (a)Zymark Rapid Trace System (b) Tomtec Quadra System (c) Gilson SPE 215 System.

5. Theoretical aspects

An optimal sorbent could provide a platform for fast analyte mass-transfer kinetics, which depends on the physicochemical properties of the sorbent (surface area, pore structure and

surface chemistry). Although the physicochemical properties of the sorbent may be used to predict SPE performance, bias towards sorbent characterization in SPE-method development is more effective, as the contribution of physicochemical properties and flow rate of solution to analyze mass transfer kinetics is significant. Initial evaluation of new sorbent materials for SPE application can be achieved without complete characterization of the physicochemical properties of the sorbent. Progress could be made towards a better understanding of new sorbent materials by relying on the theoretical prediction of the physicochemical properties of the sorbent.

For sorbent screening, does one start off with batch experiments and then transfer to packed sorbent formats? Batch experiments are important as they give information about sorbent adsorption characteristics, in particular adsorption kinetics derived from the equilibrium isotherms (Freundlich and Langmuir) [78]. Although batch and flow through SPE rely on the distribution or partition coefficient, thus directly linked, a flow through based screening experimental approach that relies on breakthrough profiles could be employed.

Given that the major sorption parameters characterizing a sorbent are analyte recovery efficiency and breakthrough volume [21], the experimental design for fabrication and evaluation of SPE devices could proceed in two steps:

i. The first involves establishing an optimal sorbent mass, packing format and SPE method at which quantitative recoveries (preferably above 80%) are achieved; and

ii. The second involves determining breakthrough curves from which sorbent retention characteristics are derived.

One of the most important characteristic parameters in establishing the suitability of a SPE sorbent bed for extracting target analytes is the breakthrough volume (V_B) as it gives an indication of the sorbent's loading capacity. Assuming that there is a measurable analyte retention, the breakthrough curve forms a sigmoid shape (see Fig.17.) that gives an indication of the analyte mass transfer kinetics as a function of the sorbent retention characteristics [21]. In addition to the breakthrough volume, two important parameters that are obtained from the breakthrough curve are holdup volume (V_M) and retention volume (V_R).

These three parameters: (V_B), (V_R), (V_M) can be defined as points corresponding (on the breakthrough curve) to 1%, 99% and 50% of the maximum concentration of analyte in the eluate. From these parameters, two important chromatographic characteristics of a sorbent bed; theoretical plates (N) and retention factor (k) are calculated.

The number of theoretical plates corresponds to the extraction efficiency and it depends on the physicochemical properties of the sorbent, particularly the available surface area for analyte retention. While the retention factor gives an indication of the quantity of sorbed analyte and it is directly related to the sorbent recovery efficiency.

Two methods have been employed for the calculation of theoretical plates for conventional SPE sorbents, the first was proposed by Werkhoheve-Goëwie and co-workers [79] Eq.2.

http://dx.doi.org/10.5772/57100

$$V_B = V_R * \left(\frac{\sqrt{N} - 2}{\sqrt{N}} \right) \tag{2}$$

While the second method was proposed by Lövkvist and Jönsson [80] who adopted a differential numerical solution to the breakthrough curve for analytes on a sorbent bed with a low number of theoretical plates Eq.3.

$$V_B = V_R \left(a_o + \frac{a_1}{N} + \frac{a_2}{N^2} \right)^{\frac{-1}{2}} \tag{3}$$

Where $a_o = (1 - b)^2$, a_1 and a_2 are complex functions of b evaluated from the tabular data [80] and b is the breakthorugh level (the fraction of the total mass of analyte which has passed through the sorbent bed).

The retention factor (k) is calculated from the fundamental equation of chromatography expressed as;

$$V_R = V_M (1 + k) \tag{4}$$

Given that the equations for calculating (N) and (k) have been applied to microparticle based sorbents (commercially available sorbents), a question raised would be whether they would be suitable for nanofibrous sorbent bed material. Moreso, bearing in mind that the research work on electrospun nanofiber based SPE sorbents is a step towards the development of electrospun nanofiber based HPLC stationary phases, it is necessary to have a fundamental understanding of their kinetic and thermodynamic properties in relation to retention characteristics.

Theoretical and experimental methods have been proposed for determining breakthrough curves [81, 82]. Although experimental breakthrough curve determination by frontal chromatography (continuously added sample to sorbent bed see Fig.16.) is more tedious, it is more useful for SPE device fabrication. This is due to the fact that it serves as a guide for understanding the effect of sorbent packing format, packing density and sorbent morphology on the flow characteristics of the sample phase.

Under ideal conditions, the breakthrough curve forms a smooth sigmoid shape (see Fig.17.) with the specific shape depending on the sorbent retention characteristics

However, experimentally the breakthrough curve is plotted by using a line of best fit as the data points do not always follow a smooth pattern.

The correct determination of breakthrough parameters is subject to debate as several methods have been proposed [83, 84]. Nevertheless, a mathematical modeling approach may be said to

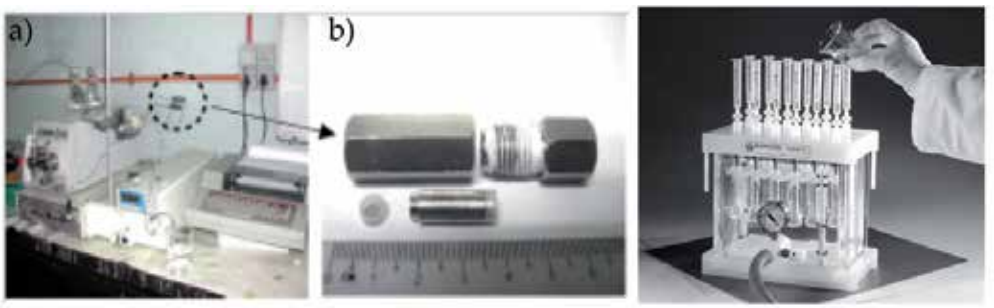

Figure 16. Representation of a (a) online (b) offline frontal chromatography set-up

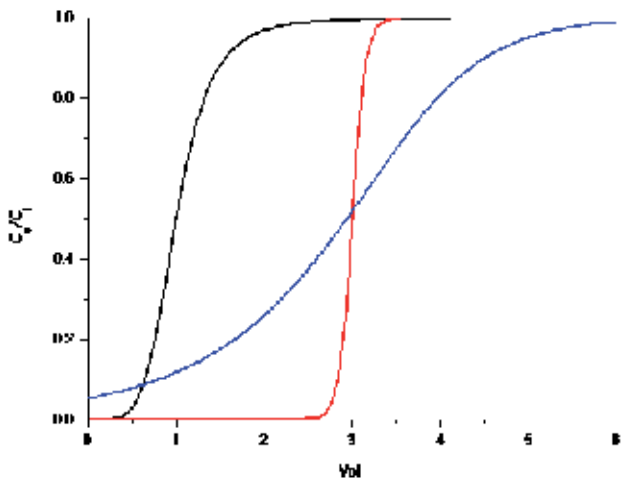

Figure 17. Mathematical simulations of breakthrough curves that can be obtained

be more preferable as it takes into consideration the actual shape of the breakthrough curve. In addition, interpreting observed experimental phenomena from the mathematical modeling perspective is invaluable as it provides a platform for linking up the various parameters influencing any system [85-89].

Our research group [68] and that of Susan Olesik were the first to report chromatographic parameters of electrospun nanofiber sorbent beds and chromatographic parameters of thin layer chromatography (TLC) plates [90], respectively. Therefore, an approach adopted in our group and results obtained will be discussed. Due to the importance of the accurate determination of breakthrough parameters, it was imperative for us to compare different mathematical models for each set of data points obtained in the experimental procedure.

A breakthrough curve typically follows a form of an "S" shape (Fig.18.). Therefore, it may be considered to be a form of a logistic function. A simple logistic function may be defined by the formula;

http://dx.doi.org/10.5772/57100

$$Y(x) = \frac{1}{1+e^{-x}} \tag{5}$$

Where the variable Y might be considered to denote analyte concentration, e is Euler's number and the variable x might be thought of as volume. For values of x in a defined range of real numbers from -∞ to +∞, exponential growth which slows to linear growth and progresses to exponential decay is observed.

The logistic function is the solution of the simple first order non-linear differential equation

$$\frac{d}{dx}Y(x) = Y(x)\left(1 - Y(x)\right) \tag{6}$$

The qualitative behavior may be understood as follows; the derivative is 0 at $Y = 0$ or 1 and the derivative is positive for Y between 0 and 1, and negative for Y above 1 or less than 0. Thus for any value of Y greater than 0 and less than 1, Y grows to 1.

Alternatively, the logistic function may be expressed symbolically as;

$$Y(x) = \frac{e^{x}}{e^{x}+e^{c}} = \frac{1}{1+e^{-x}} \tag{7}$$

Where 1 is chosen as the constant of integration $(e^{c}=1)$

Besides the logistic function, sigmoid functions include the ordinary arctangent, the hyperbolic tangent and the error function. However, for this book contribution, the logistic function was employed as the fundamental equation upon which curve fitting models were developed. The curve fitting mathematical model depends on the "S" shape of the data points and the selection is guided by by the resulting regression constants.

The Boltzmann model has been used to fit experimental data for conventional SPE sorbents as it has generally been accepted as an accurate method [84]. Thus it was the first model that was explored (see equation 8).

$$Y = A_2 + \frac{A_1 - A_2}{1+e^{\frac{x-x_o}{dx}}} \tag{8}$$

Where Y represents the ratio of the eluted (C_e) to the inlet (C_i) analyte concentration $\left(\frac{C_e}{C_i}\right)$, x is the volume of sample flowing through the sorbent, A_1 and A_2 are two regression parameters. The maximum value of $\left(\frac{C_e}{C_i}\right)$ is (A_2) and it is obtained when $x \to \infty$, while the minimum value

of $\left(\frac{C_e}{C_i}\right)$ is approximately A_1, obtained for $x \to 0$. The retention volume which corresponds to the point of inflexion on the breakthrough curve was obtained from the model and it corresponds to the $\left(\frac{C_e}{C_i}\right) = \frac{A_1 + A_2}{2}$

$$V_R = x_o \tag{9}$$

The hold-up volume (V_M) and the breakthrough volume (V_B) were calculated as the x values obtained from equating the following;

$$\left(\frac{99}{100}\right) * A_2 = A_2 + \frac{A_1 - A_2}{1 + e^{\frac{x - x_o}{dx}}} \tag{10}$$

$$\left(\frac{1}{100}\right) * A_2 = A_2 + \frac{A_1 - A_2}{1 + e^{\frac{x - x_o}{dx}}} \tag{11}$$

And by solving these equations, the formulae below were derived;

$$V_B = x_o + (dx) * \ln\left(\frac{100}{99}\left(1 - \frac{A_1}{A_2}\right) - 1\right) \tag{12}$$

$$V_M = x_o + (dx) * \ln\left(99 - 100 * \frac{A_1}{A_2}\right) \tag{13}$$

The second mathematical model employed is the sigmoid three parameter model (see equation 14)

$$Y = \frac{a}{1 + e^{-\frac{(x - x_o)}{b}}} \tag{14}$$

Similar to the Boltzmann model, Y represents the ratio of the eluted (C_e) to the inlet (C_i) analyte concentration $\left(\frac{C_e}{C_i}\right)$, x is the volume of sample flowing through the sorbent, a and b are two regression parameters. The maximum value of $\left(\frac{C_e}{C_i}\right)$ is (a). Calculation of V_M and V_B was achieved by expressing $\left(\frac{C_e}{C_i}\right)$ as a fraction of a as follows;

$$\left(\frac{C_e}{C_i}\right) = F * a \tag{15}$$

Where $F = \frac{1}{1 + e^{-\frac{(x - x_o)}{b}}}$ and solving for x (corresponding to either V_M or V_B) resulted in the expression below

$$x = x_o + b\ln\frac{F}{1 - F} \tag{16}$$

V_M and V_B were obtained from equation 16 at F values of 0.99 and 0.01 respectively.

The third model that was explored is the Weibull five parameter model (see equation 17)

$$Y = Y_o + a\left[1 - e^{-\left(\frac{x - x_o + b\ln 2^{\frac{1}{c}}}{b}\right)^c}\right] \tag{17}$$

Y_o and a correspond to the maximum and minimum points on the breakthrough curve, x_o corresponds to the point of inflexion while b and c are regression parameters.

As $x \to \infty$, Y approaches the maximum value of $\left(\frac{C_e}{C_i}\right) = Y_o + a$ thus, $\left(\frac{C_e}{C_i}\right)$ at any point of the breakthrough curve can be expressed as a fraction (F) of the maximum value of $\left(\frac{C_e}{C_i}\right)$.

If the maximum value of $\left(\frac{C_e}{C_i}\right)$ is expressed as

$$F^*\left(Y_o + a\right) = Y_o + a\left[1 - e^{-\left(\frac{x - x_o + b\ln 2^{\frac{1}{c}}}{b}\right)^c}\right] \tag{18}$$

Solving for x results in the expression below;

$$x = x_o - b\ln 2^{\frac{1}{c}} + b\left[\ln\left[\left(\frac{Y_o}{a} + 1\right)^{-1}(1 - F)^{-1}\right]\right]^{\frac{1}{c}} \tag{19}$$

Therefore, V_M and V_B can be calculated at F values corresponding to $\frac{99}{100}$ and $\frac{1}{100}$ respectively.

An example in which we compared the Boltzmann model and the sigmoid Weibull five parameter model for the evaluation of a microcolumn SPE device. The experimental approach to determine the breakthrough curves involved the use of a syringe pump (see Fig.14) to drive a sample of 500 $ngml^{-1}$ corticosteroids through a 10 mg electrospun polystyrene fiber sorbent bed at 0.1 $mlmin^{-1}$ with subsequent HPLC-DAD detection.

Analyte	V_B(µl) Observed	V_B(µl) Calculated	V_M(µl)	V_R(µl)	N_{cal}	N_{obs}	k
Betamethasone	1400	848.18	5185.39	3044.89	7.69	13.71	-0.41
Dexamethasone	1400	924.53	5189.44	3100.98	8.12	13.29	-0.40

Table 2. Chromatographic parameters of the electrospun polystyrene fiber based micro colum sorbent bed format derived from the sigmoid Boltzmann model

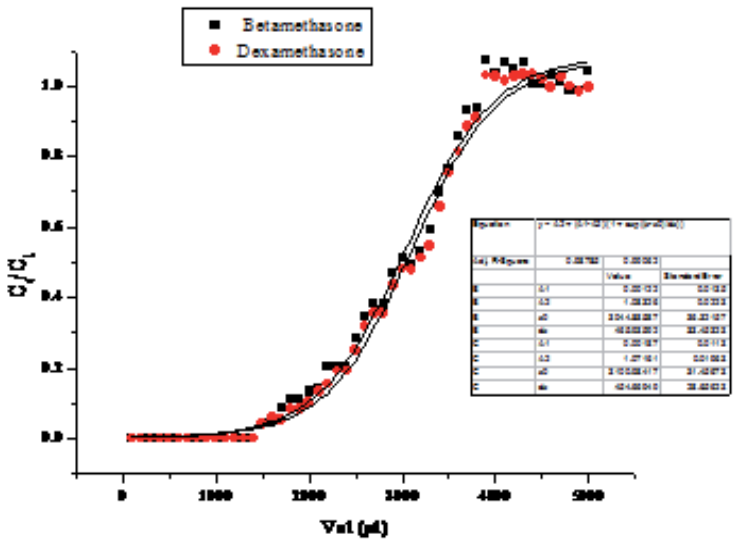

Figure 18. Breakthrough curves determined for two steroids on electrospun polystyrene fibers packed in micro column sorbent bed format presented as lines of best fit using the sigmoid Boltzmann model.

The breakthrough volumes, equilibrium volumes, retention volumes, theoretical plates and retention factor values for betamethasone and dexamethasone were very close which was consistent with the closeness of their logP values. This consistency was observed for the breakthrough curves fitted using both the Boltzmann and the Weibull five parameter model. On that basis, it may be concluded that these mathematical models would be suitable for characterisation of any electrospun fiber sorbent-analyte system that follows a similar profile.

Comparison of the calculated theoretical plates for the disk (1.39-2.82) and the micro column (7.98-9.1) SPE devices revealed that the shape of the breakthrough curve could be related to the theoretical plates [80, 91]. In addition, the observed breakthrough volumes for the disk (400-500 µl) and micro column (1400 µl) respectively were consistent with the theoretical plates. This may mean that theoretical plates could be important for the retention characteristics of a SPE sorbent bed.

Given the fact that theoretical plates are a function of the available surface area for analyte interaction, it could be concluded that a sorbent material with a larger surface area may exhibit

http://dx.doi.org/10.5772/57100

a larger number of theoretical plates and consequently a large retention capacity as mass transfer kinetics would be enhanced. Therefore, a larger number of theoretical plates would correspond to a steeper slope of the breakthrough curve as a result of fast mass transfer kinetics.

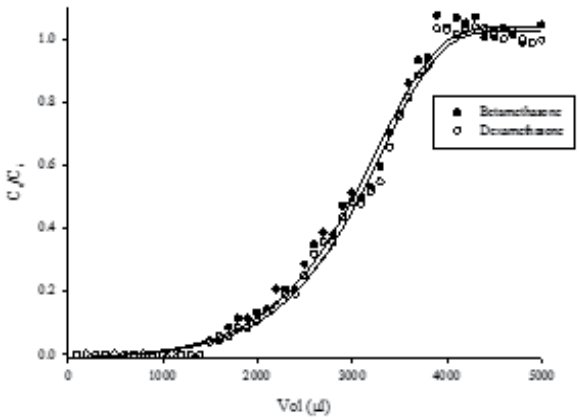

Figure 19. Breakthrough curves determined for two steroids on electrospun polystyrene fibers packed in microcolumn sorbent bed format presented as lines of best fit using the Weibull five parameter model.

	Coefficient					R^2
Analyte	**a**	**b**	**c**	**x_o**	**y_o**	
Betamethasone	1.0396 (0.01)	545252504.47 (0.30)	879140.39 (7.94)	3088.50 (40.73)	-0.0143 (0.0094)	0.9953
Dexamethasone	1.0528 (0.02)	15042770.75 (8.91)	23676.51 (7.37)	3032.19 (34.33)	-0.0159 (0.0110)	0.9943

Table 3. Regression parameters for the Weibull five parameter model

Analyte	V_B**(µl)** Observed	V_B**(µl)** Calculated	V_M**(µl)**	V_R**(µl)**	N_{cal}	N_{obs}	k
Betamethasone	1400	901	4250	3088.5	7.98	13.38	-0.27
Dexamethasone	1400	1020	4240	3032.2	9.1	13.80	-0.28

Table 4. Chromatographic parameters of the electrospun polystyrene fiber based micro column sorbent bed format derived from the Weibull five parameter model.

6. Conclusions

Given the fact that the feasibility of electrospun nanofiber based SPE has been successfully demonstrated, it is proposed that future research efforts should be channelled towards

simplifying SPE device fabrication and SPE procedures. In addition, more research efforts should be channelled towards physicochemical characterisation of electrospun nanofibers and relating to retention characteristics of the electrospun nanofiber based sorbent beds. Therefore, it is expected that with a better control of nanofiber orientation, packing procedures and pore structure, analytically useful electrospun nanofiber based chromatographic sorbent beds for HPLC could be fabricated.

By describing the wide nanofiber sorbent range of chemistries, functionalities and morphologies, it is hoped that this book chapter has provided enough evidence to support the hypothesis that electrospun nanofibers will be an effective class of SPE sorbents.

However several questions relating to the role of electrospinning, surface area to volume ratio, sorptive capacity and the miniaturisation route (should it be SPE or SPME variations?) still need to be answered. Looking into the future one wonders if nanostructured materials will mark the end of the sorbent technology development chain. In conclusion one can say with some degree of confidence that through electrospinning, a new class of sorbent based techniques/devices will eventually find their way into the analytical process either as a low or high resolution separation step.

Acknowledgements

Sasol is acknowledged for Samuel Chigome's Post Doctoral Research fellowship. Water Research Commission of South Africa, National Research Foundation of South Africa, Agilent Technologies, African Network of Analytical Chemists (SEANAC) and Rhodes University are acknowledged for financial and equipment support.

Author details

Samuel Chigome* and Nelson Torto*

*Address all correspondence to: n.torto@ru.ac.za

Department of Chemistry, Rhodes University, South Africa

References

[1] I. Liska, J. Chromatogr., A 885 (2000) 3-16.

[2] J. K. Lokhnauth, *Solid phase microextraction and stir bar sorptive extraction coupled to ion mobility spectrometry*. 2005. p. 201 pp.

[3] H. Braus, F. M. Middleton, G. Walton, Anal. Chem. 23 (1951) 1160-4.

[4] S. Chigome, G. Darko, N. Torto, Analyst 136 (2011) 2879-2889

[5] E. D.H., *Manual of symbols and terminology for physicochemical quantities and units. Appendix II. Definitions, terminology, and symbols in colloid and surface chemistry*, in *Pure Appl. Chem.* 1972. p. 577-638.

[6] R. P. Schwarzenbach, P. M. Gschwend, D. M. Imboden, *Environmental Organic Chemistry*. 1992: Wiley. 681 pp.

[7] B. S. Bahl, G. D. Tuli, A. Bahl, *Essentials of Physical Chemistry, 24th Edition*. 2000: S. Chand & Co. Ltd. 880 pp.

[8] J. Fraissard, C. W. Conner, Editors, *Physical Adsorption: Experiment, Theory and Applications. (Proceedings of the NATO Advanced Study Institute, held 19 May-1 June 1996, in La Colle sur Loup, France.) [In: NATO ASI Ser., Ser. C, 1997; 491]*. 1997: Kluwer. 619 pp.

[9] M. C. Hennion, J. Chromatogr., A 856 (1999) 3-54.

[10] K.-U. Goss R. P. Schwarzenbach, Environ. Sci. Technol. 35 (2001) 1-9.

[11] P. W. Lankford, W. W. Eckenfelder, Jr., Editors, *Toxicity Reduction in Industrial Effluents*. 1990: Van Nostrand Reinhold. 350 pp.

[12] W. J. Thomas B. Crittenden, *Adsorption Technology and Design*. 1997: Butterworth-Heinemann. 176 pp.

[13] S. Mitra J. D. Winefordner, *Sample Preparation Techniques in Analytical Chemistry*. 2003: John Wiley & Sons Inc. 400 pp.

[14] R. P. Belardi J. B. Pawliszyn, Water Pollut. Res. J. Can. 24 (1989) 179-191.

[15] S. Risticevic, V. H. Niri, D. Vuckovic, J. Pawliszyn, Anal. Bioanal. Chem. 393 (2009) 781.

[16] F. M. Musteata J. Pawliszyn, TrAC Trends in Analytical Chemistry 26 (2007) 36-45.

[17] D. Vuckovic, X. Zhang, E. Cudjoe, J. Pawliszyn, Journal of Chromatography A 1217 (2010) 4041-4060.

[18] L. Muller. *Field analysis by SPME*. 1999: Royal Society of Chemistry. p.269-283

[19] J. S. Fritz M. Macka, J. Chromatogr., A 902 (2000) 137-166.

[20] J. S. Fritz, *Analytical Solid-Phase Extraction*. 1999: Wiley. 210 pp.

[21] C. F. Poole, A. D. Gunatilleka, R. Sethuraman, J. Chromatogr., A 885 (2000) 17-39.

[22] R. Lucena, B. M. Simonet, S. Cárdenas, M. Valcárcel, Journal of Chromatography A 1218 (2011) 620-637.

[23] C. K. Liu, K. Lai, W. Liu, M. Yao, R. J. Sun, Polymer International 58 (2009) 1341-1349.

[24] G. Y. Oh, Y. W. Ju, M. Y. Kim, H. R. Jung, H. J. Kim, W. J. Lee, Science of the Total Environment 393 (2008) 341-347.

[25] W. G. Shim, C. Kim, J. W. Lee, J. J. Yun, Y. I. Jeong, H. Moon, K. S. Yang, Journal of Applied Polymer Science 102 (2006) 2454-2462.

[26] N. N. Bui, B. H. Kim, K. S. Yang, M. E. Dela Cruz, J. P. Ferraris, Carbon 47 (2009) 2538-2539.

[27] R. Lucena, B. M. Simonet, S. CÃ¡rdenas, M. ValcÃ¡rcel, Journal of Chromatography A 1218 620-637.

[28] N. Masque, R. M. Marce, F. Borrull, TrAC, Trends Anal. Chem. 17 (1998) 384.

[29] C. Shao, H. Kim, J. Gong, D. Lee, Nanotechnology 13 (2002) 635.

[30] S. S. Choi, S. G. Lee, S. S. Im, S. H. Kim, Y. L. Joo, Journal of Materials Science Letters 22 (2003) 891-893.

[31] A. C. Patel, S. Li, C. Wang, W. Zhang, Y. Wei, Chem. Mater. 19 (2007) 1231-1238.

[32] D. Qi, X. Kang, L. Chen, Y. Zhang, H. Wei, Z. Gu, Anal Bioanal Chem 390 (2008) 929-38.

[33] Z. Liu, X. Kang, F. Fang, Microchim. Acta 168 (2010) 59-64.

[34] X. Kang, C. Pan, Q. Xu, Y. Yao, Y. Wang, D. Qi, Z. Gu, Anal Chim Acta 587 (2007) 75-81.

[35] Y. Zhang, X. Kang, L. Chen, C. Pan, Y. Yao, Z. Z. Gu, Analytical and Bioanalytical Chemistry 391 (2008) 2189-2197.

[36] X. J. Kang, L. Q. Chen, Y. Y. Zhang, Y. W. Liu, Z. Z. Gu, Journal of Separation Science 31 (2008) 3272-3278.

[37] S. Chigome, G. Darko, U. Buttner, N. Torto, Anal. Methods 2 (2010) 623-626.

[38] L.-Q. Chen, X.-J. Kang, J. Sun, J.-J. Deng, Z.-Z. Gu, Z.-H. Lu, J. Sep. Sci. 33 (2010) 2369-2375.

[39] Y. Wang, L. Chen, X. Kang, Q. Xu, Z. Gu, Zhongguo Yaolixue Tongbao 23 (2007) 832.

[40] X. Kang, H. Wei, Y. Zhang, L. Chen, Z. Gu. Progress on Post-Genome Technologies, Proceedings of the International Forum on Post-Genome Technologies (4' IFPT), 4th, Hangzhou, China, Sept. 25-26, (2006) 241-245

[41] F. Fang, X. J. Kang, Z. Y. Liu, Y. Q. Ma, Z. Z. Gu, Chinese Chemical Letters 20 (2009) 1491-1494.

[42] Q. Xu, S. Y. Wu, M. Wang, X. Y. Yin, Z. Y. Wen, W. N. Ge, Z. Z. Gu, Chromatographia 71(2010) 487-492.

[43] Q. Xu, X. Yin, S. Wu, M. Wang, Z. Wen, Z. Gu, Microchimica Acta 168 (2010) 267-275.

[44] Q. Xu, N. Zhang, X. Yin, M. Wang, Y. Shen, S. Xu, L. Zhang, Z. Gu, J Chromatogr B Analyt Technol Biomed Life Sci 878 (2010) 2403-8.

[45] K. Yoshimatsu, L. Ye, J. Lindberg, I. S. Chronakis, Biosens Bioelectron 23 (2008) 1208-15.

[46] C.-h. Zheng, F.-g. Meng, X.-r. Mo, D.-y. Zhao, M.-m. Yang, Fenxi Shiyanshi 29 (2010) 80-84.

[47] C. Zheng, L. Yang, Z. Yao, D. Zhao, M. Yang, Fenxi Ceshi Xuebao 28 (2009) 926-930.

[48] Z. Yao, L. Yang, C. Zheng, M. Yang, Huaxue Tongbao 72 (2009) 845-848.

[49] L. Zhang Y.-L. Hsieh, Nanotechnology 17 (2006) 4416-4423.

[50] C. L. Casper, J. S. Stephens, N. G. Tassi, D. B. Chase, J. F. Rabolt, Macromolecules 37 (2004) 573-578.

[51] A. Gupta, C. D. Saquing, M. Afshari, A. E. Tonelli, S. A. Khan, R. Kotek, Macromolecules 42 (2009) 709-715.

[52] Q. Shi, N. Vitchuli, L. Ji, J. Nowak, M. McCord, M. Bourham, X. Zhang, J. Appl. Polym. Sci. 120 (2011) 425.

[53] N. Fontanals, R. M. Marce, F. Borrull, TrAC, Trends Anal. Chem. 24 (2005) 394-406.

[54] N. Fontanals, R. M. Marce, F. Borrull, Journal of Chromatography A 1152 (2007) 14-31.

[55] A. Kloskowski, M. Pilarczyk, A. Przyjazny, J. NamieÅ›nik, Critical Reviews in Analytical Chemistry 39 (2009) 43-58.

[56] L. S. Wan, J. Wu, Z. K. Xu, Macromolecular Rapid Communications 27 (2006) 1533-1538.

[57] E. Turiel A. Martin-Esteban, Anal. Chim. Acta 668 (2010) 87.

[58] I. S. Chronakis, B. Milosevic, A. Frenot, L. Ye, Macromolecules 39 (2006) 357-361.

[59] S. Chigome N. Torto, TrAC, Trends Anal. Chem. 38 (2012) 21-31.

[60] X. Kang, C. Pan, Q. Xu, Y. Yao, Y. Wang, D. Qi, Z. Gu, Analytica Chimica Acta 587 (2007) 75-81.

[61] F. Fang, X. J. Kang, Z. Y. Liu, Y. Q. Ma, Z. Z. Gu, Chinese Chemical Letters 20 (2009) 1491-1494.

[62] Z. Liu, X. Kang, F. Fang, Microchimica Acta 168 (2009) 59-64.

[63] X.-J. Kang, L.-Q. Chen, Y. Wang, Y.-Y. Zhang, Z.-Z. Gu, Biomedical Microdevices 11 (2009) 723-729.

[64] Y. Zhang, X. Kang, L. Chen, C. Pan, Y. Yao, Z.-Z. Gu, Analytical and Bioanalytical Chemistry 391 (2008) 2189-2197.

[65] D. Qi, X. Kang, L. Chen, Y. Zhang, H. Wei, Z. Gu, Anal. Bioanal. Chem. 390 (2008) 929-938.

[66] X.-j. Kang, L.-q. Chen, Y.-y. Zhang, Y.-w. Liu, Z.-z. Gu, Journal of Separation Science 31 (2008) 3272-3278.

[67] J. S. Fritz J. J. Masso, J. Chromatogr., A 909 (2001) 79-85.

[68] S. Chigome, G. Darko, U. Buttner, N. Torto, Analytical Methods 2 (2010) 623-626.

[69] Q. Xu, S.-Y. Wu, M. Wang, X.-Y. Yin, Z.-Y. Wen, W.-N. Ge, Z.-Z. Gu, Chromatographia 71 (2009) 487-492.

[70] Q. Xu, X. Yin, M. Wang, H. Wang, N. Zhang, Y. Shen, S. Xu, L. Zhang, Z. Gu, Journal of Agricultural and Food Chemistry 58 (2010) 11311-11317.

[71] W. Shu-Yan, X. Qian, C. Tian-Shu, W. Min, Y. Xue-Yan, Z. Ni-Ping, S. Yan-Yan, W. Zuo-Yang, G. Zhong-Ze, Fenxi Huaxue/ Chinese Journal of Analytical Chemistry 38 (2010) 503-507.

[72] Q. Xu, N. Zhang, X. Yin, M. Wang, Y. Shen, S. Xu, L. Zhang, Z. Gu, J. Chromatogr., B: Anal. Technol. Biomed. Life Sci. 878 (2010) 2403-2408.

[73] Q. Xu, X. Yin, Y. Shen, N. Zhang, M. Wang, Z. Gu, Chin. J. Chem. 29 (2011) 567-574.

[74] Q. Xu, X. Yin, S. Wu, M. Wang, Z. Wen, Z. Gu, Microchimica Acta 168 (2010) 267-275.

[75] H. Bagheri, A. Aghakhani, M. Akbari, Z. Ayazi, Analytical and Bioanalytical Chemistry 400 (2011) 3607-3613

[76] H. Bagheri, Z. Ayazi, A. Aghakhani, N. Alipour, J. Sep. Sci. 35 (2012) 114-120.

[77] M. Abdel-Rehim, J. Chromatogr., A 1217 (2010) 2569-2580.

[78] G. Darko, S. Chigome, Z. Tshentu, N. Torto, Anal. Lett. 44 (2011) 1855-1867.

[79] C. E. Werkhoven-Goewie, U. A. T. Brinkman, R. W. Frei, Anal. Chem. 53 (1981) 2072-80.

[80] P. Lövkvist J. Å. Jönsson, Analytical Chemistry 59 (1987) 818-821.

[81] K. Bielicka-Daszkiewicz A. Voelkel, Talanta 80 (2009) 614-621.

[82] R. Ferrer, J. L. Beltran, J. Guiteras, Anal. Chim. Acta 346 (1997) 253-258.

[83] M. Mihaly, E. S. Andreiadis, E. Pincovschi, Sci. Bull. - Univ. "Politeh." Bucharest, Ser. B 67 (2005) 57-64.

[84] E. Bacalum, M. Radulescu, E.-E. Iorgulescu, V. David, Rev. Roum. Chim. 56 (2011) 137-143.

[85] S. V. Romanenko A. G. Stromberg, J. Anal. Chem. 55 (2000) 1024-1028.

[86] S. D. Kolev, Anal. Chim. Acta 229 (1990) 183-9.

[87] W. D. Hillis, Curr Biol 3 (1993) 79-81.

[88] V. F. Pozhidaev, Y. B. Rubinshtein, G. Y. Golberg, S. A. Osadchii, Chem. Pet. Eng. 45 (2009) 460-467.

[89] M. Ramirez C, M. Pereira da Silva, S. G. Ferreira L, O. Vasco E, Journal of Hazardous Materials 146 (2007) 86-90.

[90] J. E. Clark S. V. Olesik, Anal. Chem. (Washington, DC, U. S.) 81 (2009) 4121.

[91] G. I. Senum, Environ. Sci. Technol. 15 (1981) 1073-5.

Chapter 2

Electrospun Nanofibers: From Rational Design, Fabrication to Electrochemical Sensing Applications

Jianshe Huang and Tianyan You

Additional information is available at the end of the chapter

http://dx.doi.org/10.5772/57099

1. Introduction

Electrospinning is a convenient and versatile technique to prepare continuous fibers with diameters ranging from tens nanometers to several micrometers [1]. In early works, electrospinning was limited to the fabrication of nanofibers from organic polymers due to the stringent requirement on the viscoelastic behavior of the electrospinning solution [2]. Recent efforts have greatly expanded the application scope of electrospinning technique. Various one-dimensional (1D) nanomaterials can be prepared by electrospinning besides the common polymer fibers, such as polymer fibers loaded with nanoparticles and functional molecules, ceramics fibers and metal/metal oxide fibers. Additionally, with the development of electrospinning method and setup, electrospun fibers have not been limited to the morphology of solid interior and smooth surface. Fibers with novel secondary structures, such as core/sheath, hollow and porous, can also be prepared if appropriate processing parameters or new designs of setups are employed.

Due to the small diameter, extremely long length, high surface area and complex pore structures, electrospun fibers have being attracted extensive research interests for their applications in biomedical field [1, 3, 4], such as tissue engineering, drug delivery and wound healing, as well as energy and environmental engineering [5, 6]. The relatively large specific surface area and high porosity make electrospun nanomaterials attract significant attentions in developing ultrasensitive sensors [7-9]. Various electrospun nanomaterial-based sensors have been designed, including resistive sensor, electrochemical sensor, fluorescent sensor, acoustic wave sensor, colorimetric sensor, photoelectric sensor, etc. Among these read-out modes, electrochemical read-out, featured with high sensitivity and selectivity, inexpensive equipment and easy miniaturization, has attracted remarkable attentions in the ultrasensitive detection. In this chapter, we focus on the synthesis of nanofibers with different composition,

and the design and preparation of electrospun nanofibers with novel secondary structures. Following this, the application of electrospun nanomaterials in constructing electrochemical sensors and their analytical performance is discussed.

2. General process of electrospinning

The basic setup for electrospinning consists of three major components: a high voltage power supply, a spinneret, and a collector (a counter electrode) (Fig. 1). In the process of electrospinning, the applied voltage causes a cone-shaped deformation of the drop of polymer solution (Taylor cone). Once the strength of electric field exceeds a threshold value, the electrostatic force on the deformed polymer drop can overcome the surface tension and thus a liquid jet is formed. This electrified jet then moves toward counter electrode, leading to the formation of a long and thin thread. As the liquid jet is continuously elongated and the solvent is evaporated, solid fibers with diameters as small as tens nanometers are deposited on the colletor.

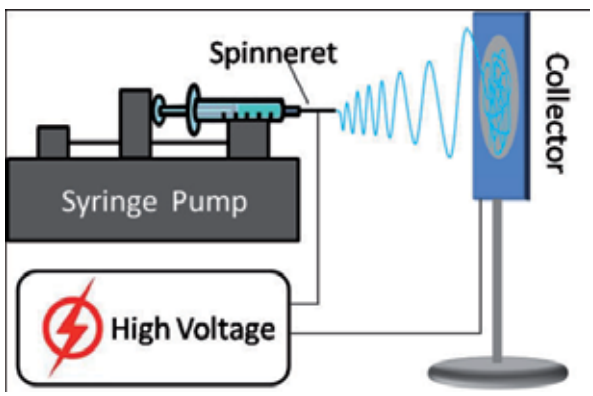

Figure 1. Schematic illustration of the basic setup of electrospinning.

In spite of the simple setup, there are a number of parameters that can greatly affect the morphology and diameter of electrospun fibers, including: (1) the intrinsic properties of solution such as the type of polymer, concentration, conductivity, and solvent volatility; and (2) the processing parameters such as the strength of the applied electric field, solution flow rate, and the distance between spinneret and collector [2, 10, 11]. In addition, the humidity and temperature of the surroundings may also play an important role in determining the morphology and diameter of electrospun fibers. Numerous experimental investigations and theoretical models have drawn some general relationships between these parameters and fiber morphology. For example, the higher applied voltage will lead to a larger fiber diameter, but this trend is not monotonic; the higher polymer concentration (higher viscosity) or faster flow rate usually results in the larger nanofiber diameters. In contrast, the increase of solution conductivity can significantly reduce the fiber diameter. These results are instructive to some extent in experiment design and predicting the resultant fiber morphology. However,

empirical knowledge is crucial because the ideal values of these parameters vary considerably with the polymer/solvent system.

3. Fabrication of nanofibers by electrospinning

Electrospinning has been proved to be a versatile method to prepare 1D nanomaterials of polymer, ceramics, metal, and metal oxide. Various functional elements, such as drugs, dyes, DNA, proteins, and nanoparticles, could be incorporated into electrospun nanofibers to form composite nanofibers. Additionally, except for the nanofibers with solid interior and smooth surface, nanofibers with various secondary structures, including core/sheath, hollow, and porous, could be fabricated by electrospinning. In this section, the preparation of electrospun nanofibers with different composition and secondary structures is introduced, and the parameters that control the composition and morphology are highlighted.

3.1. Electrospun nanofibers with different composition

In principle, almost all natural and synthetic polymers can be electrospun into their 1D nanostructures through judicious selection of solution and processing parameters [1]. Besides itself nanofibers, polymers can also be used as template or host to load nanoparticles or functional molecules. The produced composite nanofibers exhibit various electronic, optical, magnetic, and biological properties.

In order to incorporate nanoparticles into electrospun fibers, pre-synthetic Au [12], Fe_3O_4 [13], SiO_2 nanoparticles [14], CdTe quantum dots [15], and Au nanorods (AuNRs) [16] were introduced in polymer solution and then electrospinning was conducted. For example, AuNRs/poly(vinyl alcohol) (PVA) nanofiber was prepared by electrospinning the mixture solution of AuNRs and PVA [16]. The AuNRs were well aligned along the axis direction of the fibers due to the external fields (Fig. 2A). In a one-step method, silver nitrate was dissolved in poly(vinyl pyrrolidone) (PVP)/N, N-dimethylformamide (DMF) [17], or nylon 6/formic acid [18] solution, where DMF and formic acid acted as both a solvent for polymer and a reducing agent for the Ag^+ ion, followed by electrospinning to form Ag nanoparticle-filled composite nanofibers. In addition, the introduction of nanoparticles into polymer nanofibers have also been accomplished by adding appropriate precursors to the electrospinning solution, after that a chemical or physical method was used to reduce the metal precursor. For example, $PdCl_2$ and copolymers of acrylonitrile and acrylic acid (PAN-AA) are dissolved in DMF for electrospinning. And then, the fiber mat was immersed into diluted hydrazine water solution to reduce Pd cations [19]. The as-prepared Pd/PAN-AA composite material showed high catalytic activity toward hydrogenation of dehydrolinalool. Li et al. prepared Ag nanoparticle-loaded PAN nanofibers via electrospinning of PAN/$AgNO_3$-DMF solution followed by UV-irradiation photoreduction [20].

Carbon nanotubes (CNTs), an actively studied nano-object, can also be incorporated into electrospun fibers. The goal of most studies in this direction is to improve the electrical conductivity and mechanical strength of the fibers [21-25]. Some exciting properties were also

observed for CNT-incorporated polymer fibers, such as enhanced thermal stability [21], anisotropic electrical conductivity [24], and the preferential orientation of the CNTs along the fiber axis. These composite fibers can find promising applications in high strength membrane and electronics. Graphene, a single layer of aromatic carbon nanomaterial, has also been used as nanofiller in polymer nanofibers to reinforce the mechanical, electrical, thermal, and optical properties. For example, Bao et al. prepared graphene-poly(vinyl acetate) (PVAc) composite nanofibers by electrospinning [26]. The results indicated that the dispersity of pristine or functionalized graphene greatly influenced the morphology of fibers. When graphene modified by 1-pyrenebutanoic acid succinimidyl ester (G-PBASE) or 4-(2-(pyridin-4-yl)vinlyl) phenyl group (G-dye) was used as nanofillers, uniform and smooth nanofibers were readily obtained (Fig. 2B). In contrast, some micrometer-sized beads were formed when plain graphene oxide (GO) was used due to the poor dispersion of GO in the DMF solvent.

In addition to the nano-objects, drugs, dyes, proteins, DNA, virus, and other compounds can be readily incorporated into electrospinning solutions to produce functional fibers. For example, collagen could be electrospun into fibers from a solution of 1, 1, 1, 3, 3, 3-hexafluoro-2-propanol (HFP) [27, 28], or from a blend with poly(ethylene oxide) (PEO) [29]. Other proteins and enzymes, such as elastin [29], casein [30], α-chymotrypsin [31], bovine serum albumin (BSA) [32, 33], silk fibroin [34], lipase [30, 35], cellulose [36, 37], lysozyme [38, 39], glucose oxidase [40], luciferase [32], alkaline phosphatase and β-galactosidase [41], diisopropylfluorophosphatase [42], and lactate dehydrogenase [43], could only be processed by electrospinning as blends with synthetic polymers. The catalytic activity of encapsulated enzyme is usually lower than that of free enzyme, but more active than that in the cast membrane due to the higher surface area and porous structures of electrospun fibers. In addition, DNA molecules can also be encapsulated in electrospun fibers from blends with polymers [44, 45]. DNA molecules incorporated into electrospun nanofiber could reserve structurally intact and bioactive. More interestingly, virus could be used to fabricate 1D micro- and nanosized diameter fibers by electrospinning [46]. M13 virus was dispersed in HFP solution to form a homogeneous virus suspension, and then was directly electrospun into fibers (Fig. 2C). Due to the toxicity of HFP to the M13 virus, infectibility of M13 virus in HFP solution was dramatically decreased, showing no infectibility. In order to improve processing ability and preserve the intact viral structure and infecting ability, the M13 virus suspension was blended with a water soluble polymer PVP. Uniform fibers with the diameter of 100-200 nm could then be obtained.

For inorganic compounds, it is very difficult to directly process by electrospinning due to the strict requirement of solution viscoelasticity. Only a few types of inorganic fibers could be obtained by carefully selecting metallic precursors and solvents [47-49]. Recent studies demonstrated that the combination of electrospinning and sol-gel process could be used for direct producing inorganic fibers, for example TiO_2/SiO_2 and Al_2O_3 [50], SiO_2 [51], V_2O_5/SiO_2 [52], SiO_2/ZrO_2 [53]. The key point of this method was to control the hydrolysis rate of sol-gel precursors by adjusting the pH value or aging conditions. However, the fibers prepared via direct electrospinning of inorganic sols are usually several hundred nanometers in diameter with poor monodispersity, and only a limited number of materials can be prepared by this

http://dx.doi.org/10.5772/57099

method. In order to reduce the diameter of electrospun fibers, Li and Xia developed a new approach in which polymer was introduced into the sol-gel precursor to control the viscoelastic behavior, at the same time the sol-gel reaction was controlled to take place mainly in the spinning jet rather than in the stock solution [54-56]. In a typical procedure [55], a sol-gel precursor of titanium tetraisopropoxide ($Ti(OiPr)_4$) was mixed with PVP in alcohol solution. After the solution had been electrospun into a thin jet, the metal alkoxide immediately started to hydrolyze by reacting with the moistrure in air to generate a continuous gel network within the polymer matrix. As a result, TiO_2/PVP composite nanofibers would be obtained (Fig. 2D). These composite nanofibers could subsequently be converted into TiO_2 nanofibers without changing their morphology via calcinations at the elevated temperature (Fig. 2E). The average diameter of these ceramic nanofibers could be controlled in the range of 20-200 nm with relatively narrow size distribution by varying a number of parameters. This method has also been extended to process many other oxide ceramics into nanofibers. Similarly, a great number of metal oxide or sulfide nanofibers have been produced by electrospinning the solutions of appropriate metal precursors and polymers, followed by calcination at elevated temperatures. Electrospun metal oxide nanofibers could be further converted into continuous and thin metal nanofibers in reducing atmosphere, such as Cu [57, 58], Fe, Co, and Ni [59]. Shui and Li prepared long Pt nanowires with a few nanometers in diameter by electrospinning of H_2PtCl_6/PVP mixture solution and heat treatment [60]. A series of processing parameters were optimized to control the morphology and diameter of the nanowires. Very recently, Greiner's group prepared Au nanowires by electrospinning of highly concentrated aqueous dispersions of gold nanoparticles in the presence of PVA and subsequent annealing at 300-500 ℃ in air [61]. The produced Au nanowires represented solid structures like bulk gold (Fig. 2F). The electrospun metal nanofibers with ultrahigh aspect ratio and ultralow junction resistance are of great interest for foundational research and applications in nanoelectronics, fuel cells, and sensors.

Carbon fibers or nanofibers, which have many noticeable properties in mechanical strength, electrical conductivity, and special surface area, have been considered as one of the most important materials for modern science and technology. Various electrospun polymer nanofibers could be converted into carbon nanofibers, such as polyacrylonitrile (PAN), polyimide (PI), PVA, poly(vinylidene fluoride) (PVDF) and pitch. Inagaki et al. recently composed a review on the preparation of carbon nanofibers from electrospun polymer nanofibers [62]. Carbon precursors and the control of structure and texture in the resultant carbon nanofibers were highlighted.

3.2. Nanofibers with core/sheath structures

Nanofibers with core/sheath structures have many potential applications in microfluidics, photonics, and energy storage. Electrospinning provides a simple method for the large-scale fabrication of such nanofibers. Up to now, several methods have been developed to prepare core/sheath structured nanofibers by electrospinning. For example, in template-directed method, polymer fibers (template) were produced by ordinary electrospinning, and then the as-prepared fibers were coated with the shell component by various chemical and physical methods [63-67]. With the use of conventional single-nozzle electrospinning, it is also possible

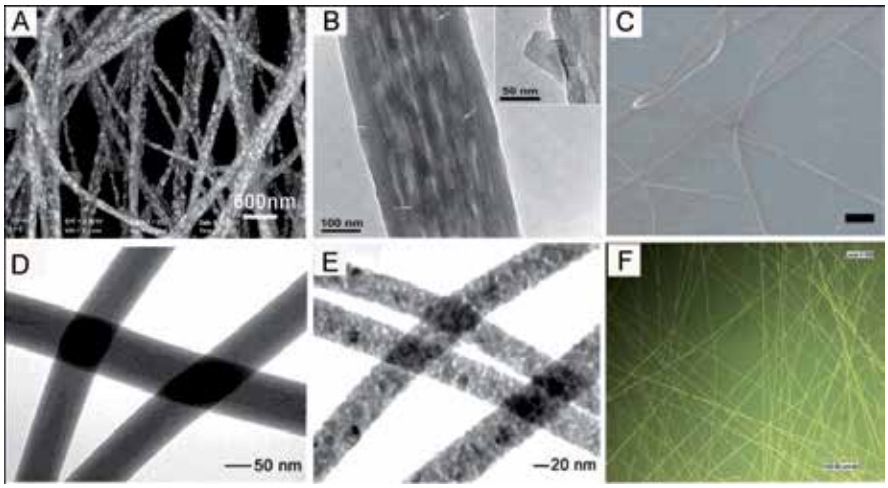

Figure 2. Electrospun nanofibers with different composition. (A) Typical backscattering SEM image of the AuNRs/PVA nanofibers [16]. (B) High-magnification TEM image of G-PBASE/PVAc nanofiber. The arrows indicate the graphene flakes inside the nanofiber. The inset shows an enlarged image of G-PBASE embedded in the sidewall of a PVAc nanofiber [26]. (C) SEM image of electrospun M13 virus-only fibers. (Scale bars: 5 μm) [46]. (D) TEM image of TiO_2/PVP composite nanofibers fabricated by electrospinning an ethanol solution that contained 0.03 g/mL PVP and 0.1 g/mL $Ti(OiPr)_4$ [55]. (E) TEM image of TiO_2 nanofibers prepared by calcining (D) sample in air at 500 ℃ for 3 h [55]. (F) Optical microscopy image of gold nanowires on a mica slide, scale bar: 100 μm [61].

to prepare core/sheath nanofibers from emulsion or homogeneous polymer solutions. In the case of emulsion electrospinning, a core/sheath jet was formed in the electrospinning process due to the stretching and collapse of emulsion. This method has been used to prepare poly(methyl methacrylate) (PMMA)/PAN [68, 69], protein-methyl cellulose/poly(D, L-lactide) (MC/PDLLA) [39, 70], and PEO/poly(ethylene glycol)-poly(L- lactic acid) (PEG-PLA) (Fig. 3) [71] core/sheath nanofibers, and has the potential to extend to any pair of water-soluble polymer and hydrophobic (or amphiphilic) polymer. In the case of homogeneous solution electrospinning, the formation of core/sheath structure was mainly attributed to the phase separation of polymer blends, different solubility of the two components, and some other rheological factors [72-76]. The type of polymers, the ratios of components and the additives play key roles in the formation of core/sheath structures, rather than co-continuous morphologies. Recently, Jo et al. reported a one-step, single-nozzle electrospinning method for producing core-sheath nanofibers with cross-linked polymeric colloids as core and polymer as sheath (Fig. 4) [77]. Cross-linked PMMA colloids or poly(N-isopropylacrylamide) (PNIPAm) microgels were dispersed in a concentrated polymer solution, e.g. poly(ε-caprolactone) (PCL) in chloroform solution, for electrospinning. In the electrospinning process, fast evaporation of the solvent from the Taylor cone and following solution jet enhanced the phase separation of colloids from the condensed polymer solution, which resulted in a continuous colloidal packing at the inner region of fibers. If a small amount of colloids was used, the beanpod-like morphology of the nanofibers could be obtained; while a larger amount of colloids would lead to the colloids closely packing at the central area of the fibers, and core/sheath fibers consisting of a colloidal core could be produced.

http://dx.doi.org/10.5772/57099

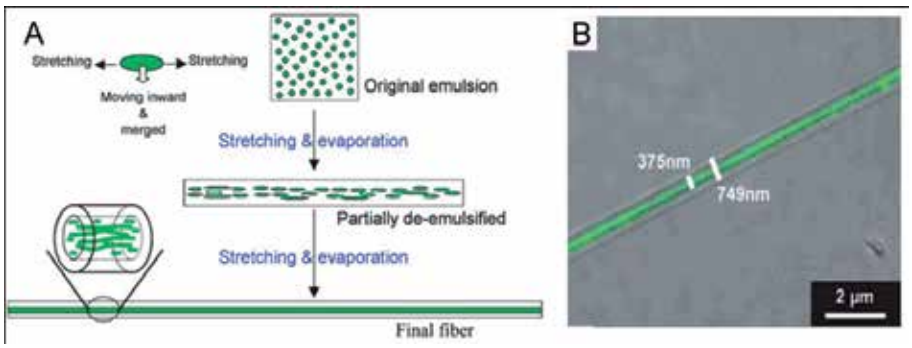

Figure 3. (A) Schematic mechanism for the formation of core/sheath composite fibers during emulsion electrospinning. (B) Confocal laser scanning microscope image of core/sheath structured PEO/PEG-PLA nanofiber prepared from W/O emulsions [71].

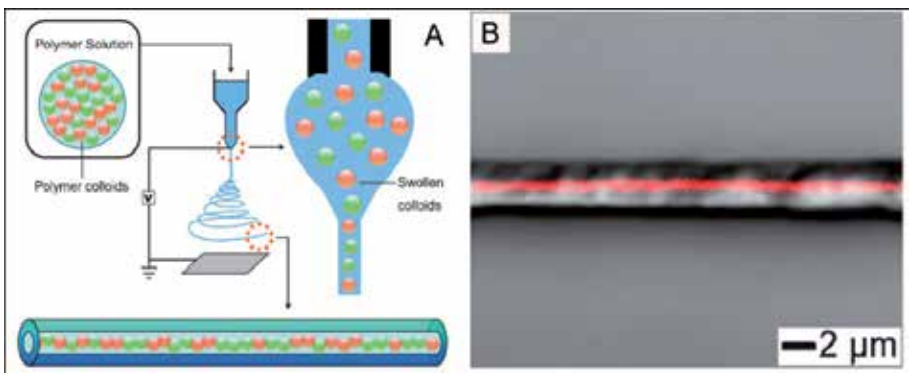

Figure 4. (A) Schematic illustration of the method for producing core/sheath nanofibers that contain an array of colloids in the core. (B) Combination of optical and fluorescent mode images of the core/sheath fiber, consisting of a PCL sheath and PNIPAm microgel particles in the core [77].

Coaxial electrospinning, in which coaxial two spinnerets replaced the single nozzle in the conventional setup for electrospinning, is a more convenient and direct method for the preparation of core/sheath structured nanofibers. Loscertales et al. initially designed a coaxial spinneret to generate steady core/sheath liquid jet from immiscible liquids [78]. However, in their experiment, the liquid jet was broke up to form core/sheath capsules, rather than fibers. Sun and co-workers overcame the instability problem in the coaxial electrospinning process to obtain continuous core/sheath jet, and then core/sheath polymer fibers [79]. The experimental setup for coaxial electrospinning is shown in Fig. 5A. It was proposed that undesirable mixing of the two polymer solutions could be prevented by the low diffusion coefficients relative to the fast stretching and solidification processes taking place in the electrospinning process. Core/sheath fibers with identical polymers PEO/PEO, or two different polymers polysulfone (PSU)/PEO could be obtained using this method. More importantly, non-spinnable solutions, such as poly(dodecylthiophene) (PDT) and $Pd(OAc)_2$, could also be used as core

components to obtain core/sheath structured PDT/PEO (Fig. 5B) and Pd/PLA composite fibers. Yu et al. detailedly studied the coaxial electrospinning process for producing fibers with smaller diameters and core/sheath structure from difficult-to process fluids [80]. They pointed out that the stabilization of the core fluid in the sheath against breakup into droplets were mainly accomplished through two mechanisms: (1) The viscoelastic sheath fluid could delayed or completely suppressed the Rayleigh instability (which resulted in the breakup of fluid jet into droplets) in the core fluid. In the electrospinning process, stretching of the sheath component imparted great elasticity to the interface due to strain hardening, further stabilizing the core fluid. (2) The sheath fluid also reduced the surface forces at the boundary of the core fluid by replacing the relatively high fluid-vapor surface tension typically present in single-fluid electrospinning by a lower fluid-fluid interfacial tension. Additionally, the fast travelling speed of fluids in electrospinning process prevented the two fluids from mixing significantly. Li and Xia also systematiclly investigated the coaxial electrospinning process by using two immiscible liquids of heavy mineral oil and an ethanol solution of PVP and $Ti(OiPr)_4$ as the materials for core and sheath [81]. They argued that rapid stretching of the sheath caused strong viscous stress, which would stretch the oil phase and elongate it along with the sheath solution via the mechanisms of viscous dragging and/or contact friction.

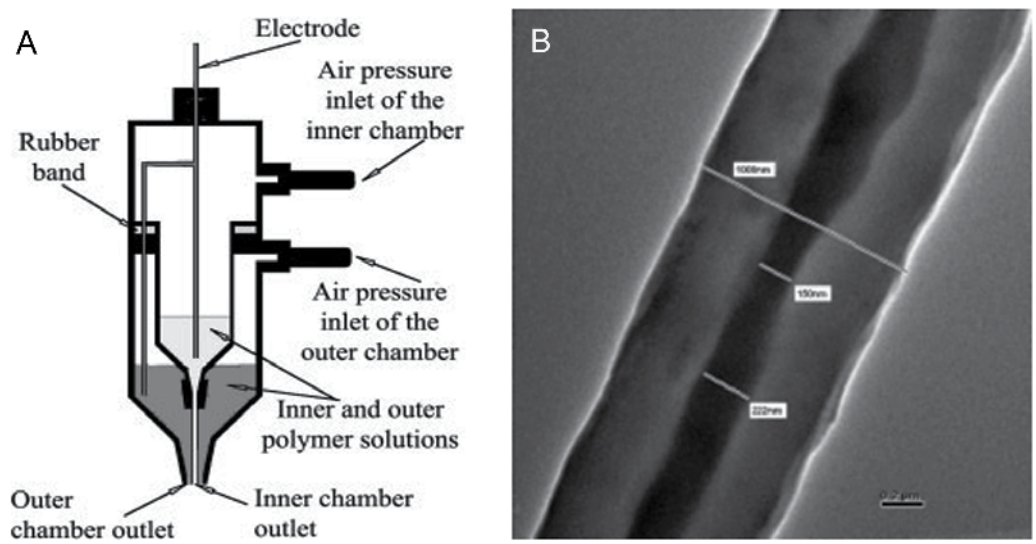

Figure 5. (A) Experimental setup used for coaxial electrospinning of core/sheath nanofibers. (B) TEM image of co-electrospun PEO (shell) and PDT (core) composite nanofibers [79].

With the development of theoretical and experimental aspects, this coaxial electrospinning method has been extended to prepare core/sheath fibers of various composition, such as gelatin/PCL [82, 83], poly(ethylene glycol) (PEG)/PCL [38], PCL/collagen [84], polyurethane/polycarbonate (PU/PC) [85], PCL/PEG [86], PVP/PDLLA [87], polypyrrole (PPy)/PVP [88], poly(lactide-co-glycolide) (PLGA)/chitosan [89], PVP/poly(L-lactide-co-epsilon-caprolactone) (PLCL) [90], dextran/PLCL [91], Alq3/PVP [92], poly(glycerol sebacate) (PGS)/gelatin [93],

http://dx.doi.org/10.5772/57099

poly(lactic acid) (PLA)/chitosan [94], PEO/chitosan [95], poly(L-lactide-co-caprolactone) (PLLACL)/collagen [96], and poly(hydroxybutyrate-co-hydroxyvalerate) (PHBV)/chitosan [97]. Other functional components, for example, FePt nanoparticles [98], Si nanoparticles [99], multi-walled carbon nanotube (MWNT) [100], O_2 indicator (PtOEP) and γ-Fe_3O_4 [101], proteins [102], and drug molecules [103], have also been used as core components to fabricate core/sheath fibers. In combination of coaxial electrospinning and sol-gel process, inorganic fibers with core/sheath structures were also prepared, such as $LiCoO_2$/MgO [104], TiN/VN [105], $CoFe_2O_4$/$Pb(Zr_{0.52}Ti_{0.48})O_3$ [106], and SnO_2/TiO_2 [107].

3.3. Nanofibers with hollow structures

Tubular nanostructures with dimensions in the range of submicrometer to a few nanometers are of great interest for applications in catalysis, fluid transportation, drug release, sensing, and gas storage. Various methods have been demonstrated to fabricate such structures from a broad range of materials. Similar to the preparation of core/sheath nanofibers, electrospun nanofibers have been used as sacrificial templates for preparing tubular fibers. For example, Bognitzki and co-workers designed a method termed tubes by fiber templates (TUFT) process for fabricating nano- and mesotubes [108]. They selected electrospun PLA nanofibers as templates. Polymer, polymer-metal hybrid and metal tubes could be obtained after coating and removing the template fibers. In this template method, various coating techniques have been employed, such as chemical vapor deposition [108, 109], physical vapor deposition [108], sol-gel process [110], electrochemical deposition [111], in-situ polymerization [112], layer-by-layer assembly [113-115], vapor deposition polymerization [116], atomic layer deposition [117], and sputtering [118]. After the formation of core/sheath fibers, the templates could be removed by heat treatment [108-110, 117, 118], or solvent extraction [109, 111-116], to obtain tubular structures. Additionally, nanofibers with hollow interior could be prepared by using electrospun nanofibers as sacrificial templates without post-treatment process. For example, Te and Bi_xTe_{1-x} hollow nanofibers were directly synthesized by galvanic displacement reaction of electrospun Ni nanofibers at room temperature [119]. In general, additional coating and etching steps are required in these template methods, and the quality of the resultant tubes is strongly dependent on the control of each step.

Nanofibers with hollow structures were also prepared by single-nozzle electrospinning, followed by appropriate post-treatment. For example, ceramics or metal oxide tubes have been fabricated by calcining the composite fibers, which were produced by electrospinning the mixture solution of polymer and procursors. $LiNiO_2$ [120], CeO_2 [121], Y_2O_3-ZrO_2 [122], $LaMgAl_{11}O_{19}$ [122, 123], ZnO [124], MgO [125], TiO_2 [126], $BaFe_{12}O_{19}$ [127], SiO_2 [128], α-Fe_3O_4 and Co_3O_4 [129], Fe_2O_3 [130], $CoFe_2O_4$ [131], CuO and Cu [132], and SnO_2 [133] tubes have been prepared by this method. Several groups have systematically investigated the preparation process and proposed the formation mechanism of hollow fibers [120, 121, 129, 130, 133]. Cheng et al. [130] proposed that: In the electrospinning process, the evaporation of solvent would result in the formation of a gel layer on the surface of composite nanofibers, which has an important function to keep fiber texture during heat treatment. During heating, the gas produced by the decomposition of polymer would

diffuse through the fiber surface. Once the rate of gas release was larger than gas diffusion through the fiber surface, the pressure inside the fibers increased to be larger than that outside of the composite fibers; consequently, hollow fibers could be obtained. However, Xia and co-workers argued that polymer template and Kirkendall effect played an important role to build hollow fibers [133]. Vacancies generated by the diffusion of metal precursors to the fiber surface and the decomposition of polymers finally formed the hollow structures. Although the exact mechanism is ambiguous and not consistent, a necessary condition for the formation of tubular structures is that a rigid "skin" must form before the complete removal of polymer. In this method, the concentration of precursor, the ratio of precursor to polymer, the calcination temperature and heating rate significantly influence the morphology of the final products. In another single-nozzle electrospinning method, tetraethyl orthosilicate (TEOS) [134], PEO [135], or mineral oil [136] was introduced into the electrospinning solution to induce phase separation, and finally hollow fibers were obtained. Yu et al. prepared Sn nanoparticle encapsulated multichannel carbon microtubes by single-nozzle electrospinning process of tin octoate-PMMA-PAN in DMF emulsion and subsequent calcinations [137]. Because PAN solution is easier to stretch than PMMA/DMF fluid, thus a core-shell jet was formed and the subsequent formation of core-shell fibers. The as-collected electrospun fibers were stabilized in air at 250 ℃, leading to the thermal degradation of the core components to create SnO_2 nanoparticles encapsulated in porous hollow fibers. After carbonization under an Ar/H_2 atmosphere, the fibers were transformed into multichannel hollow porous carbon microtubes and SnO_2 was reduced to Sn nanoparticles.

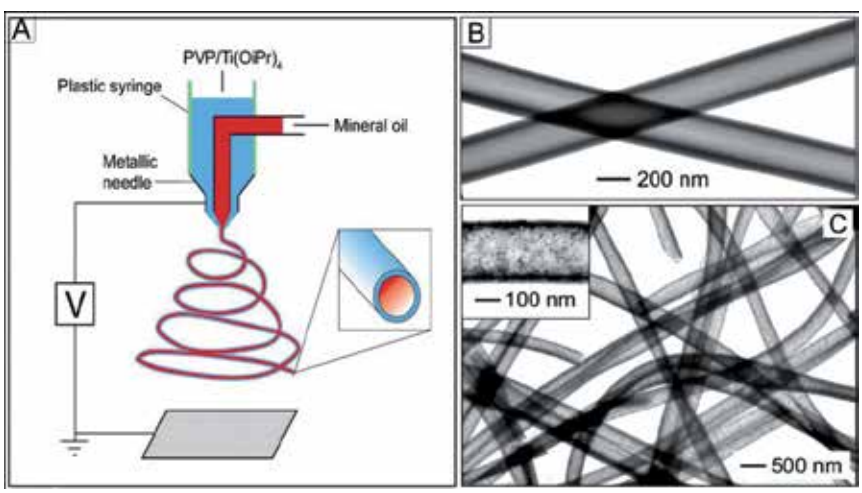

Figure 6. (A) Schematic illustration of the setup for electrospinning nanofibers with a core/sheath structure. The spinneret was fabricated from two coaxial capillaries, through which heavy mineral oil and an ethanol solution containing PVP and $Ti(OiPr)_4$ were simultaneously ejected to form a continuous, coaxial jet. (B) TEM image of two as-spun hollow fibers after the oil cores had been extracted with octane. The walls of these tubes consisted of amorphous TiO_2 and PVP. (C) TEM image of TiO_2 (anatase) hollow fibers that were obtained by calcining the composite nanotubes in air at 500 ℃ [81].

http://dx.doi.org/10.5772/57099

The studies in several groups have demonstrated that electrospinning could be directly utilized to prepare hollow nanofibers. For example, Li and Xia developed a coaxial electrospinning setup to fabricate ceramic hollow fibers by co-electrospinning viscous mineral oil as the core and a mixture ethanol solution of PVP and $Ti(OiPr)_4$ as the shell (Fig. 6A) [81]. The mineral oil was subsequently extracted to form amorphous TiO_2/PVP composite tubes (Fig. 6B). After calcination at elevated temperatures in air, hollow TiO_2 fibers were obtained (Fig. 6C). The wall thickness and inner diameter of the hollow nanofibers could be varied in the range from tens of nanometers to several hundred nanometers by controlling the processing parameters. The same group also demonstrated that functional nanoparticles (iron oxide, SnO_2, Au) or molecular species (dye, octadecyltrichlorosilane) could be directly incorporated into the hollow interiors by pre-dissolving these functional materials into the core liquid [138]. Using a similar setup, Loscertales and co-workers prepared polymer-free SiO_2 and ZrO_2 tubes by co-electrospinning an aged inorganic sol and an immiscible (or poorly miscible) liquid such as olive oil or glycerin, followed by selective removal of the inner liquid [139]. Turbostratic carbon nanotubes with inner diameter of 500 nm and wall thickness of 200 nm could also be obtained via coelectrospinning of PAN and PMMA with subsequent thermal degradation of the PMMA core and finally carbonization of the PAN shell [140]. Besides the ceramics and carbon tubes, polymeric microtubes were also fabricated in a single step by using the co-electrospinning of two polymeric solutions [141]. In this approach, two mechanisms, fast evaporation of the shell solvent and contact with a nonsolvent, were responsible for the formation and stabilization of the microtubes. Using the coaxial electrospinning, hollow fibers with various composition have been prepared, such as zeolite [142], SiO_2 [143, 144], TiO_2 [145], $LiNiO_2$ [146], $LiCoO_2$ [147], $BaTiO_3$ [148], $LiNi_{0.8}Co_{0.1}Mn_{0.1}O_2$-MgO [149], PMMA [150, 151], PC [151], poly(3-hydroxy butyrate) (PHB) [152], Sn@carbon nanoparticles encapsulated carbon [153], and carbon [154].

Except for the spinneret with two coaxial capillaries, tri-axial spinneret was also designed to fabricate hollow nanostructures. For example, Lallave et al. [155] prepared Alcell lignin hollow nanofibers by tri-axial spinneret co-electrospinning Alcell lignin solutions at room temperature without any added polymer. The outmost sheath flow of ethanol was used to avoid solidification of the Taylor cone. After stabilization and carbonization of the as-spun fibers at elevated temperatures, hollow carbon nanofibers were obtained. Zhao and co-workers developed a multifluidic compound-jet electrospinning technique to fabricate bio-mimic hierarchical multichannel microtubes (Fig. 7a) [156]. They used an ethanol solution of $Ti(OiPr)_4$ and PVP as outer liquid and paraffin oil as inner liquid. After a compound fluidic electrospinning process and removing the organics, TiO_2 three-channel tubes were obtained (Fig. 7b, c and d). With the rational design of the spinneret, tubes with two to five channels have been successfully fabricated. Such multichannel structure greatly improved photocatalytic activity of TiO_2 for degrading gaseous acetaldehyde due to a cooperative effect of trapping more gaseous molecules inside the channels and multiple reflection of incident light [157].

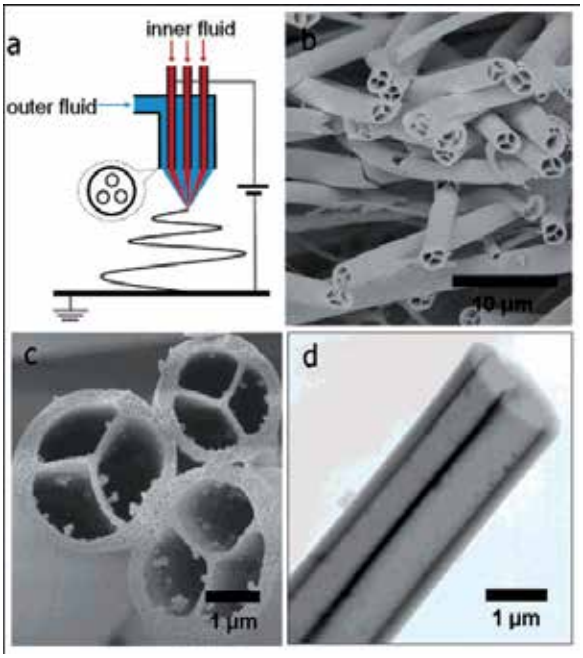

Figure 7. (a) Schematic illustration of the three-channel tube fabrication system. The immiscible inner and outer fluids were paraffin oil (red), and ethanol solution containing Ti(O*i*Pr)$_4$ and PVP (blue). The inset shows the outlet section of the spinneret. (b) Side-view SEM image of sample after the organics have been removed. (c) Magnified SEM image of tubes in which the channels were divided into three independent flabellate parts by a Y-shape inner ridge. (d) TEM image of a three-channel tube; the individual channels of tube are straight and continuous [156].

3.4. Nanofibers with porous structures

Nanofibers with porous structures have excited immense interest because of their ultrahigh surface area, and thus potential applications in filtration, absorption, fuel cell, catalysis, tissue engineering, and sensors. Several methods have been reported for fabricating porous electrospun nanofibers. In one method, phase separation was utilized to induce the formation of porous nanostructures in the electrospinning process. For example, Bognitzki et al. prepared porous polymer fibers of poly(L-lactic acid) (PLLA), PC, and polyvinylcarbazole by using dichloromethane as solvent [158]. For PLLA fibers, the average pore size is in the order of 100 nm in width and 250 nm in length with the long axis being oriented along the fiber axis (Fig. 8). The fast evaporation of solvent gave rise to local phase separation, and the solvent-rich regions transformed into pores during the electrospinning process. Rabolt's group systematically investigated the influence of polymer/solvent properties on the fiber surface morphology [159]. A variety of solvents (tetrahydrofuran (THF), CS_2, toluene, THF/DMF) with different boiling points and vapor pressures were examined to prepare polystyrene (PS) fibers. It was found that a very high density of pores were observed on PS fibers electrospun from THF, while the microtexture and nanopores disappeared as substitution of THF with DMF. This result indicated that the volatility of the solvent significantly influenced the pore formation.

http://dx.doi.org/10.5772/57099

In addition to PS, the polymers including PMMA, PC, and PEO were also investigated. In general, electrospun PMMA fibers from $CHCl_3$ and THF exhibited a nanoporous surface texture. PC fibers electrospun from $CHCl_3$ showed elongated nanopores of about 100-250 nm, while those formed from THF exhibited irregular-shaped micropores with diameters of about 20 μm. However, no nanopores were observed on electrospun PEO fibers under any processing conditions. They also investigated the effect of humidity and molecular weight on the surface morphology of electrospun PS fibers from PS/THF solution [160]. They found that increasing humidity caused an increase in the number, diameter, shape, and distribution of the pores, and increasing the molecular weight of PS resulted in larger, less uniform shaped pores. From these systematic studies, they ascribed the formation of porous surface morphology to the combinative effect of both phase separation and breath figure formation. Dayal and co-workers studied experimentally and theoretically the formation of porous structures from electrospinning of PMMA/CH_2Cl_2 and PS/THF systems [161]. They proposed that the porous fibers were favored to form if the polymer/solvent system was partially miscible showing an upper critical solution temperature (UCST) envelope at the electrospinning temperature, especially if the solvent utilized were volatile and sensitive to moisture absorption. The pore size depends on various factors such as surface energy and the solvent evaporation rates. With the use of phase separation mechanism, ultrafine porous cellulose triacetate (CTA) fibers were also prepared by electrospinning CTA dissolved in CH_2Cl_2 or a mixed solvent of CH_2Cl_2/ethanol [162]. Similarly, PS fibers with micro- and nanoporous structures both in the core and/or on the fiber surfaces were prepared in a single process by varying solvent compositions (THF/DMF) and the concentration of PS solutions [163]. Porous polymer fibers of PLLA [164], PAN [165], and cellulose acetate [166] were also prepared by electrospinning with appropriate binary solvent system. The formation of porous structures was mainly due to the spinodal decomposition phase separation occurred during the electrospinning process.

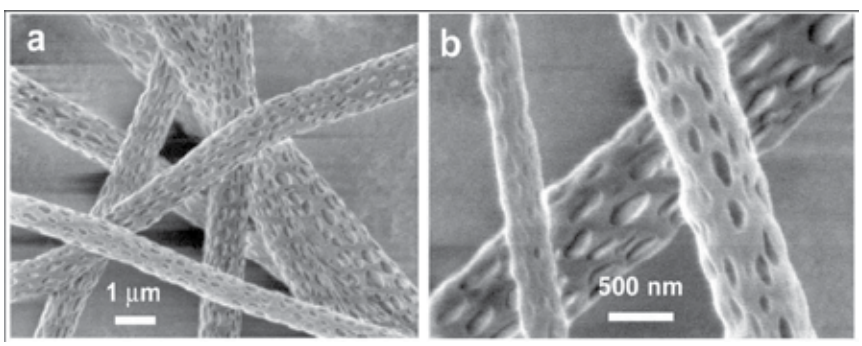

Figure 8. SEM micrographs of porous PLLA fibers obtained via electrospinning of a solution of PLLA in dichloromethane. a) Survey; b) Magnification [158].

In another method, porous nanofibers could be prepared by the selective removal of a component from nanofibers made of a composite or blend material. For example, the structural changes for fibers consisting of a PLA/PVP blend were investigated when one of the two components was selectively removed [167]. It was found that porous nanofibers were obtained

after selective removal of PVP by water extraction or PLA by annealing at elevated temperatures when equal amount of the two polymers were loaded into the electrospinning solution. However, the fibers remained compact without any alteration of the surface structure after removing the minor component when another component was the major one in the composite fibers. This morphological change was believed to result from the rapid phase separation and rapid solidification in the electrospinning process. Porous inorganic nanofibers of TiO_2 [55, 81], SiO_2 [168-170], SnO_2 [171, 172], $NaYF_4$:Yb_3, Er_3@silica [173], and $ZnCo_2O_4$ [174] have been fabricated by electrospinning the blend solutions of polymer and procursors, followed by selective removal of the polymer component. Porous polymer fibers, such as PEI [175], poly(glycolic acid) (PGA) [176], and PAN [177] were also prepared by electrospinning of a blend solution, followed by thermal degradation or solvent extraction of another component. Salts, such as $GaCl_3$ and $NaHCO_3$, were also introduced into the electospinning solution to induce porous structures after the removal of the salts [178, 179].

Xia's group reported a novel method to produce porous nanofibers by modifying the electrospinning setup [180]. In this setup, the collector was immersed in a bath of liquid nitrogen. Porous polymer fibers can be obtained through thermally induced phase separation (TIPS) between the solvent-rich and solvent-poor regions in the fiber during electrospinning, followed by removal of solvent in vacuum. PS fibers with ~1 μm in diameter were obtained by using this method (Fig. 9A). Examination of the end of a broken fiber (inset) indicated that the fiber was porous throughout. It should be noted that the fibers prepared by this method had larger diameters than those prepared without the use of a liquid nitrogen bath. The reason is that the fibers were collected with a smaller distance between the spinneret and the liquid nitrogen (10 cm), which greatly weakened the size reduction caused by whipping and solvent evaporation. This method could be extended to prepare porous fibers from a variety of different polymers, such as PAN, PVDF, and PCL (Fig. 9B). Similarly, Pant et al. developed a water-bath electrospinning setup, and highly porous PCL fibers were prepared by electrospinning from pure PCL, and its blends with methoxy poly(ethylene glycol) (MPEG) [181]. A simultaneous phase separation and dissolution of MPEG from electrospun PCL fibers caused the formation of porous structure during water-bath electrospinning.

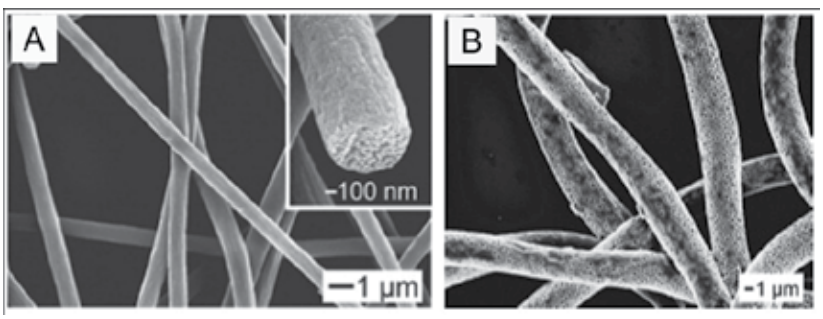

Figure 9. (A) SEM images of PS porous fibers prepared by electrospinning into liquid nitrogen, followed by drying in vacuum. The inset is a SEM micrograph of the broken end of a fiber at a higher magnification, showing that the fiber was porous throughout. (B) PCL fibers obtained by electrospinning into liquid nitrogen followed by drying in vacuum [180].

http://dx.doi.org/10.5772/57099

Porous carbonaceous materials have been widely used in gas storage, separation, purification, or as catalyst carriers, electrode materials for fuel cells, and electrochemical double-layer supercapacitors, because of their unique mechanical properties, heat resistance, chemical inertness, etc. Porous carbon nanofibers could be prepared by the combination of electrospinning and post-spun treatment. For example, PAN-based carbon fibers with porous structures have been fabricated by electrospinning the mixture solutions of PAN and other polymers, followed by removal of the polymer and carbonization of the remaining PAN [177, 182, 183]. Kim et al. prepared porous carbon nanofibers by the electrospinning of PAN solution containing zinc chloride [184]. Zinc chloride trapped in the electrospun PAN nanofibers acted as a dehydrating agent and thus enhanced the oxidation rate, affording a shortened stabilization time. During carbonization process, zinc oxide was formed and acted as the catalyst for creating micropores on the outer surface of carbon nanofibers by etching carbon atoms. Porous structures were also produced on carbon nanofibers during the stabilization and carbonization process by activation using chemical activation regents, such as zinc chloride [185], and KOH [186], or activation using SiO_2 nanoparticles [187-189].

3.5. Nanofibers with other secondary structures

In addition to the structures aforementioned, beaded, necklace-like, and ribbon nanofibers could be prepared by adjusting the processing and solution parameters for electrospinning. The beads formed in the electrospinning process were usually regarded as by-products, and the formation mechanism was studied by several groups [190, 191]. It was found that the viscoelasticity of the solution, charge density carried by the jet, and the surface tension of the solution were the key factors that influence the formation of the beaded fibers. Jin et al. fabricated necklace-like structure via electrospinning aqueous solution of PVA and SiO_2 particles [192]. The results indicated that the diameter of SiO_2 particles, the weight ratio of PVA to SiO_2, the voltage, and the relative content of PVA/SiO_2/H_2O greatly influenced the morphology of electrospun fibers. Especially, the diameter of SiO_2 particles greatly influenced the morphology of produced fibers. For example, SiO_2 particles with diameter of 143 nm tended to aggregate into bunches in the fibers, while 265 and 910 nm SiO_2 particles tended to align along the fibers one by one, resembling necklaces. In addition to round nanofibers, electrospinning a polymer solution can produce thin fibers with a variety of cross-sectional shapes. Koombhongse and co-workers studied a series of polymer solutions, and various shaped fibers were observed, including branched fibers, flat ribbons, ribbons with other shapes, and fibers that were split longitudinally from larger fibers [193]. In the electrospinning process, a thin polymer skin was formed due to the rapid evaporation of the solvent. Following the escape of solvent inside the fibers, tube-like fibers were formed, which collapsed due to atmospheric pressure to create ribbon-like fibers. Branched fibers were formed by the ejection of smaller jets from the surface of the primary jets, while split fibers were obtained by the separation of a primary jet into two smaller jets. They proposed that fluid mechanical effects, electrical charge carried with the jet, and evaporation of the solvent all contributed to the formation of these special shaped fibers.

4. Application of electrospun nanofibers in electrochemical sensors

Electrospun nanofibers are featured with small diameter, extremely long length, high surface area and complex pore structure. As mentioned above, electrospinning has been applied to fabricate nanofibers with various compositions and secondary structures. These electrospun nanofibers readily assemble into three-dimensional membranes, which characterized as high porosity, interconnectivity, and a large surface-to-volume ratio, makes electrospun nanomaterials highly attractive to different applications, including sensors. Several reviews on the application of electrospun nanofibers in constructing sensors with different read-out mode and for different target were published in past several years [7-9, 194, 195]. Among various read-out modes, electrochemical read-out has attracted remarkable attentions in the ultrasensitive detection due to its high sensitivity and selectivity, inexpensive equipment and easy miniaturization. Various electrospun nanofibers, including polymer nanofibers, composite nanofibers, and metal or metal oxide nanofibers, have been used to prepare electrochemical sensors for a wide range of analytes. A summary of electrochemical sensors based on electrospun nanomaterials is illustrated in Table 1.

Materials	Fiber diameter (nm)	Analytes	Detection potential (V)	Linear Rang (μM)	Limit of Detection (μM)	Ref.
PVA	70-250	glucose	0.65	1000-10000	50	[40]
PVA/F108/AuNPs/Lac	~	4-CP 2,4-DCP 2,4,6-TCP	0.0 -0.15 0.1	1-25 1-25 1-25	12.09 2.70 9.33	[196]
nylon-6	95(RSD 27%)	glucose	~	1000-10000	6	[197]
nylon-6	~	glucose	0.70	1000-9000	2.5	[198]
nylon-6	~	glucose	0.50	1000-10000	6	[199]
nylon-6	~	pyrocatechol	-0.2	~100	0.05	[200]
PMMA/PANi-Au_{nano}	400-500	superoxide anion ($O_2^{\cdot -}$)	0.3	~	0.3	[201]
Pt/PANi	~	urea	-0.1	~20000	10	[202]
DNA/SWNT/PEO	50-300	glucose	0.5	~20000		[203]
PANCAA MWNT/PANCAA	~ ~	glucose glucose	0.8 0.8	0-7000 0-7000	557 668	[204]
PVDF/PAPBA	150	glucose	0.04	100-1600		[205]
nylon-6	140±15	cysteine	0.3	100-400	15	[206]
P_2W_{18}/PVA	~500	nitrite	-0.2	100-1500	0.96	[207]
CNF	200-500	NADH	0.45	0.02-11.47	0.02	[208]

Materials	Fiber diameter (nm)	Analytes	Detection potential (V)	Linear Rang (μM)	Limit of Detection (μM)	Ref.
CNF	200-500	DA UA AA	0.376 0.475 0.200	0.04-5.6 0.8-16.8 2-64	0.04 0.2 2	[209]
CNF	200-400	L-tryptophan L-tyrosine L-cysteine	0.9 0.8 0.75	0.1-119 0.2-107 0.15-64	0.1 0.1 0.1	[210]
CNF	200-400	xanthine	0.85	0.03-21.19	0.02	[211]
CNF	400-600	catechol hydroquinone	~ ~	1-200 1-200	0.2 0.4	[212]
CNF	100±25	glucose	0.2	~	~	[213]
Pd/CNF	200-500	H_2O_2 NADH	-0.2 0.5	0.2-20000 0.2-716.6	0.2 0.2	[214]
Pd/CNF	200-500	DA UA AA	0.402 0.550 0.158	0.5-160 2-200 50-4000	0.2 0.7 15	[215]
Pd/CNF	200-500	hydrazine	-0.32	10-4000	2.9	[216]
Pd/CNF	300-500	oxalic acid	1.07	200-13000 13000-45000	200	[217]
Ni/CNF	200-400	glucose	0.6	2 -2500	1	[218]
Ni/CNF	200-400	ethanol	0.55	250-87500	250	[219]
Rh/CNF	300-500	hydrazine	0.4	0.5-175	0.3	[220]
Pt/CNF	200-500	H_2O_2	0.0	1-800	0.6	[221]
ZnO	195-350	glucose	0.8	250-19000	1	[222]
Mn_2O_3-Ag	~	glucose	-0.45	~1100	1.73	[223]
Au	990±490	fructose	0.2	100-3000	11.7	[224]
Co_3O_4	105 ±10	glucose	0.59	~2040	0.97	[225]
CuO	90-240	glucose	0.4	6-2500	0.8	[226]
CuO	~2 μm	glucose	0.4	0.2 -600	0.0022	[227]
NiO	10 μm	glucose	0.5	1-270	0.033	[228]
Pd-CuO	90-140	glucose	0.35	0.2-2500	0.019	[229]
NiO-Ag	82.1± 13.8	glucose	0.1 0.6	~590 ~2630	1.37 0.72	[230]
NiO-Au	width 580 ±44,	glucose	0.2 0.6	~2790 ~4550	0.65 1.32	[231]

Materials	Fiber diameter (nm)	Analytes	Detection potential (V)	Linear Rang (μM)	Limit of Detection (μM)	Ref.
	thickness 60 ±21					
NiO-Pt	214±77	glucose	0.6	~3670	0.313	[232]
CuO-NiO	10 μm	glucose	0.5	3-510	0.001	[233]
NiO-CdO	~	glucose	0.6	~6370	0.35	[234]
Mn_2O_3	105	hydrazine	0.6	~644	0.3	[235]
CuO/Co_3O_4	150-350	fructose	0.3	10-6000	3	[236]
Hb	width ~2.5μm, thickness ~600 nm	nitrite H_2O_2	-0.65 -0.377	~4500 ~27	0.47 0.61	[237]
SWNTs-Hb	width ~2.5μm, thickness ~600 nm	TCA nitrite H_2O_2	-0.65 -0.65 -0.364	12-108 ~207 ~27.3	2.41 0.30 0.22	[238]
TiO_2-Pt	72.61±15.04	hydrazine	0.5	~1030	0.142	[239]
SiO_2@Au	~	H_2O_2	-0.4	5-1000	2	[240]

Table 1. Electrospun nanofibers based electrochemical sensors.

Abbreviations in the table: PVA: poly(vinyl alcohol); F108: PEO-PPO-PEO; Lac: laccase; 4-CP: 4-chlorophenol; 2, 4-DCP: 2, 4-dichlorophenol; 2, 4, 6-TCP: 2, 4, 6-trichlorophenol; PMMA: Poly(methyl methacrylate); PANi: polyaniline; PEO: poly(ethylene oxide); PANCAA: poly(acrylonitrile-co-acrylic acid); SWNT: Single-walled carbon nanotube; MWNT: Multi-walled carbon nanotube; PVDF: poly(vinylidene fluoride); PAPBA: poly(aminophenyl boronic acid); P_2W_{18}: α-$K_6[P_2W_{18}O_{62}]$ $14H_2O$; CNF: carbon nanofiber; Hb: hemoglobin; TCA: trichloro-acetic acid.

4.1. Polymer nanofibers based electrochemical sensors

Since the first enzyme-based electrochemical biosensor was proposed by Clark and Lyons [241], numerous efforts have been afforded in this direction because of the simplicity and high selectivity of enzyme electrodes. The immobilization of enzymes on a suitable matrix and their stability are important factors in the fabrication of biosensors. Several methods have been developed for immobilization of enzymes, including physical adsorption, cross-linking, self-assembly, as well as entrapment in polymers or sol-gels. Due to the merits of high specific surface area and porous structure, electrospun polymer fibers would be a promising biocompatible material for enzyme immobilization [1]. For example, Ren and co-workers prepared a

http://dx.doi.org/10.5772/57099

glucose biosensor by electrospinning a solution of glucose oxidase (GOx) and PVA, and directly collecting the fibers on a electrode [40]. Then GOx was immobilized by cross-linking the electrospun PVA/GOx composite membranes with glutaraldehyde. The immobilized GOx remained active inside the electrospun PVA fibrous membranes after the harsh process of electrospinning. The apparent Michaelis-Menten constant (K_M^{app}) for this biosensor was determined to be 23.66 mM. Liu et al. developed laccase (Lac) biosensor for the determination of phenolic compounds by in situ electrospinning of a mixture of PVA, Lac, PEO-PPO-PEO (F108) and Au nanoparticles, where F108 was used as an enzyme stabilizing additive and Au NPs were used to enhance the conductivity of the biosensor [196]. Under the optimal conditions, the biosensor showed a sensitivity following the order of 2, 4-dichlorophenol (2, 4-DCP) > 2, 4, 6-trichlorophenol (2, 4, 6-TCP) > 4-chlorophenol (4-CP). The obtained K_M^{app} values were 426.06, 9.41 and 73.36 μM for 4-CP, 2, 4-DCP and 2, 4, 6-TCP, respectively. The results indicated that Lac encapsulated into electrospun nanofibers retained its high catalytic activity. The sensing performance of this biosensor was attributed to the suitable electrochemical interface (e.g. biocompatibility, high surface area-to-volume ratio and superior mechanical properties) of PVA/F108/Au NPs/Lac.

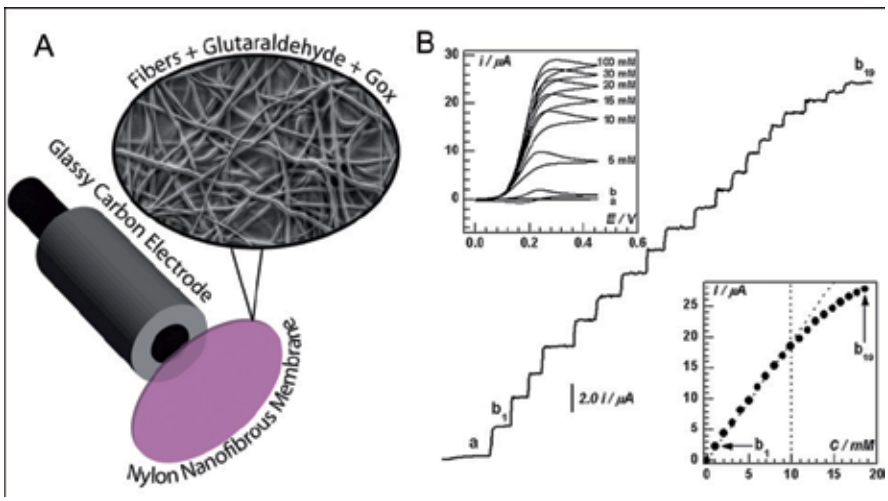

Figure 10. (A) Schematic picture of the nylon nanofibrous biosensing unit coupled with a glassy carbon electrode. Also shown a scanning electron microscopy detail of the nanofibrous structure. (B) Response current of nylon nanofiber-based glucose biosensors after the addition of glucose (1 mM each). Detection potential, + 0.5 V vs. Ag/AgCl. Supporting electrolyte, 0.1 M PBS (pH 6.5) containing 0.1 mM ferrocene methanol. Inset (bottom-right) shows the corresponding calibration plot. Inset (top-left) shows the catalyzed electrochemical oxidation of glucose mediated by ferrocene methanol, where curve a and b are the cyclic voltammograms (CVs) of the blank and of the ferrocene methanol (0.1 mM) in the absence of glucose. Other CVs are obtained upon addition of glucose from 5 to 100 mM. In all the CVs, scan rate=0.02 V s^{-1}; 0.1 M PBS (pH 6.5) [199].

In addition to the direct incorporation of enzyme into polymer nanofibers, post-spun modification is a widely used method for constructing enzyme-based biosensors. Mannino's group developed glucose biosensors by using electrospun nylon-6 nanofibrous membranes (NFM) as the enzyme immobilization matrix [197-199]. A piece of NFM was placed over the electrode

surface and secured with an o-ring (Fig. 10A). The highly porous morphology of the NFM allowed the analytes to diffuse toward the transducer, while the proteins might be retained by physical or chemical bonding with its large available surface. With the presence of mediator (ferrocene methanol) in the detection cell, a linear current response of this biosensor was obtained in the range of 1-10 mM, with detection limit of micromole-level (Fig. 10B). The K_M^{app} value for the immobilized GOx was 17 mM, which was greater than that obtained for homogeneous enzyme catalysis, but was comparable to that of GOx covalently bound to nylon [199]. These results indicated that this NFM provided favorable environment for the immobilization of GOx enzyme. Additionally, the nylon nanofibers membrane was also used to immobilize tyrosinase and construct an amperometric biosensor for the detection of phenolic compounds [200]. This biosensor showed excellent performance in respect to sensitivity, selectivity and reproducibility. Santhosh et al. developed an electrochemical sensor for the detection of superoxide anion ($O_2^{\cdot -}$) based on Au nanoparticles loaded PMMA-polyaniline (PANi) core-shell electrospun nanofiber membrane [201]. This membrane provided high surface area and porous structure for effective immobilization of superoxide dismutase (SOD), as well as offered excellent biocompatible microenvironment for SOD. Direct electron transfer was achieved between SOD and the electrode with an electron transfer rate constant of 8.93 s^{-1}. Jia et al. prepared a urea biosensor based on Pt nanoflower/PANi nanofibers [202]. PANi nanofibers were prepared by in situ polymerization of aniline on an electrospun PAN nanofiber template in an acidic solution with ammonium persulfate as the oxidant. Pt nanoflowers were further electrodeposited onto the PANi nanofibers backbone by cyclic voltammetry. Then, urease was physically adsorbed on the Pt/PANi modified electrode, followed with Nafion entrapment. This biosensor was applied for the sensitive urea detection in a flow injection analysis (FIA) system.

Carbon nanotubes (CNTs) have become the subject of intense investigation due to their remarkable electrical, chemical, mechanical and structural properties. Recent studies have demonstrated that CNT could greatly promote the electron-transfer reaction of proteins [242]. Therefore, CNT-filled electrospun nanofibers as matrix for the immobilization of enzyme are expected to further improve the analytical performance of enzyme electrode. Liu et al. prepared CNT-filled composite nanofibers by electrospinning DNA/SWNT/PEO blended suspension [203]. The noncovalent binding of DNA to the sidewalls of SWNTs was used to highly disperse SWNTs in the solution. The DNA/SWNT/PEO composite nanofibers were deposited on Pt-coated glass slides, and then directly used as substrate electrode for immobilization of GOx. This biosensor displayed the direct electrochemistry of GOx, suggesting that GOx immobilized on the nanofibers still maintained its electrochemical properties and the composite nanofibers promoted the electron transfer between the electrode and the redox center of enzyme. Nanofibrous membranes filled with multiwalled carbon nanotube (MWNT) were also electrospun from the mixture of poly(acrylonitrile-co-acrylic acid) (PANCAA) and MWNTs [204]. These nanofibrous membranes were directly deposited on Pt electrodes for the fabrication of glucose biosensors. Glucose oxidase (GOx) was covalently immobilized on the membranes through the activation of carboxyl groups on the PANCAA nanofiber surface. Compared with PANCAA nanofiber membrane, MWNT-filled PANCAA nanofiber membrane enhanced the maximum current response, while the electrode response time was

http://dx.doi.org/10.5772/57099

delayed. The MWNT filling also increased the K_M^{app} value, indicating that the secondary structure of immobilized GOx was disturbed.

Although good selectivity and high sensitivity were obtained with these enzyme-based biosensors, inevitable drawbacks such as the chemical and thermal instabilities originated from the intrinsic nature of enzymes as well as the tedious fabrication procedures might limit their analytical applications. Therefore, it is desirable to develop sensitive and selective non-enzymatic sensors. Manesh et al. prepared a non-enzymatic glucose sensor based on the composite electrospun nanofibrous membrane of PVDF and poly(aminophenyl boronic acid) (PAPBA), which was collected on indium tin oxide (ITO) glass plate [205]. The smaller size of PVDF/PAPBA nanofibers provided a large number of active sites for sensing action and the boronic acid groups in PAPBA were the sources for the preferential selectivity and sensing of glucose. The sensor retained 90% of the original activity after 50 days repeated usage and storage at 4 ℃, indicating an excellent long-term stability.

Scampicchio et al. studied the protective properties of nylon-6 nanofiber membrane against fouling and passivation of the carbon working electrode [243]. For example, the polyphenols oxidation usually results in the severe passivation of carbon electrode due to the adsorption of analytes or reaction intermediates. However, no voltammetric waves appeared at the nylon-6 nanofiber membrane coated electrode for the flavonoids (quercetin, myricetin and cathechin) oxidation. On the contrary, when phenol acids (caffeic, synapic, syringic, vanillic and gallic acid) were used, their typical oxidation waves emerged. Therefore, nylon-6 nanofiber membrane could be used as a selective barrier to preserve the active surface of the electrode from passivation of flavonoids and to construct sensors with high selectivity. Furthermore, this protective nylon-6 nanofiber membrane was used to adsorb MWNTs and construct a sensor for the electrochemical detection of sulfhydryl compounds [206]. The membrane was easily peeled off, leaving the bare electrode surface back to its original electrochemical behaviour. Preliminary experiments indicated that the membrane coating protected the bare electrode from the passivation occurred during oxidation of cysteine. Cao and co-workers prepared a nitrite sensor based on polyoxometalate hybrid nanofibers, which was fabricated by electrospinning of a mixture of PVA and α-$K_6[P_2W_{18}O_{62}]$ $14H_2O$ (P_2W_{18}) onto the surface of an ITO electrode [207]. After thermal crosslinking at 135 ℃ for 24 hours, the P_2W_{18} hybrid nanofibers were insoluble in aqueous solutions even after a period of 24 hours, which ensured the electrochemical stability of the hybrid nanofiber-modified ITO electrode. This P_2W_{18} hybrid nanofiber modified electrode presented excellent electrocatalytic activity toward the reduction of nitrite, which could be attributed to the large electroactive surface area of the P_2W_{18} hybrid nanofibers.

4.2. Carbon nanofiber based electrochemical sensors

Carbon nanofibers (CNFs), a unique 1D carbon nanomaterial, have attracted great interests due to their high mechanical strength and excellent electric properties similar to carbon nanotubes (CNTs), but larger surface-active groups-to-volume ratio than that of the glassy-like surface of CNTs [244]. CNFs can be used as immobilization matrixes for biomolecules, while at the same time they can relay the electrochemical signal acting as transducers.

Therefore, a great number of CNF-based sensors or biosensors have been developed [245]. In combination with the carbonization process, electrospinning has been actively exploited as a valuable and versatile method for preparation of CNFs with the controllable structure and texture [62]. As a result, electrospun CNFs or their composite materials are expected to be a promising material for constructing ultrasensitive electrochemical sensors.

Our group has successfully prepared CNFs by electrospinning, followed by stabilization and carbonization processes. These electrospun CNFs were directly used to modify carbon paste electrode (CNF-CPE) and construct a sensor for mediatorless detection of NADH (Fig. 11) [208]. This electrochemical sensor showed low detection limit down to nM-level, wide linear range and good selectivity for determination of NADH in the presence of ascorbic acid (AA). CNF-CPE was also employed for the simultaneous determination of AA, dopamine (DA), and uric acid (UA) by using differential pulse voltammetry (DPV) method [209]. Three well-defined peaks with remarkably increased peak current could be achieved at the CNF-CPE. Low detection limits of 0.04 μM, 2 μM and 0.2 μM for DA, AA and UA were obtained. Some oxidizable amino acids such as L-tryptophane, L-tyrosine and L-cysteine play important roles in many biochemical processes. However, the determination of these amine acids usually suffers from high overpotential and poor reproducibility. We found that the electrospun CNF modified electrode displayed high electrocatalytic activity toward the oxidation of these amino acids with enhanced peak currents and low overpotentials [210]. This sensor showed excellent analytical performance for the detection of the three amino acids. In addition, electrospun CNF modified electrode was also used for non-enzymatic electrochemical detection of xanthine [211], and simultaneous determination of dihydroxybenzene isomers (catechol and hydroquinone) [212]. These sensors exhibited high sensitivity, stability and selectivity, as well as good anti-fouling properties. The practical application of these sensors for determining the target analytes was evaluated, and satisfactory results were obtained. Recently, we fabricated a novel composite electrode by mixing the electrospun CNF with the ionic liquid 1-butyl-4-methyl-pyridinium hexaflurophosphate (PFP) [246]. This CNF/PFP electrode exhibited strong current response and low background noise at the studied composite ratio. When used as electrochemical sensor, it showed high sensitivity and good selectivity for simultaneous detection of DA, AA and UA, guanine and adenine, as well as high signal-to-noise ratio (S/N) and good stability for amperometric detection of NADH under physiological conditions.

Recently, Lee's group prepared porous carbon nanomaterials by electrospinning, thermal treatment and activation process, and then constructed GOx-based glucose biosensors [213, 247, 248]. Silica nanoparticles with average size of 16±2 nm were used as physical activation agent. It was found that micro- and mesopores were induced through the physical activation process, which increased the specific surface area by over 42-fold compared to the untreated materials [247]. These carbon nanomaterials were also treated by oxyfluorination at 1 bar for 5 min using a mixed gas of oxygen and fluorine to introduce hydrophilic functional groups. After the activation and oxyfluorination treatment, the GOx immobilization was maximized by enlarged sites of carbon electrode and improved interfacial affinity between the carbon surface and the GOx. Subsequently, high sensitivity was obtained for this glucose sensor. They also investigated the influence of carbonization temperature on the carbon structure, and

http://dx.doi.org/10.5772/57099

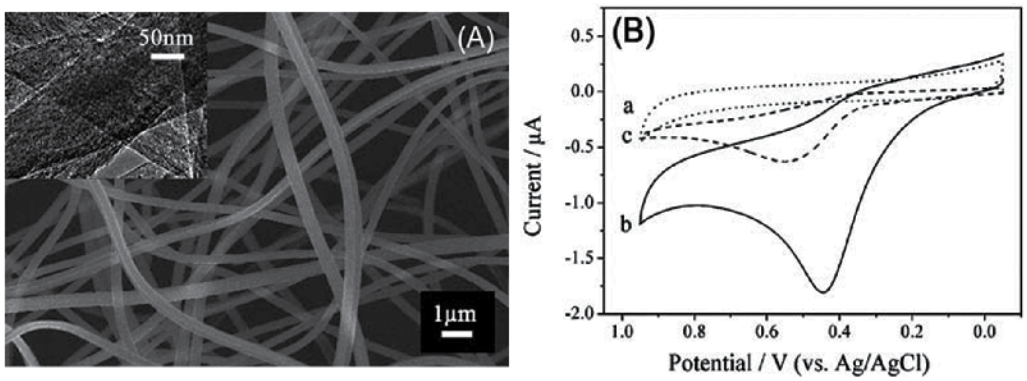

Figure 11. (A) SEM image of electrospun CNFs. Inset shows TEM image of CNFs. (B) CVs of 0.1 M PBS (pH 7.0) a) plain and b) containing 1 mM NADH at the CNF-CPE; c) Corresponding CV of (b) with the CPE. Scan rate: 50 mV s^{-1} [208].

subsequent analytical performance [213]. Raman spectra indicated the crystallization and orientation of the carbon fibers was improved with the increase of carbonization temperature. The electrical conductivity was also improved after heat treatment at higher temperature. The sample treated at 2473 K showed the highest sensitivity for glucose detection among the tested samples, which was ascribed to the high porosity, crystallization and orientation of the carbon structure. Additionally, CNTs were used as an electrically conductive additive to prepare CNT-embedded carbon fibers [248]. Combined with physical activation and oxyfluorination treatment, the prepared glucose sensor showed improved sensitivity and rapid response time as a result of more efficient GOx immobilization and electron transfer.

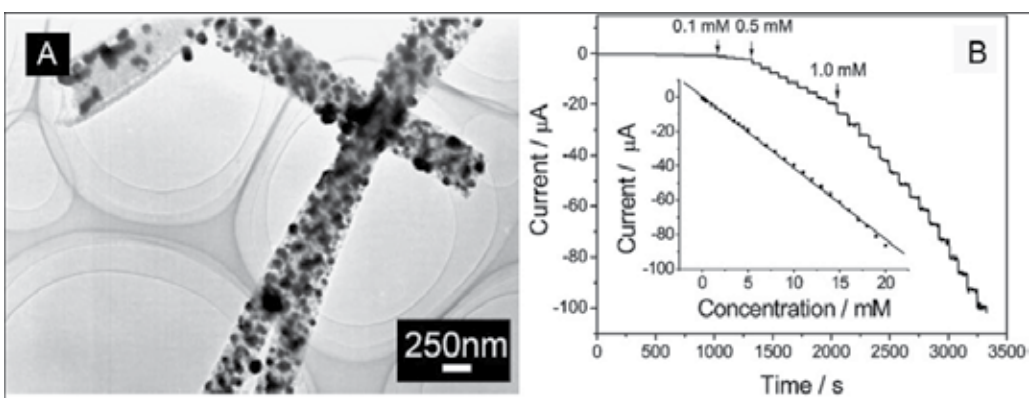

Figure 12. (A) Typical TEM image of Pd/CNF nanocomposites; (B) Current-time responses of the Pd/CNF-CPE on successive injection of specific concentration of H_2O_2 into N_2-saturated PBS (0.1 M, pH 7.0), inset shows the calibration curve for H_2O_2 concentration between 0.2 μM and 20 mM [214].

Metal nanoparticle/CNF nanocomposites have received great attention in catalysis, fuel cell, and chemical/biological sensing applications. In conventional synthesis method, CNFs usually suffer from harsh oxidation or modification with polymers in order to realize

selective deposition of metal nanoparticles on the surface of CNFs. These surface functionalization approaches provide efficient avenues for the deposition of metal nanoparticles, but tend to degrade the mechanical and electronic properties of CNFs because of the introduction of a large number of defects or polymer shell. Electrospinning provided a simple and efficient method to prepare metal nanoparticle/CNF nanocomposites with high quality and purity. Recently, palladium nanoparticle-loaded carbon nanofibers (Pd/CNFs) were synthesized by the combination of electrospinning, reduction and carbonization processes [214]. The metallic Pd nanoparticles were well-dispersed on the surface or completely embedded into CNFs (Fig. 12A), which rendered the Pd nanopatticles high stability and resistance to the aggregation and desquamation. Pd/CNF-modified electrode exhibited high electrocatalytic activities towards the reduction of H_2O_2 and the oxidation of NADH. For H_2O_2, the Pd/CNF-modified electrode displayed a wider linear range from 0.2 μM to 20 mM with a detection limit of 0.2 μM at -0.2 V (Fig. 12B), and the detection was free of interference from the coexisted AA and UA. In the case of NADH, the linear range at the Pd/CNF-modified electrode was from 0.2 μM to 716.6 μM with a detection limit of 0.2 μM at 0.5 V. The high sensitivity, wide linear range, good reproducibility, and the minimal surface fouling make this Pd/CNF-modified electrode a promising candidate for amperometric H_2O_2 or NADH sensor. Pd/CNFs modified electrode also displayed excellent electrocatalytic activities towards DA, UA and AA [215]. The oxidation overpotentials of DA, UA and AA were decreased significantly compared with those obtained at the bare electrode. Due to the different extent of the peak potential shift, these three compounds could be determined simultaneously by CV or DPV at the Pd/CNF modified electrode. The Pd/CNF composite materials were also applied for the detection of hydrazine and oxalic acid with attractive analytical performances [216, 217]. Nickel nanoparticle-loaded carbon nanofibers (NiCF) were also fabricated by using the similar method to that of Pd/CNF [218]. NiCF paste (NiCFP) electrode exhibited excellent electrocatalytic performance for the oxidation of glucose. The amperometric responses of the NiCFP electrode to glucose showed a linear range from 2 μM to 2.5 mM with the detection limit of 1 μM at the applied potential of 0.6 V. The proposed electrode, featured with good resistance to surface fouling and high operational stability, could be used as a promising nonenzymatic glucose sensor. The NiCFP electrode also showed high electrocatalytic activity toward the ethanol oxidation, and was used as enzyme-free ethanol sensor [219]. The detection exhibited high response, good stability and acceptable reproducibility. Similarly, Hu et al. prepared rhodium nanoparticle-loaded carbon nanofibers by electrospinning [220]. Rh nanoparticles with the diameter of 30-70 nm were uniformly distributed on the CNF surface. This nanocomposite was used for determination of hydrazine with high sensitivity and selectivity. Very recently, a Pt nanoparticle-loaded electrospun carbon nanofiber electrode was prepared by a simple wet-chemical method [221]. CNF paste electrode was firstly prepared using electrospun CNFs, then it was immersed into H_2PtCl_6 solution to adsorb $[PtCl_6]^{2-}$. After that, HCOOH was added to reduce the metal precursors. Large amounts of Pt nanoparticles could be well deposited on the surface of the electrospun CNF electrode without using any stabilizer or pretreatment procedure. In application to electrochemical

sensing platform, the Pt/CNF electrode exhibited high sensitivity and good selectivity for amperometric detection of H_2O_2.

4.3. Metal/metal oxide nanofiber based electrochemical sensors

Electrospinning has been proved to be a simple method for large-scale producing metal or metal oxide nanofibers. One of the most important applications of these nanomaterials is to develop their potential in chemical sensing or biosensing, profiting from their small size, large surface-to-volume ratios and high aspect ratios. Reliable and fast determination of glucose is of considerable importance in biotechnology, clinical diagnostics and food industry. Up to now, numerous electrospun metal/metal oxide nanofiber based glucose sensors or biosensors have been reported. For example, Ahmad and co-workers prepared an amperometric glucose biosensor based on a single ZnO nanofiber which was produced by electrospinning of PVP/zinc acetate mixture solution and subsequent high-temperature calcination [222]. A single ZnO nanofiber was transferred on Au electrode and functionalized with GOx via physical adsorption. The K_M^{app} value was estimated to be 2.19 mM, indicated that the immobilized GOx possessed a high enzymatic activity. Huang et al. fabricated highly porous Mn_2O_3-Ag nanofibers by a two-step procedure (electrospinning and calcinations) [223]. The as-prepared Mn_2O_3-Ag nanofibers were employed as the immobilization matrix for GOx to construct oxygen-reduction based glucose biosensor. The Mn_2O_3-Ag nanofibers could effectively mediated the direct electron transfer between the electroactive center of GOx and the electrode. This biosensor displayed good analytical performance for glucose detection due to the merits of this porous nanofiber, such as high surface area for enzyme loading, and high electrocatalytic activity toward the reduction of oxygen. Recently, electrospun Au nanofiber based biosensor for the detection of fructose and glucose was also developed by Russell's group [224]. The gold fibers were prepared by electroless deposition of gold nanoparticles on an electrospun PAN-$HAuCl_4$ fiber. Fructose dehydrogenase was covalently coupled to the Au fiber surface through glutaraldehyde crosslink to a cystamine monolayer. The enzyme exhibited mediated electron transfer directly to the gold electrode, and catalytic currents characteristic of fructose oxidation in the presence of a ferrocene methanol mediator were observed. This fructose sensor could also be used to determine glucose by using glucose isomerase to convert glucose to fructose.

Compared with the enzyme-based glucose biosensors, nonenzymatic glucose sensors are preferential because they avoid the problem of enzyme denature and intricate enzyme immobilization process. The nonenzymatic electrochemical glucose sensors significantly depend on the properties of electrode materials, on which glucose is oxidized directly. Various electrospun metal oxide nanofibers have been used to construct nonenzymatic glucose sensors. For example, Ding et al. fabricated Co_3O_4 nanofibers by electrospinning and subsequent calcination [225]. The as-prepared Co_3O_4 nanofibers were applied to construct a non-enzymatic sensor for glucose detection in alkaline solution. The catalytic property of the as-prepared Co_3O_4 nanofibers towards glucose oxidation was related to CoOOH and CoO_2. The negatively charged Co_3O_4 nanofibers surface could strongly repel

the negatively charged UA and AA molecules, thus resulting in good selectivity. Other metal oxide nanofibers, such as CuO [226, 227], and NiO [228] were also prepared by using the similar method and used for nonenzymatic detection of glucose. The direct glucose detection on these metal oxide nanofiber modified electrodes usually carried out in alkaline electrolyte and mediated by $Ni(OH)_2$/NiO(OH) or $Cu(OH)_2$/CuO(OH) redox couples. The study also demonstrated that the content of metal precursor in the electrospinning solution and the calcination temperature greatly influenced the morphology and catalytic activity of the produced nanomaterials [227, 228]. In contrast to the monometallic nanomaterials, bimetallic ones usually show enhanced electrocatalytic activity due to the synergistic effect. Wang et al. initially prepared electrospun palladium (IV)-doped CuO composite nanofiber based non-enzymatic glucose sensors [229]. The as-prepared nanofibers had a rough surface and consisted of the agglomeration of oxide nanoparticles with average size of about 40 nm. This sensor exhibited high sensitivity for the determination of glucose with the detection limit of 19 nM. Following a facile two-step synthesis route of electrospinning and calcination, Ding and co-workers prepared NiO-Ag hybrid nanofibers, NiO nanofibers, and porous Ag [230]. The NiO-Ag hybrid nanofibers consisted of homogeneous distribution of NiO and irregular distribution of Ag nanoclusters. The as-prepared samples were then applied to construct non-enzymatic sensors for glucose detection. The NiO-Ag hybrid nanofiber modified electrode showed 55-fold higher sensitivity than that obtained on the porous Ag modified electrode at 0.1 V, and 5.2-fold higher sensitivity, lower detection limit and wider linear range than that of the NiO nanofiber modified electrode at 0.6 V (Fig. 13). The significant improvement obtained with NiO-Ag nanofiber were attributed to the use of abundant nanofibers which could provide numerous electron transfer tunnels, the highly porous structure which minimized the diffusion resistance of analytes, and the synergetic effect between NiO and Ag. This method have also been extended to prepare NiO-Au [231], and NiO-Pt [232] bimetallic nanofibers. The as-prepared hybrid nanofibers were employed for the nonenzymatic glucose detection in alkaline electrolyte and showed improved analytical performance compared to the monometallic counterparts. Binary metal oxide nanofibers, including CuO-NiO [233], and NiO-CdO [234] have also exploited as the candidates for developing nonenzymatic glucose sensors. These binary metal oxide nanofibers showed good analytical properties for glucose detection due to the large amounts of reactive sites on the electrode surface and improved conductivity of NiO nanofibers by the incorporation of secondary metal oxide.

In addition to the predominant glucose sensors, the applications of electrospun metal/metal oxide nanofibers in the preparation of sensors for other important analytes were also investigated. For example, Ding et al. constructed an amperometric sensor for hydrazine detection by using electrospun Mn_2O_3 nanofibers [235]. Wang and co-workers exploited electrospun CuO-Co_3O_4 nanofibers as active electrode materials for direct enzyme-free fructose detection [236]. These works demonstrated that electrospun metal/metal oxide nanometerial is one of the promising catalytic electrode materials for constructing ultrasensitive electrochemical sensors.

http://dx.doi.org/10.5772/57099

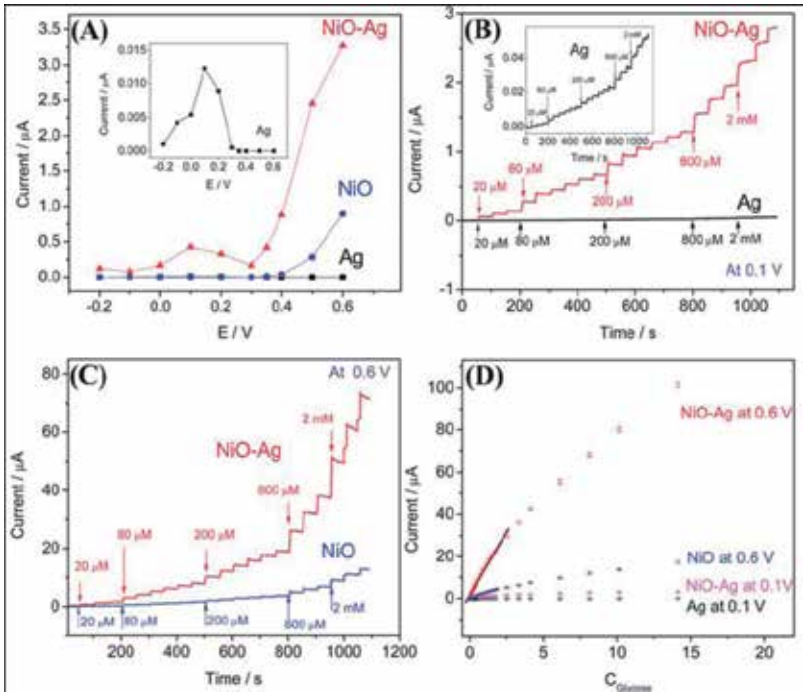

Figure 13. (A) Hydrodynamic voltammograms of 200 μM glucose at the porous Ag/GCE, NiO NFs/GCE and NiO-Ag NFs/GCE; (B) Amperometric response of porous Ag/GCE and NiO-Ag NFs/GCE to successive additions of glucose at an applied potential of 0.1 V; (C) Amperometric response of porous NiO NFs/GCE and NiO-Ag NFs/GCE to successive additions of glucose at an applied potential of 0.6 V; (D) the corresponding calibration curves [230].

4.4. Other electrospun nanofibers based electrochemical sensors

Ding et al. developed an amperometric biosensor by directly electrospinning deposition of hemoglobin (Hb) microbelts on the surface of glassy carbon electrode (Fig. 14A) [237]. This porous Hb microbelt coating closely contacted to the electrode surface and showed enhanced direct electrochemistry of Hb (Fig. 14B). The Hb microbelts based amperometric biosensor showed a fast response to the analytes and low detection limits of 0.61 μM for H_2O_2 and 0.47 μM for nitrite. The K_M^{app} value of 0.093 mM was obtained for the electrocatalytic reduction of H_2O_2, reflecting the high affinity of Hb to the substrate H_2O_2. SWNT-Hb composite microbelts were also fabricated by the same group and employed as active material to prepare mediator-free biosensors [238]. The direct electrochemistry of Hb at SWNT-Hb/GCE was more prominent than that obtained at the Hb microbelt/GCE because of the enhanced electron transfer by incorporated/embedded SWNTs and the porous 3D structure of Hb microbelt coating. Sensitive amperometric detection of trichloroacetic acid (TCA), nitrite, and H_2O_2 was obtained with the detection limits of 2.41 μM, 0.30 μM and 0.22 μM, respectively. TiO_2-Pt nanofibers were fabricated by electrospinning PVP/ethanol solution containing platinum acetate and $Ti(OiPr)_4$, followed by calcination in air at 500 °C for 3 h [239]. The as-prepared TiO_2-Pt hybrid nanofibers were used as the electrochemical catalyst for hydrazine detection. Au-coated SiO_2

core-shell nanofibers were prepared by the seed-mediated growth Au shell on electrospun SiO_2 nanofibers [240]. Then horseradish peroxidase (HRP) was immobilized on the SiO_2@Au nanofibers modified electrode via physical adsorption to construct an amperometric H_2O_2 biosensor. This biosensor exhibited high biological affinity to H_2O_2 and the HRP enzyme on the gold shell kept its activity with a low-diffusion barrier.

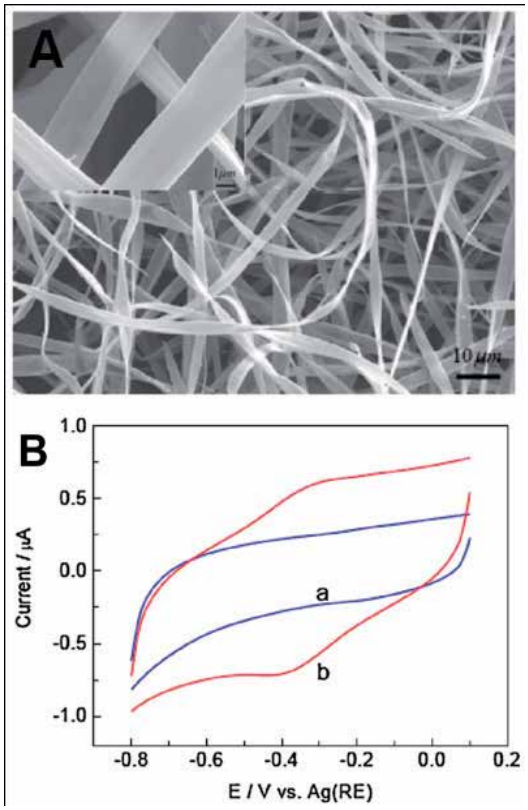

Figure 14. (A) Typical SEM images of Hb microbelts at low (scale bar=10 μm) and high (inset, scale bar=1 μm) magnification; (B) CVs of the bare GC electrode (a) and Hb microbelts modified GC electrode (b) in 0.1 M pH 7.0 phosphate buffer solution. Scan rate, 100 mV s^{-1} [237].

5. Conclusions and remarks

In past few years, numerous studies have demonstrated that elctrospinning is a simple and versatile method for fabricating nanofibers of organic or inorganic materials. Various functional components, such as nanoparticles, CNTs, proteins, DNA and so on, have been incorporated into the electrospun nanofibers. These composite nanofibers exhibited excellent properties and extended the applications of electrospun nanomaterials. With the profound understanding the electrospinning process and the development of setup for electrospinning,

http://dx.doi.org/10.5772/57099

nanofibers with core/sheath, hollow and porous structures have been directly generated by electrospinning or prepared through the combination of electrospinning with some post-spun treatments. Due to the small size, high surface area, and high porosity, electrospun nanomaterials have been witnessed as a promising candidate for a wide range of applications. One of the important applications is the construction of electrochemical sensors or biosensors, where electrospun nanomaterials acted as matrix for the immobilization of enzyme or as the active electrocatalysts. Electrospun nanofiber-based electrochemical sensors or biosensors have exhibited excellent analytical performances for a number of analytes.

In spite of the significant progress in the area of electrospinning, several challenges have to be resolved before large-scale fabrication and extensive applications of electrospun nanomaterials. Most important is that more experimental studies and theoretical modeling are required in order to achieve a better control over the size and morphology of electrospun fibers. To date, it is still not easy to generate uniform nanofibers with diameters below 100 nm, in particular, on the scale of 10-30 nm. Additionally, it is still necessary to systematically investigate the correlation between the processing/solution parameters and the secondary structures of produced nanofibers. Frankly speaking, the application of electrospun nanomaterials in electrochemical sensors is still in its infancy stage, where the applied materials and analytical targets are limited. The majority of polymers have poor conductivity, which limited their direct applications in electrochemical sensors. In this case, it is desirable to develop conductive polymer nanofibers based electrochemical sensors. However, it is still rarely reported in the literatures. Electrospun carbon nanofiber is another good alternative, but the limited catalytic activity and larger diameters confined their analytical performances. Metal nanoparticle loaded carbon nanofibers showed great promise in the preparation of ultrasensitive electrochemical sensors, while the diameter of nanoparticles is difficult to control by using the current one-step method. For the analytical targets, it is still focused on the small molecules at the present research, predominated by glucose. Therefore, there is a large scope to extend the analytes to other significant molecules, particularly the biomolecules such as DNA, proteins, and cells.

There is no doubt that electrospinning has become one of the most powerful techniques for fabricating 1D nanomaterials with broad range of functionalities. Electrospun nanofibers have emerged as a kind of great promising material for constructing ultrasensitive electrochemical sensors or biosensors. We can believe that with the extensive interdisciplinary research more and more electrspun nanofiber-based electrochemical sensors or biosensors with excellent properties will emerge in the near future and will be practically applied in environmental monitoring, food analysis and clinical diagnostics.

Acknowledgements

This work was financially supported by the National Nature Science Foundation of China (NO. 21155002, 21105098, 21222505).

Author details

Jianshe Huang and Tianyan You*

*Address all correspondence to: youty@ciac.jl.cn

State Key Laboratory of Electroanalytical Chemistry, Changchun Institute of Applied Chemistry, Chinese Academy of Sciences, Changchun, PRC

References

[1] Greiner A, Wendorff JH. Electrospinning: A fascinating method for the preparation of ultrathin fibres. Angewandte Chemie-International Edition 2007; 46(30) 5670-5703.

[2] Li D, Xia YN. Electrospinning of nanofibers: Reinventing the wheel? Advanced Materials 2004; 16(14) 1151-1170.

[3] Liang D, Hsiao BS, Chu B. Functional electrospun nanofibrous scaffolds for biomedical applications. Advanced Drug Delivery Reviews 2007; 59(14) 1392-1412.

[4] Yoo HS, Kim TG, Park TG. Surface-functionalized electrospun nanofibers for tissue engineering and drug delivery. Advanced Drug Delivery Reviews 2009; 61(12) 1033-1042.

[5] Thavasi V, Singh G, Ramakrishna S. Electrospun nanofibers in energy and environmental applications. Energy & Environmental Science 2008; 1(2) 205-221.

[6] Cavaliere S, Subianto S, Savych I, Jones DJ, Roziere J. Electrospinning: designed architectures for energy conversion and storage devices. Energy & Environmental Science 2011; 4(12) 4761-4785.

[7] Ding B, Wang M, Wang X, Yu J, Sun G. Electrospun nanomaterials for ultrasensitive sensors. Materials Today 2010; 13(11) 16-27.

[8] Kim I-D, Rothschild A. Nanostructured metal oxide gas sensors prepared by electrospinning. Polymers for Advanced Technologies 2011; 22(3) 318-325.

[9] Ding B, Wang M, Yu J, Sun G. Gas sensors based on electrospun nanofibers. Sensors 2009; 9(3) 1609-1624.

[10] Huang ZM, Zhang YZ, Kotaki M, Ramakrishna S. A review on polymer nanofibers by electrospinning and their applications in nanocomposites. Composites Science and Technology 2003; 63(15) 2223-2253.

[11] Sill TJ, von Recum HA. Electrospinning: Applications in drug delivery and tissue engineering. Biomaterials 2008; 29(13) 1989-2006.

[12] Kim GM, Wutzler A, Radusch HJ, Michler GH, Simon P, Sperling RA, Parak WJ. One-dimensional arrangement of gold nanoparticles by electrospinning. Chemistry of Materials 2005; 17(20) 4949-4957.

[13] Huang C, Soenen SJ, Rejman J, Trekker J, Chengxun L, Lagae L, Ceelen W, Wilhelm C, Demeester J, De Smedt SC. Magnetic electrospun fibers for cancer therapy. Advanced Functional Materials 2012; 22(12) 2479-2486.

[14] Friedemann K, Corrales T, Kappl M, Landfester K, Crespy D. Facile and large-scale fabrication of anisometric particles from fibers synthesized by colloid-electrospinning. Small 2012; 8(1) 144-153.

[15] Li M, Zhang J, Zhang H, Liu Y, Wang C, Xu X, Tang Y, Yang B. Electrospinning: A facile method to disperse fluorescent quantum dots in nanofibers without Forster resonance energy transfer. Advanced Functional Materials 2007; 17(17) 3650-3656.

[16] Zhang C-L, Lv K-P, Cong H-P, Yu S-H. Controlled assemblies of gold nanorods in PVA nanofiber matrix as flexible free-standing SERS substrates by electrospinning. Small 2012; 8(5) 648-653.

[17] Jin W-J, Lee HK, Jeong EH, Park WH, Youk JH. Preparation of polymer nanofibers containing silver nanoparticles by using poly(N-vinylpyrrolidone). Macromolecular Rapid Communications 2005; 26(24) 1903-1907.

[18] Shi Q, Vitchuli N, Nowak J, Noar J, Caldwell JM, Breidt F, Bourham M, McCord M, Zhang X. One-step synthesis of silver nanoparticle-filled nylon 6 nanofibers and their antibacterial properties. Journal of Materials Chemistry 2011; 21(28) 10330-10335.

[19] Demir MM, Gulgun MA, Menceloglu YZ, Erman B, Abramchuk SS, Makhaeva EE, Khokhlov AR, Matveeva VG, Sulman MG. Palladium nanoparticles by electrospinning from poly(acrylonitrile-co-acrylic acid)-$PdCl_2$ solutions. Relations between preparation conditions, particle size, and catalytic activity. Macromolecules 2004; 37(5) 1787-1792.

[20] Li ZY, Huang HM, Shang TC, Yang F, Zheng W, Wang C, Manohar SK. Facile synthesis of single-crystal and controllable sized silver nanoparticles on the surfaces of polyacrylonitrile nanofibres. Nanotechnology 2006; 17(3) 917-920.

[21] Ko F, Gogotsi Y, Ali A, Naguib N, Ye HH, Yang GL, Li C, Willis P. Electrospinning of continuons carbon nanotube-filled nanofiber yarns. Advanced Materials 2003; 15(14) 1161-1165.

[22] Sen R, Zhao B, Perea D, Itkis ME, Hu H, Love J, Bekyarova E, Haddon RC. Preparation of single-walled carbon nanotube reinforced polystyrene and polyurethane nanofibers and membranes by electrospinning. Nano Letters 2004; 4(3) 459-464.

[23] Hou HQ, Ge JJ, Zeng J, Li Q, Reneker DH, Greiner A, Cheng SZD. Electrospun polyacrylonitrile nanofibers containing a high concentration of well-aligned multiwall carbon nanotubes. Chemistry of Materials 2005; 17(5) 967-973.

[24] Ra EJ, An KH, Kim KK, Jeong SY, Lee YH. Anisotropic electrical conductivity of MWCNT/PAN nanofiber paper. Chemical Physics Letters 2005; 413(1-3) 188-193.

[25] McCullen SD, Stevens DR, Roberts WA, Ojha SS, Clarke LI, Gorga RE. Morphological, electrical, and mechanical characterization of electrospun nanofiber mats containing multiwalled carbon nanotubes. Macromolecules 2007; 40(4) 997-1003.

[26] Bao Q, Zhang H, Yang J-x, Wang S, Tang DY, Jose R, Ramakrishna S, Lim CT, Loh KP. Graphene–polymer nanofiber membrane for ultrafast photonics. Advanced Functional Materials 2010; 20(5) 782-791.

[27] Matthews JA, Wnek GE, Simpson DG, Bowlin GL. Electrospinning of collagen nanofibers. Biomacromolecules 2002; 3(2) 232-238.

[28] Rho KS, Jeong L, Lee G, Seo B-M, Park YJ, Hong S-D, Roh S, Cho JJ, Park WH, Min B-M. Electrospinning of collagen nanofibers: Effects on the behavior of normal human keratinocytes and early-stage wound healing. Biomaterials 2006; 27(8) 1452-1461.

[29] Buttafoco L, Kolkman NG, Engbers-Buijtenhuijs P, Poot AA, Dijkstra PJ, Vermes I, Feijen J. Electrospinning of collagen and elastin for tissue engineering applications. Biomaterials 2006; 27(5) 724-734.

[30] Xie J, Hsieh Y-L. Ultra-high surface fibrous membranes from electrospinning of natural proteins: casein and lipase enzyme. Journal of Materials Science 2003; 38(10) 2125-2133.

[31] Herricks TE, Kim S-H, Kim J, Li D, Kwak JH, Grate JW, Kim SH, Xia Y. Direct fabrication of enzyme-carrying polymer nanofibers by electrospinning. Journal of Materials Chemistry 2005; 15(31) 3241-3245.

[32] Zeng J, Aigner A, Czubayko F, Kissel T, Wendorff JH, Greiner A. Poly(vinyl alcohol) nanofibers by electrospinning as a protein delivery system and the retardation of enzyme release by additional polymer coatings. Biomacromolecules 2005; 6(3) 1484-1488.

[33] Tang C, Ozcam AE, Stout B, Khan SA. Effect of pH on Protein distribution in electrospun PVA/BSA composite nanofibers. Biomacromolecules 2012; 13(5) 1269-1278.

[34] Okhawilai M, Rangkupan R, Kanokpanont S, Damrongsakkul S. Preparation of Thai silk fibroin/gelatin electrospun fiber mats for controlled release applications. International Journal of Biological Macromolecules 2010; 46(5) 544-550.

[35] Song J, Kahveci D, Chen M, Guo Z, Xie E, Xu X, Besenbacher F, Dong M. Enhanced catalytic activity of lipase encapsulated in PCL nanofibers. Langmuir 2012; 28(14) 6157-6162.

[36] Wu L, Yuan X, Sheng J. Immobilization of cellulase in nanofibrous PVA membranes by electrospinning. Journal of Membrane Science 2005; 250(1–2) 167-173.

[37] Tran DN, Yang D-J, Balkus Jr KJ. Fabrication of cellulase protein fibers through concentric electrospinning. Journal of Molecular Catalysis B: Enzymatic 2011; 72(1–2) 1-5.

[38] Jiang H, Hu Y, Li Y, Zhao P, Zhu K, Chen W. A facile technique to prepare biodegradable coaxial electrospun nanofibers for controlled release of bioactive agents. Journal of Controlled Release 2005; 108(2–3) 237-243.

[39] Yang Y, Li X, Qi M, Zhou S, Weng J. Release pattern and structural integrity of lysozyme encapsulated in core–sheath structured poly(dl-lactide) ultrafine fibers prepared by emulsion electrospinning. European Journal of Pharmaceutics and Biopharmaceutics 2008; 69(1) 106-116.

[40] Ren G, Xu X, Liu Q, Cheng J, Yuan X, Wu L, Wan Y. Electrospun poly(vinyl alcohol)/glucose oxidase biocomposite membranes for biosensor applications. Reactive & Functional Polymers 2006; 66(12) 1559-1564.

[41] Dror Y, Kuhn J, Avrahami R, Zussman E. Encapsulation of enzymes in biodegradable tubular structures. Macromolecules 2008; 41(12) 4187-4192.

[42] Han D, Filocamo S, Kirby R, Steckl AJ. Deactivating chemical agents using enzyme-coated nanofibers formed by electrospinning. ACS Applied Materials & Interfaces 2011; 3(12) 4633-4639.

[43] Moreno I, González-González V, Romero-García J. Control release of lactate dehydrogenase encapsulated in poly (vinyl alcohol) nanofibers via electrospinning. European Polymer Journal 2011; 47(6) 1264-1272.

[44] Luu YK, Kim K, Hsiao BS, Chu B, Hadjiargyrou M. Development of a nanostructured DNA delivery scaffold via electrospinning of PLGA and PLA–PEG block copolymers. Journal of Controlled Release 2003; 89(2) 341-353.

[45] Bellan LM, Cross JD, Strychalski EA, Moran-Mirabal J, Craighead HG. Individually resolved DNA molecules stretched and embedded in electrospun polymer nanofibers. Nano Letters 2006; 6(11) 2526-2530.

[46] Lee SW, Belcher AM. Virus-based fabrication of micro- and nanofibers using electrospinning. Nano Letters 2004; 4(3) 387-390.

[47] Wang Y, Santiago-Aviles JJ. Synthesis of lead zirconate titanate nanofibres and the Fourier-transform infrared characterization of their metallo-organic decomposition process. Nanotechnology 2004; 15(1) 32-36.

[48] Wang Y, Furlan R, Ramos I, Santiago-Aviles JJ. Synthesis and characterization of micro/nanoscopic $Pb(Zr_{0.52}Ti_{0.48})O_3$ fibers by electrospinning. Applied Physics A: Materials Science & Processing 2004; 78(7) 1043-1047.

[49] Wang Y, Serrano S, Santiago-Aviles JJ. Electrostatic synthesis and characterization of $Pb(Zr_xTi_{1-x})O_3$ micro/nano-fibers. In: Wallenberger FT, Weston NE, Ford R, Wool RP,

Chawla K. (ed.) Advanced Fibers, Plastics, Laminates and Composites. 2002. p359-364.

[50] Larsen G, Velarde-Ortiz R, Minchow K, Barrero A, Loscertales IG. A method for making inorganic and hybrid (organic/inorganic) fibers and vesicles with diameters in the submicrometer and micrometer range via sol-gel chemistry and electrically forced liquid jets. Journal of the American Chemical Society 2003; 125(5) 1154-1155.

[51] Choi SS, Lee SG, Im SS, Kim SH, Joo YL. Silica nanofibers from electrospinning/sol-gel process. Journal of Materials Science Letters 2003; 22(12) 891-893.

[52] Panels JE, Joo YL. Incorporation of vanadium oxide in silica nanofiber mats via electrospinning and sol-gel synthesis. Journal of Nanomaterials 2006.

[53] Ko JB, Lee S, Kim D, Kim Y, Li G, Lee S, Chang TS, Kim D, Joo Y. Fabrication of SiO_2/ZrO_2 composite fiber mats via electrospinning. Journal of Porous Materials 2006; 13(3) 325-330.

[54] Li D, Wang YL, Xia YN. Electrospinning of polymeric and ceramic nanofibers as uniaxially aligned arrays. Nano Letters 2003; 3(8) 1167-1171.

[55] Li D, Xia YN. Fabrication of titania nanofibers by electrospinning. Nano Letters 2003; 3(4) 555-560.

[56] Li D, Herricks T, Xia YN. Magnetic nanofibers of nickel ferrite prepared by electrospinning. Applied Physics Letters 2003; 83(22) 4586-4588.

[57] Bognitzki M, Becker M, Graeser M, Massa W, Wendorff JH, Schaper A, Weber D, Beyer A, Golzhauser A, Greiner A. Preparation of sub-micrometer copper fibers via electrospinning. Advanced Materials 2006; 18(18) 2384-2386.

[58] Wu H, Hu L, Rowell MW, Kong D, Cha JJ, McDonough JR, Zhu J, Yang Y, McGehee MD, Cui Y. Electrospun metal nanofiber webs as high-performance transparent electrode. Nano Letters 2010; 10(10) 4242-4248.

[59] Wu H, Zhang R, Liu X, Lin D, Pan W. Electrospinning of Fe, Co, and Ni nanofibers: synthesis, assembly, and magnetic properties. Chemistry of Materials 2007; 19(14) 3506-3511.

[60] Shui J, Li JCM. Platinum nanowires produced by electrospinning. Nano Letters 2009; 9(4) 1307-1314.

[61] Gries K, Vieker H, Goelzhaeuser A, Agarwal S, Greiner A. Preparation of continuous gold nanowires by electrospinning of high-concentration aqueous dispersions of gold nanoparticles. Small 2012; 8(9) 1436-1441.

[62] Inagaki M, Yang Y, Kang F. Carbon nanofibers prepared via electrospinning. Advanced Materials 2012; 24(19) 2547-2566.

[63] Fu GD, Lei JY, Yao C, Li XS, Yao F, Nie SZ, Kang ET, Neoh KG. Core-sheath nanofibers from combined atom transfer radical polymerization and electrospinning. Macromolecules 2008; 41(18) 6854-6858.

[64] Nair S, Hsiao E, Kim SH. Fabrication of electrically-conducting nonwoven porous mats of polystyrene-polypyrrole core-shell nanofibers via electrospinning and vapor phase polymerization. Journal of Materials Chemistry 2008; 18(42) 5155-5161.

[65] Fragala ME, Cacciotti I, Aleeva Y, Lo Nigro R, Bianco A, Malandrino G, Spinella C, Pezzotti G, Gusmano G. Core-shell Zn-doped TiO_2-ZnO nanofibers fabricated via a combination of electrospinning and metal-organic chemical vapour deposition. CrystEngComm 2010; 12(11) 3858-3865.

[66] Kang H, Zhu Y, Yang X, Shen J, Chen C, Li C. Gold/mesoporous silica-fiber core-shell hybrid nanostructure: a potential electron transfer mediator in a bio-electrochemical system. New Journal of Chemistry 2010; 34(10) 2166-2175.

[67] Kazemi A, Lahann J, Madani M, Sharifi-Sanjani N, Hasan-Kaviar A. Preparation of core-shell and hollow fibers using layer by layer (LbL) self-assembly of polyelectrolytes on electrospun submicrometer-scale silica fibers. Polymer Science Series B 2010; 52(9) 571-574.

[68] Bazilevsky AV, Yarin AL, Megaridis CM. Co-electrospinning of core-shell fibers using a single-nozzle technique. Langmuir 2007; 23(5) 2311-2314.

[69] Zander NE, Strawhecker KE, Orlicki JA, Rawlett AM, Beebe TP. Coaxial electrospun poly(methyl methacrylate)-polyacrylonitrile nanofibers: Atomic force microscopy and compositional characterization. Journal of Physical Chemistry B 2011; 115(43) 12441-12447.

[70] Yang Y, Li X, Cui W, Zhou S, Tan R, Wang C. Structural stability and release profiles of proteins from core-shell poly(D, L-lactide) ultrafine fibers prepared by emulsion electrospinning. Journal of Biomedical Materials Research Part A 2008; 86A(2) 374-385.

[71] Xu X, Zhuang X, Chen X, Wang X, Yang L, Jing X. Preparation of core-sheath composite nanofibers by emulsion electrospinning. Macromolecular Rapid Communications 2006; 27(19) 1637-1642.

[72] Wei M, Lee J, Kang B, Mead J. Preparation of core-sheath nanofibers from conducting polymer blends. Macromolecular Rapid Communications 2005; 26(14) 1127-1132.

[73] Wei M, Kang B, Sung C, Mead J. Core-sheath structure in electrospun nanofibers from polymer blends. Macromolecular Materials and Engineering 2006; 291(11) 1307-1314.

[74] Na H, Liu X, Li J, Zhao Y, Zhao C, Yuan X. Formation of core/shell ultrafine fibers of PVDF/PC by electrospinning via introduction of PMMA or BTEAC. Polymer 2009; 50(26) 6340-6349.

[75] Zhang JF, Yang DZ, Xu F, Zhang ZP, Yin RX, Nie J. Electrospun core-shell structure nanofibers from homogeneous solution of poly(ethylene oxide)/chitosan. Macromolecules 2009; 42(14) 5278-5284.

[76] Kuo CC, Lin CH, Chen WC. Morphology and photophysical properties of light-emitting electrospun nanofibers prepared from poly(fluorene) derivative/PMMA blends. Macromolecules 2007; 40(19) 6959-6966.

[77] Jo E, Lee S, Kim KT, Won YS, Kim H-S, Cho EC, Jeong U. Core-sheath nanofibers containing colloidal arrays in the core for programmable multi-agent delivery. Advanced Materials 2009; 21(9) 968-972.

[78] Loscertales IG, Barrero A, Guerrero I, Cortijo R, Marquez M, Gañán-Calvo AM. Micro/nano encapsulation via electrified coaxial liquid jets. Science 2002; 295(5560) 1695-1698.

[79] Sun ZC, Zussman E, Yarin AL, Wendorff JH, Greiner A. Compound core-shell polymer nanofibers by co-electrospinning. Advanced Materials 2003; 15(22) 1929-1932.

[80] Yu JH, Fridrikh SV, Rutledge GC. Production of submicrometer diameter fibers by two-fluid electrospinning. Advanced Materials 2004; 16(17) 1562-1566.

[81] Li D, Xia YN. Direct fabrication of composite and ceramic hollow nanofibers by electrospinning. Nano Letters 2004; 4(5) 933-938.

[82] Zhang Y, Huang Z-M, Xu X, Lim CT, Ramakrishna S. Preparation of core–shell structured PCL-r-gelatin bi-component nanofibers by coaxial electrospinning. Chemistry of Materials 2004; 16(18) 3406-3409.

[83] Gulfam M, Lee JM, Kim JE, Lim DW, Lee EK, Chung BG. Highly porous core-shell polymeric fiber network. Langmuir 2011; 27(17) 10993-10999.

[84] Zhang YZ, Venugopal J, Huang ZM, Lim CT, Ramakrishna S. Characterization of the surface biocompatibility of the electrospun PCL-collagen nanofibers using fibroblasts. Biomacromolecules 2005; 6(5) 2583-2589.

[85] Han X-J, Huang Z-M, He C-L, Liu L, Wu Q-S. Coaxial electrospinning of PC(shell)/PU(core) composite nanofibers for textile application. Polymer Composites 2006; 27(4) 381-387.

[86] Liao IC, Chew SY, Leong KW. Aligned core-shell nanofibers delivering bioactive proteins. Nanomedicine 2006; 1(4) 465-471.

[87] Sun B, Duan B, Yuan X. Preparation of core/shell PVP/PLA ultrafine fibers by coaxial electrospinning. Journal of Applied Polymer Science 2006; 102(1) 39-45.

[88] Srivastava Y, Loscertales I, Marquez M, Thorsen T. Electrospinning of hollow and core/sheath nanofibers using a microfluidic manifold. Microfluidics and Nanofluidics 2008; 4(3) 245-250.

[89] Wu L, Li H, Li S, Li X, Yuan X, Li X, Zhang Y. Composite fibrous membranes of PLGA and chitosan prepared by coelectrospinning and coaxial electrospinning. Journal of Biomedical Materials Research Part A 2010; 92A(2) 563-574.

[90] Sun B, Li S, Zhang H, Li H, Zhao CG, Yuan XY, Cui YL. Controlled release of Berberine Chloride by electrospun core/shell PVP/PLCL fibrous membranes. International Journal of Materials & Product Technology 2010; 37(3-4) 338-349.

[91] Li H, Zhao C, Wang Z, Zhang H, Yuan X, Kong D. Controlled release of PDGF-bb by coaxial electrospun dextran/poly(L-lactide-co-ε-caprolactone) fibers with an ultrafine core/shell structure. Journal of Biomaterials Science, polymer Edition 2010; 21(6-7) 803-819.

[92] Yang PP, Chen JF, Huang ZH, Zhan SM, Jiang ZJ, Qiu YQ, Shao C. A novel 1D organic optic–electronic nanomaterial using PPV (p-type) as shell and Alq3 (n-type) as core. Materials Letters 2009; 63(23) 1978-1980.

[93] Ravichandran R, Venugopal JR, Sundarrajan S, Mukherjee S, Ramakrishna S. Poly(glycerol sebacate)/gelatin core/shell fibrous structure for regeneration of myocardial infarction. Tissue Engineering Part A 2011; 17(9-10) 1363-1373.

[94] Nguyen TTT, Chung OH, Park JS. Coaxial electrospun poly(lactic acid)/chitosan (core/shell) composite nanofibers and their antibacterial activity. Carbohydrate Polymers 2011; 86(4) 1799-1806.

[95] Pakravan M, Heuzey M-C, Ajji A. Core–shell structured PEO-chitosan nanofibers by coaxial electrospinning. Biomacromolecules 2012; 13(2) 412-421.

[96] Su Y, Su Q, Liu W, Lim M, Venugopal JR, Mo X, Ramakrishna S, Al-Deyab SS, El-Newehy M. Controlled release of bone morphogenetic protein 2 and dexamethasone loaded in core–shell PLLACL–collagen fibers for use in bone tissue engineering. Acta Biomaterialia 2012; 8(2) 763-771.

[97] Tong H-W, Zhang X, Wang M. A new nanofiber fabrication technique based on coaxial electrospinning. Materials Letters 2012; 66(1) 257-260.

[98] Song T, Zhang Y, Zhou T, Lim CT, Ramakrishna S, Liu B. Encapsulation of self-assembled FePt magnetic nanoparticles in PCL nanofibers by coaxial electrospinning. Chemical Physics Letters 2005; 415(4–6) 317-322.

[99] Hwang TH, Lee YM, Kong BS, Seo JS, Choi JW. Electrospun core-shell fibers for robust silicon nanoparticle-based lithium ion battery anodes. Nano Letters 2012; 12(2) 802-807.

[100] Longson TJ, Bhowmick R, Gu C, Cruden BA. Core–shell interactions in coaxial electrospinning and impact on electrospun multiwall carbon nanotube core, poly(methyl methacrylate) shell fibers. Journal of Physical Chemistry C 2011; 115(26) 12742-12750.

[101] Medina-Castillo AL, Fernandez-Sanchez JF, Fernandez-Gutierrez A. One-step fabrication of multifunctional core-shell fibres by co-electrospinning. Advanced Functional Materials 2011; 21(18) 3488-3495.

[102] Li X, Su Y, Chen R, He C, Wang H, Mo X. Fabrication and properties of core-shell structure P(LLA-CL) nanofibers by coaxial electrospinning. Journal of Applied Polymer Science 2009; 111(3) 1564-1570.

[103] Huang H-H, He C-L, Wang H-S, Mo X-M. Preparation of core-shell biodegradable microfibers for long-term drug delivery. Journal of Biomedical Materials Research Part A 2009; 90A(4) 1243-1251.

[104] Gu Y, Chen D, Jiao X, Liu F. $LiCoO_2$-MgO coaxial fibers: co-electrospun fabrication, characterization and electrochemical properties. Journal of Materials Chemistry 2007; 17(18) 1769-1776.

[105] Zhou XH, Shang CQ, Gu L, Dong SM, Chen X, Han PX, Li LF, Yao JH, Liu ZH, Xu HX, Zhu YW, Cui GL. Mesoporous coaxial titanium nitride-vanadium nitride fibers of core-shell structures for high-performance supercapacitors. ACS Applied Materials & Interfaces 2011; 3(8) 3058-3063.

[106] Xie S, Ma F, Liu Y, Li J. Multiferroic $CoFe_2O_4$-$Pb(Zr_{0.52}Ti_{0.48})O_3$ core-shell nanofibers and their magnetoelectric coupling. Nanoscale 2011; 3(8) 3152-3158.

[107] Peng X, Santulli AC, Sutter E, Wong SS. Fabrication and enhanced photocatalytic activity of inorganic core-shell nanofibers produced by coaxial electrospinning. Chemical Science 2012; 3(4) 1262-1272.

[108] Bognitzki M, Hou HQ, Ishaque M, Frese T, Hellwig M, Schwarte C, Schaper A, Wendorff JH, Greiner A. Polymer, metal, and hybrid nano- and mesotubes by coating degradable polymer template fibers (TUFT process). Advanced Materials 2000; 12(9) 637-640.

[109] Liu TQ. Preparation of a novel micro/nano tubes via electrospun fiber as a template. Journal of Materials Science & Technology 2004; 20(5) 613-616.

[110] Caruso RA, Schattka JH, Greiner A. Titanium dioxide tubes from sol-gel coating of electrospun polymer fibers. Advanced Materials 2001; 13(20) 1577-1579.

[111] Abidian MR, Kim DH, Martin DC. Conducting-polymer nanotubes for controlled drug release. Advanced Materials 2006; 18(4) 405-409.

[112] Dong H, Jones WE. Preparation of submicron polypyrrole/poly(methyl methacrylate) coaxial fibers and conversion to polypyrrole tubes and carbon tubes. Langmuir 2006; 22(26) 11384-11387.

[113] Ge L, Pan C, Chen H, Wang X, Wang C, Gu Z. The fabrication of hollow multilayered polyelectrolyte fibrous mats and its morphology study. Colloids and Surfaces A: Physicochemical and Engineering Aspects 2007; 293(1–3) 272-277.

[114] Pan C, Ge L-Q, Gu Z-Z. Fabrication of multi-walled carbon nanotube reinforced polyelectrolyte hollow nanofibers by electrospinning. Composites Science and Technology 2007; 67(15–16) 3271-3277.

[115] Zhang T, Ge L, Wang X, Gu Z. Hollow TiO_2 containing multilayer nanofibers with enhanced photocatalytic activity. Polymer 2008; 49(12) 2898-2902.

[116] McCann JT, Lim BK, Ostermann R, Rycenga M, Marquez M, Xia YN. Carbon nanotubes by electrospinning with a polyelectrolyte and vapor deposition polymerization. Nano Letters 2007; 7(8) 2470-2474.

[117] Peng Q, Sun XY, Spagnola JC, Hyde GK, Spontak RJ, Parsons GN. Atomic layer deposition on electrospun polymer fibers as a direct route to Al_2O_3 microtubes with precise wall thickness control. Nano Letters 2007; 7(3) 719-722.

[118] Choi S-H, Ankonina G, Youn D-Y, Oh S-G, Hong J-M, Rothschild A, Kim I-D. Hollow ZnO nanofibers fabricated using electrospun polymer templates and their electronic transport properties. ACS Nano 2009; 3(9) 2623-2631.

[119] Lee KJ, Song H, Lee YI, Jung H, Zhang M, Choa YH, Myung V. Synthesis of ultralong hollow chalcogenide nanofibers. Chemical Communications 2011; 47(32) 9107-9109.

[120] Gu Y, Chen D, Jiao X. Synthesis and characterization of hollow $LiNiO_2$ fibers via sol-electrospinning method. Journal of Sol-gel Science and Technology 2007; 43(2) 245-249.

[121] Cui Q, Dong X, Wang J, Li M. Direct fabrication of cerium oxide hollow nanofibers by electrospinning. Journal of Rare Earths 2008; 26(5) 664-669.

[122] Li JY, Tan Y, Xu FM, Sun Y, Cao XQ, Zhang YF. Hollow fibers of yttria-stabilized zirconia (8YSZ) prepared by calcination of electrospun composite fibers. Materials Letters 2008; 62(16) 2396-2399.

[123] Zhang Y, Li Q, Li H, Cheng Y, Zhang J, Cao X. Sintering-resistant hollow fibers of LaMgAl11O19 prepared by electrospinning. Journal of Crystal Growth 2008; 310(16) 3884-3889.

[124] Chen WS, Huang DA, Chen HC, Shie TY, Hsieh CH, Liao JD, Kuo CS. Fabrication of polycrystalline ZnO nanotubes from the electrospinning of Zn^{2+}/Poly(acrylic acid). Crystal Growth & Design 2009; 9(9) 4070-4077.

[125] Hota G, Sundarrajan S, Ramakrishna S, WunJern N. One step fabrication of MgO solid and hollow submicrometer fibers via electrospinning method. Journal of the American Ceramic Society 2009; 92(10) 2429-2433.

[126] Cheng Y, Huang W, Zhang Y, Zhu L, Liu Y, Fan X, Cao X. Preparation of TiO_2 hollow nanofibers by electrospining combined with sol-gel process. CrystEngComm 2010; 12(7) 2256-2260.

[127] Mou F-z, Guan J-g, Sun Z-g, Fan X-a, Tong G-x. In situ generated dense shell-engaged Ostwald ripening: A facile controlled-preparation for $BaFe_{12}O_{19}$ hierarchical hollow fiber arrays. Journal of Solid State Chemistry 2010; 183(3) 736-743.

[128] Zampetti E, Pantalei S, Scalese S, Bearzotti A, De Cesare F, Spinella C, Macagnano A. Biomimetic sensing layer based on electrospun conductive polymer webs. Biosensors & Bioelectronics 2011; 26(5) 2460-2465.

[129] Chen X, Unruh K, Ni CY, Ali B, Sun Z, Lu Q, Deitzel J, Xiao JQ. Fabrication, formation mechanism, and magnetic properties of metal oxide nanotubes via electrospinning and thermal treatment. Journal of Physical Chemistry C 2011; 115(2) 373-378.

[130] Cheng Y, Zou B, Wang C, Liu Y, Fan X, Zhu L, Wang Y, Ma H, Cao X. Formation mechanism of Fe_2O_3 hollow fibers by direct annealing of the electrospun composite fibers and their magnetic, electrochemical properties. CrystEngComm 2011; 13(8) 2863-2870.

[131] Cheng Y, Zou B, Yang J, Wang C, Liu Y, Fan X, Zhu L, Wang Y, Ma H, Cao X. Fabrication of $CoFe_2O_4$ hollow fibers by direct annealing of the electrospun composite fibers and their magnetic properties. CrystEngComm 2011; 13(7) 2268-2272.

[132] Xiang H, Long Y, Yu X, Zhang X, Zhao N, Xu J. A novel and facile method to prepare porous hollow CuO and Cu nanofibers based on electrospinning. CrystEngComm 2011; 13(15) 4856-4860.

[133] Xia X, Dong XJ, Wei QF, Cai YB, Lu KY. Formation mechanism of porous hollow SnO_2 nanofibers prepared by one-step electrospinning. Express Polymer Letters 2012; 6(2) 169-176.

[134] Li XH, Shao CL, Liu YC. A simple method for controllable preparation of polymer nanotubes via a single capillary electrospinning. Langmuir 2007; 23(22) 10920-10923.

[135] Hong Y, Chen X, Jing X, Fan H, Gu Z, Zhang X. Fabrication and drug delivery of ultrathin mesoporous bioactive glass hollow fibers. Advanced Functional Materials 2010; 20(9) 1503-1510.

[136] Lu B, Guo X, Bao Z, Li X, Liu Y, Zhu C, Wang Y, Xie E. Direct preparation of carbon nanotubes and nanobelts from polymer. Nanoscale 2011; 3(5) 2145-2149.

[137] Yu Y, Gu L, Zhu CB, van Aken PA, Maier J. Tin nanoparticles encapsulated in porous multichannel carbon microtubes: Preparation by single-nozzle electrospinning and application as anode material for high-performance Li-Based batteries. Journal of the American Chemical Society 2009; 131(44) 15984-15985.

[138] Li D, McCann JT, Xia Y. Use of Electrospinning to directly fabricate hollow nanofibers with functionalized inner and outer surfaces. Small 2005; 1(1) 83-86.

[139] Loscertales IG, Barrero A, Marquez M, Spretz R, Velarde-Ortiz R, Larsen G. Electrically forced coaxial nanojets for one-step hollow nanofiber design. Journal of the American Chemical Society 2004; 126(17) 5376-5377.

[140] Zussman E, Yarin AL, Bazilevsky AV, Avrahami R, Feldman M. Electrospun polyaniline/poly(methyl methacrylate)-derived turbostratic carbon micro-/nanotubes. Advanced Materials 2006; 18(3) 348-353.

[141] Dror Y, Salalha W, Avrahami R, Zussman E, Yarin AL, Dersch R, Greiner A, Wendorff JH. One-step production of polymeric microtubes by co-electrospinning. Small 2007; 3(6) 1064-1073.

[142] Di JC, Chen HY, Wang XF, Zhao Y, Jiang L, Yu JH, Xu RR. Fabrication of zeolite hollow fibers by coaxial electrospinning. Chemistry of Materials 2008; 20(11) 3543-3545.

[143] Zhan S, Chen D, Jiao X. Co-electrospun SiO_2 hollow nanostructured fibers with hierarchical walls. Journal of Colloid and Interface Science 2008; 318(2) 331-336.

[144] Katoch A, Kim SS. Synthesis of hollow silica fibers with porous walls by coaxial electrospinning method. Journal of the American Ceramic Society 2012; 95(2) 553-556.

[145] Zhang X, Thavasi V, Mhaisalkar S, Ramakrishna S. Novel hollow mesoporous 1D TiO_2 nanofibers as photovoltaic and photocatalytic materials. Nanoscale 2012; 4(5) 1707-1716.

[146] Zhan S, Li Y, Yu H. Sol-gel co-electrospun $LiNiO_2$ hollow nanofibers. Journal of Dispersion Science and Technology 2008; 29(6) 823-826.

[147] Zhan S, Li Y, Yu H. $LiCoO_2$ hollow nanofibers by co-electrospinning sol-gel precursor. Journal of Dispersion Science and Technology 2008; 29(5) 702-705.

[148] Zhan S, Yu H, Li Y, Jiang B, Zhang X, Yan C, Ma S. Co-electrospun $BaTiO_3$ hollow fibers combined with sol-gel method. Journal of Dispersion Science and Technology 2008; 29(9) 1345-1348.

[149] Gu YX, Jian FF. Hollow $LiNi_{0.8}Co_{0.1}Mn_{0.1}O_2$-MgO coaxial fibers: Sol-gel method combined with co-electrospun preparation and electrochemical properties. Journal of Physical Chemistry C 2008; 112(51) 20176-20180.

[150] Chan KHK, Kotaki M. Fabrication and morphology control of poly(methyl methacrylate) hollow structures via coaxial electrospinning. Journal of Applied Polymer Science 2009; 111(1) 408-416.

[151] Lee G, Song J-C, Yoon K-B. Controlled wall thickness and porosity of polymeric hollow nanofibers by coaxial electrospinning. Macromolecular Research 2010; 18(6) 571-576.

[152] Wang C, Yan K-W, Lin Y-D, Hsieh PCH. Biodegradable core/shell fibers by coaxial electrospinning: Processing, fiber characterization, and its application in sustained drug release. Macromolecules 2010; 43(15) 6389-6397.

[153] Yu Y, Gu L, Wang C, Dhanabalan A, van Aken PA, Maier J. Encapsulation of Sn@carbon nanoparticles in bamboo-like hollow carbon nanofibers as an anode material in lithium-based batteries. Angewandte Chemie-International Edition 2009; 48(35) 6485-6489.

[154] Lee B-S, Son S-B, Park K-M, Yu W-R, Oh K-H, Lee S-H. Anodic properties of hollow carbon nanofibers for Li-ion battery. Journal of Power Sources 2012; 199(0) 53-60.

[155] Lallave M, Bedia J, Ruiz-Rosas R, Rodríguez-Mirasol J, Cordero T, Otero JC, Marquez M, Barrero A, Loscertales IG. Filled and hollow carbon nanofibers by coaxial electrospinning of Alcell lignin without binder polymers. Advanced Materials 2007; 19(23) 4292-4296.

[156] Zhao Y, Cao XY, Jiang L. Bio-mimic multichannel microtubes by a facile method. Journal of the American Chemical Society 2007; 129(4) 764-765.

[157] Zhao T, Liu Z, Nakata K, Nishimoto S, Murakami T, Zhao Y, Jiang L, Fujishima A. Multichannel TiO_2 hollow fibers with enhanced photocatalytic activity. Journal of Materials Chemistry 2010; 20(24) 5095-5099.

[158] Bognitzki M, Czado W, Frese T, Schaper A, Hellwig M, Steinhart M, Greiner A, Wendorff JH. Nanostructured fibers via electrospinning. Advanced Materials 2001; 13(1) 70-72.

[159] Megelski S, Stephens JS, Chase DB, Rabolt JF. Micro- and nanostructured surface morphology on electrospun polymer fibers. Macromolecules 2002; 35(22) 8456-8466.

[160] Casper CL, Stephens JS, Tassi NG, Chase DB, Rabolt JF. Controlling surface morphology of electrospun polystyrene fibers: Effect of humidity and molecular weight in the electrospinning process. Macromolecules 2004; 37(2) 573-578.

[161] Dayal P, Liu J, Kumar S, Kyu T. Experimental and theoretical investigations of porous structure formation in electrospun fibers. Macromolecules 2007; 40(21) 7689-7694.

[162] Han SO, Son WK, Youk JH, Lee TS, Park WH. Ultrafine porous fibers electrospun from cellulose triacetate. Materials Letters 2005; 59(24–25) 2998-3001.

[163] Lin J, Ding B, Yu J, Hsieh Y. Direct fabrication of highly nanoporous polystyrene fibers via electrospinning. ACS Applied Materials & Interfaces 2010; 2(2) 521-528.

[164] Qi Z, Yu H, Chen Y, Zhu M. Highly porous fibers prepared by electrospinning a ternary system of nonsolvent/solvent/poly(L-lactic acid). Materials Letters 2009; 63(3–4) 415-418.

[165] Yu X, Xiang H, Long Y, Zhao N, Zhang X, Xu J. Preparation of porous polyacrylonitrile fibers by electrospinning a ternary system of PAN/DMF/H_2O. Materials Letters 2010; 64(22) 2407-2409.

[166] Celebioglu A, Uyar T. Electrospun porous cellulose acetate fibers from volatile solvent mixture. Materials Letters 2011; 65(14) 2291-2294.

[167] Bognitzki M, Frese T, Steinhart M, Greiner A, Wendorff JH, Schaper A, Hellwig M. Preparation of fibers with nanoscaled morphologies: Electrospinning of polymer blends. Polymer Engineering & Science 2001; 41(6) 982-989.

[168] Kanehata M, Ding B, Shiratori S. Nanoporous ultra-high specific surface inorganic fibres. Nanotechnology 2007; 18(31) 315602.

[169] Patel AC, Li SX, Wang C, Zhang WJ, Wei Y. Electrospinning of porous silica nanofibers containing silver nanoparticles for catalytic applications. Chemistry of Materials 2007; 19(6) 1231-1238.

[170] Hou Z, Zhang C, Li C, Xu Z, Cheng Z, Li G, Wang W, Peng C, Lin J. Luminescent porous silica fibers as drug carriers. Chemistry – A European Journal 2010; 16(48) 14513-14519.

[171] Wang Y, Ramos I, Santiago-Aviles JJ. Synthesis of ultra-fine porous tin oxide fibres and its process characterization. Nanotechnology 2007; 18(29) 295601.

[172] Yang A, Tao X, Pang GKH, Siu KGG. Preparation of porous tin oxide nanobelts using the electrospinning technique. Journal of the American Ceramic Society 2008; 91(1) 257-262.

[173] Hou Z, Li C, Ma P, Li G, Cheng Z, Peng C, Yang D, Yang P, Lin J. Electrospinning preparation and drug-delivery properties of an up-conversion luminescent porous $NaYF_4$:Yb^{3+}, Er^{3+}@silica fiber nanocomposite. Advanced Functional Materials 2011; 21(12) 2356-2365.

[174] Luo W, Hu X, Sun Y, Huang Y. Electrospun porous $ZnCo_2O_4$ nanotubes as a high-performance anode material for lithium-ion batteries. Journal of Materials Chemistry 2012; 22(18) 8916-8921.

[175] Han SO, Son WK, Cho D, Youk JH, Park WH. Preparation of porous ultra-fine fibres via selective thermal degradation of electrospun polyetherimide/poly(3-hydroxybutyrate- co-3-hydroxyvalerate) fibres. Polymer Degradation and Stability 2004; 86(2) 257-262.

[176] You Y, Youk JH, Lee SW, Min B-M, Lee SJ, Park WH. Preparation of porous ultrafine PGA fibers via selective dissolution of electrospun PGA/PLA blend fibers. Materials Letters 2006; 60(6) 757-760.

[177] Zhang Z, Li X, Wang C, Fu S, Liu Y, Shao C. Polyacrylonitrile and carbon nanofibers with controllable nanoporous structures by electrospinning. Macromolecular Materials and Engineering 2009; 294(10) 673-678.

[178] Gupta A, Saquing CD, Afshari M, Tonelli AE, Khan SA, Kotek R. Porous nylon-6 fibers via a novel salt-induced electrospinning method. Macromolecules 2009; 42(3) 709-715.

[179] Ma G, Yang D, Nie J. Preparation of porous ultrafine polyacrylonitrile (PAN) fibers by electrospinning. Polymers for Advanced Technologies 2009; 20(2) 147-150.

[180] McCann JT, Marquez M, Xia Y. Highly porous fibers by electrospinning into a cryogenic liquid. Journal of the American Chemical Society 2006; 128(5) 1436-1437.

[181] Pant HR, Neupane MP, Pant B, Panthi G, Oh H-J, Lee MH, Kim HY. Fabrication of highly porous poly(ε-caprolactone) fibers for novel tissue scaffold via water-bath electrospinning. Colloids and Surfaces B: Biointerfaces 2011; 88(2) 587-592.

[182] Peng M, Li D, Shen L, Chen Y, Zheng Q, Wang H. Nanoporous structured submicrometer carbon fibers prepared via solution electrospinning of polymer blends. Langmuir 2006; 22(22) 9368-9374.

[183] Zhang L, Hsieh Y-L. Carbon nanofibers with nanoporosity and hollow channels from binary polyacrylonitrile systems. European Polymer Journal 2009; 45(1) 47-56.

[184] Kim C, Ngoc BTN, Yang KS, Kojima M, Kim YA, Kim YJ, Endo M, Yang SC. Self-sustained thin webs consisting of porous carbon nanofibers for supercapacitors via the electrospinning of polyacrylonitrile solutions containing zinc chloride. Advanced Materials 2007; 19(17) 2341-2346.

[185] Im JS, Park S-J, Kim TJ, Kim YH, Lee Y-S. The study of controlling pore size on electrospun carbon nanofibers for hydrogen adsorption. Journal of Colloid and Interface Science 2008; 318(1) 42-49.

[186] Song X, Wang C, Zhang D. Surface structure and adsorption properties of ultrafine porous carbon fibers. Applied Surface Science 2009; 255(7) 4159-4163.

[187] Ji L, Lin Z, Medford AJ, Zhang X. Porous carbon nanofibers from electrospun polyacrylonitrile/SiO_2 composites as an energy storage material. Carbon 2009; 47(14) 3346-3354.

[188] Ji LW, Saquing C, Khan SA, Zhang XW. Preparation and characterization of silica nanoparticulate-polyacrylonitrile composite and porous nanofibers. Nanotechnology 2008; 19(8) 085605.

[189] Lee S, Lee K, Moon GD, Won YS, Yoon YJ, Park SS, Kim YR, Jeong U. Preparation of macroporous carbon nanofibers with macroscopic openings in the surfaces and their applications. Nanotechnology 2009; 20(44) 445702.

[190] Jaeger R, Schönherr H, Vancso GJ. Chain packing in electro-spun poly(ethylene oxide) visualized by atomic force microscopy. Macromolecules 1996; 29(23) 7634-7636.

[191] Fong H, Chun I, Reneker DH. Beaded nanofibers formed during electrospinning. Polymer 1999; 40(16) 4585-4592.

[192] Jin Y, Yang D, Kang D, Jiang X. Fabrication of necklace-like structures via electrospinning. Langmuir 2010; 26(2) 1186-1190.

[193] Koombhongse S, Liu W, Reneker DH. Flat polymer ribbons and other shapes by electrospinning. Journal of Polymer Science Part B: Polymer Physics 2001; 39(21) 2598-2606.

[194] Chigome S, Torto N. A review of opportunities for electrospun nanofibers in analytical chemistry. Analytica Chimica Acta 2011; 706(1) 25-36.

[195] Scampicchio M, Bulbarello A, Arecchi A, Cosio MS, Benedetti S, Mannino S. Electrospun nonwoven nanofibrous membranes for sensors and biosensors. Electroanalysis 2012; 24(4) 719-725.

[196] Liu J, Niu J, Yin L, Jiang F. In situ encapsulation of laccase in nanofibers by electrospinning for development of enzyme biosensors for chlorophenol monitoring. Analyst 2011; 136(22) 4802-4808.

[197] Arecchi A, Scampicchio M, Brenna O, Mannino S. Biocatalytic nylon nanofibrous membranes. Analytical and Bioanalytical Chemistry 2010; 398(7) 3097-3103.

[198] Scampicchio M, Arecchi A, Bianco A, Bulbarello A, Bertarelli C, Mannino S. Nylon nanofibrous biosensors for glucose determination. Electroanalysis 2010; 22(10) 1056-1060.

[199] Scampicchio M, Arecchi A, Lawrence NS, Mannino S. Nylon nanofibrous membrane for mediated glucose biosensing. Sensors and Actuators B-chemical 2010; 145(1) 394-397.

[200] Arecchi A, Scampicchio M, Drusch S, Mannino S. Nanofibrous membrane based tyrosinase-biosensor for the detection of phenolic compounds. Analytica Chimica Acta 2010; 659(1–2) 133-136.

[201] Santhosh P, Manesh KM, Lee S-H, Uthayakumar S, Gopalan AI, Lee K-P. Sensitive electrochemical detection of superoxide anion using gold nanoparticles distributed poly(methyl methacrylate)-polyaniline core-shell electrospun composite electrode. Analyst 2011; 136(8) 1557-1561.

[202] Jia W, Su L, Lei Y. Pt nanoflower/polyaniline composite nanofibers based urea biosensor. Biosensors & Bioelectronics 2011; 30(1) 158-164.

[203] Liu Y, Chen J, Anh NT, Too CO, Misoska V, Wallace GG. Nanofiber mats from DNA, SWNTs, and poly(ethylene oxide) and their application in glucose biosensors. Journal of the Electrochemical Society 2008; 155(5) K100-K103.

[204] Wang Z-G, Wang Y, Xu H, Li G, Xu Z-K. Carbon nanotube-filled nanofibrous membranes electrospun from poly(acrylonitrile-co-acrylic acid) for glucose biosensor. Journal of Physical Chemistry C 2009; 113(7) 2955-2960.

[205] Manesh KM, Santhosh P, Gopalan A, Lee K-P. Electrospun poly(vinylidene fluoride)/poly(aminophenylboronic acid) composite nanofibrous membrane as a novel glucose sensor. Analytical Biochemistry 2007; 360(2) 189-195.

[206] Li F, Scampicchio M, Mannino S. Carbon nanotube-adsorbed electrospun nanofibrous membranes as coating for electrochemical sensors for sulfhydryl compounds. Electroanalysis 2011; 23(8) 1773-1775.

[207] Cao F, Guo S, Ma H, Gong J. ITO electrode modified by a-$K_6P_2W_{18}O_{62}$ hybrid nanofibers for nitrite determination. Electroanalysis 2012; 24(2) 418-424.

[208] Liu Y, Hou HQ, You TY. Synthesis of carbon nanofibers for mediatorless sensitive detection of NADH. Electroanalysis 2008; 20(15) 1708-1713.

[209] Liu Y, Huang JS, Hou HQ, You TY. Simultaneous determination of dopamine, ascorbic acid and uric acid with electrospun carbon nanofibers modified electrode. Electrochemistry Communications 2008; 10(10) 1431-1434.

[210] Tang XF, Liu Y, Hou HQ, You TY. Electrochemical determination of L-Tryptophan, L-Tyrosine and L-Cysteine using electrospun carbon nanofibers modified electrode. Talanta 2010; 80(5) 2182-2186.

[211] Tang X, Liu Y, Hou H, You T. A nonenzymatic sensor for xanthine based on electrospun carbon nanofibers modified electrode. Talanta 2011; 83(5) 1410-1414.

[212] Guo Q, Huang J, Chen P, Liu Y, Hou H, You T. Simultaneous determination of catechol and hydroquinone using electrospun carbon nanofibers modified electrode. Sensors and Actuators B-chemical 2012; 163(1) 179-185.

[213] Bae T-S, Shin E, Im JS, Kim JC, Lee Y-S. Effects of carbon structure orientation on the performance of glucose sensors fabricated from electrospun carbon fibers. Journal of Non-crystalline Solids 2012; 358(3) 544-549.

[214] Huang J, Wang D, Hou H, You T. Electrospun palladium nanoparticle-loaded carbon nanofibers and their electrocatalytic activities towards hydrogen peroxide and NADH. Advanced Functional Materials 2008; 18(3) 441-448.

[215] Huang JS, Liu Y, Hou HQ, You TY. Simultaneous electrochemical determination of dopamine, uric acid and ascorbic acid using palladium nanoparticle-loaded carbon nanofibers modified electrode. Biosensors & Bioelectronics 2008; 24(4) 632-637.

[216] Zhang HJ, Huang JS, Hou HQ, You TY. Electrochemical detection of hydrazine based on electrospun palladium nanoparticle/carbon nanofibers. Electroanalysis 2009; 21(16) 1869-1874.

[217] Liu Y, Huang J, Wang D, Hou H, You T. Electrochemical determination of oxalic acid using palladium nanoparticle-loaded carbon nanofiber modified electrode. Analytical Methods 2010; 2(7) 855-859.

[218] Liu Y, Teng H, Hou HQ, You TY. Nonenzymatic glucose sensor based on renewable electrospun Ni nanoparticle-loaded carbon nanofiber paste electrode. Biosensors & Bioelectronics 2009; 24(11) 3329-3334.

[219] Liu Y, Zhang L, Guo Q, Hou H, You T. Enzyme-free ethanol sensor based on electrospun nickel nanoparticle-loaded carbon fiber paste electrode. Analytica Chimica Acta 2010; 663(2) 153-157.

[220] Hu G, Zhou Z, Guo Y, Hou H, Shao S. Electrospun rhodium nanoparticle-loaded carbon nanofibers for highly selective amperometric sensing of hydrazine. Electrochemistry Communications 2010; 12(3) 422-426.

[221] Liu Y, Wang DW, Xu L, Hou HQ, You TY. A novel and simple route to prepare a Pt nanoparticle-loaded carbon nanofiber electrode for hydrogen peroxide sensing. Biosensors & Bioelectronics 2011; 26(11) 4585-4590.

[222] Ahmad M, Pan C, Luo Z, Zhu J. A single ZnO nanofiber-based highly sensitive amperometric glucose biosensor. Journal of Physical Chemistry C 2010; 114(20) 9308-9313.

[223] Huang S, Ding Y, Liu Y, Su L, Filosa R, Jr., Lei Y. Glucose biosensor using glucose oxidase and electrospun Mn_2O_3-Ag nanofibers. Electroanalysis 2011; 23(8) 1912-1920.

[224] Marx S, Jose MV, Andersen JD, Russell AJ. Electrospun gold nanofiber electrodes for biosensors. Biosensors & Bioelectronics 2011; 26(6) 2981-2986.

[225] Ding Y, Wang Y, Su L, Bellagamba M, Zhang H, Lei Y. Electrospun Co_3O_4 nanofibers for sensitive and selective glucose detection. Biosensors & Bioelectronics 2010; 26(2) 542-548.

[226] Wang W, Zhang L, Tong S, Li X, Song W. Three-dimensional network films of electrospun copper oxide nanofibers for glucose determination. Biosensors & Bioelectronics 2009; 25(4) 708-714.

[227] Cao F, Gong J. Nonenzymatic glucose sensor based on CuO microfibers composed of CuO nanoparticles. Analytica Chimica Acta 2012; 723 39-44.

[228] Cao F, Guo S, Ma H, Shan D, Yang S, Gong J. Nickel oxide microfibers immobilized onto electrode by electrospinning and calcination for nonenzymatic glucose sensor and effect of calcination temperature on the performance. Biosensors & Bioelectronics 2011; 26(5) 2756-2760.

[229] Wang W, Li Z, Zheng W, Yang J, Zhang H, Wang C. Electrospun palladium (IV)-doped copper oxide composite nanofibers for non-enzymatic glucose sensors. Electrochemistry Communications 2009; 11(9) 1811-1814.

[230] Ding Y, Wang Y, Su L, Zhang H, Lei Y. Preparation and characterization of NiO-Ag nanofibers, NiO nanofibers, and porous Ag: towards the development of a highly

sensitive and selective non-enzymatic glucose sensor. Journal of Materials Chemistry 2010; 20(44) 9918-9926.

[231] Ding Y, Liu Y, Parisi J, Zhang L, Lei Y. A novel NiO-Au hybrid nanobelts based sensor for sensitive and selective glucose detection. Biosensors & Bioelectronics 2011; 28(1) 393-398.

[232] Ding Y, Liu Y, Zhang L, Wang Y, Bellagamba M, Parisi J, Li CM, Lei Y. Sensitive and selective nonenzymatic glucose detection using functional NiO-Pt hybrid nanofibers. Electrochimica Acta 2011; 58 209-214.

[233] Cao F, Guo S, Ma H, Yang G, Yang S, Gong J. Highly sensitive nonenzymatic glucose sensor based on electrospun copper oxide-doped nickel oxide composite microfibers. Talanta 2011; 86 214-220.

[234] Ding Y, Wang Y, Zhang L, Zhang H, Lei Y. Preparation, characterization and application of novel conductive NiO-CdO nanofibers with dislocation feature. Journal of Materials Chemistry 2012; 22(3) 980-986.

[235] Ding Y, Hou C, Li B, Lei Y. Sensitive hydrazine detection using a porous Mn_2O_3 nanofibers-based sensor. Electroanalysis 2011; 23(5) 1245-1251.

[236] Wang Y, Wang W, Song W. Binary CuO/Co_3O_4 nanofibers for ultrafast and amplified electrochemical sensing of fructose. Electrochimica Acta 2011; 56(27) 10191-10196.

[237] Ding Y, Wang Y, Li B, Lei Y. Electrospun hemoglobin microbelts based biosensor for sensitive detection of hydrogen peroxide and nitrite. Biosensors & Bioelectronics 2010; 25(9) 2009-2015.

[238] Ding Y, Wang Y, Lei Y. Direct electrochemistry and electrocatalysis of novel single-walled carbon nanotubes–hemoglobin composite microbelts—Towards the development of sensitive and mediator-free biosensor. Biosensors & Bioelectronics 2010; 26(2) 390-397.

[239] Ding Y, Wang Y, Zhang L, Zhang H, Li CM, Lei Y. Preparation of TiO_2-Pt hybrid nanofibers and their application for sensitive hydrazine detection. Nanoscale 2011; 3(3) 1149-1157.

[240] Shen J, Yang X, Zhu Y, Kang H, Cao H, Li C. Gold-coated silica-fiber hybrid materials for application in a novel hydrogen peroxide biosensor. Biosensors & Bioelectronics 2012; 34(1) 132-136.

[241] Clark LC, Lyons C. Electrode systems for continuous monitoring in cardiovascular surgery. Annals of the New York Academy of Sciences 1962; 102(1) 29-45.

[242] Wang J. Carbon-nanotube based electrochemical biosensors: A review. Electroanalysis 2005; 17(1) 7-14.

[243] Scampicchio M, Bulbarello A, Arecchi A, Mannino S. Electrospun nanofibers as selective barrier to the electrochemical polyphenol oxidation. Electrochemistry Communications 2008; 10(7) 991-994.

[244] Vamvakaki V, Tsagaraki K, Chaniotakis N. Carbon nanofiber-based glucose biosensor. Analytical Chemistry 2006; 78(15) 5538-5542.

[245] Huang JS, Liu Y, You TY. Carbon nanofiber based electrochemical biosensors: A review. Analytical Methods 2010; 2(3) 202-211.

[246] Liu Y, Wang DW, Huang JS, Hou HQ, You TY. Highly sensitive composite electrode based on electrospun carbon nanofibers and ionic liquid. Electrochemistry Communications 2010; 12(8) 1108-1111.

[247] Im JS, Kim JG, Bae T-S, Yu H-R, Lee Y-S. Surface modification of electrospun spherical activated carbon for a high-performance biosensor electrode. Sensors and Actuators B-chemical 2011; 158(1) 151-158.

[248] Im JS, Yun J, Kim JG, Bae T-S, Lee Y-S. The effects of carbon nanotube addition and oxyfluorination on the glucose-sensing capabilities of glucose oxidase-coated carbon fiber electrodes. Applied Surface Science 2012; 258(7) 2219-2225.

Chapter 3

Chitin Nanofibers, Preparations and Applications

Shinsuke Ifuku, Zameer Shervani and
Hiroyuki Saimoto

Additional information is available at the end of the chapter

http://dx.doi.org/10.5772/57095

1. Introduction

Chitin nanofibers (CNFs) are mainly extracted from crab and prawn shells [1, 2] and recetly found in small amount in edible species of mushrooms [3]. CNFs are composed of chitin compound. Chitin in powder form is obtained from fish industry wastes which is otherwise thrown as industrial waste. Since CNFs are biodegradable having typical width 10-20 nm and large surface-to-mass ratio thus they are being prepared, studied, and applied more recently world wide along with rapidly growing field nanotechnology dealing with the better properties of materials when their sizes are smaller in the range 1-100 nm. Fibrilated chitin in the form of highly viscous gel suspension in water has found scope in pharmaceuticals [4], chiral separation [5], fillers in silsesquioxane [6]. When blended with inorganic metals to prepare advanced hybrid organic-inorganic composites they can have applications in electronics, electrical, optical devices and much needed solar energy production.

To introduce NFs, cellulose NFs are most important as cellulose is most abundant and readily available from plant cell walls and also produced by bacteria. Thus cellulose NFs must be most existing and easily available in nature. Attempt was successful to apply the cellulose NFs by using bacterial cellulose of the width 50 nm [7]. Though the diameter of NFs was 50 nm, larger compared to latter extracted by researchers [8], fibers worked as nanofillers in the cavities of polymerized acrylic resin. A visible light (400-800 nm) transparent flexible sheet of cellulose NFs reinforced acrylic resin polymer was obtained that showed a transmittance value of 85% at 600 nm wavelength when NFs content was 60 wt%. Prepared sheet was highly transparent due to the nanosized effect of NFs as the size of fibers was one-tenth of the wavelength of light that made material free from scattering therefore sheet was transparent. Thus authors claimed that the NFs of 50 nm width can have scope in optical devices such as displays. In year 2007, Abe et al. [8] extracted cellulose NFs of 15 nm width from Radiata pine tree wood powder

using a series of chemical treatments followed by mechanical grinding. The width of the fibers was measured by field emission scanning electron microscopy (FE-SEM). The authors were first successfully reduced the size of extracted NFs from 50 to 15 nm from any natural resources.

Chitin is second most plentiful biomaterial [9] next to cellulose exists on earth with yearly production of 10^{11} tons. Chitin raw dried powder is manufactured from exoskeleton of sea food shellfish, crabs, shrimps, and insects and edible mushrooms of fungus species and sea weed algae. Chitin content in fish industrial waste is 8-33% which is thrown if not used. Thus our group is actively engaged in developing chitin research to make a number of products from atomized or fibrillated chitin in the form of chitin nanofibers (CNFs) and its derivatives [10-13]. Chitin obtained from its natural resources is highly crystalline and most of it is α-chitin conformation though the contents of α- and βchitin depends on the source.

We have published a number of review articles [11, 14, 15] covering back ground of CNFs in detail, method of preparation, sources, composition, physical and chemical properties, characterization, their composites and derivatives preparations, surface modification. Commercialization of dry chitin powder and CNFs has also been described. For atomization or fibrillation of 1 wt.% wet chitin to CNFs three types of methods were used and compared. A very recently developed [10] Star Burst atomization system which employed high pressure water jet system where slurry of chitin in high acetic acid medium is introduced in chamber of Star Burst system machine where it is fibrilized into NFs of width (18.0-19.0 nm). Atomizataion occurred in this newly developed machine chamber by collision to ceramic ball that throws out fine fibrillated NFs at extremely high pressure of 245 MPa through an out let nozzle. The two other commonly used apparatus used for fibrillation are a blender and grinder. The advantages of Star Burst system over blender or grinder for fibrillation have been described in article [10] published recently. CNFs obtained by Star Burst system were studied thoroughly recording FE-SEM images of fibers obtained after a number of passes up to ten. The width of NFs decreased from 19.0 nm to 16.5 nm when number of passes increased from one to ten, respectively. Effect of number of passes on the CNFs properties was investigated by FT-IR, XRD profiles of chitin. In review article [11] molecular structure of chitin, hierarchical organization on the surface of crab shell exoskeleton and isolation from crab and prawn shell has been described. Method of isolation of CNFs from crab or prawn shell using a number of chemical treatments followed by grinder treatment has been explained. The width of NFs was determined by FE-SEM recordings, NFs of 10-20 nm diameter with high aspect ratio were obtained after one pass. FE-SEM images were recorded of stepwise isolation of NFs, just after removing the matrix components and after one pass treatment in acetic acid and without acetic acid condition. Without grinding treatment the fibers were like accumulated ribbons, after one pass treatment without acid the fibers were not separated but in acidic condition after one pass the fibers separated due to repulsion among the positive charges generated on the surface of fibers in acidic conditions. Chitin NFs were modified to produce novel green materials into nano-whiskers of width 6.2 nm and length 250 nm when fibers were deacetylated by treating with 33% NaOH. This contribution discusses most recent advances in preparation, derivatization, characterization and applications of CNFs. Most of the work has been conducted in our laboratory and we have also discussed the results from other groups as well.

http://dx.doi.org/10.5772/57095

2. Preparation of CNFs from crab and prawn shells, and mushrooms

2.1. CNFs from crab shells

Commercial grade dried crab shell flakes of species *Paralithodes camtschaticus* (red king crab) were used as a raw starting material to isolate NFs. Flakes from red king crab shell are so cheap and abundant that they are used in fertilizer industry. Crab shells were crushed to powder and purified according to the well established method. 1 wt.% slurry of crab chitin was prepared by a series of chemical treatment described in a previous chapter [14]. In brief minerals were removed by HCl treatment, suspension was filtered and washed thoroughly with distilled water, removal of proteins was done by refluxing the suspension with NaOH, pigments and lipids were removed by ethanol. After completion of above the treatments, suspension was filtered washed with distilled water and kept wet for mechanical grinding for fibrillation, this wet slurry was made to a concentration of 1 wt.% and called chitin slurry. Chemical treatment loosened the tightly bonded fibrils bundles to larger extent apart from removal of minerals, proteins, pigments, and lipids as shown in Fig. 1a and b.

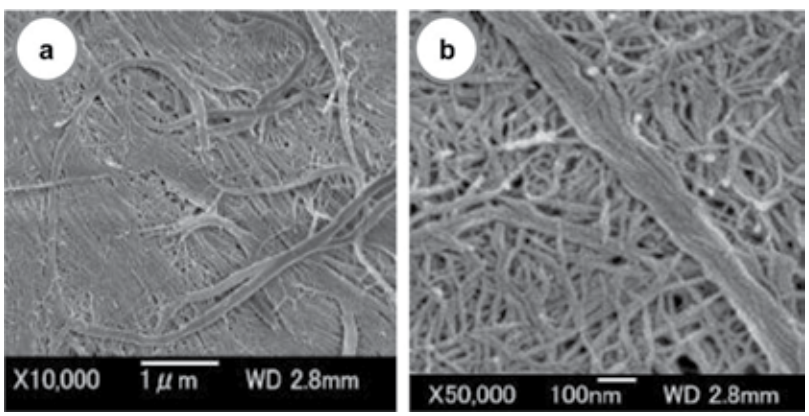

Figure 1. FE-SEM images of crab shell surface after removal of matrix from shell surface by chemical treatment without mechanical grinding at different magnification scales; a) 1000 nm; b) 100 nm. Reprinted with permission from ref. 1. Copyright 2009, American Chemical Society.

Bundles of NFs of width 30 nm are visible in micrographs without mechanical grinding. For fibrillation, 1 wt.% slurry was passed through a grinder of the model (MKCA6-3; Masuko Sangyo Co., Ltd.). After passing through the grinder, chitin slurry changed to highly viscous stable wet gel of CNFs. To record FE-SEM picture of sample, sheet of chitin material was prepared. Sheet was coated with 2 nm layer of platinum by an ion sputter coating before recording SEM micrographs. Chitin slurry was passed for one cycle through grinder at pH 7 and 3. As shown in Fig. 2a at neutral pH, fibers had width in wider range 10-100 nm. The bundles of embedded chitin-protein fibers were fibrillated successfully by grinding of wet chitin. It was easy to remove protein from water soaked chitin to isolate chitin fibrils. Authors [16] reported preparation method of CNFs from wet squid pen β-chitin at pH 3–4. In acidic

condition at low pH cationization of C2 amino groups in β-chitin occurred resulted in more dispersed and stable phase because of electrostatic repulsion. Similar electrostatic phenomena occurred at low pH of 3 when amino groups cationized in preparation of CNFs from α-chitin obtained from crab shell in one grinding pass in acidic condition by our research group [1]. Fine fibrils in the narrow range of 10-20 nm were obtained as shown in Fig. 2b and c. Chitin slurry of 1 wt.% became a highly viscous gel phase after one cycle of grinding treatment is due to large surface area of NFs. Viscous gel phase formation is the indication that fibrillation was successful in one cycle of grinding and it was more facilitated in acidic medium as unbroken high aspect ratio NFs were visible in FE-SEM images.

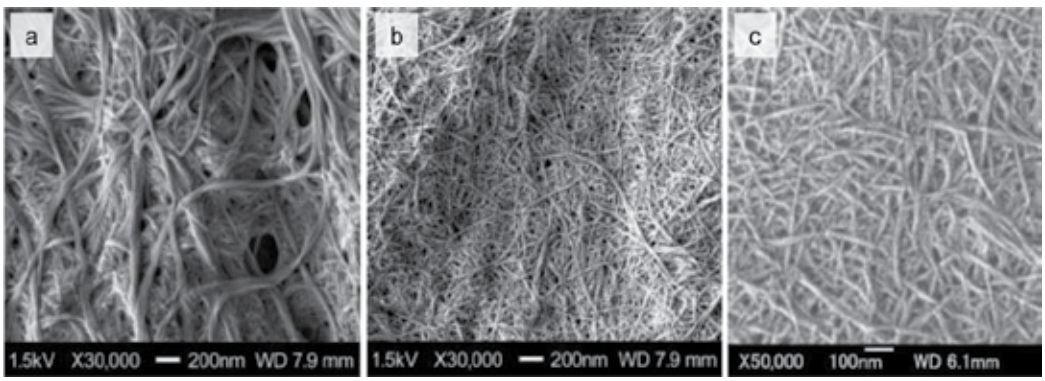

Figure 2. FE-SEM pictures CNFs prepared from crab shell after one cycle of grinding at pH values; a) pH 7; b and c) pH 3; the scale is a and b) 400 nm, c) 200 nm. Reprinted with permission from ref. 1. Copyright 2009, American Chemical Society.

2.2. CNFs from prawn shell

In section 2.1, CNFs were isolated successfully from crab shells flakes in acidic medium with uniform width (10-20 nm) and high aspect ratio after series of chemical treatments followed by one pass of mechanical grinding. Acidic pool and excess acetic acid, however, in CNFs is a matter of worry for applications of NFs especially in pharmaceutical, cosmetic, biomedical industries. Acidic contamination of NFs for above applications is an important issue to address from toxicity viewpoint. Removal of acid from NFs is difficult, complicated, and make products expensive. Therefore preparation of CNFs in normal condition of neutral pH is utmost and immediate necessity to apply them for above products. CNFs from prawn shells have been extracted under neutral conditions without addition of any acid. Fresh shells of prawn species *Penaeus monodon* (black tiger prawn) was used to prepare CNFs. Prawns are cultivated on large scale world wide and its shells are thrown as industrial waste. Chemical treatments to remove minerals, pigments and proteins and lipids are same for prawn [2] as described for isolation of chitin from crab shells. In brief, addition of NaOH and HCl removed proteins and minerals, respectively leaving the chitin and pigments in shell. Pigments were removed with ethanol extraction. Yield of dry chitin from prawn shells was 16.7%. Degree of deacetylation (DDA) of prepared samples determined by the content of C and N by elemental analysis was 7%. SEM

http://dx.doi.org/10.5772/57095

micrograph of the black tiger prawn shell surface after removal of the matrix components is shown in Fig. 3. SEM picture shows exocuticle which is the main part of the prawn shells. It is important that uniform CNFs with an elaborate interwoven structure is clearly visible in the image. 1 wt.% chemically treated chitin suspension was crushed by a domestic blender and passed through a grinder for fibrillation without addition of acid. Chitin slurry obtained was high viscous gel after a single grinding treatment similar to that observed in CNFs from crab shell. Fig 4a and b are the SEM images of one pass NFs at different magnifications. The width of NFs was 10–20 nm. In crab shell NFs at neutral pH, width of the fibers was widely distributed in range 10-100 nm after single grinding pases. Thus preparation of NFs from prawn shells is much advantageous than crab shell. Using prawn shells, thin, homogeneous, uniformly distributed, well separated, and large aspect ratio CNFs were successfully prepared in neutral medium with much superiority over acidic crab shell preparations to apply for a number of industrial applications. The explanation we have given of fibrillation of prawn shell achieved at neutral pH unlike to crab shell that occurred at pH 3 is following. The outer most skeleton (exoskeleton) of prawn or crab shell is made up of two parts exocuticle and endocuticle. Exocuticle has a very fine interwoven plywood type structure, endocuticle is rather more coarse and has thick fibers as shown in Fig.1. 90% of crab shell is made up of these thicker endocuticular fibers [17]. Thus a low pH of 3 medium is used to obtain nanofibrils in crab shell. On the other hand the exoskeleton of prawn including black tiger prawn made up of mostly semitransparent soft shell of fine exocuticle as shown in Fig. 3, thus their fibrillation occurs easier than crab shell at neutral pH. The preparation for CNFs from prawn shells in neutral pH is also valid to other species of prawn as described in article [2].

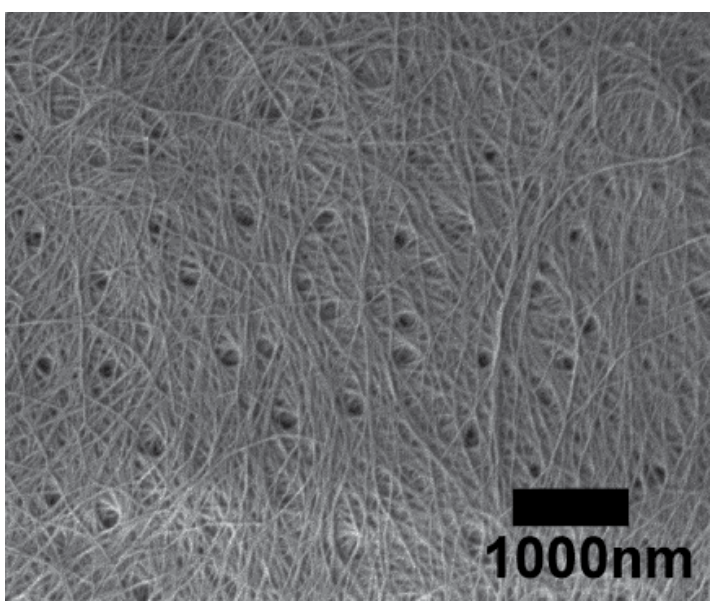

Figure 3. FE-SEM image of black tiger prawn after chemical treatment. Reproduced with permission from ref. 2. Copyright 2011, Elsevier.

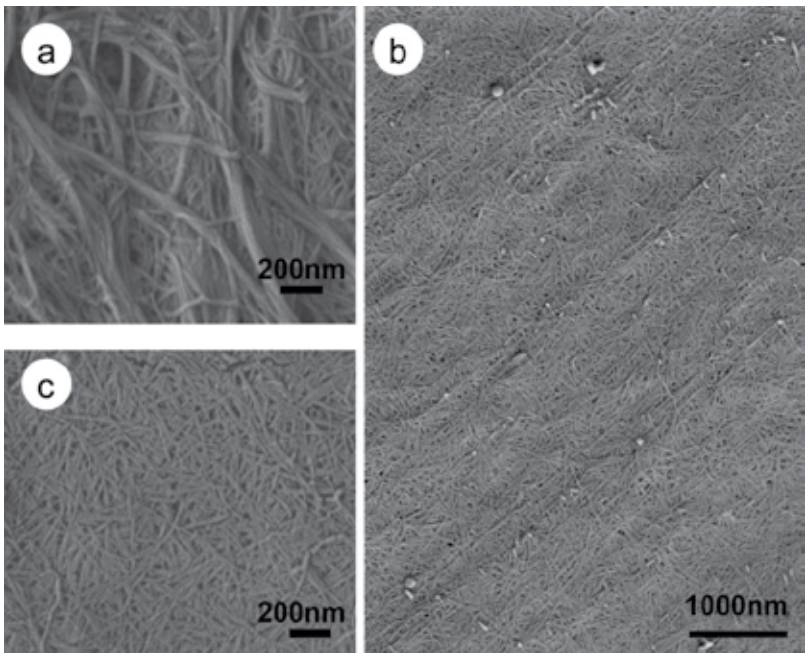

Figure 4. FE-SEM image of black tiger prawn NFs after one pass in grinder at neutral pH; a) scale: 1000 nm, b) scale: 200 nm. Reproduced with permission from ref. 2. Copyright 2011, Elsevier.

2.3. Nanofibrillation of dry chitin powder by Star Burst system

Authors [10] used new fibrillation machine Star Burst system (SBS) developed by Sugino Machine Co., Ltd. to prepare NFs from commercially available dry α-chitin powder from crab shell with and without acetic acid medium. The working principle of SBS instrument has been described in introduction part of the review. Instrument uses high pressure water jet to atomized the chitin slurry into NFs. FE-SEM showed that NFs became thinner as the number of SB passes increased. Fibers were thinner in acidic medium than neutral conditions. NFs prepared in SBS were thinner than reported earlier [1] using grinder in acidic medium. XRD recording showed that SBS did not damage NFs and did not reduce crystallinity.

Fig. 5 shows FE-SEM micrographs of CNFs after SB treatments under a neutral aqueous condition. After one pass, the chitin was not fibrillated (Fig. 5(a)). Thick aggregates of CNFs were observed. There was a significant change in the morphology of CFs after the treatment with five and ten passes (Fig. 5b, c, d, and e). In five and ten passes the NFs are fibrillated as shown in Fig. 5c and e on maginification of 300 nm. The width of fibers in five passes is 18.2 and it reduced to 17.3 nm in ten passes. Thus SBS is powerful tools to give fibers of very thin diameter even without acetic acid solution pool. If we consider the atomization of CNFs in SBS with acetic acid then even in one pass fibrillation occurred as shown in Fig. 6a, b.). Fibrillation completed in five passes as can be seen from SEM pictures Fig. 6d, c.), while processing the fibers in ten passes the thickness of fibers decreases while aspect ratio reduced as fibers breaks

due to over processing as can be seen from SEM pictures Fig. 6e and f.). Fiber thickness in one, five, and ten passes are 19.0, 18.0, and 16.5 nm, respectively. It is very noteworthy that advatage of very renetly developed advanced technology high pressure jet SBS can atomized chitin slurry with or wthout acetic acid in just five passes to give NFs of small diameter (18.0-18.2 nm) and with high aspect ratio. Increasing number of passes to ten that is considered over processing decreases the width of NFs to very smaller extent. So five passes are optimum with or wthout acetic acid medium.

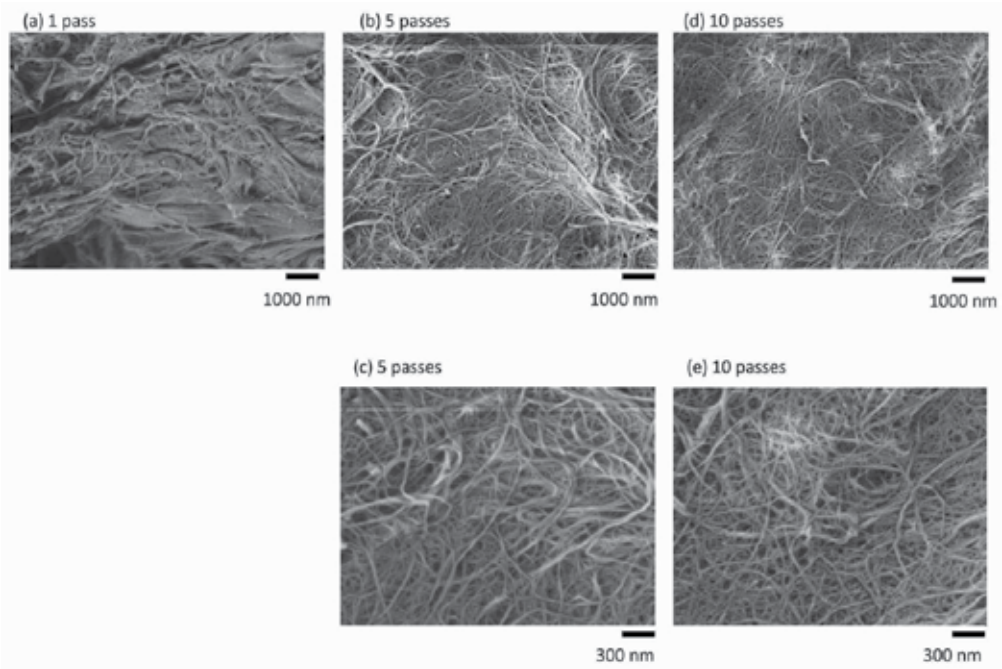

Figure 5. FE-SEM of CNFs; a) one pass, b and c) 5 passes, d and e) 10 passes prepared by SBS instrument without acetic acid. The scales are shown in the pictures. Reprinted from ref. 10.

2.4. Characterization of CNFs by FT-IR and XRD recoding

Fig. 7 shows the FT-IR spectra of chitin fibers treated by the Star Burst system after 1, 5, and 10 passes under both neutral and acidic conditions. All spectra of obtained of CNFs showed that spectral features are in excellent agreement with the spectrum of commercial chitin. In particular the OH stretching band at 3424 cm^{-1}, NH stretching band at 3259 cm^{-1}, amide band I at 1652 and 1621 cm^{-1}, and amide II band at 1554 cm^{-1} of the CNFs are observed. These absorption peaks are especially characteristic of chitin. This suggests that original chemical structures of chitin were maintained even after 10 passes of Star Burst mechanical treatments with or without acidic pool. Fig. 8 are the XRD pattern of commercial chitin and processesed CNFs. X-ray diffraction profiles of CNFS processed by the Star Burst system after several passes under both neutral and acidic conditions. All diffraction patterns coincide closely with

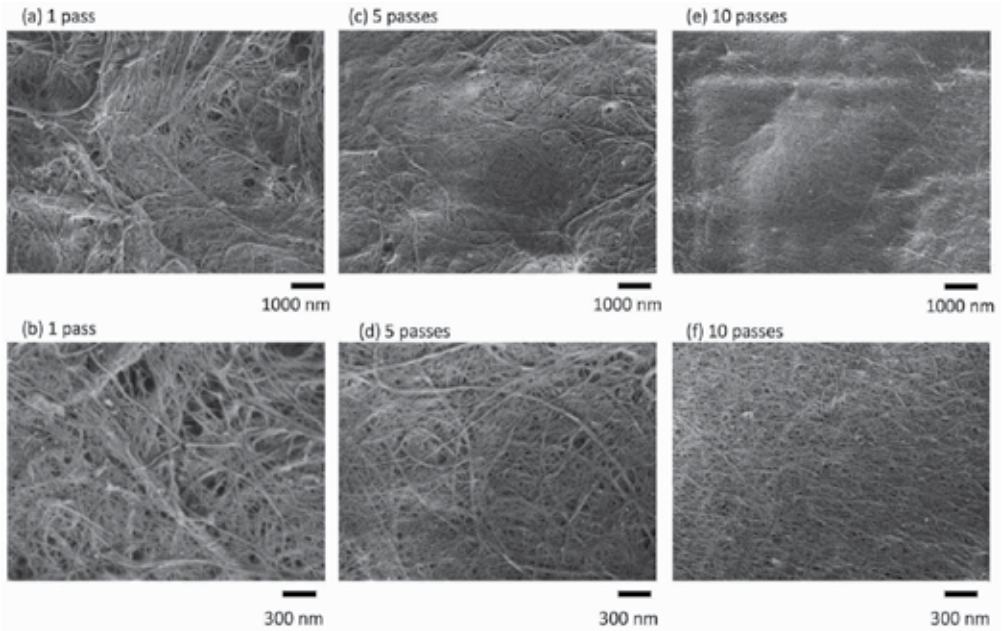

Figure 6. FE-SEM of CNFs; a and b) one pass, c and d) 5 passes, e and f) 10 passes prepared by SBS instrument with acetic acid. The scales are shown in the pictures. Reprinted from ref. 10.

original chitin powder. The four diffraction peaks of the CNFs observed at two θ= 9.2, 19.1, 20.9, and 23.1◦ corresponded to 020, 110, 120, and 130 planes, respectively [18]. They were typical antiparallel crystal patterns of α-chitin. Thus, the original crystalline structure was maintained after the purification process followed by the Star Burst treatments. Following are the relative crystalline indices of CNFs determined from X-ray diffraction profiles. Original chitin powder has a comparatively high crystallinity of 83.7%. After the Star Burst process under both acidic and neutral conditions, there was no significant difference in the relative degree of crystallinity after the various numbers of passes. This result indicates that at least 10 mechanical treatments with the SBS did not damage the CFs, even though the system used a super high pressure water jet operated at 245 MPa.

2.5. Preparation of CNFs from edible mushrooms

CNFs were isolated and charecterized [3] from cell wall of edible mushrooms by a number of chemical treatments to remove glucans, minerals, and proteins associated with mushrooms followed by grinding treatment in acidic medium. NFs width was in the range 20-28 nm depending on the type of mushroom used. The goal of extraction of CNFs from edible mushrooms of nano-sized scale fibers is to develop novel functional food materials. The detailed extraction method and final SEM images of NFs extracted and methods employed to characterize them have been described below. The mushrooms species *Pleuotus eryngii* (king trumpet mushroom), *Agaricus bisporus* (common mushroom), *Lentinula edodes* (shiitake), *Grifola frondosa* (maitake), and *Hypsizygus marmoreus* (buna-shimeji) commonly used for human

http://dx.doi.org/10.5772/57095

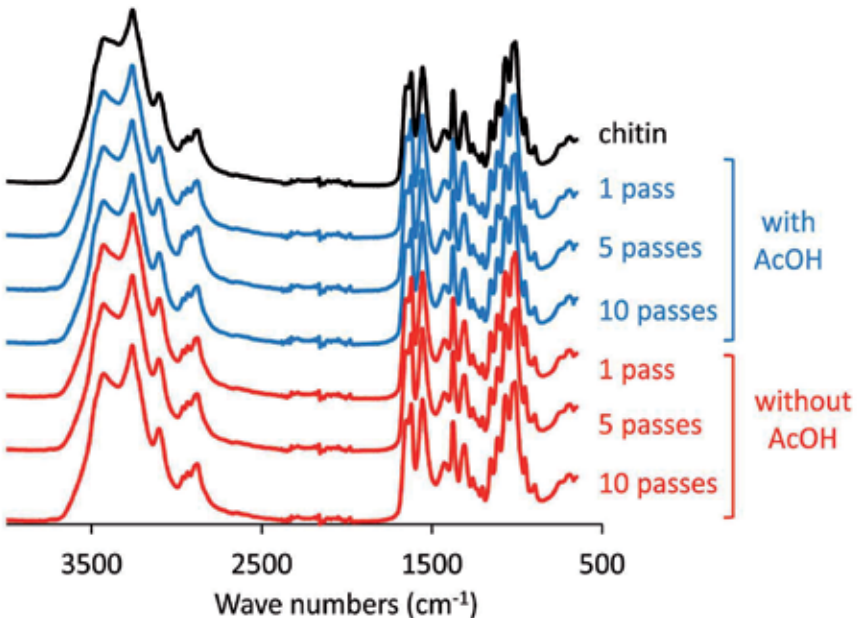

Figure 7. FT-IR spectra of chitin fibers after 1, 5, and 10 passes through Star Burst with and without acetic acid. Reprinted from ref. 10.

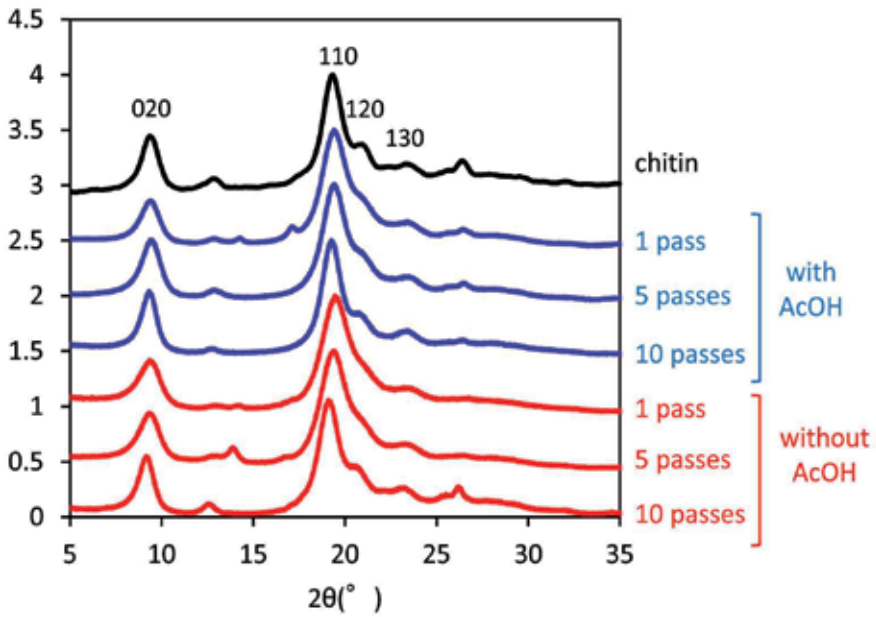

Figure 8. X-ray diffraction profiles of chitin fibers after 1, 5, and 10 passes through Star Burst with and without acetic acid. Reprinted from ref. 10.

consumption were used in this study. The purification was done by a series of chemical treatments to remove associated compounds: proteins, pigments, glucans, and minerals according to the following procedure. Sodium hydroxide was used to dissolve, hydrolyze, and remove proteins and alkali soluble glucans. Hydorochloric acid was used to remove minerals. At this stage partial neutral saccharides and acid soluble protein compounds were also removed. The extraction step with sodium chlorite and acetic acid removed pigments from the sample. At final stage, the sample was treated with sodium hydroxide again to eliminate and remove the residual glucans including trace amount of proteins. After chemical treatment if the extracted mass allowed to dry, it causes strong hydrogen bonding between CNFs when all matrix substances are washed away which makes it difficult to fibrillate chitin to NFs. Thus the sample was kept wet after removal of the matrix for preparation of CNFs. The purified sample with 1 wt.% content of chitin was passed through a grinder for nano-fibrillation in acetic acid medium at pH 3. After grinder treatment, the chitin homogeneous stable dispersed slurry of chitin with high viscosity was obtained resulted due to high surface-to-volume ratio of NFs thus finally the sample was successfully fibrillated. Fig. 9 shows SEM images of CNFs from five mushrooms after removing matrix components and one pass though the grinder. The isolated chitins are well fibrillated and uniform. The width of the fibers was in the range 20-28 nm depending on the species of mushroom. The yield of CNFs contents in mushrooms was not so high as in crab or prawn shells, it was merely in the range 1.3-3.5 wt.% depending on the species of mushrooms.

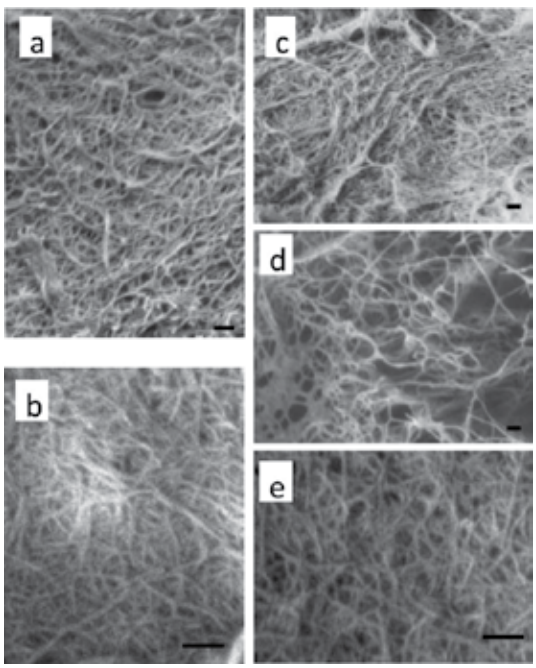

Figure 9. FE-SEM images of CNFs prepared from a) *Pleuotus eryngii*, b) *Agaricus bisporus*, c) *Lentinula edodes*, d) *Grifola frondosa*, e) *Hypsizygus marmoreus*. The scale bars are 200 nm. Reprinted from ref. 3.

http://dx.doi.org/10.5772/57095

FT-IR and XRD spectrometry were employed to characterized the CNFs from mushrooms. FT-IR spectra (Fig. 10) of commercially available chitin derived from crab shell and CNFs from 5 types of mushroom were compared for analysis. The major bands of the spectra of CNFs are in agreement with commercial chitin. Similarly XRD of commercially available chitin and the CNFs prepared from five types of mushrooms were compared (Fig. 11). The four diffraction bands of CNFs are typical crystal patterns of α-chitin. Thus, CNFs extracted from several types of mushroom maintained α-chitin crystalline structures after the removal of matrix substances followed by grinder treatment. However, in the case of *Hypsizygus marmoreus*, X-ray diffractogram (Fig. 11f) contains crystal patterns of cellulose (Fig. 11g). The diffraction peaks observed from 15° to 17°, and 22.5°, corresponding to the 110, 1–10, and 200 planes, respectively are typical for the cellulose I crystal.

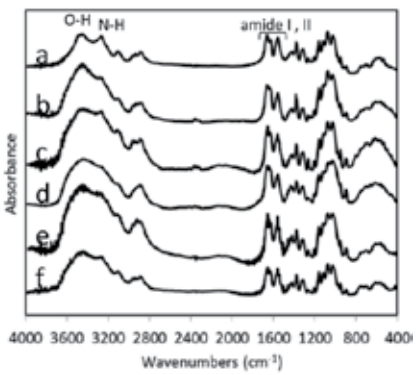

Figure 10. FT-IR spectra of a) commercial chitin, and CNFs from mushroom source of species b) *Lentinula edodes*, c) *Pleuotus eryngii*, d) *Hypsizygus marmoreus,* e) *Grifola frondos,* and f) *Agaricus bisporus*. Reprinted from ref. 3.

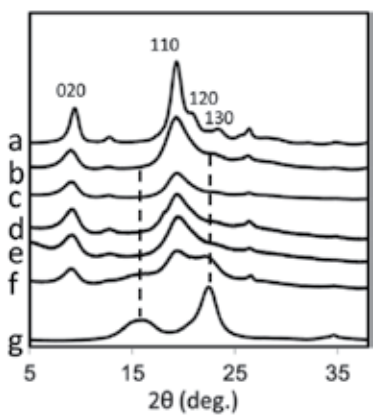

Figure 11. XRD pattern of a) commercial chitin, and CNFs from mushroom source of species b) *Pleuotus eryngii*, c) *Agaricus bisporus*, d) *Lentinula edodes*, e) *Grifola frondos*, f) *Hypsizygus marmoreus,* and g) commercially available cellulose. Reprinted from ref. 3.

3. CNFs nanocomposites

Very recently [6] new nanocomposite films of CNFs reinforced silsesquioxane-urethaneacrylate (SSQ-UA) copolymer were prepared. CNFs-SSQ-UA nanocomposite films were highly transparent due to filling of nanometer sized (10-20 nm) CNFs inside the hybrid inorganic-organic SSQ-UA copolymer. CNFs due their crystalline structure drastically increased the Young's moduli and the tensile strengths of the composite and decreased the coefficient of thermal expansion (CTE). High thermal stability of polysilsesquioxane improved heat resistance of CNFs. The composite in the ratio of SSQ/UA = 5/0, 4/1, 3/2, 2/3, and 1/4, was prepared and blended with CNFs and copolymerized using a photo initiator 2-Hydroxy-2-methylpropiophenone then cured for free radical polymerization by UV irradiation for 8 min at 40 mW cm^{-1} (SPOT CURE SP-7, Ushio Inc).

3.1. Optical properties of CNFs composites

Fig. 12 shows % transmittance vs wavelength (nm) of composite film. Neat CNF sheet was not transparent as % transmittance is nil in visible region and interpreted at 600 nm for all composites. While neat poly-SSQ film had approximately 90% transmittance. After SSQ-UA matrix impregnation and subsequent polymerization, the obtained CNFs nanocomposites in different ratio of SSQ/UA became highly transparent for visible light. CNFs sheets blended with SSQ-UA had good transparency (85% at 600 nm) in case of SSQ/UA ratio 5/0. Blending with 1/4 ratio of SSQ/UA, CNFs sheet transparency decreased slightly to 80% compared with 85% for 5/0 blending ratio of SSQ/UA. The composite films became transparent due to nano-sized composition of CNF sheet. Since the width (10-20 nm) of CNFs was much shorter than the wavelength of visible light (approximately 400-800 nm), the nanocomposites cause less light scattering than a microfiber reinforced composite at the interface between nanofiber and SSQ-UA matrix. At 600 nm since transmittance of nanocomposites were 85-80%, the optical loss caused by nanofiber reinforcement were only in the range 5-10% despite the high fiber content of 50 wt.%. The transmittance of nanocomposites increased as ratio of SSQ increased. The chitin nanofiber sheet obtained in this study can be available like a paper, though the novelty of the paper is composed of nano-meter thick fibers. Several patterns can be printed on the nanofiber paper that we have prepared using a domestic inkjet printer (Fig. 13a). The printed NF paper became transparent (Fig. 13b) after matrix impregnation. This newly established technique of transparent printing on such a thin (70 μm) composite sheet can have application in printing of wiring used in electronic devices or electronic papers.

3.2. Thermal properties of composites

Fig. 14 shows the CTE of neat CNFs and its composites. Although neat poly-SSQ (SSQ/UA = 5/0) was too fragile to measure the thermal expansion, the CNF reinforced nanocomposite was tough for CTE measurement. CTE of CNF sheet without SSQ matrix was only 8.0×10^{-6} K^{-1}. While CTE of SSQ-UA copolymer films without CNFs were high in the range $96.2\text{-}164.0 \times 10^{-6}$ K^{-1} depending on the ratio of SSQ/UA as shown by bars in Fig. 14. CTEs of all nanocomposites decreased significantly to a constant value of 30×10^{-6} K^{-1}. These values corresponded to 66 to

http://dx.doi.org/10.5772/57095

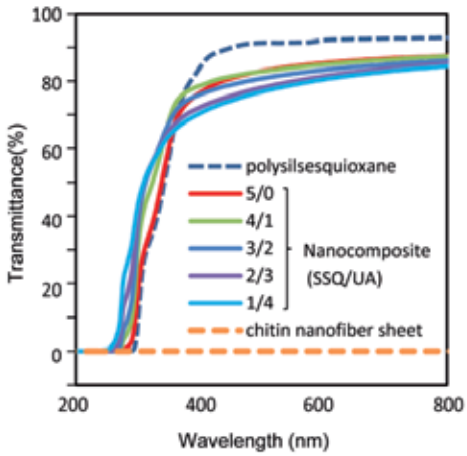

Figure 12. Regular light transmittance spectra of CNFs composite film, the material of which measurements were conducted are shown in the inset of figure. Reproduced with permission from ref. 6. Copyright 2012, Elsevier.

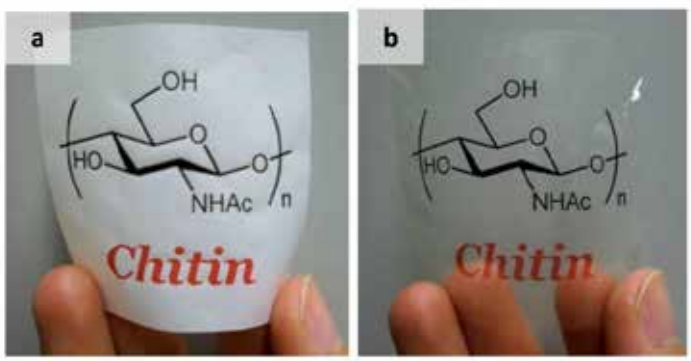

Figure 13. CNFs sheet a) without blending with SSQ-UA matrix; b) after blending with SSQ-UA matrix followed by copolymerization by UV irradiation. Reproduced with permission from ref. 6. Copyright 2012, Elsevier.

81% decreased compared to the corresponding to neat SSQ-UA matrices. Thus, CNFs with low CTE worked effectively to decrease the thermal expansion of SSQ-UA copolymer film as a result of reinforcement.

3.3. Mechanical characterization of composites

Fig. 15 shows Young's moduli and tensile strengths of SSQ-UA copolymer films and their CNFs composites. The Young's moduli of SSQ-UA with the ratio of 3/2, 2/3, and 1/4 without CNFs decreased from 1,571 to 128 MPa with increasing the ratio of reactive diluent UA oligomer. This is due to decrease in crosslinking density with decreasing the amount of strengthening hybrid component SSQ. The SSQ-UA films with the ratio of 5/0 and 4/1 were too fragile to measure the mechanical properties so their bars are not shown in the Young's

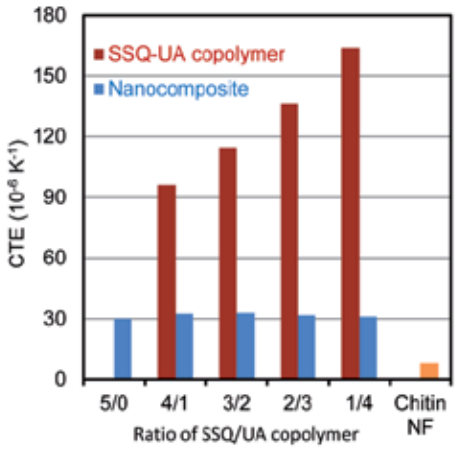

Figure 14. Coefficient of thermal expansion (CTE) of SSQ-UA copolymer films and SSQ-UA-CNFs composites. Reproduced with permission from ref. 6. Copyright 2012, Elsevier.

moduli plot. Nanocomposites were tough enough for the testing due to CNF support. The Young's moduli of these nanocomposites significantly increased and reached in the range 3.36 to 4.29 GPa. The tensile strengths also significantly increased in the range 31 to 59 MPa. It is important to notice that each Young's moduli and tensile strength of the chitin nanofiber composites were higher than that of CNF sheet or SSQ-UA copolymer. The higher Young's moduli and tensile strength of composite is due to SSQ-UA matrix embedded in every space of CNF sheet and strongly interacts with NF at the interface thus resulted in the increase of the reinforcement effect. The enhancements of mechanical properties of composite strongly support that a CNF sheet with a high Young's modulus (1.80 GPa) and a high tensile strength (30 MPa) worked effectively as a reinforcement filler for SSQ-UA copolymer.

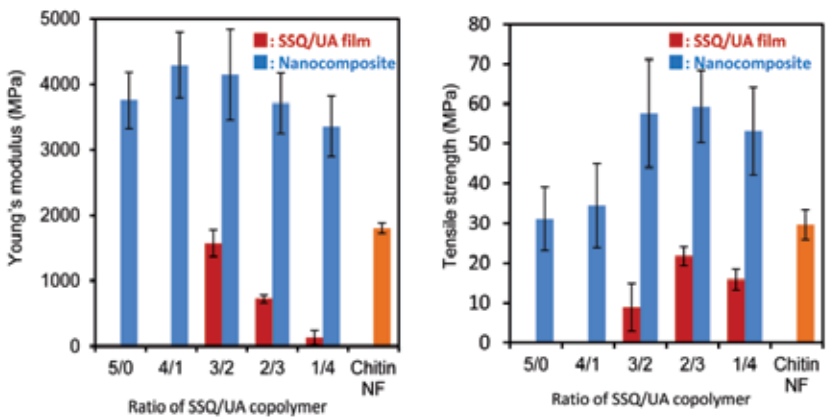

Figure 15. Young's modulus and tensile strength of SSQ-UA copolymer and SSQ-UA-CNFs composites. Reproduced with permission from ref. 6. Copyright 2012, Elsevier.

http://dx.doi.org/10.5772/57095

4. Preventive effect of CNF on dextran sulfate sodium (DSS)-induced ulcerative colitis (UC)

In this section we describe the medical aspect of CNFs taking a model of DSS- induced colitis in mouse as investigated by Azuma et al [4]. The effect of CNFs on disease activity index such as weight loose, loose stools, and bleeding symptoms in colitis were studied. CNFs administered mouse exhibited a significant reduced in disease activity index. Colon length increased that was shortened due to DSS induction by administration of CNFs compared to control. Damage in intestinal mucosa was microscopically monitored as shown in Fig. 16. In CNFs group on 6th day erosion, crypt destruction, and edema were markedly suppressed compared to control. The number of myeloperoxidase (MPO)-positive cells lowered significantly compared to control group. Thus CNFs improved clinical symptoms in DSS-induced acute UC mouse model.

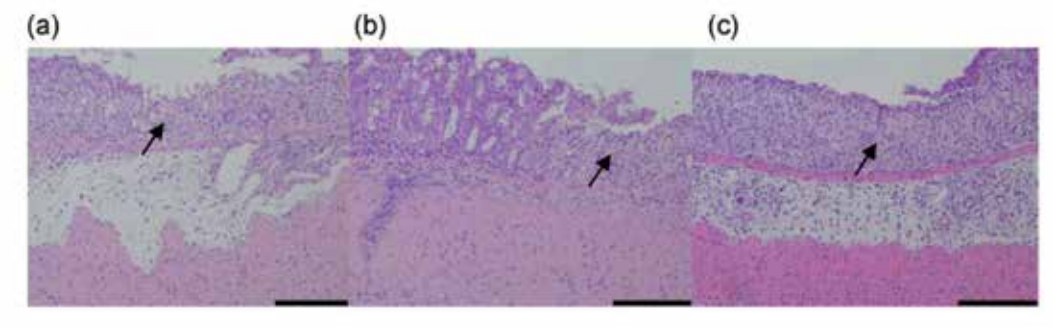

Figure 16. Effect of CNFs administration on histopathologicucedal changes in DSS-induced acute UC mice; a) control, b) CNFs, and c) chitin powder. Reproduced with permission from ref. 4. Copyright 2012, Elsevier.

5. Conclusion

Preparation of CNFs from crab, prawn shells, and a number of species of mushrooms have been discussed. Both chemical treatments and mechanical processing have been described in detail. CNFs prepared from crab shell, the presence of acidic medium was important to reduce the size of NFs. While in case of prawn shells the fibrillation was achieved in neutral conditions. Width of CNFs was 10-20 nm with high aspect ratio. After completion of fibrillation the CNFs were in physical state of wet gel of very high viscosity. Size of NFs was determined by recording FE-SEM of flakes or thin film of NFs. Apart from using grinder a newly developed high pressure jet atomization machine (Star Burst System; SBS) was also employed to fibrillate the NFs. Fibrillation was more effective when SBS was used that gave more thinner (19.0-16.5 nm) and homogeneous NFs compared to girder. NFs were characterized for chitin content by XRD and FT-IR measurements. CNFs were also prepared from five different species of edible

mushrooms, NFs of width 20-28 nm were obtained. But the chitin yield in mushroom was lower (1.3-3.5 wt.%) compared to crab (12.2 wt.%) or prawn (16.7 wt.%). SSQ-UA copolymer-CNFs transparent composite sheets or thin film ware prepared and their optical, thermal, and mechanical properties were investigated. The properties improved on blending CNFs with copolymer to larger extent which has increased the scope of CNFs. CNFs were found effective to DSS-induced UC disease in mouse colon, the UC symptoms removed and lowered the MPO-positive cell count decreased significantly.

Author details

Shinsuke Ifuku, Zameer Shervani and Hiroyuki Saimoto

Graduate School of Engineering, Tottori University, Koyama-cho Minami, Tottori, Japan

References

[1] Ifuku S., Nogi M., Abe K., Yoshioka M., Morimoto M., Saimoto H., Yano H. Preparation of chitin nanofibers with a uniform width as α-chitin from crab shells. Biomacromolecules, 2009; 10: 1584-1588.

[2] Ifuku S., Nogi M., Yoshioka M., Morimoto M., Yano H., Saimoto H. Simple preparation method of chitin nanofibers with a uniform width of 10-20 nm from prawn shell under neutral conditions. Carbohydrate Polymers, 2011; 84: 762-764.

[3] Ifuku S., Nomura R., Morimoto M., Saimoto H. Fabrication of chitin nanofibers with a width of 20 nm from mushrooms. Materials, 2011; 4: 1417-1425.

[4] Azuma K., Osaki T., Wakuda T., Ifuku S., Saimoto H., Tsuka T., Imagawa T., Okamoto Y., Minami S. Beneficial and preventive effect of chitin nanofibrils in a dextran sulfate sodium-induced acute ulcerative colitis model. Carbohydrate Polymers, 2012; 87: 1399-1403.

[5] Sueyoshi Y., Hashimoto T., Yoshikawa M., Ifuku S. Chitin nanofiber membranes for chiral separation. Sustainable Agriculture Research, 2012; 1(1): 42-47.

[6] Ifuku S., Ikuta A., Hosomi T., Kanaya S., Shervani Z., Morimoto M., Saimoto H. Preparation of polysilsesquioxane-urethaneacrylate copolymer film reinforced with chitin nanofibers. Carbohydrate Polymers, 2012; 89: 865-869.

[7] Yano H., Sugiyama J., Nakagaito AN., Nogi M., Matsuura T., Hikita M., Handa K. Optical transparent composites reinforced with networks of bacterial nanofibers. Advanced Materials, 2005; 17: 153-155.

[8] Abe K., Iwamoto S., Yano H. Obtaining cellulose nanofibers with a uniform width of 15 nm from wood. Biomacromolecules, 2007; 8: 3276–3278.

[9] Gopalan NK., Dufresne, A. Crab shell chitin whisker reinforced natural rubber nanocomposites. 1. Processing and swelling behavior. Biomacromolecules, 2003; 4: 657–665.

[10] Ifuku S., Yamada K., Morimoto M., Saimoto H. Nanofibrillation of dry chitin powder by star burst system. Journal of Nanomaterials, 2012; 2012.

[11] Ifuku S., Saimoto H. Chitin nanofibers: preparations, modification, and applications. Nanoscale, 2012; 4: 3308-3318.

[12] Ifuku S., Iwasaki M., Morimoto M., Saimoto H. polymerization of acrylic acid onto chitin nanofibers to improve dispersibility in basic water. Carbohydrate Polymers, 2012; 90: 623-627.

[13] Azuma K., Osaki T., Ifuku S., Saimoto H., Tsuka T., Imagawa T., Okamoto Y., Minami S. α-Chitin nanofibrils improve inflammatory and fibrosis responses in inflammatory bowel disease mice model. Carbohydrate Polymers, 2012; 90: 197-200.

[14] Ifuku S, Nakagaito AN., Saimoto M. Chitin nanofibers with a uniform width of 10 to 20 nm and their transparent nanocomposite films. In: Lin T. (ed.) Nanofibers, Production properties and functional applications. Rijeka: InTech; 2012. p59-84.

[15] Ifuku S, Nakagaito AN., Saimoto H. Preparation of Chitin Nanofibers with a Uniform Width of 10-20 nm from Crab and Prawn Shells and their Transparent Nanocomposite Films. In: Wythers MC. (ed.) Advances in materials science research. volume 12. New York: Nova Scientific Publishers; 2012. p313-322.

[16] Fan Y., Saito T., Isogai A. Preparation of chitin nanofibers from squid pen α-chitin by simple mechanical treatment under acid conditions. Biomacromolecules 2008; 9: 1919–1923.

[17] Chen PY., Lin, AY., McKittrick J., Meyers MA. Structure and mechanical properties of crab exoskeletons. Acta Biomateralia, 2008; 4: 587–596.

[18] Minke R., Blackwell J. The structure of α-chitin. Journal of Molecular Biology, 1978; 120: 167–181.

Chapter 4

Fabrication of Nanofibrous Scaffolds by Electrospinning

Kai Wei and Ick-Soo Kim

Additional information is available at the end of the chapter

http://dx.doi.org/10.5772/57093

1. Introduction

Continuous progress in surgical technologies and biomedical science has allowed tissue or whole-organ transplantation to become potential options to restore native functions such as regeneration of fractured or diseased bones. Unfortunately, the increasing demand for function transplants and the human aspiration for longer living far exceed the available supply of usable donor tissues. Transplantation technology has encountered severe limitations. Therefore, new technologies are needed to reduce this gap in clinical need versus available healthy tissue and organ supplies. In recent years, electrospinning has been employed as a leading technique for generating biomimetic scaffold made of synthetic and natural polymers for tissue engineering. This method can produce electrospun fibers with diameters in the range from several micrometers down to less than 100 nm that have a very high surface area to mass ratio. This kind of thee dimensional, fibrous scaffold with high porosity can closely biomimic that of native extracellular matrix. Thus, facilitate cell attachment, support cell growth and regulate cell differentiation [1, 2].

Silk filament derived from silkworm *Bombyx mori* is a natural protein mainly made of sericin and fibroin proteins, *i.e.*, sericin (the outer coating) and fibroin (the inner brins). The sericin protein is removed by a process called degumming in industry, so that the term silk is commonly improperly used to define only one of its two components, the silk fibroin. Silk fibroin is a typical fibrous protein that has been studied as a scaffold for tissue engineering because of its excellent biocompatible, bioabsorbability and low level of inflammatory potential [3–5]. In recent years regenerated silk fibroin nanofibers have been developed using electrospinning technique for tissue engineering [4, 5].

In tissue engineering *in vitro*, many researches were directed towards the development of novel hybrid nanofibers scaffold using regenerated silk fibroin by electrospinning technique [6–9] in order to improve cell adhesion, proliferation and differentiation behavior. In current

research, various electrospun nanofibers have been devised to prepare biomimetic nanocomposites for potential application in tissue engineering. For instance, Mather *et al.* prepared silica from nanofibers by immersion of the PEI/PVP (poly(ethylene imine)/poly(vinyl pyrrolidone)) nanofibers in silica precursor tetramethylorthosilicate (TMOS) and then calcinations [10]. A simple alternative to create silk/silica composites is to coat silk-based material templates with silica precursors (such as tetraethylorthosilicate (TEOS)) and subsequently heat them at 105 °C for several h, as was demonstrated with cocoon fibers of *Bombyx mori* fibroin silkworms [11]. Furthermore, the silk template can subsequently be removed by calcinations, yielding a porous material in which the pore structure is determined by the silk-based material.

Bioactive ceramics, such as hydroxyapatite (HA) has also been used in many medical applications in orthopedic and dental surgery owing to its osteoconductivity and osteophilicity [12–14]. In the past few years, various electrospun nanocomposite fibers, such as PCL/$CaCO_3$ [15], HA/gelatin [16], silk/HA [17], PLA/HA [18], and triphasic HA/collagen/PCL [19] had been devised and explored for potential bone regeneration applications. However, since most of these electrospun composite fibers were prepared by electrospinning of blends made by simply mixing the prior obtained inorganic nanoparticles with viscous spinning solutions of polymers, it usually results in nanocomposites with very limited or lacking of specific interactions between the organic and inorganic phases [20].

Besides the widely recognized merits of electrospun fibers, Core-sheath structural nanofibrous scaffold incorporated with bioactive agents is supposed to promote cell migration, proliferation, and gene expressions because the controllable and sustainable release of bioactive agents from the fibers and the preservation of bioactivity. A functional nanofibrous scaffolds incorporated with bioactive agents depends on two factors: the controllable and sustainable release of bioactive agents from the fibers and the preservation of bioactivity. A majority of the reported works on drug release scaffolds tends to adopt the route of simple mixing of bioactive agents and the carrier polymers for blend-electrospinning. The resultant blend formulation would usually lead to initial burst release of drug, which is undesirable for an effective and controllable device. [11] Moreover, simple blending of electrospinning dopes leads to the direct exposure of bioactive agent to aggressive solvent environment that potentially denatures the biomolecules and loses the bioactivity. Therefore, developing novel processes capable of providing controllable system for the release of biomolecules from the electrospun fibers while preserving the bioactivity is of great importance.

In this study, three kinds of nanocomposite scaffold were prepared by electrospinning for improving cell cultivation. Firstly, we describe the formation of regenerated silk fibroin/tetramethoxysilane (TMOS) nanofibers hybrid nanocomposites obtained by electrospinning of their blends. Hydrolysis and condensation of alkoxy silicon monomer (TMOS) shows that the Si–O–Si bonds join together in order to form a network made of porosities. Moreover, the amine groups catalyze the hydrolysis process due to the alternating presence of protonated and non-protonated amine groups in the fibroin molecular chains, which allows hydrogen bond formation with the oxygen adjacent to silicon in the precursor and thus facilitate –Si–O–Si– bond formation [21]. Here we hypothesize that the hybrid of silk fibroin and TMOS could improve hydrophilicity of the fibrous nanocomposites, furthermore, it would improve cell

http://dx.doi.org/10.5772/57093

activity by accelerating adhesion behavior in the early stages. Secondly, a silk-nHA (nano-hydroxyapatite) biocomposite scaffold was also developed by an electrospinning technique and then post-treated by employing a calcium phosphate (Ca–P) alternate soaking method. We hypothesized that well-distributed HA nanoparticles on the silk nanofibrous would improve cell activity by accelerating differentiation in the late stages. Extensive material characterizations and cell culture studies using MC3T3-E1 were conducted to assess the viability and potential application of this material for future bone grafts applications. Furthermore, we present a novel and effective emulsion electrospinning method in obtaining Fluorescein isothiocyanate-dextran (FITC-dextran)/poly (lactic-co-glycolic acid) (PLGA) and Type I collagen/poly (lactic-co-glycolic acid) (PLGA) fibrous composite scaffolds. Core-sheath structured fibers are successfully fabricated with average diameters of 665 nm and 567 nm for FITC-dextran/PLGA and collagen/PLGA, respectively. *In vitro* release profile shows sustained release of encapsulated FITC-dextran from FITC-dextran/PLGA fibers as long as 7 weeks. The osteoblastic activities of collagen/PLGA nanofibrous scaffold are also investigated by employing osteoblastic-like MC3T3-E1 cell line. Lactate dehydrogenase assay results suggest the excellent cytocompatibility. Cell proliferation and alkaline phosphatase (ALP) activity is also ameliorated on this emulsion electrospun collagen/PLGA fibrous scaffold. All the results indicated that this composited scaffold could support the early stages of osteoblast behavior as well as immediate/late stages. The emulsion electrospinning process has good potential for application in drug release device and three-dimensional scaffold in bone regeneration.

2. Fabrication of silk/TMOS composite nanofibers by co-electrospinning

In the electrospinning system [22, 23], a high-voltage power supply (Har-100*12, Matsusada Co., Tokyo, Japan), capable of generating voltages up to 100 kV, was used as the source of the electric field. The regenerated silk protein solution was contained in a plastic tube connected with a capillary tip with an inner diameter of 0.6 mm. The copper wire connected to a positive electrode (anode) was inserted into the polymer solution, and a negative electrode (cathode) was attached to a metallic collector. The solution volume was controlled to keep proper flow rate for spinning.

Silkworm Bombyx mori is a natural protein that is mainly made of sericin and fibroin proteins, *i.e.*, sericin (the outer coating) and fibroin (the inner brins). The sericin protein is removed by a process called degumming in industry, so that the term silk is commonly improperly used to define only one of its two components. In this work, the cocoons of Bombyx mori were degummed three times in an aqueous Na_2CO_3 (0.02 M) at 100 °C for 30 min and washed with distilled water in order to remove sericin from the surface of silk fibers and then the silk fibroin was obtained. The silk fibroin was then dissolved in a ternary solvent system of $CaCl_2$/CH_3CH_2OH/H_2O in 1:2:8 molar ratio at 70 °C with vigorous stirring. After dialysis against distilled water with cellulose tubular membrane with molecular weight cutoffs (MWCO) ranging from 12,000 to 16,000 Daltons for 4 days at 25 °C, the regenerated silk fibroin sponge was obtained by lyophilization (−20 °C, 24 h). the solutions were prepared by dissolving 8% (w/w) regenerated silk protein in 1,1,1,3,3,3-Hexafluoro-2-propanol (HFIP), after 24 h stirring,

5% and 15% (on the weight of silk fibroin) of TMOS was added to the fibroin solution within 30mins under stirring [24–26].

2.1. Morphology of silk/TMOS nanocomposites scaffolds

Electrospun nanofibers of regenerated silk fibroin and its blends with TMOS from their HFIP solutions were obtained using conditions specified above. Figure 1(a) shows SEM image of pure regenerated silk fibroin nanofibers electrospun from a regenerated silk solution dissolved in HFIP at a concentration of 8 wt %. SEM analysis indicates a broad diameter distribution, with an average diameter of 1252 nm and standard deviation (SD) of 410 nm.

The silk/TMOS nanofibers, shown in Figure 1(b, c), were obtained by adding 5 wt % TMOS in 8 wt % regenerated silk fibroin solution within 30 mins under stirring, electrospinning at a voltage of 16 kV and a TCD of 10 cm, and finally drying at 25 °C for 24 h under humidity of 20%. Interestingly, the adjacent fibers in silk/TMOS hybrid electrospun nanofibers caused to 'weld' at fiber contact points [27], as evident in the SEM images (Figure 1(b)). Compared to welded hybrid fibers, the pure silk nanofibers shown in Figure 1(a) are intact and do not show flash welding. Additionally, the fiber diameters showed almost same to 1,287 nm (SD = 367 nm) (Figure 1(b)), to fibers spun from the pure silk solution (Figure 1(a)). The observed 'weld' at contact points may be due to the equilibrium water content, as was verified by TGA analysis shown later. Moreover, as the TMOS concentration increased to 15%, the fibers became belts and the juncture extended like a sheet which could not be identified as nanofiber mats at all (Figure 1(c)). So in this study we just investigated the hybrid nanofibers with the TMOS concentration of 5%.

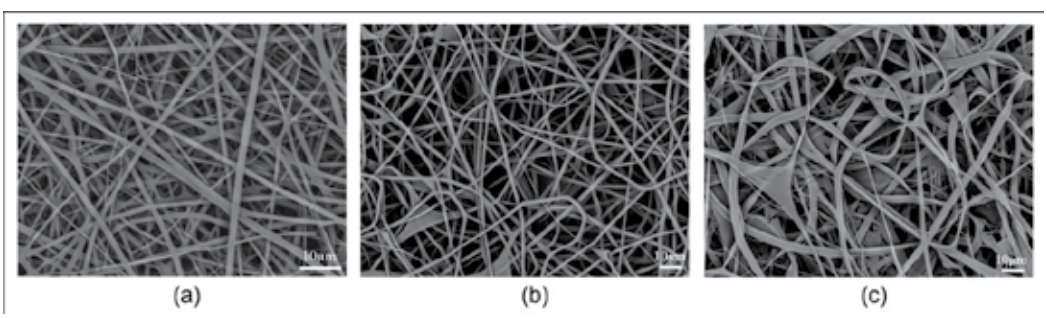

Figure 1. SEM images of the nanofibers (a) regenerated silk fibroin nanofibers; (b) silk/TMOS hybrid nanofibers with TMOS concentration of 5 wt %; and (c) silk/TMOS hybrid nanofibers with TMOS concentration of 15 wt %.

2.2. Hydrophilicity properties of electrospun regenerated silk/TMOS nanofibers

The hydrophilicity of electrospun nanofibers composites can be seen from Figure 2. Water contact angle showed a sharp decrease of electrospun silk nanofibers incorporated with TMOS than pure regenerated silk fibroin nanofiber from 116.2° to 84.8°. Although silk fibroin has many hydrophilic groups such as –OH and –COOH, the incorporation of TMOS result in higher water capacity in the fibers due to the formation of spatial net structure formed *via* Si–

O–Si– linkages as proved by TG result. Furthermore, the water contact of silk/TMOS hybrid nanocomposites was closed to that of TCD (Tissue culture Dish) template (75.6°), which indicated that it may be more suitable for cell attachment than pure silk nanofibers because the optimum water contact of the surface for fibroblast adhesion is reported in the range between 55° and 75° [28]. The adhesion behavior will be discussed in the following text.

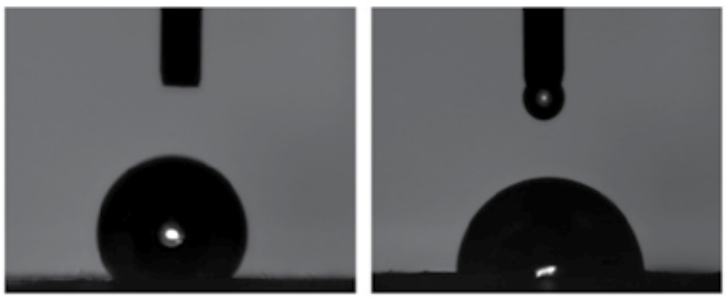

Figure 2. Water contact angle of (a) pure silk nanofibers; and (b) silk/TMOS nanofibers.

2.3. Cytotoxicity assay

Lactate dehydrogenase (LDH) leakage assay results in Figure 3(a) suggest that cell culturing on silk/TMOS fibrous scaffolds cause LDH release near 8% while that on silk is near 7%. Both of them are of no significant difference with the LDH release from TCD as a control. The results showed that the incorporation of TMOS in the fibrous material didn't affect the excellent biocompatibility of silk fibroin. From the live/dead fluorescence micrographs in Figure 3(b) and (c), the majority of cells incubated for 12 h on silk/TMOS and silk scaffolds were alive and parts of them revealed spindle shaped morphology. Cytotoxicity assays indicate that L929 cells on silk/TMOS fibrous scaffold have comparable viability on silk fibrous scaffold.

2.4. Adhesion behavior of electrospun regenerated silk/TMOS nanofibers

The adhesion ratio of L929 cells on pure silk, silk/TMOS nanofibers and TCD controls were shown in Figure 4(a). The cell adhesion ratio of silk/TMOS nanofibers was significantly higher than pure silk nanofibers and TCD controls in all the culture times, it reached as high as 95% after 90 mins' cultivation while that on pure silk was near 85%. Although an increase in adhesion ratio on both pure silk nanofibers and TCD controls after 30 to 90 mins of cell culture were observed, results of adhesion ratio of silk/TMOS nanofibers showed excellent attachment behavior to L929 cells which could be attributed to the melioration of hydrophilicity. The incorporation of TMOS on silk fibroin nanofibers had enhanced the adhesion behavior of L929 cells as expected.

Immunofluorescence microscopy of L929 cells grown on pure silk, silk/TMOS fibrous scaffold and TCD after 6 h cultivation are shown in Figure 4(b-d). Blue fluorescence of cell nuclei

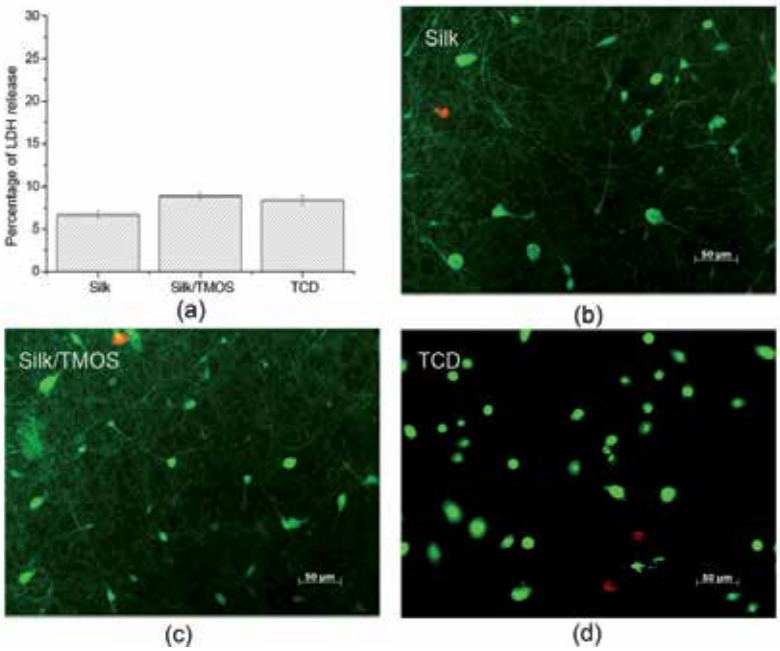

Figure 3. LDH release (a) and fluorescence micrographs of Calcein AM/PI-stained L929 cells with live cells fluorescing green and dead cells fluorescing red after 12 h culture on the Silk/TMOS; (b), silk; (c) nanofibrous scaffold; and TCD (d).

revealed round, well-spaced, and regularly distributed nuclei across the surface of both fibrous scaffolds. Compared to the L929 cells on pure silk that showed round shaped, the cytoskeletal organization (green fluorescence) of most cells on silk/TMOS scaffold showed obvious spindle-shaped morphology, while both round and spindle-shaped L929 cells have been investigated on TCD as a control. Moreover, only L929 cells on silk/TMOS showed vinculin signals (red fluorescence) at the extremities of cellular extensions. Consisting with the adhesion ration in Figure 4 (a), these results mean a better adhesion and stretching behavior of L929 cells on silk/TMOS nanofibrous scaffold than that on pure silk scaffold.

Accordingly, intensive researches have been carried out in order to manipulate cellular behavior by modifying the relative properties of materials. Y. Sasai *et al.* induce durable hydrophilicity on the hydrophobic of polystyrene surface and further modified it by RGD sequence which can be recognized by the receptor protein on the cellular membrane to enhance the adhesion and proliferation of PC12 cell [29]. Vera A. *et al.* induced stable cell adhesion by manipulating the surface topography to the hydrogel poly (ethylene glycol) although fibroblast is intrinsically non-adhesive to the smooth surface [30]. Mohammad *et al.* found that the positive surface of the titanium cylinder results in favorable NCTC clone 929 fibroblast cell adhesion [31]. The results in our study suggested that the cell adhesion ratio and spreading on silk/TMOS has been enhanced comparing to the pure silk. This can be explained by the change of fibrous surface properties in the terms of hydrophilicity and surface morphology change. First of all, water contact angle showed that silk/TMOS have better hydrophilicity than

http://dx.doi.org/10.5772/57093

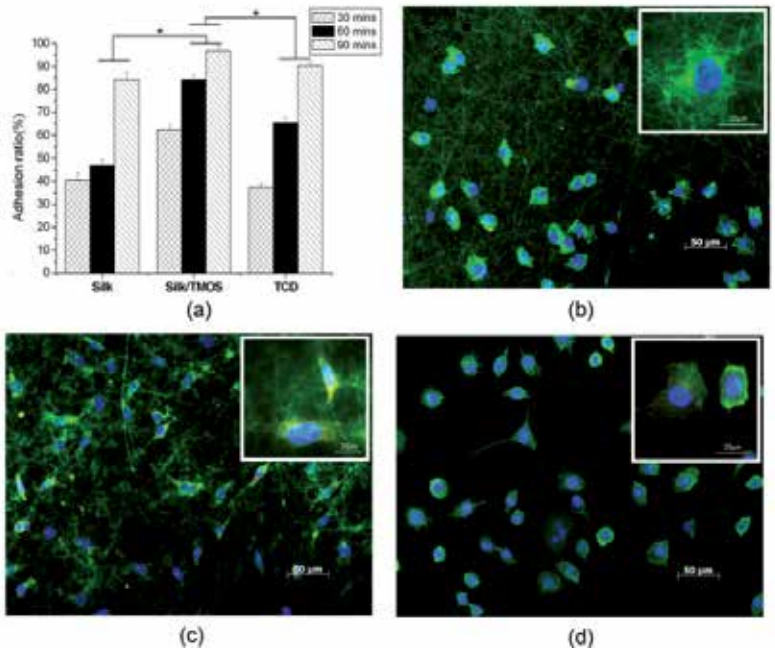

Figure 4. The adhesion ratio (a) for L929 cells after 90 min culture on pure silk, silk/TMOS nanofibers and TCD controls. Significant difference between different materials groups were denoted as * ($p < 0.05$). and Fluorescent staining of F-actin (green), vinculin (red), and cell nuclei (blue) for L929 cells after 6 hs culture on silk; (b) fibrous scaffold, silk/TMOS; (c); and TCD (d).

neat silk because of the formation of spatial net structure formed *via* Si–O–Si– linkages. Studies about the wettability, initial protein adsorption, and the cell adhesion showed that one of the fibronectin state has more active conformation (secondary structure rearrangements) being on a hydrophilic surface [32, 33]. This will consequently lead to more spreading of fibroblasts and ultimately the sufficient cell adhesion and spreading. It has been reported that the optimum wettability of the surface for fibroblast adhesion is in the range between 55° and 75° [28]. The TCD used in this study as control has a water contact of 75.6° (data not shown) and the incorporation of TMOS has change the hydrophobic silk surface of 116.2° to hydrophilic 84.8°. Secondly, SEM images in Figure 1(b, c) showed the interesting adjacent fibers in silk/TMOS hybrid electrospun nanofibers caused to 'weld' at contact points. It has been known that the substrate's topography has a great influence on the behavior of cells at interface. Studies showed that contact guidance happened to cells of different types on different materials with different sizes and shapes of patterns [34–36]. Probably, this kind of 'weld' in silk/TMOS nanofibrous mats influence the surface microstructure of the fiber that might has positive effect to the L929 cell adhesion, though more intensive study is necessary for the conclusion. Nevertheless, considering the complexity of cell surface interaction, which involves protein absorption and specific binding, the function groups that existed in TMOS and net charges presented on the silk/TMOS hybrid scaffold might also influence the protein adsorption and therefore cell adhesion in some degree [37, 38].

3. Fabrication of silk/nHA composite nanofibers

The regenerated silk fibroin sponge was obtained using the same method as described above. Silk fibroin solutions in the concentration of 18% (w/w) were prepared by dissolving the regenerated silk protein sponge into 98% formic acid, and used for electrospinning [39]. The electrospun silk nanofiber was post-treated by a Calcium–Phosphate (Ca–P) alternate soaking method. That is, mineralization of nHA was achieved by subjecting the nanofibers in a series of calcium and phosphate treatments, deemed as the alternate soaking method [40]. Silk nanofibrous scaffolds were first immersed in 0.5 M of $CaCl_2$ (pH of 7.2) (Aldrich Chemical Company, Inc., St. Louis, State Abbreviation, USA), followed by rinsing with deionized (DI) water. Afterwards, the scaffolds were subsequently immersed in 0.3 M of Na_2HPO_4 (pH of 8.96) (Merck & Co. Inc., City, NJ, USA) and rinsed with DI water. The above-mentioned step was referred to as 1 cycle of Ca–P treatment. All nanofibers were subjected to 3 cycles of Ca–P treatments, where the first cycle was 10 min (in each chemical solution) and the second and third cycles were 5 min (in each chemical solution). After mineralization, the nanofibers were freeze-dried overnight.

3.1. Morphology of silk/nHA nanofibrous scaffolds

Mineralization of nHA was successfully deposited on pure silk fibroin nanofibers after 3 cycles [41] of Ca–P treatment as depicted in Figure 7. As shown in Figure 5(b,c), the diameter of obtained silk fibroin nanofibers was around 242 ± 34 nm. It was observed that nHA was homogenously formed on pure silk nanofiber substrates. As evidenced in the high resolution FE-SEM micrograph (Figure 5(d)), nHA particles formed on silk fibroin nanofibrous scaffolds were nanocrystalline in structure and the deposition was occurred predominately on the surfaces of the nanofibrous scaffolds. The size of nHA particles was approximately 30–35 nm in diameter, which was proved by WAXD (see below).

3.2. Crystal Structure of Silk/nHA Nanofibrous Scaffolds

XRD results as can be seen in Figure 8 clearly demonstrated the presence of nHA in the mineralized silk/nHA nanofibrous scaffolds (Figure 6(b): nHA residues and Figure 6(c): mineralized silk/nHA nanofibers). The broad halo peak at 20.6° in Figure 6(c) was attributed to the silk II form of β-sheet crystalline structure [42, 43]. All the peaks in Figures 6(b) and (c) were consistent with the peaks associated with pure nHA (Figure 6(a)), suggesting that rapid mineralization approach used in our study was effective in producing nHA phases on the silk nanofibrous substrates. But unfortunately, both the EDX and XRD analyses indicate the poor crystallinity of the nHA formed on silk nanofibers. It can be explained that the hydroxyl or amide group, which existed in the silk fibroin macro chains, captured calcium or phosphate ions in the solution by chelation. The supply of calcium or phosphate ions to the apatite nuclei was retarded, and the apatite crystals grew under the condition that the calcium or phosphate ions were not sufficiently supplied. Therefore, the crystal growth of apatite was inhibited along a particular axis and resulted in random orientations of crystals in the mineralized fibroin [44].

http://dx.doi.org/10.5772/57093

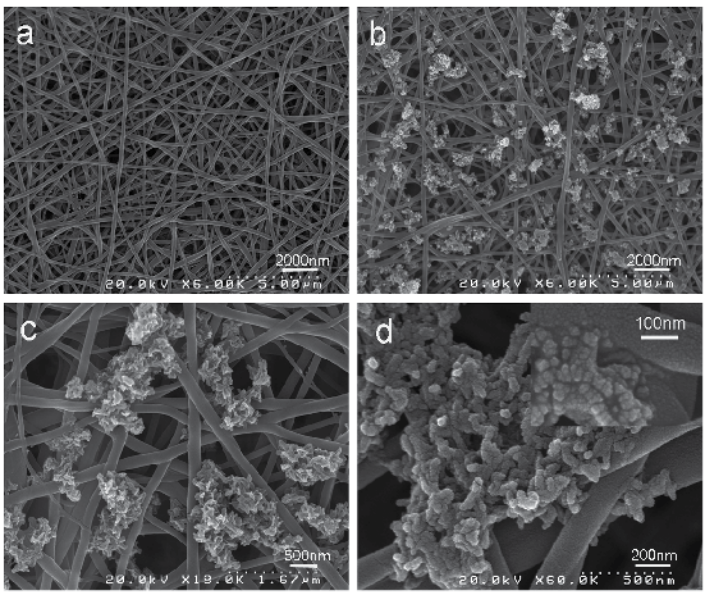

Figure 5. FE-SEM images of pure silk and mineralized silk/nHA nanofibers after 3 cycles of Ca–P treatment. (a) pure silk nanofibers (6000 ×; scale bar, 500 nm), (b–d) mineralized silk/nHA nanofibers after 3 cycles of Ca–P treatment with different magnification.

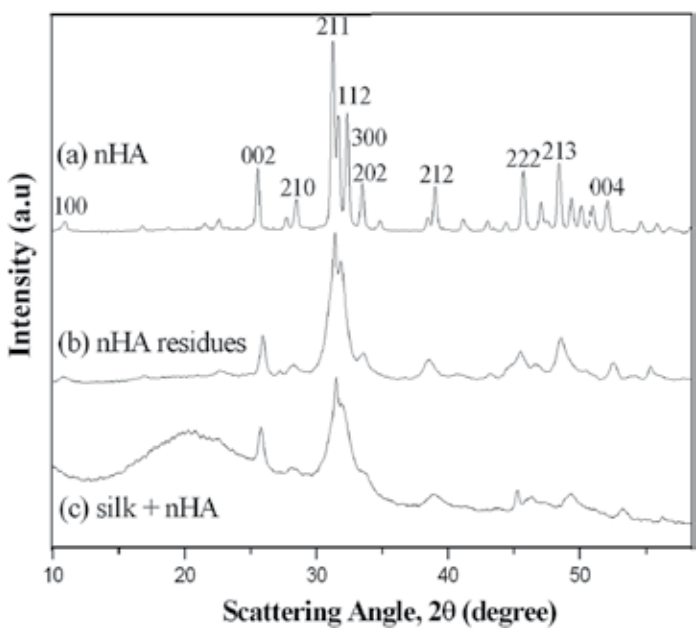

Figure 6. X-ray diffraction (XRD) patterns of (a) pure HA (control); (b) nHA residues; and (c) mineralized silk/nHA nanofibers.

3.3. Proliferation behavior of silk/nHA nanofibrous scaffolds

In Figure 7, immunofluorescence of actin filaments demonstrates the cytoskeletal organization (green). Since the high surface area to volume of nanofibers which is used to mimic the extracellular matrix environment of cells, the MC3T3-E1 cells in Figure 7(I) is investigated to spread in spindle or polygonal morphology after 24 h cultivation. Moreover, intensive vinculin signals can be found along the stretching cellular axis. The MC3T3-E1 cell's adhesion activity in Figure 7(I) suggested that the mineralization of nHA on silk fibrous mats didn't outweigh the benefit of silk nanofibrous scaffold. 3D network culturing morphology of MC3T3-E1 in Figure 7(II) was determined by laser depth-of-focus scanning about 20μm of the silk-nHA scaffold. Together with the cross-section image of Figure 7(III) where a portion of cells are penetrated into fabricated channels, silk-nHA fibrous mats were proved to be suitable for supporting the MC3T3-E1's 3D cultivation.

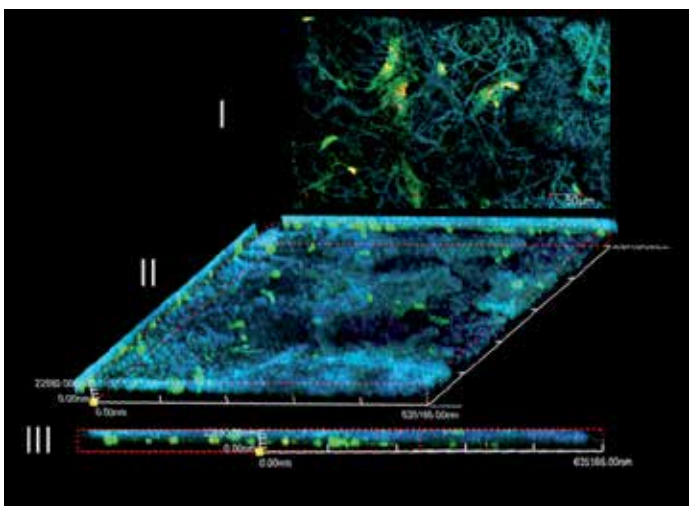

Figure 7. Fluorescent staining of F-actin (green), vinculin (red), and cell nuclei (blue) for MC3T3-E1 cells after 24 h cultivation on silk/nHA fibrous scaffold. (I) 2D morphology of cultivation; (II) 3D morphology by laser scanning of fibrous scaffold; and (III) cross section of II.

As evidenced in the FE-SEM micrographs, osteoblasts were successfully seeded on both pure and mineralized silk nanofibers where the cells were partly adhered to nHA regions in the silk/nHA nanofibers (Figure 8(b)). The deposition of nHA did not affected the MC3T3-E1 attachment compared to those on those grown on pure silk nanofibers after 1 day cultivation (Figures 8(a) and 8(b)) [45, 46], Likewise, cell spreading in a spindle-like shape was also observed on HA-based composites after 2 days of cell culture due to the physical contacts between cells which is maintained *via* the formation of filopodia or lamellipodia [47]. As seen in Figure 8(d), the cells were strongly anchored on the silk/nHA nanofibrous scaffolds, with

http://dx.doi.org/10.5772/57093

preferential attachment of the pseudopodia to nHA regions. In addition, a greater cell spreading on silk/nHA nanofibers was observed after 2 days of cell culture (Figure 8(d)), compared to that after 1 day (Figure 8(b)). When the culture period is prolonged in our study, full cell coverage was found on the nanofibers, and eventually osteoblasts covered most of the nanofiber surfaces after 7 days of cell culture with extended lamellipodia, creating a cell multi-layers on the fibers (Figure 8(f)).

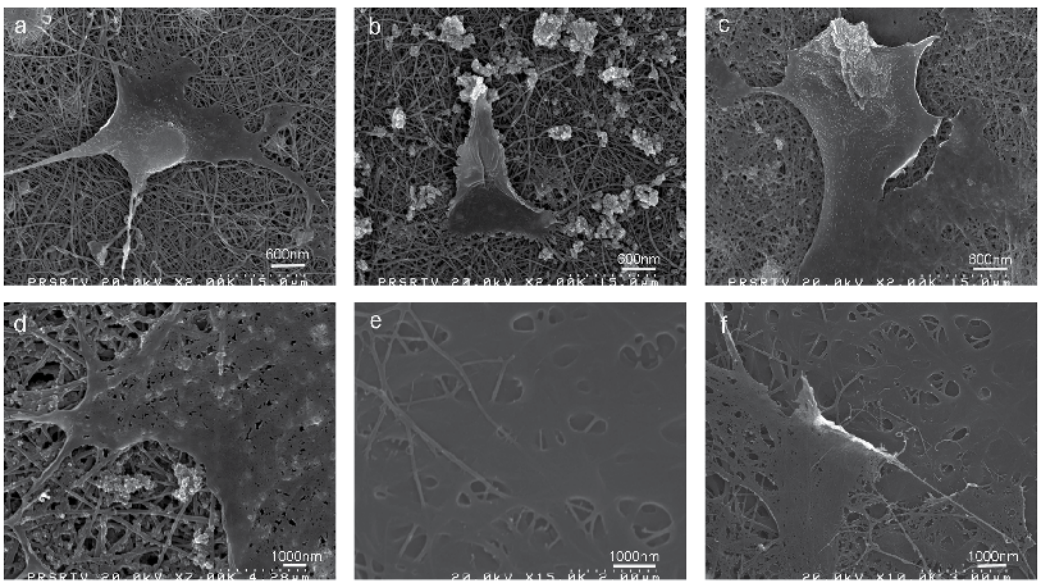

Figure 8. Osteoblasts on pure and mineralized silk/nHA nanofibers. (a) pure silk (day 1); (b) silk/nHA (day 1); (c) pure silk (day 2); (d) silk/nHA (day 2); (e) pure silk (day 7); and (f) silk/nHA (day 7).

Figure 9 shows cell proliferation on pure and mineralized silk nanofibers onward 3 days of cultivation. It was observed that when compared with the pure silk nanofibers, the cell numbers were smaller for mineralized silk/nHA nanofiber scaffold and TCD until 7 days cultivation. This is different from what was observed in other studies where osteoblast proliferation was improved on nanophase HA materials [48, 49]. Probably, the difference was due to the size effect of hydroxyapatite nanoparticles on proliferation as well as the density or bulk distribution. Moreover, previous studies showed that curved nHA surface at a nanometer level could decrease osteoblast-like cells on early period of proliferation [50]. The previously reported results [51–53] were also coincided with those observed in our study: surface topography had a crucial influence on cell behavior, which was accompanied by attenuated proliferation rates on rougher surfaces. Nevertheless, after 14 days of cultivation, cell number on mineralized silk is of no significant differences between pure silk and TCD controls ($p \geq 0.05$), suggesting that the addition of nHA had no negative effect on later period of cell proliferation.

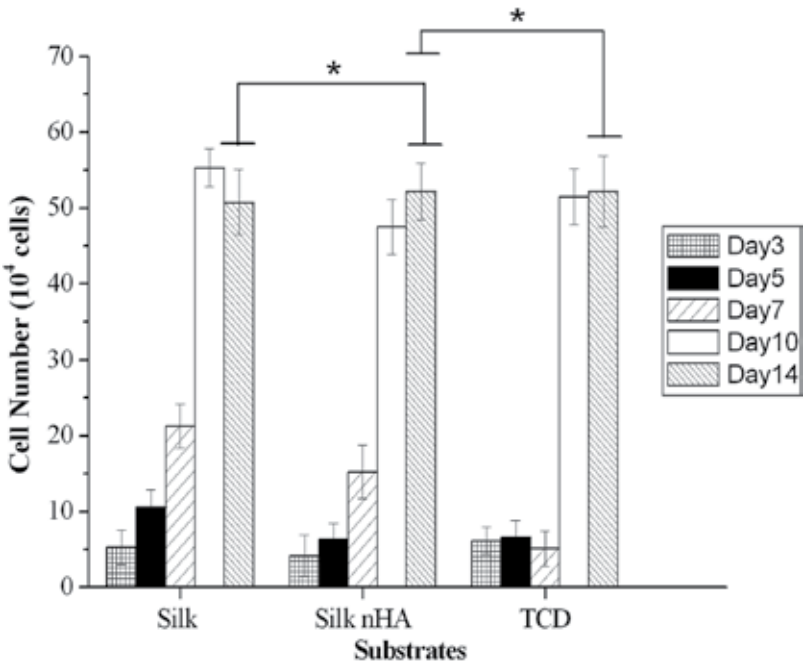

Figure 9. Cell proliferation on pure and mineralized silk nanofibers after 3 to 14 days of cell culture. Significant difference between different materials groups were denoted as * ($p \geq 0.05$).

3.4. Alkaline phosphatase (ALP) activity of silk/nHA nanofibrous scaffolds

One of the properties of nHA is its bioactive nature which promotes osteoblastic differentiation *in vitro* [54–56]. ALP-hydrolyzed phosphate esters play an essential role in the initiation of the cell differentiation process. Thus, ALP activity, as a marker of osteoblastic activity and a standard to evaluate the differentiation of MC3TC-E1 cells, were measured and shown in Figure 10. There was a slight reduction in ALP activity on the pure silk and mineralized silk/nHA nanofibers than TCD after 5 days of cell culture, while a significant increase in ALP activity on both pure silk and mineralized silk/nHA nanofibers after 7 to 14 days of cell culture, compared to TCD counterparts. Results of ALP activity of pure silk and mineralized silk/nHA nanofibers were comparable on an early stage after 5 days of cell culture, but after 7 days of cell culture ALP activity was meliorated in mineralized silk/nHA than pure silk substrates. The incorporation of nHA on silk fibroin nanofibers had enhanced the differentiation activity of MC3T3-E1 from day 7 to 14. After 14 days of cell culture, ALP activity on mineralized silk/nHA nanofibers was nearly 1.6 times higher than that of pure silk nanofibers. One noteworthy observation was that ALP activity in pure silk and mineralized silk/nHA nanofibers was superior to that of TCD as a control from 7 to 14 days of cell culture.

http://dx.doi.org/10.5772/57093

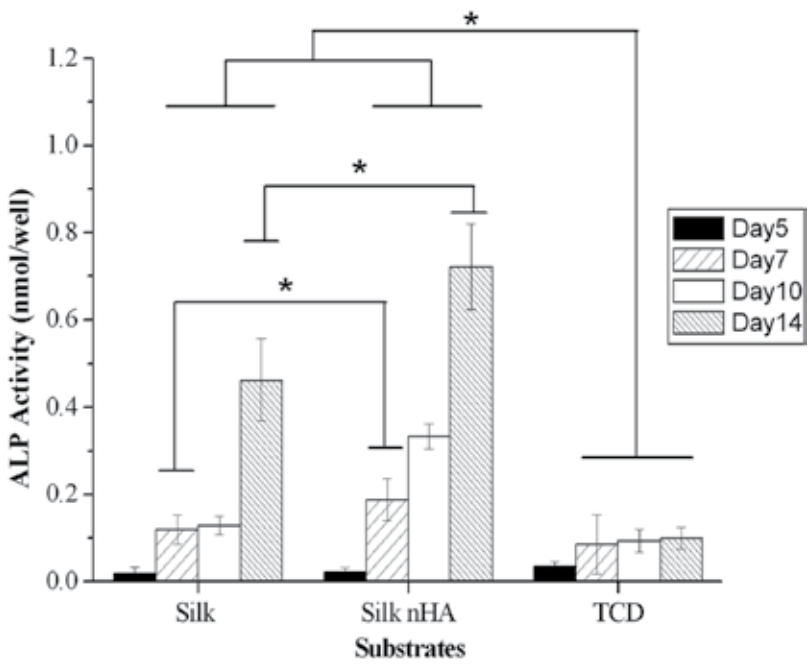

Figure 10. ALP activity on pure and mineralized silk/nHA nanofibers after 5, 7, 10 and 14 days of cell culture. Significant difference between different materials groups were denoted as * ($p < 0.05$).

4. Fabrication of core-sheath structured nanofibers by emulsion electrospinning

There are two possible approaches of incorporating biomolecules in the fibers during electrospinning. These approaches include coaxial electrospinning and emulsion electrospinning. The coaxial electrospinning utilizes two feeding capillary channels for different solutions thus maintaining the functional activity of bimolecular. [57] However, special apparatus is required for coaxial electrospinning and it demands careful adjustment of the operational conditions in order to obtain desirable results. On the other hand, emulsion electrospinning has attracted growing interests, [58-60] due to its relative simplicity and capability of preparing core-sheath type nanofibers using normal solution electrospinning process. In emulsion electrospinning, an aqueous drug solution is prepared and dispersed into a polymer solution in an organic solvent to form a water-in-oil emulsion electrospinning dope. However, the emulsifying process by ultra-sonication might cause conformational changes of biomolecules that affect its bioactivity. Thus, it is necessary not only to prepare emulsion electrospun fibrous scaffold where encapsulated proteins can be controllably released but also to preserve the bioactivities of the encapsulated biomolecules during the emulsifying process.

In this study, poly (lactic-co-glycolic acid) (PLGA), a hydrophilic polymer with excellent biocompatibility and biodegradability which has been widely used in drug delivery and scaffold application, [61-63] was dissolved in chloroform/toluene (C/T) mixed solvent to form the oil phase of the emulsion. SPAN80 (Sorbitan Monooleate) was selected as a non-ionic surfactant widely used in pharmaceuticals and presumed to be non-toxic for biomedical use. The Fol-8Col dissolved in aqueous solution was emulsified with the PLGA oil phase to prepare the emulsion electrospinning dope. (Figure.11) The past work in emulsion electrospinning has been limited to relatively low water content of 4 vol.% (volume percent). [64] For some biomacromolecules that have comparatively low solubility in water, higher water content in the emulsions may be advantageous for their desirable encapsulation in fibers. The concept of using emulsion as a modulator in electrospinning was reported by J.C. Sy *et al*. [65] Here, we propose to introduce emulsions with high water content of 10 wt.% (weight percent). The distribution and inner layer structure of the encapsulated Fol-8Col was investigated. Moreover, release profiles of encapsulated Fol-8Col from the fibrous mats and its short-term cell cytocompatibility to fibroblasts cell line L929 were tested for its potential application as a drug release device as well as tissue engineering scaffold.

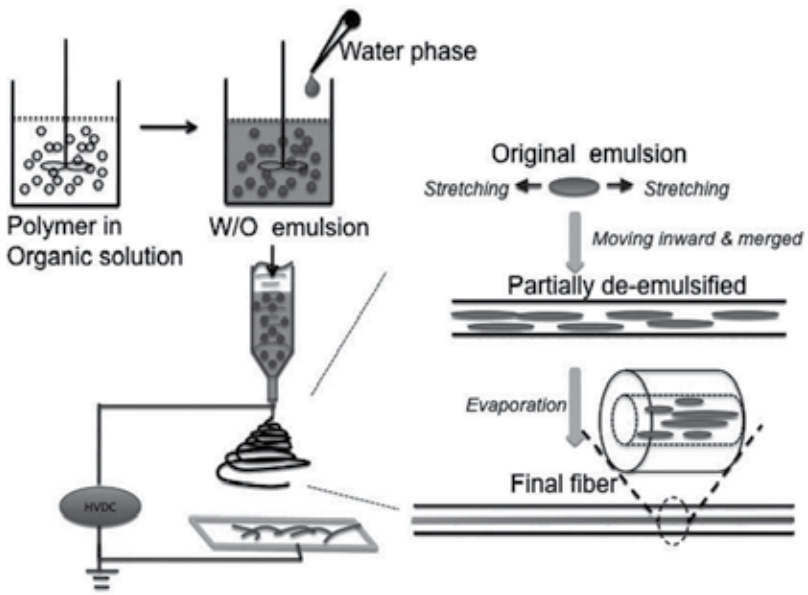

Figure 11. Schematic of emulsion electrospinning.

4.1 Characterization of the encapsulation

In order to clarify the encapsulation of Fol-8Col inside the fibers, two means were employed to characterize the encapsulation effect. FITC produces green fluorescence at 490nm. The

http://dx.doi.org/10.5772/57093

fluorescence micrographs of NHS-Fluorescein labeled Fol-8Col/PLGA showed fluorescence emitting fibers (Figure 12), suggesting the homogeneous presence of Fol-8Col in the emulsion electrospun fibers. Consisting with the SEM images in Figure 1, bead defects of fibrous morphology were not observed.

TEM observation was further conducted to identify the layer structure of emulsion electrospun fibers in this study. The TEM image of Figure 13 suggested that the inner component Fol-8Col of W/O emulsion was properly wrapped in the centre of resultant composite fiber. The boundary in the TEM images reflects the difference of electron transmission ability between the core (Fol-8Col) and sheath (PLGA). However, a slanted portion of boundary can be observed which is associated with the miscibility of amphiphilic surfactant (SPAN80) molecule.

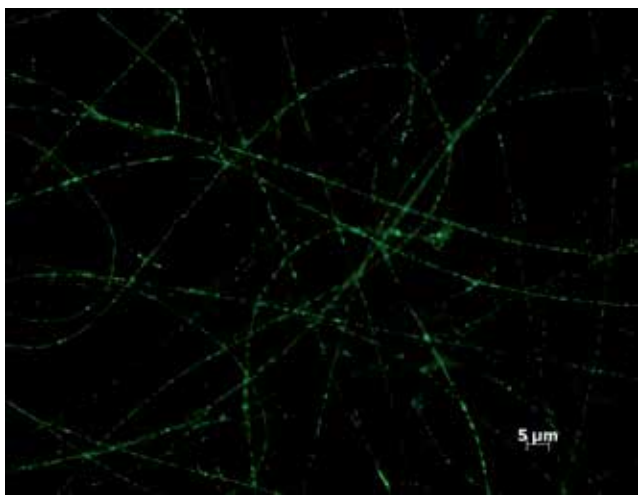

Figure 12. Fluorescence microphotograph of Fol-8Col/PLGA fibers electrospun with Fol-8Col (5 wt% aqueous content), a C/T weight ratio of 75/25, and 10wt% PLGA.

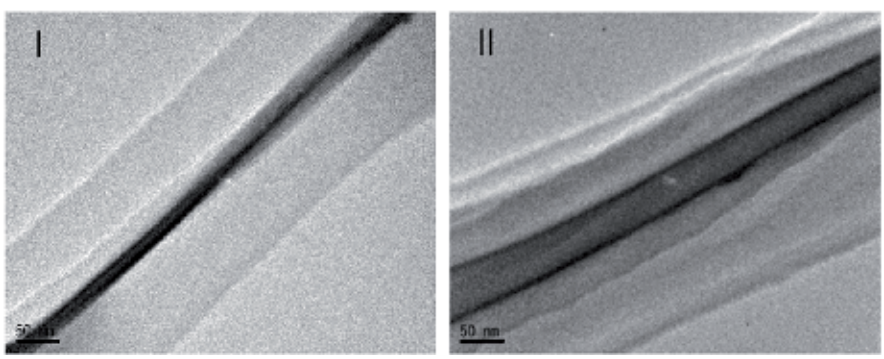

Figure 13. TEM images of Fol-8Col/PLGA fibers electrospun from Fol-8Col [5 (I) and 10wt%(II) aqueous content], with a C/T weight ratio of 75/25 and a PLGA concentration of10 wt%.

4.2 Cytotoxicity assay and live/dead cell staining

The cytocompatibility test of murine fibroblast L929 on Fol-8Col/PLGA emulsion electrospun fibrous scaffold was performed to investigate its potential for tissue engineering application. Here we chose the fibrous scaffold prepared from the electrospinning dope of Fol-8Col aqueous 5 wt.%, PLGA 10 wt.%, C/T 75:25. Collagen/PLGA fibrous mat (morphological data not shown) produced under the same electrospinning condition were tested as control. Figure 14 shows that LDH release after 24 hours' cultivation on all the samples was approximately 10% percent without significant difference ($p>0.05$). From the live/dead fluorescence micrographs, the majority of live cells incubated on Fol-8Col/PLGA scaffold can be observed with stretching spindle shaped morphology. The cytotoxicity assays indicate that the L929 cells have comparable viability on Fol-8Col/PLGA scaffold as that on Collagen/PLGA scaffold.

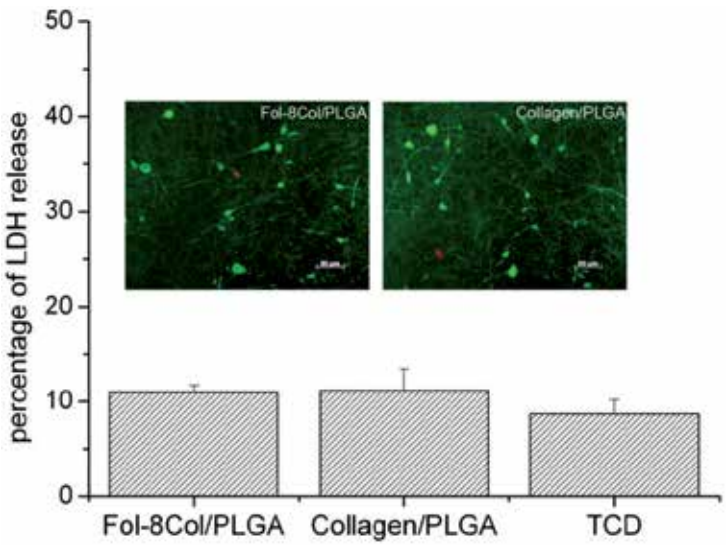

Figure 14. L929 cell LDH leakage results and fluorescence micrographs of Calcein AM/PI-stained L929 cells with live cells fluorescing green and dead cells fluorescing red after 24 h culture on the Fol-8Col/PLGA and collagen/PLGA as a control. Fibers are electrospun at 5 wt% protein aqueous content, C/T 75/25, and 10wt% PLGA.

4.3 Adhesion ratio and cell morphology

The adhesion activity of L929 cells on Fol-8Col/PLGA scaffold is shown in Figure 15. After 6 hours of cultivation, the adhesion ratio of L929 cells on Fol-8Col/PLGA achieved 62±2.3% while that on PLGA is 45±3.4%. This can be attributed to the effect of the Fol-8Col, which is a hydrophilic compared to PLGA molecule; where in the RGD sequences in Fol-8Col molecule has been proven effective at improving cell adhesion. [66] The result shows that the adhesion

ratio (87.6±2.5%) of L929 cells on Fol-8Col/PLGA scaffold after 24 hours cultivation remains higher than that on neat PLGA (68±1.8%).

The immunocytofluorescence staining for nuclei, vinculin, and filamentous actin of L929 cell after 24 hours adhesion shows that L929 cells on both scaffolds exhibited obvious stretching spindle morphology. The filament bundles (green stain) are oriented in a parallel direction following the main cellular axis. A comparatively intensive vinculin signals (red) was investigated on the higher magnificent (630x) image of cells on Fol-8Col/PLGA scaffolds compared to that on PLGA. Our previous results have proved that the biocompatibility of Fol-8Col matrix to L929 cell line is higher than that of the native collagen. [67] The immunocytofluorescence staining results on Fol-8Col/PLGA scaffold in this section is consistent with the adhesion ratio analysis, showing that good cytocompatibility has been preserved after the emulsion electrospinning process.

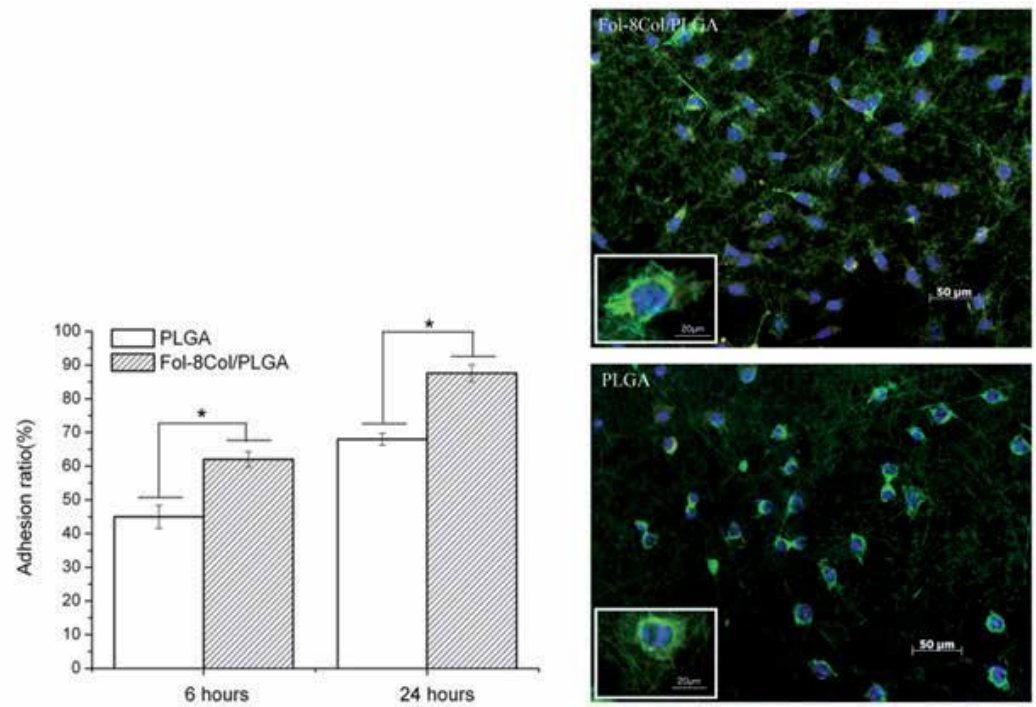

Figure 15. Adhesion ratio and fluorescent staining of F-actin (green), vinculin (red), and cell nuclei (blue) for L929 cells after 24 h culture on a Fol-8Col/PLGA fibrous scaffold (electrospun from 5 wt% Fol-8Col aqueous content, C/T 75/25, and 10wt% PLGA). A neat PLGA fibrous scaffold was used as a control.

Previous studies have addressed the issue of preserving the biomolecular activity through various methods. [68, 69] Our previous research on Fol-8Col has shown that it has excellent biocompatibility to L929 cell line. [4] The results in Figure 14 and 15, show that the cytocompatibility of encapsulated Fol-8Col released from Fol-8Col/PLGA fibrous scaffold to L929 cells were preserved. The effectiveness of SPAN80 in the formation of W/O emulsion is thought to

facilitate the production of core-sheath structure via the electrospinning process. The core-sheath structure lessens the possibility of the exposure of Fol-8Col to the harsh organic solvents and thus protects Fol-8Col from activity loss. We assumed that the collagen derivate sequences, RGD sequences, and the triple-helix have been preserved in Fol-8Col, which is an essential element of its bioactivity.

5. Conclusions

We have successfully prepared three different nanofibrous scaffolds *via* co-electrospinning, post-treatment processes and emulsion electrospinning.

Regenerated silk fibroin/TMOS hybrid nanofibers showed superior fibroblast attachment, compared to pure silk fibroin nanofibers, due to relatively higher hydrophilicity. Accordingly, the silk/TMOS nanofibrous composites showed a sharp decrease in water contact angle than pure regenerated silk fibroin nanofiber due to the spatial net structure formed *via* Si–O–Si– connection which was responsible for water capacity. Interestingly, the electrospinning process caused adjacent fibers to 'weld' at contact points, as confirmed by SEM analysis. This study of simple incorporation silk with TMOS has merit of preserving the excellent biocompatibility of silk, and the fibrous three-dimensional silk/TMOS scaffold can support significantly enhanced L929 adhesion than pure silk. Thus this method might open a new pathway to preparing various functional scaffolds with enhanced bioactivity for in vitro tissue engineering application.

Nano hydroxyapatite was successfully deposited on regenerated silk fibroin nanofibrous scaffolds by a biomimetic Ca–P method. It was found that the primary nHA crystals with a diameter about 30 nm were well-distributed on the surface of the nanofibrous substrates. The ALP expression of the cells was improved on mineralized silk/nHA nanofibers during the cell culture periods, irrespective of the cell number which was leveling off (3 to 7 days). It appeared that the nHA presenting in mineralized silk/nHA nanofibers had a greater improvement on differentiation stages than in an early stage of cultivation, such as adhesion and proliferation. The cell cultivation in this study demonstrated that silk/nHA nanocomposite scaffold could support the early stage of osteoblast adhesion and had a significant effect on the differentiation stage, suggesting that this composite scaffold may be a promising biomaterial for bone tissue engineering.

Furthermore, Fol-8Col, an original designed recombinant collagen-like protein, has been successfully encapsulated in PLGA in the form of core-sheath fibrous structure via emulsion electrospinning. The homogenous encapsulation of the Fol-8Col in a core-sheath form was characterized by the fluorescence micrographs of NHS-Fluorescein labeled Fol-8Col/PLGA and transmission electron microscope. The cytocompatibility of Fol-8Col/PLGA fibers proved its superior ability for L929 cells adhesion compared to that of the neat PLGA. In this regard, this emulsion electrospinning process might open a new pathway to preparing tailored core-sheath fibers to ultimately fulfill the functions of drug release device as well as tissue engineering scaffold.

Acknowledgements

The authors acknowledge the support of Shinshu University Global COE Program "International Center of Excellence on Fiber Engineering".

Author details

Kai Wei* and Ick-Soo Kim

*Address all correspondence to: sudaweikai@hotmail.com

Nano Fusion Technology Research Group, Faculty of Textile Science & Technology, Shinshu University, Ueda, Japan

References

[1] Huang, L.; Nagapudi, K.; Apkarian, R.P.; Chaikof, E.L. *J. Biomater Sci. Polym. Ed.* 2001, *12*, 979–993.

[2] Matthews, J.A.; Wnek, G.E.; Simpson, D.G.; Bowlin, G.L. *Biomacromolecules* 2002, *3*, 232–238.

[3] Altman, G.H.; Diaz, F.; Jakuba, C.; Calabro, T.; Horan, R.L.; Chen, J.S.; Lu, H.; Richmond, J.; Kaplan, D.L. *Biomaterials* 2003, *24*, 401–416.

[4] Meinel, L.; Hofmann, S.; Karageorgiou, V.; Kirker-Head, C.; Mccool, J.; Gronowicz, G.; Zichner L.; Langer, R.; Vunjak-Novakovic, G.; Kaplan, D.L. *Biomaterials* 2005, *26*, 147–155.

[5] Panilaitis, B.; Altman, G.H.; Chen, J.S.; Jin, H.J.; Karageorgiou, V.; Kaplan, D.L. *Biomaterials* 2003, *24*, 3079–3085.

[6] Caruso, R.A.; Schattka, J.H.; Greiner, A. *Adv. Mater.* 2001, *13*, 1577–1579.

[7] Hou, H.; Ge, J.J.; Zeng, J.; Li, Q.; Reneker, D.H.; Greiner, A.; Cheng, S.Z.D. *Chem. Mater.* 2005, *17*, 967–973.

[8] Patel, A.C.; Li, S.; Yuan, J.M.; Wei, Y. *Nano Lett.* 2006, *6*, 1042–1046.

[9] Wei, K.; Ohta, T.; Kim, B.S.; Lee, K.H.; Kim, K.W.; Khil, M.S.; Kim, H.Y.; Kim, I.S. *Polym. Adv. Technol.* 2010, *21*, 746–751.

[10] Pritesh, A.P.; Jessica, E.; Maria, C.A.; A. Jon, G.; Patrick, T.M. *Polymer* 2009, *50*, 1214–1222.

[11] Xu, Q.; Li, J.B.; Peng, Q.; Wu, L.L. Li, S.P. *Mater. Sci. Eng. B* 2006, *127*,212–217.

[12] LeGeros, R.Z. Karger: Basel, Switzerland, 1991.

[13] Aoki, H. Tokyo: Ishiyaku Euro America, 1994; 90–130.

[14] Feenstra, L.; de Groot, K. Medical Use of Calcium Phosphate Ceramics. In *Bioceramics of Calcium Phosphate*; de Groot, K, Ed.; CRC Press: Boca Raton, FL, USA, 1982.

[15] Fujihara, K.; Kotaki, M.; Ramakrishna, S. *Biomaterials* 2005, *26*, 4139–4147.

[16] Kim, H.W.; Song, J.H.; Kim, H.E. *Adv. Funct. Mater.* 2005, *15*, 1988–1994.

[17] Li, C.; Vepari, C.; Jin, H.J.; Kim, H.; Kaplan, D.L. *Biomaterials* 2006, *27*, 3115–3124.

[18] Sui, G.; Yang, X.; Mei, F.; Hu, X.; Chen, G.; Deng, X.; Ryu, S. *J. Biomed. Mater. Res. Part A.* 2007, *82A*, 445–454.

[19] Venugopal, J.; Vadgama, P.; Kumar, T.; Ramakrishna, S. *Nanotechnology* 2007, *18*, 055101–055101.

[20] Zhang, Y.; Venugopal, J.R.; El-Turki, A.; Ramakrishna, S.; Su, B.; Lim, C.T. *Biomaterials* 2008, *29*, 4314–4322.

[21] Pohnert, G.; Angewandte, C. *Int. Ed.* 2002, *41*, 3167–3169.

[22] Ohsawa, O.; Lee, K.H.; Kim, B.S.; Lee, S.; Kim, I.S. *Polymer* 2010, *51*, 2007–2012.

[23] Wei, K.; Li, Y.; Kim, K.O.; Nakagawa, Y.; Kim, B.S.; Abe, K.; Chen, G.Q.; Kim, I.S. *J. Biomed. Mater. Res. Part A* 2011, *97*, 272–280.

[24] Zhang, M.; Yi, T.T.; Zhang, Y.M.; Zhang, L.; Wu, W.; Zhang, A.L.; Pan, Z.J. *Polym. Adv. Technol.* 2011, *22*, 151–157.

[25] Yao, C.; Li, X.; Song, T.; Li, Y.; Pu, Y. *Polym. Int.* 2009, *58*, 396–402.

[26] Park, K.E.; Jung, S.Y.; Lee, S.J.; Min, B.M.; Park, W.H. *Int. J. Biol. Macromol., 38*, 165–173.

[27] Li, Y.; Bao. X.X.; Matsuda, N.; Yao, J.M.; Teramoto, A.; Abe, K.; Ko, F.K. *J. Mater. Sci.* 2011, *46*, 1396–1404.

[28] Jang, S.Y.; Seshadri, V.; Khil, M.S.; Kumar, A.; Marquez, M.; Mather, P.T. *Adv. Mater.* 2005, *17*, 2177–2180.

[29] Groth, T.; Altankov, G. *Biomaterials* 1996, *17*, 1227–1234.

[30] Sasai, Y.; Matsuzaki, N.; Kondo, S.; Yamauchi, Y.; Kuzuya, M. *Surf. Coat. Technol.* 2008, *202*, 5724–5727.

[31] Schulte, V.A.; Díez, M.; Möller, M.; Lensen, M.C. *Biomacromolecules* 2009, *10*, 2795–2801.

[32] Hamdan, M.; Blanco, L.; Khaisat, A.; Tresguerres, I.F. *Clin Implant Dent Relat Res.* 2006, *8*, 32–38.

[33] Grinnell, F.; Feld, M.K. *J. Biol. Chem.* 1982, *257*, 4888–4893.

[34] Wei, J.H.; Yoshinari, M.; Takemoto, S.; Hattori, M.; Kawada, E.; Liu, B.L.; Oda, Y.J. *Biomed. Mater. Res.* 2007, *81B*, 66–75.

[35] Lim, J.Y.; Donahue, H.J. *Tissue Eng.* 2007, *13*, 1879–1891.

[36] Curtis, A.; Wilkinson, C. *Biomaterials* 1997, *18*, 1573–1583.

[37] Kidambi, S.; Udpa, N.; Schoeder, S.A.; Findlan, R.; Lee, I.; Chan, C. *Tissue Eng.* 2007, *13*, 2105–2117.

[38] Keselowsky, B.G.; Collard, D.M.; Garcia, A.J. *Biomaterials* 2004, *25*, 5947–5954.

[39] Wang, Y.X.; Robertson, J.L.; Spillman, W.B.; Claus, R.O. *Pharm. Res.* 2004, *21*, 1362–1373.

[40] Wei, K.; Xia, J.H.; Kim, B.S.; Kim, I.S. *J. Polym. Res.* 2010, *18*, 579–585.

[41] Taguchi, T.; Kishida, A.; Akashi, M. *Chem. Lett.* 1998, *8*, 711–712.

[42] Ngiam, M.; Liao, S.; Patil, A.J.; Cheng, Z.; Chan, C.K.; Ramakrishna, S. *Bone* 2009, *45*, 4–16.

[43] Kim, U.J.; Park, J.Y.; Kim, H.J.; Wada, M.; Kaplan, D.L. *Biomaterials* 2005, *26*, 2775–2785.

[44] Furuzono, T.; Taguchi, T.; Kishida, A.; Akashi, M.; Tamada, Y.; Biomed, J. *J. Biomed. Mater. Res.*, 2000, *50*, 344–352.

[45] Zhai, Y.; Cui, F.Z. *J. Cryst. Growth* 2006, *291*, 202–206.

[46] Smith, I.O.; McCabe, L.R.; Baumann, M.J. *Int. J. Nanomed.* 2006, *1*, 189–194.

[47] Itoa, Y.; Hasudaa, H.; Kamitakaharac, M.; Ohtsukic, C.; Taniharac, M.; Kangd, I.K.; Kwon, O.H. *J. Biosci. Bioeng.* 2005, *100*, 43–49.

[48] Ogata, K.; Imazato, S.; Ehara, A.; Ebisu, S.; Kinomoto, Y.; Nakano, T. *J. Biomed. Mater. Res.* 2005, *72*, 127–135.

[49] Liao, S.S.; Cui, F.Z.; Zhu, Y. *J. Bioact. Comp. Poly.* 2004, *19*, 117–130.

[50] Webster, T.J.; Siegel, R.W.; Bizios, R. *Biomaterials* 1999, *20*, 1221–1227.

[51] Zhu, X.; Eibl, O.; Scheideler, L.; Geis-Gerstorfer, J. *J. Biomed. Mater. Res.* 2006, *79*, 114–127.

[52] Bacakova, L.; Stary, V.; Kofronova, O.; Lisa, V. *J. Biomed. Mater. Res.* 2001, *54*, 567–578.

[53] Anselme, K.; Bigerelle, M.; Noel, B.; Dufresne, E.; Judas, D.; Iost, A. *J. Biomed. Mater. Res.* 2000, *49*, 155–166.

[54] Martin, J.Y.; Schwartz, Z.; Hummert, T.W.; Schaub, D.M.; Simpson, J.; Lankford, J. *J. Biomed. Mater. Res.* 1995, *29*, 389–401.

[55] Ayers, R.; Nielsen-Preiss, S.; Ferguson, V.; Gotolli, G.; Moore, J.J.; Kleebe, H.J. *Mater. Sci. Eng. C* 2006, *26*, 1333–1337.

[56] Redey, S.A.; Nardin, M.; Bernache-Assolant, D.; Rey, C.; Delannoy, P.; Sedel, L. *J. Biomed. Mater. Res.* 2000, *50*, 353–364.

[57] Thian, E.S.; Huang, J.; Best, S.M.; Barber, Z.H.; Brooks, R.A.; Rushton, N. *Biomaterials* 2006, *27*, 2692–2698.

[58] Y.Z. Zhang, X. Wang, Y. Feng, J. Li, C.T. Lim, S. Ramakrishna, *Biomacromolecules* 2006, *7*, 1049-1057.

[59] X.L. Xu, X.L. Zhuang, X.S. Chen, X.R. Wang, L.X. Yang, X.B. Jing, *Macromol. Rapid Commun*. 2006, *32*, 1637–1642.

[60] J.F. Zhang, D.Z. Yang, F. Xu, Z.P. Zhang, R.X. Yin, J. Nie, *Macromolecules* 2009, *42*, 5278–5284.

[61] S. Agarwala, A. Greiner, *Polym. Adv. Technol.* 2011, *22*, 372–378.

[62] J. Wang, B.M. Wang, S.P. Schwendeman, *J. Control Release* 2002, *82*, 289–307.

[63] T.B. Bini, S. Gao, T.C. Tan, S. Wang, A. Lim, L.B. Hai, S. Ramakrishna, *Nanotechnology* 2004, *15*, 1459–1464.

[64] H. Pan, H. Jiang, W. Chen, *Biomaterials* 2008, *29*, 1583–1592.

[65] X. Xu, L. Yang, X. Xu, X. Wang, X. Chen, Q. Liang, J. Zeng, X. Jing, *J. Control Release* 2005, *108*, 33–42.

[66] J.C. Sy, A.S. Klemm, V.P. Shastri, *Adv. Mater*. 2009, *21*, 1814–1819.

[67] W. Chen, C.E. Chang, M.K. Gilson, *J. Am. Chem. Soc*. 2006, *128*, 4675–4687.

[68] C. Du, M. Wang, J. Liu, M. Pan, Y. Cai, J. Yao, *Appl. Microbiol. Biotechnol*. 2008, *79*, 195–202.

[69] X. Zong, K. Kwangsok, F. Dufei, R. Shaofeng, B.S. Hsiao, B. Chu, *Polymer* 2002, *43*, 4403–4412.

[70] J. Zeng, A. Aigner, F. Czubayko, T. Kissel, J.H. Wendorff, A. Greiner, *Biomacromolecules* 2005, *6*, 1484–1488.

Chapter 5

Carbon Nanofiber Concrete for Damage Detection of Infrastructure

Y.L. Mo and Rachel Howser Roberts

Additional information is available at the end of the chapter

http://dx.doi.org/10.5772/57096

1. Introduction

Fiber research in concrete construction is an ongoing field and the use of carbon nanofibers (CNF) is examined. Fibers improve brittle materials such as concrete by enhancing tensile strength, ductility, toughness, and conductivity. Short-fiber composites are a class of strain sensor based on the concept of short electrically conducting fiber pull-out that accompanies slight and reversible crack opening. For a fiber composite to have strain sensing ability, the fibers must be more conducting than the matrix in which they are embedded, of diameter smaller than the crack length, and well dispersed. Their orientations can be random, and they do not have to touch one another. The electrical conductivity of the fibers enables the direct current (DC) electrical resistivity of the composites to change in response to strain change or temperature, allowing sensing.

2. Nanotechnology in concrete

Despite the fact that nanotechnology is a relatively recent development in scientific research, the introduction of the concept is credited to Nobel Prize winner Richard Feynman from his 1959 lecture, "There's Plenty of Room at the Bottom" [1]. Feynman considered the possibility of direct manipulation of individual atoms as a powerful form of synthetic chemistry. Decades later, Feynman's concept morphed into the field of nanotechnology. According to the National Science Foundation and National Nanotechnology Initiative, the definition of nanotechnology includes three elements [2]:

- The size range of the material structures under consideration should be approximately 100 nanometers;

- The nanotechnology should have the ability to measure or transform at the nanoscale;
- There should be properties that are specific to the nanoscale as compared to the macro or micro scale.

Following this definition, in the past 25 years nanotechnology has expanded from Feynman's idea and now finds applications in fields ranging from medical devices to nano-reinforced concrete [3, 4].

To date, the awareness and application of nanotechnology in the construction industry are increasing; however, progress is uneven in the current early stages of its practical exploitation. Bartos [5] presents three reasons for this phenomenon:

- The nature of the construction industry differs greatly from the other industries doing research in nanotechnology. The final products coming from the construction industry are not mass-produced and require relatively long service lives, differentiating it from the products from the microelectronics, information technology, and automotive industries.
- Historically, there is a very low level of investment in construction research and development.
- Research in nano-related research and development requires very high initial capital investment

Despite these difficulties, there have been significant advances in nanoscience of cementitious materials with an increase in the understanding of basic phenomena in cement at the nanoscale. These include structure and mechanical properties of the hydrate phases, origins of cement cohesion, cement hydration, interfaces in concrete, and mechanisms of degradation [6]. A major nanotechnology application is to include nano-sized reinforcement in cement-based materials such as carbon nanotubes or nanofibers.

3. Fiber reinforced concrete

Concrete, composed of fine and coarse aggregates held together by a hydrated cement binder, is one of the most important construction materials and is used in diverse project areas including house foundations, high rise tower components, highways, and dams. Hydrated cement is a brittle material that is an order of magnitude stronger in compression than in tension. To compensate for this weakness reinforcement consisting typically of rebar or fibers are added to the concrete.

The use of fibers to reinforce brittle materials can be traced back to ancient times when straw and hair was added to mud bricks. The modern development of the use of fibers in construction began in the 1960s with the addition of steel fibers to reinforced concrete structures. This was closely followed by the addition of polymeric fibers, glass fibers, and carbon fibers in the 1970s, 80s, and 90s, respectively [7].

Fibers improve brittle materials such as concrete by enhancing tensile strength, ductility, toughness, and conductivity [8-13]. Fibers are typically used in two forms: short randomly

http://dx.doi.org/10.5772/57096

dispersed fibers in a cementitious matrix or a continuous mesh of fibers used in thin sheets. Here we will focus on randomly dispersed fibers used to arrest cracks. The cracking process within concrete begins with the onset of isolated nanocracks. These nanocracks grow together to form localized microcracks, which in turn grow together to form macrocracks. These macrocracks widen to form cracks visible with the naked eye. Fibers arrest these cracks by forming bridges across them. With increasing tensile stress, a bond failure eventually occurs, and the fiber will pull out of the concrete allowing the crack to widen. Fig. 1 shows the bridging action of fibers across micro and macrocracks in concrete.

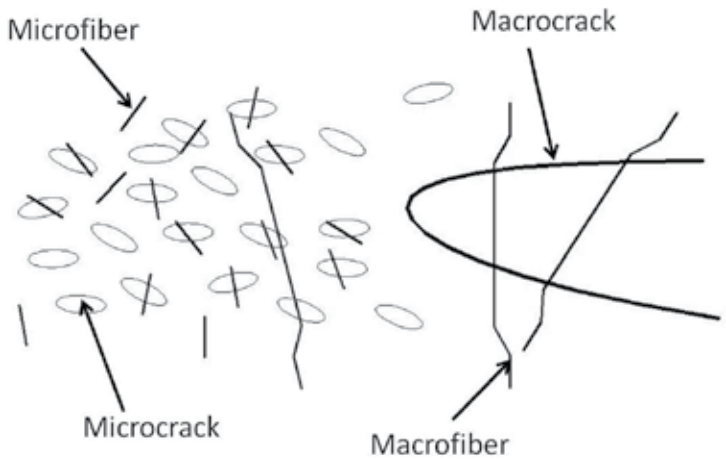

Figure 1. Bridging Action of Fibers Across Micro and Macrocracks

4. Nanoreinforcement in cement-based materials

Since the discovery of carbon nanotubes (CNT) in 1991 [14], researchers have desired to implement the unique mechanical, thermal, and electronic properties of CNT and CNF in cement-based composites. Single-wall CNT (SWCNT), multi-wall CNT (MWCNT) and CNF are graphene ring-based materials with aspect ratios greater than 1000 and high surface areas [6, 15]. CNT and CNF have moduli of elasticity in the range of terrapascals and tensile strength on the order of gigapascal [6, 16, 17]. SWCNT consist of a single graphene sheet wrapped into a seamless cylinder, while, as the name suggests, MWCNT inhere of multiple concentric sheets of graphene wrapped around a hollow core. CNF are cylindric nanostructures with graphene layers arranged as stacked cones, cups, or plates. CNF are adventagious because their stacked structure presents exposed edge planes not present in CNT that intoduce increased surface area and better bond characteristics. Because of their structure, CNF are easier to produce and cost 100 times less than SWCNT [18]. Because of the increased bond surface and lower cost, CNF are more attactive than CNT for application in cement-based composites.

5. CNT and CNF dispersion

The majority of nanoreinforced composite research has been completed on polymers containing CNT or CNF [6, 19, 20]. One of the main reasons for this is because uniform dispersion is difficult in cement-based materials. Well dispersed CNF results in uniform calcium-silicate-hydrate (CSH) gel formation, which improves the structural and electrical properties of the concrete [21]. CNT and CNF are inherently hydrophobic and are attracted due to Van der Waals forces, causing the fibers to tend to agglomerate hindering their dispersion in solvants [17, 22-24].

Several solutions have been proposed to solve this issue including dispersing the fibers through milling, ultrasonication, high shear flow, elongational flow, functionalization, in addition to surfactant and chemical dispersement systems [24]. These methods primarily fall into two categories: mechanical and chemical dispersion. The mechanical dispersion methods, such as ultrasonification, while effective in seperating the fibers, can fracture them decreasing their aspect ratio. Chemical methods use surfactants or functionalization to make the fibers less hydrophobic, reducing their tendancy to agglomerate. However, many of the chemicals used can digest the fibers causing the fibers to become less effective. The surfactants also often cause bubbles to form in the composite negatively effecting the strength of the material.

Gao et al [12] proposed a dispersion method specifically used for CNF/CNT dispersion in cement-based materials that eliminates the beforementioned drawbacks. In this method, a high-range water reducer (HRWR) is used to create a self-consolidating concrete (SCC). ACI Committee 237 Self-Consolidating Concrete offers the following definition for SCC [25]:

Self-consolidating concrete (SCC) is highly flowable, non-segregating concrete that can spread into place, fill the formwork, and encapsulate the reinforcement without any mechanical consolidation.

SCC is a product of technological advancements in the area of under-water concrete technology where the mixtures must ensure high fluidity and high resistance to washout and segregation. Okamura originally advocated SCC in 1986, and the first success with SCC occurred in 1988 [26]. The use of SCC has gained wide acceptance for savings in labor costs, shortened construction time, a better finish, and an improved work environment [27-30].

Advancement in SCC technology was primarily possible due to the introduction of new chemical admixtures that improved and controlled the SCC rheological properties. Better performing SCC mixes were produced on the advent of melamine, naphthalene, polycarboxylate, and acrylic based HRWR superplasticizers and viscosity modifying agents (VMA).

Gao et al [12] proposed using SCC because acceptable SCC is not only highly flowable, but it is also highly stable and homogenious on a macro scale. The Prestressed Concrete Institute (PCI) stipulates the following criteria for SCC [26]:

- Filling ability – The property that determines how fast SCC flows under its own weight and completely fills intricate spaces with obstacles, such as reinforcement, without losing its stability.

http://dx.doi.org/10.5772/57096

- Passing ability – the ability of SCC to pass through congested reinforcement and adhere to it without application of external energy.
- Stability – the ability of SCC to remain homogenous by resisting segregation, bleeding, and air popping during transport and placing as well as after placement.

Gao et al [12] studied SCC containing CNF to see if the same effect was present on the nano scale. In Gao et al's mixing procedure, HRWR, water, and CNF are mixed in a laboratory-grade blender. Simultaneously, fine aggregate, course aggregate, and cement are combined in a centrifugal mixer. The CNF mixture is then slowly added to the mixer to gain a homogenous mix. The fresh concrete was used to create cylinders that were tested in compression. After the test, pieces of the cylinders were observed under a scanning electron microscope (SEM). The SEM showed significant CNF clumping in specimens made of normal CNF concrete and uniform distribution in SCC containing CNF, as shown in Figs. 2 and 3, respectively.

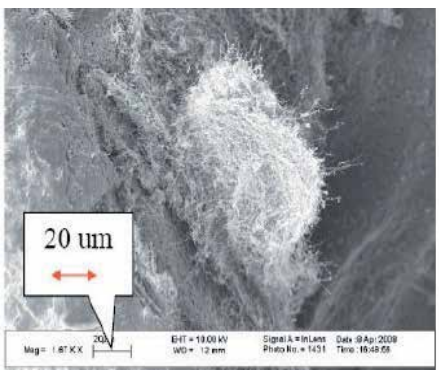

Figure 2. Scanning Electron Microscope Image of CNF Clump in Normal Cement (1670x Magnification)

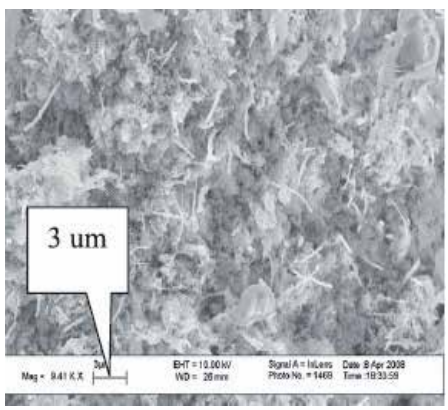

Figure 3. Scanning Electron Microscope Image of Well Dispersed CNF in a Uniform Self-Consolidating Cement (9410x Magnification)

6. Strain sensing ability of CNT/CNF cement-based materials

Smart materials are materials that sense their environment and respond to changes in strain, temperature, moisture, pH, and/or electric or magnetic fields. CNT/CNF composites qualify as smart materials since they can be used to measure strain and temperature [4, 13, 32-35]. There are two types of strain sensing, reversible and irreversible. The measurement of irreversible strain allows structural health monitoring, while the sensing of reversible strain permits dynamic load monitoring. Structural health monitoring is the process of implementing a damage detection and characterization strategy for engineering structures. Dynamic load monitoring can detect loads on structures as they are applied and removed in real time. These are important technologies because they gauge the ability of a structure to perform its intended function despite aging, degradation, or disasters. Typically, monitoring reversible strain is more difficult because it can only be monitored in real time. Additionally, reversible strain tends to be smaller than irreversible strain [31].

Strain sensing refers to the ability to measure an electrical or optical response corresponding to a strain. Chen and Chung [31] give the following requirements for a structural sensor:

a. Wide strain/stress range of detection (from small strains up to failure)

b. Response being reversible upon stimulus removal (necessary for repeated use of the sensor)

c. Ease of measuring the response (without the need of expensive peripheral equipment)

d. Presence of the sensor having no bad effect on the structural properties of the structure

e. Chemical stability and durability

f. Low cost

Current commonly used strain sensors include strain gages, fiber optic sensors, and piezoelectric sensors, which all suffer from high cost, poor durability, and the need for expensive peripheral equipment including electronics and lasers. Because of this, the use of sensors in civil structures is uncommon [31]. CNT/CNF composites could become a better option as a strain sensor because however, technology may provide a way to make them more cheaply in the future.

CNT and CNF cement-based materials exhibits properties necessary for reversible strain monitoring and electromagnetic interference (EMI) shielding. Short-fiber composites were found to be a class of strain sensor based on the concept of short electrically conducting fiber pull-out that accompanies slight and reversible crack opening. For a CNT/CNF composite to have strain sensing ability, the fibers must be more conducting than the matrix in which they are embedded, of diameter smaller than the crack length, and well dispersed. Their orientations can be random, and they do not have to touch one another [32, 33]. The electrical conductivity of the fibers enables the DC electrical resistivity of the composites to change in response to strain damage or temperature, allowing sensing [13, 32-35].

http://dx.doi.org/10.5772/57096

7. Carbon fiber cement and mortar self-sensing applications

Around the same time that CNT were discovered, reseachers were adding carbon microfibers to cement-based materials and studying their mechanical properties. In 1992 while studying the mechanical properties of carbon microfibers dispersed in mortar, Yang and Chung [35] noted that the electrical resitivity of mortar containing these fibers dramatically decreased by up to several orders of magnitude.

This idea of electrically conducting concrete led to Chen and Chung proposing an intrinsically smart concrete containing carbon microfibers [8]. Chen and Chung prepared mortar cubes containing carbon microfibers and tested them cyclically. They discovered that the electrical resistivity of the concrete increased irreversibly upon compressive loading up to approximately 1/3 the compressive strength of the mortar. After this point, the resistance reversibly increased and decreased upon loading and unloading of the specimens. Chen and Chung concluded that carbon fiber reinforced concrete can serve as a smart structural material. Chen and Chung followed this experiment with a more detailed cyclic experiment on carbon fiber mortar under cyclic loads [31]. After this test, they concluded that the initial irreversible behavior is due to permanent damage associated with the fiber/matrix interface weakening. They attributed the reversible behavior to crack opening with fiber pull-out and crack closing with fibers pushing back in.

CNT are the most conductive fibers presently known and are, therefore, more ideal for electrical applications than their micro-scale counterparts [36, 37]. CNT and CNF are also attractive for use in cement-based composites because of strength and high aspect ratios [6, 16, 17]. Li et al proposed adding MWCNT to mortar for improved mechanical properties [14]. Li et al confirmed that the flexural and compressive strength of the concrete was enhanced, but they did not study the electrical properties. The same group later studied the electrical volume resistivity of cement paste containing CNT measured using the four-probe method [39]. They applied a cyclic compressive load to a 40.0 mm by 40.0 mm by 160.0 mm (1.575 in. by 1.575 in. by 6.30 in.) rectangular prism made of the material. The fractional change in the volume resistivity oscillated up to approximately 10% with the oscillation of the compressive load.

8. Damage detection of CNF concrete columns

Gao et al expanded the work on self-sensing cement-based materials by studying 152.4 mm by 305 mm (6.00 in. by 12.00 in.) cylindars made of concrete containing CNF [12]. Gao et al crushed the cylinders monotonically and studied the electrical resistance variation. They observed electrical resistance variations up to 80% and concluded that concrete containing CNF can be used for self structural health monitoring.

Howser et al continued Gao et al's work and extended it to a full scale reinforced concrete column containing CNF [4, 12]. A self-consolidating CNF concrete (SCCNFC) column was built and tested under a reversed cyclic load. The structural behavior and the self-sensing ability were examined. The results were compared to the structural and self-sensing ability of

a traditional self-consolidating reinforced concrete (SCRC) and a self-consolidating steel fiber concrete (SCSFC) specimen.

All of the columns were 508 mm (20.0 in.) tall with cross-sections of 305 mm by 305 mm (12.00 in. by 12.00 in.). Each specimen contained six #8 (25.4 mm or 1.00 in. diameter) rebar, which corresponded to 3.27% logitudinal steel by volume of concrete. The SCRC and SCCNFC columns contained #2 stirrups with a spacing of 120.7 mm (4.75 in.) providing transverse reinforcement of 0.287% by volume of concrete. Since the columns were designed to be shear critical, the maximum reinforcement spacing was chosen based on the ACI 318 specifications [25]. See Fig. 4 for the cross-section used for the SCRC and SCCNFC columns. SCSFC column contained no transverse reinforcement, as shown in Fig. 5. Each of the columns was rigidly connected to similar foundations. See Fig. 6 for the elevation view of the SCRC and SCCNFC columns and foundations. The SCSFC column is identical to that shown in Fig. 6, except it does not contain transverse reinforcement. Fig. 7 shows the experimental set-up.

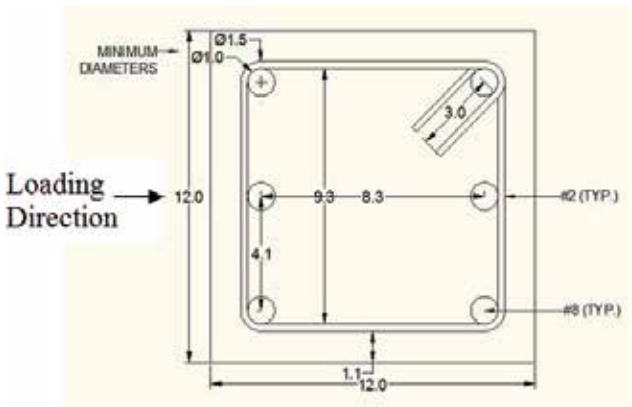

Figure 4. Cross-Section of SCRC and SCCNFC Columns (dimensions in inches)

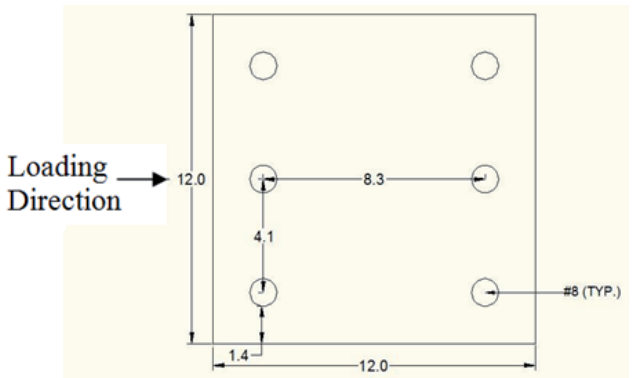

Figure 5. Cross-Section of SCSFC Column (dimensions in inches)

http://dx.doi.org/10.5772/57096

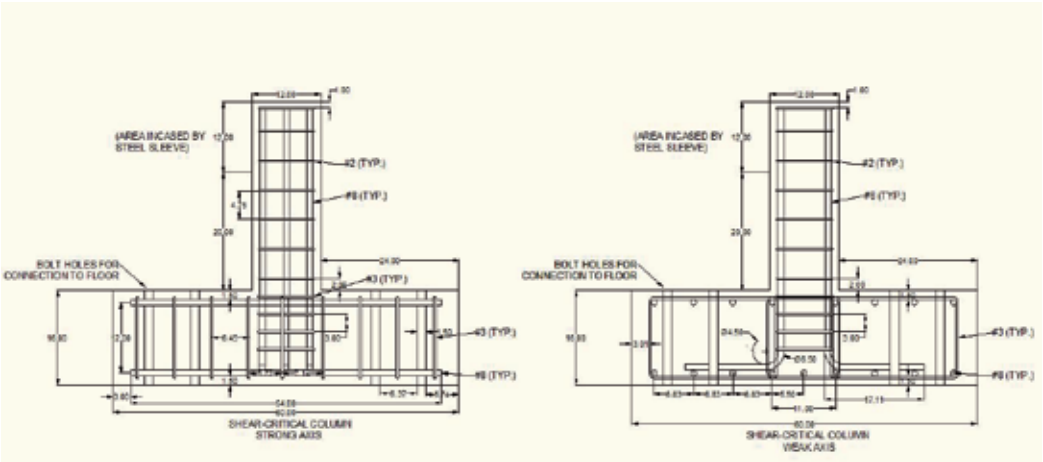

Figure 6. Elevation View of the Strong Axis of the Shear-Critical SCRC and SCCNFC Columns and Foundations (dimensions in inches)

Figure 7. Experimental Set-Up

The properties of the materials used for the three mixes were as follows:

a. Cement: The cement used in all mixtures was ASTM Type III Portland cement.

b. Fly Ash: Class C fly ash was used for the SCSFC mix and Class F fly ash was used for the SCRC mix.

c. Coarse Aggregate: Crushed limestore with a maximum diameter of ¾″ was used in the SCCNFC column. River rock with a maximum diameter of ¾″ was used in the other columns.

d. Fine Aggregate: Natural river sand with a fineness modulus of 2.71 was used in all mixes.

e. High Range Water Reducer (HRWR): Glenium® 3200HES was used in the SCCNFC column and Glenium® 3400 HES was used in the other columns. Both chemicals were polycarboxylate admixtures from BASF Chemical Co.

f. Viscosity Modifying Agent (VMA): RHEOMAC® VMA 450 was used in the specimens and also supplied by BASF Chemical Co.

g. Steel Fibers: Dramix® ZP305 fibers were used in the SCSFC mix. This was a hooked fiber with a specific gravity of 7.85. The diameter of the fiber is 0.55 mm (0.0217 in.) and the length is 30 mm (1.18 in.) resulting in an aspect ratio of 55.

h. Carbon Nanofibers: Pyrograf Products, Inc. PR-19-XT-LHT-OX fibers were used in this study. The specific gravity of the fibers was 0.0742. The diameter of the fibers was 149 nm (5.87e-6 in.) and the length was 19 μm (7.48e-4 in.) resulting in an aspect ratio of 128.

The mix proportions used for the three columns can be seen in Table 1. One percent fiber by volume was used for both of the fiber columns chosen based on literature review. It was discovered by Gao et al that CNF has an optimal dosage of approximately 1% by volume [12] [12]. It was found by many researchers that increased steel fiber increases concrete properties; however, after a percentage of 1% fibers by volume, the concrete becomes increasingly less workable, which could cause problems in construction such as honeycombing [39-41].

Material	SCRC Mix	SCSFC Mix	SCCNFC Mix
Cement	446 (752)	446 (752)	457 (771)
Fly Ash (Class C)	-	299 (504)	-
Fly Ash (Class F)	299 (504)	-	-
Fine Aggregate	937 (1580)	937 (1580)	898 (1514)
Coarse Aggregate (Limestone)	-	-	859 (1448)
Coarse Aggregate (River Rock)	491 (827)	491 (827)	-
Water	224 (377)	224 (377)	182 (307)
Glenium® 3400HES	2.81 (4.73)	2.81 (4.73)	-
Glenium® 7700HES	-	-	2.34 (3.94)
REHEOMAC® VMA 450	5.69 (9.59)	5.69 (9.59)	-
Steel Fibers	-	79.8 (134)	-
Carbon Nanofibers	-	-	3.23 (5.45)

Table 1. Mix Proportions in kg/m^3 (lb/yd^3) of Concrete

http://dx.doi.org/10.5772/57096

The main goal of testing the SCCNFC column was to prove that concrete containing CNF can be used as a sensor. To test the electrical properties of the concrete, wire meshes were constructed and embedded in each of the columns. The wire meshes were made of 12.7 mm (1/2 in.) hardware cloth with 14 gauge copper wire soldered to it. The wire extended outside of the column. The four probe method for measuring resistance was implemented, and the meshes were placed in the column as shown in Fig. 8. A power supply was attached to the top mesh that provided a current of approximately 31 V DC. An ammeter was attached to the bottom mesh and connected back to the power supply to complete a circuit. The current measured by the ammeter was recorded continuously during the tests by hand. Additional voltmeters were attached to the two middle meshes on both the north and south sides of the column to measure voltage. The voltage readings were also recorded continuously throughout the test.

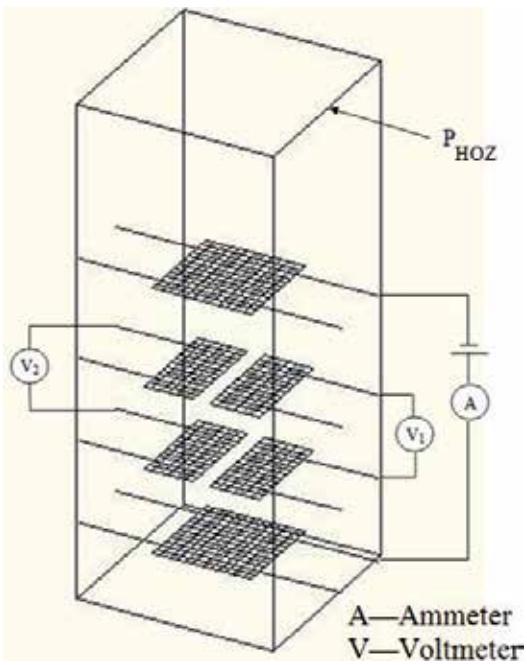

Figure 8. Four Probe Method of Resistance Measurement

The first step of the load program was to apply an axial load that would remain constant during the course of the test. The axial load equaled one-tenth of each of the columns calculated axial capacity. The axial capacity is dependent on the compressive strength of the concrete, so the axial force for each specimen varied.

After the application of the axial load, a reversed-cyclic load was added using a 649 kN (146 kip) capacity actuator. The intended load path was to use force control to complete two cycles each of ±89 kN (20 k), ±178 kN (40 k), and ±267 kN (60 k). A positive force denotes a push by the actuator while a negative force represents a pull. At the point of longitudinal steel yielding, the test switched to displacement control and completed two cycles each at a displacement

ductility of 2, 3, 4, etc. Once failure occurred, a descending branch on the load versus displacement curve was obtained in displacement control mode.

The load path followed for the SCRC column specimen can be seen in Fig. 9 with the first cracks, switch to displacement control and failure marked. The first crack on the south side of the column occurred at -178 kN (-40 k). The first shear crack formed on the column during the first -178 kN (-40 k) cycle at -178 kN (-40 k) on the west side. The column failed in shear and crushing of concrete at 276 kN (62 k). The west side of the column exhibited crushing of the concrete struts with large shear cracks. The east side exhibited local crushing at the actuator connection. The maximum displacement at the top of the column (drift) was 12.7 mm (0.50 in.).

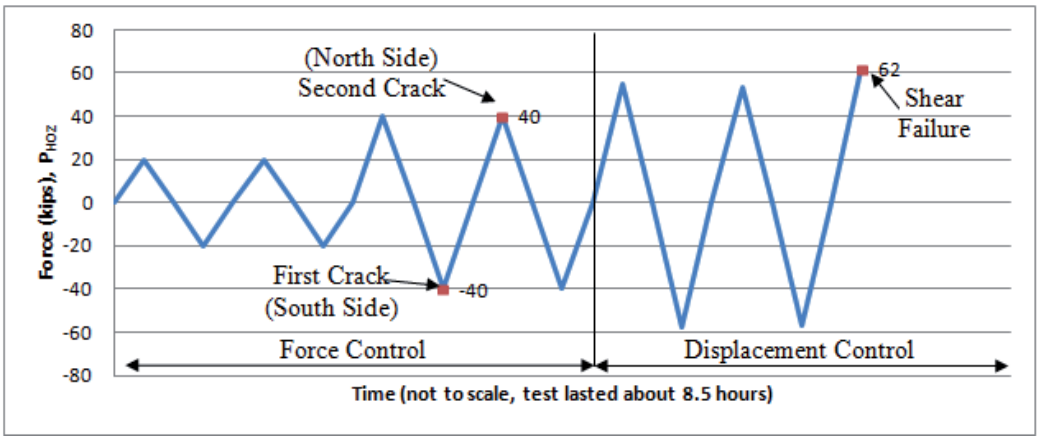

Figure 9. SCRC Column Load Path

The load path followed for the SCSFC column can be seen in Fig. 10 with the first cracks and failure marked. The first shear and flexural cracks formed on the column during the second 178 kN (40 k) cycle at 178 kN (40 k) on the west and north sides, respectively. The second flexural crack formed on the south side during the second -178 kN (-40 k) cycle at -178 kN (-40 k). The column failed suddenly in shear and crushing at 347 kN (78.0 k) on the west side of the column before the rebar yielded. The maximum displacement was 8.38 mm (0.33 in.).

The actual load path followed for the SCCNFC column can be seen in Fig. 11. The pump shut down during the test, and the actuator unloaded during the fifth cycle of the test. The pump was turned back on and the test resumed. The first flexural crack formed on the column at 160 kN (36 k) on the east, west and north sides. The second flexural crack formed on the east, west and south sides at a load of -158 kN (-35.6 k). The column failed in the combined modes of shear and concrete crushing due to flexure at 298 kN (67 k) on the west side of the column. The maximum displacement was 10.16 mm (0.4 in.).

During each of the column tests, the electrical resistance was determined to check the self-sensing ability of the concrete. The electrical readings showed a great correlation between the peaks in the applied horizontal force, strain, and resistance plots for the SCCNFC column but

http://dx.doi.org/10.5772/57096

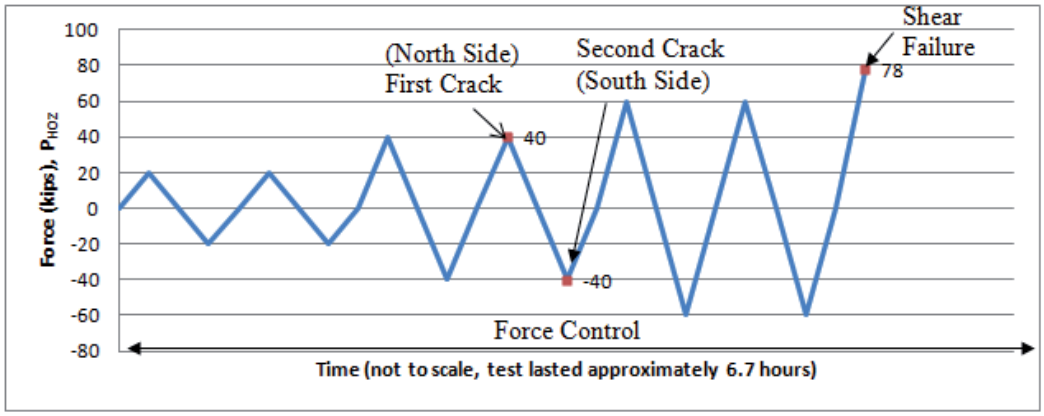

Figure 10. SCSFC Column Load Path

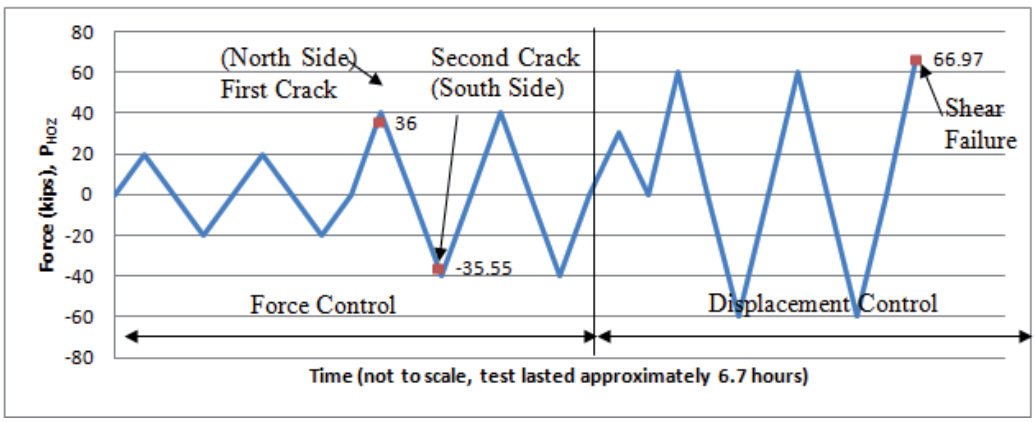

Figure 11. SCCNFC Column Load Path

little correlation between the resistance plots and the force or strain plots for the SCRC or SCSFC column. Fig. 12 shows the relationship between the SCRC column's horizontal force, LVDT strain, and electrical resistance versus time on the north side of the column. There is no relationship between the peaks and valleys in the electrical resistance and the load or strain on the north side of the column.

Fig. 13 shows the SCSFC column's force, strain, and resistance versus time on the north and south sides of the column, respectively. As shown by the grey vertical lines, there is not a relationship between the peaks and valleys in the resistance and load or strain until major cracking began to occur. After major cracking began to occur, the peaks and valleys in the electrical resistance began to correspond with the load and strain peaks and valleys. This point is shown by the dashed line in Fig. 13.

Fig. 14 shows relationship between the SCCNFC column's horizontal load, LVDT strain and electrical resistance versus time on the north side of column. As shown by the vertical lines in

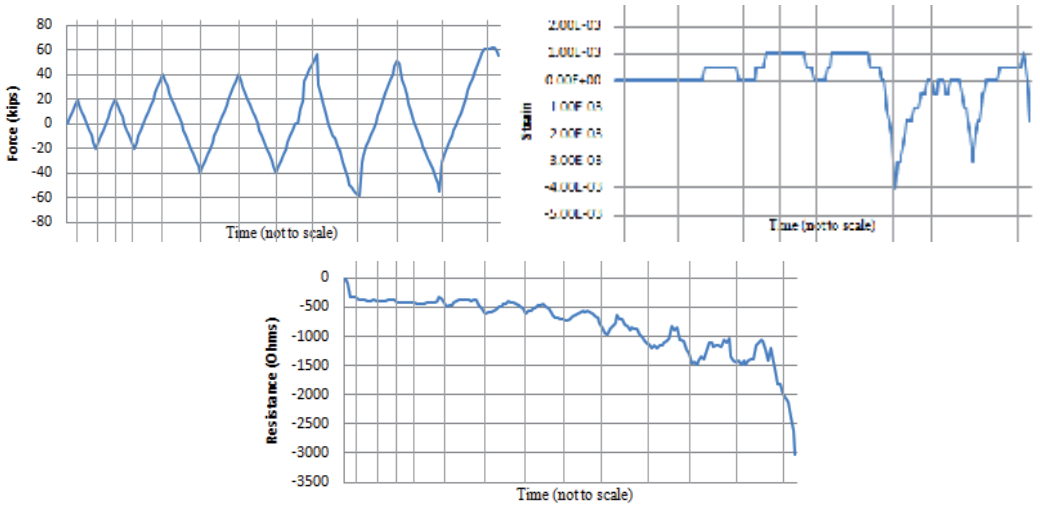

Figure 12. SCRC Column Comparison of Horizontal Force, LVDT Strain and Electrical Resistance on North Side

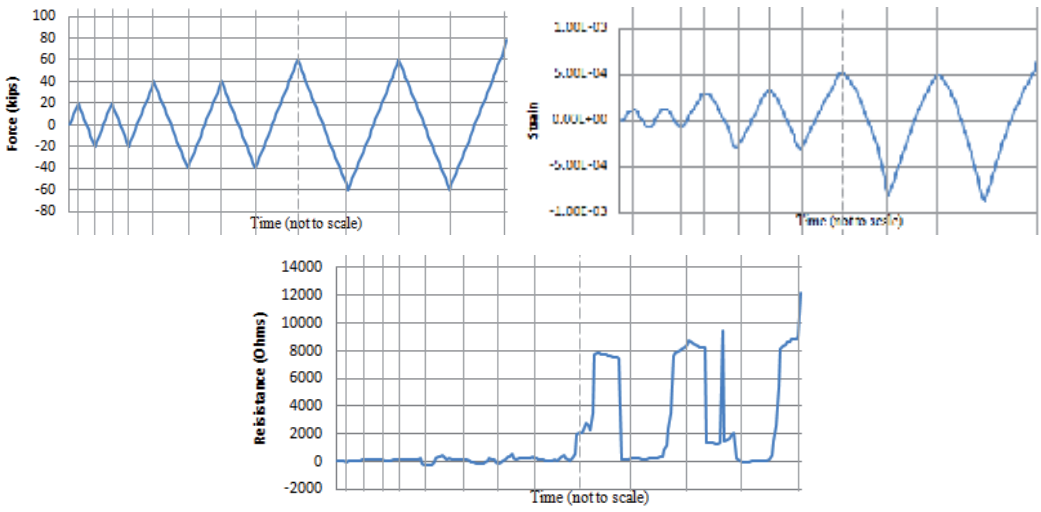

Figure 13. SCRC Column Comparison of Horizontal Force, LVDT Strain and Electrical Resistance on North Side

the grid, there is very good correlation between the force, strain and resistance. On the north side of the column, the peaks and valleys matched up until the point that the column was greatly damaged.

Because of the strong correlation found between the horizontal load, LVDT strain, and electrical resistance verses time graphs for the SCCNFC column, the electrical resistance variation (ERV) was calculated and compared to the deflection at the top of the column. ERV is the measured electrical resistance minus the initial electrical resistance quantity divided by the initial electrical resistance. Fig. 15 shows the relationship between the ERV and deflection

http://dx.doi.org/10.5772/57096

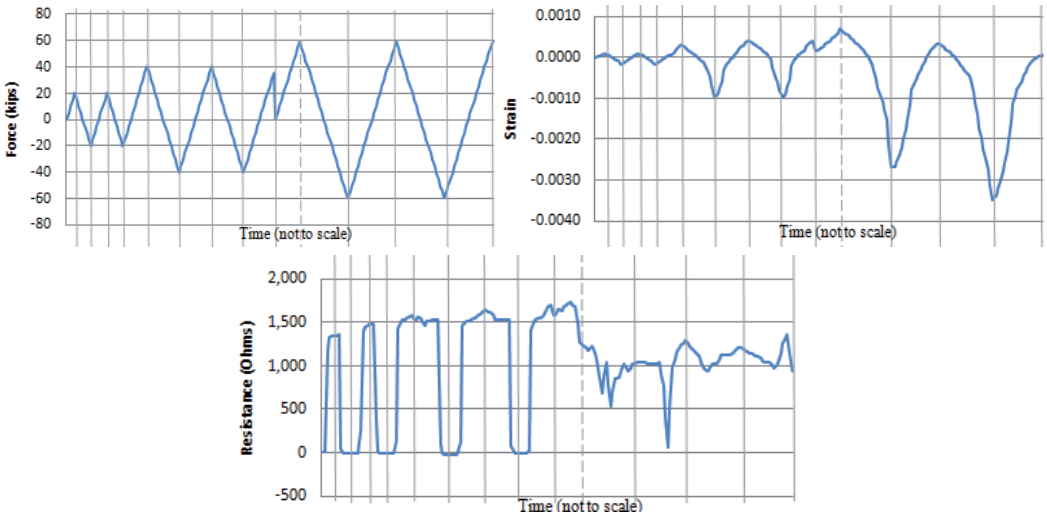

Figure 14. SCCNFC Column Comparison of Horizontal Force, LVDT Strain and Electrical Resistance on North Side

at the top of the column for the first five cycles of the test. It is obvious from Fig. 15 that the column shows major damage at approximately a deflection of 2.03 mm (0.08 in.). This corresponds to the steel yielding in the SCCNFC column. This proves that SCCNFC can be used as a type of self-structural health monitoring system.

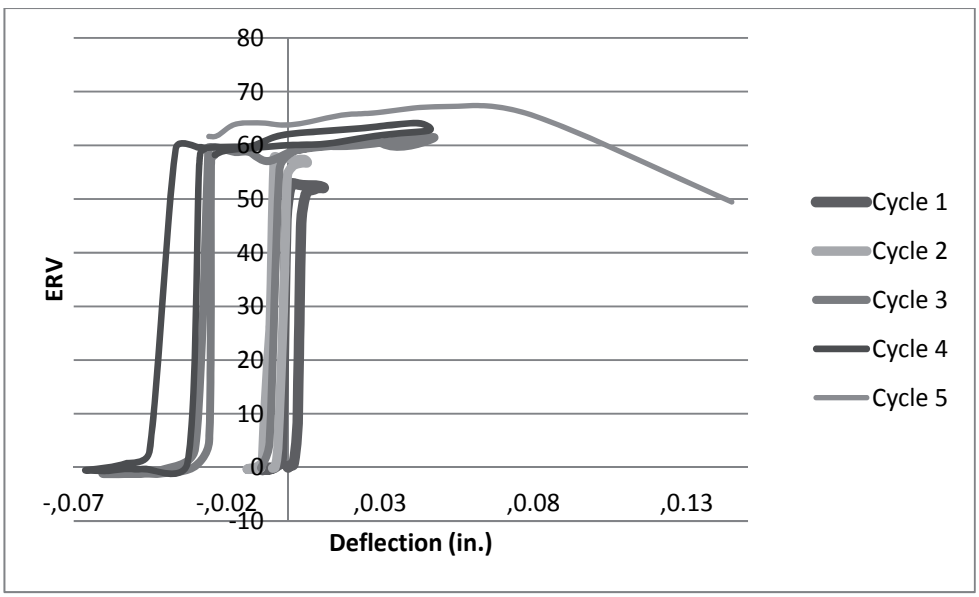

Figure 15. SCCNFC Column ERV versus Horizontal Deflection

9. Conclusions

Self-consolidating carbon nanofiber concrete (SCCNFC) follows the definition for nanotechnology set forth by the National Science Foundation and National Nanotechnology Initiative [2]. The size range of the carbon nanofibers (CNF) is approximately 100 nanometers, the SCCNFC is able to measure damage in the composite, and the CNF have properties that are specific to the nanoscale.

Well-dispersed CNF improves the strength and stiffness of concrete. Excess concentration leads to poorly dispersed CNF clumps inside the concrete and has a negative effect on both strength and electrical sensitivity. Highly workable and stable self-consolidation concrete (SCC) can maintain its workability and stability with the addition of fibers. SCC greatly increases the dispersion of carbon nanofibers (CNF) [12].

As proven by Gao et al [12] and Howser et al [4], SCCNFC can be used as a reversible strain sensor. In Howser et al's test [4], the peaks and valleys in the electrical resistance readings of the SCCNFC match the peaks and valleys of the applied force and the strain in the concrete. While the peaks and valleys in the electrical resistance readings of the self-consolidating reinforced concrete and self-consolidating steel fiber concrete specimens occasionally matched, there was not enough correspondence to safely assume that these concretes could be used as a reversible strain sensor. It was concluded that when an appropriate dosage of CNF is used, SCCNFC can be used for self-structural health monitoring.

Author details

Y.L. Mo and Rachel Howser Roberts

University of Houston, USA

References

[1] Feynman, R. There's Plenty of Room at the Bottom. Engineering and Science 1960; 23, 22-36.

[2] Roco, M. C. National Nanotechnology Initiative - Past, Present, Future. In W. A. Goddard, D. Brenner, S. E. Lyshevski, & G. J. Iafrate (Eds.), Handbook of Nanoscience, Engineering, and Technology (2nd ed.). Boca Raton, FL: CRC Press 2007; 3.1-3.26.

[3] Narayan, R. J., Kumta, P. N., Sfeir, C., Lee, D.-H., Choi, D., Olton, D. Nanostructured ceramics in medical devices: Applications and prospects. Journal of the Minerals, Metals and Materials Society 2004; 56 (10), 38-43.

[4] Howser, R. N., Dhonde, H. B., Mo, Y. L. Self-sensing of carbon nanofiber concrete columns subjected to reversed cyclic loading. Smart Materials and Structures 2011; 20 (8).

[5] Bartos, P. Nanotechnology in Construction: A Roadmap for Development. American Concrete Institute Special Publication 2008; 254, 1-14.

[6] Sanchez, F., Sobolev, K. Nanotechnology in concrete - A review. Construction and Building Materials 2010; 24, 2060-2071.

[7] Shah, S. P., Naaman, A. E. Mechanical Properties of Glass and Steel Fiber Reinforced Mortar. ACI Journal 1976; 73 (1), 50-53.

[8] Chen, P.-W., Chung, D. D. Concrete reinforced with up to 0.2 vol% of short carbon fibres. Composites 1993; 24 (1), 33-52.

[9] Li, H., Xiao, H.-g., Yuan, J., Ou, J. Microstructure of cement mortar with nano-particles. Composites Part B: Engineering 2004; 35 (2), 185-189.

[10] Li, H., Zhang, M.-h., Ou, J.-p. Abrasion resistance on concrete containing nano-particles for pavement. Wear 2006; 260 (11-12), 1262-1266.

[11] Li, H., Zhang, M.-h., Ou, J.-p. Flexural fatigue performance of concrete containing nano-particles for pavement. International Journal of Fatigue 2007; 29 (7), 1292-1301.

[12] Gao, D., Strum, M., Mo, Y. L. Electrical resistance of carbon-nanofiber concrete. Smart Materials and Structures 2009; 18 (9), 1-7.

[13] Iijima, S. Helical microtubules of graphitic carbon. Nature 1991, 354, 56-58.

[14] Li, G. Y., Wang, P. M., Zhao, X. Mechanical behavior and microstructre of cement composites incorporating surface-treated multi-walled carbon nanotubes. Carbon 2005; 43, 1239-1245.

[15] Salvetat, J. P., Bonard, J. M., Thomson, N. H., Kulik, A. J., Forro, L., Benoit, W., et al. Mechanical properites of carbon naonotubes. Applied Physics A 1999; 69, 255-260.

[16] Makar, J. M., Beaudoin, J. J. Carbon nanotubes and their application in the construction industry. 1st International Symposium on Nanotechnology in Construction, Paisley, Scotland 2003; 331-341.

[17] Kang, I., Heung, Y. Y., Kim, J. H., Lee, J. W., Gollapudi, R., Subramaniam, S., et al. Introduction to carbon nanotube and nanofiber smart materials. Composites: Part B 2006; 382-394.

[18] Coleman, N. N., Khan, U., Blau, W. J., Gun'ko, Y. K. Small but strong: A review of the mechanical properties of carbon nanotube-polymer composites. Carbon 2006; 44, 1624-1652.

[19] Makar, J. M., Margeson, J. C., Luh, J. Carbon nanotube/cement composites-early results and potential applications. 3rd International Conference on Construction Mate-

rials: Performance, Innovation and Structural Implications. Vancouver, B.C.: NRC Institute for Research in Construction; National Research Council Canada 2005; 1-10.

[20] Chung, D. D. Dispersion of Short Fibers in Cement. Journal of Materials in Civil Engineering, ASCE 2005; 17 (4), 379-383.

[21] Tzeng, Y., Huang, T. S., Chen, Y. C., Liu, C., Liu, Y. K. Hydration Properties of Carbon Nanotubes and Their Effects on Electrical and Biosensor Applications. New Diamond and Frontier: Carbon Technology 2004; 14 (3), 193-201.

[22] Baughman, R. H., Cui, C., Zakhidov, A. A., Iqbal, Z., Barisci, J. N., Spinks, G. M., et al. Carbon Nanotube Actuators. Science 1999; 284 (5418), 1340-1344.

[23] Baughman, R. H., Zakhldov, A. A., de Heer, W. A. Carbon Nanotubes--the Route Towards Applications. Science 2002; 297, 787-792.

[24] Hilding, J., Grulke, E. A., Zhang, Z. G., & Lockwood, F. Dispersion of Carbon Nanotubes in Liquids. Journal of Dispersion Science and Technology 2003; 24 (1), 1-41.

[25] ACI 318. Building Code Requirements for Structural Concrete. Farmington Hills, Michigan: American Concrete Institute; 2008.

[26] PCI, TR-6-03. Interim Guidelines for the Use of Self-Consolidating Concrete in Precast/Prestressed Concrete Institute Member Plants. Chicago: Precast/Prestressed Concrete Institute; 2003.

[27] Gaimster, R., Foord, C. Self-compacting concrete. Concrete 2000; 34, 23-25.

[28] Khayat, K. H., Hu, C., Monty, H. Stability of Self-Consolidating Concrete, Advantages, and Potential Applications. Proceedings of First International RILEM Symposium on Self-Compacting Concrete. Stockholm, Sweden 1999; 143-152.

[29] Okamura, H., Ozawa, K. Mix-Design for Self-Compacting Concrete. Concrete Library of the Japanese Society of Civil Engineers 1995; 107-120.

[30] Tanaka, K., Sato, K., Watanabe, S., Arima, I., Seunaga, K. Development and Utilization of High-Performance Concrete for the Construction of the Akashi Kaikyo Bridge. High Performance Concrete in Severe Environments, ACI SP-140 1993; 25-51.

[31] Chen, P.-W., Chung, D. D. Concrete as a new strain/stress sensor. Composites Part B: Engineering 1996; 27 (1), 11-23.

[32] Chung, D. D. Strain sensors based on the electrical resistance change accompanying the reversible pull-out of conducting short fibers in a less conducting matrix. Smart Materials and Structures 1995; 4 (1), 59-61.

[33] Chung, D. D. Cement-matrix composites for smart structures. Smart Materials and Structures 2000; 9 (4), 389-401.

[34] Xiao, H., Lan, C., Ji, X., Li, H. Mechanical and sensing properties of structural materials with nanophase materials. Pacific Scientific Journal 2003; 5, 11-17.

[35] Yang, X., Chung, D. D. Latex-modified cement mortar reinforced by short carbon fibres. Composites 1992; 23 (6), 453-460.

[36] Thess, A., Lee, R., Nikolaev, P., Dai, H., Petit, P., Robert, J., et al. Crystalline Ropes of Metallic Carbon Nanotubes. Science 1996; 273, 483-487.

[37] Wei, B. Q., Vajtai, R., Ayayan, P. M. Reliability and current carrying capactiy of carbon nanotubes. Applied Physics Letters 2001; 79 (8), 1172-1174.

[38] Li, G. Y., Wang, P. M., Zhao, X. Pressure-sensitive properties and microstructure of carbon nanotube reinforced cement composites. Cement & Concrete Composites 2007; 29, 377-382.

[39] Narayan, R. J., Kumta, P. N., Sfeir, C., Lee, D.-H., Choi, D., Olton, D. Nanostructured ceramics in medical devices: Applications and prospects. Journal of the Minerals, Metals and Materials Society 2004; 56 (10), 38-43.

[40] Padmarajaiah, S. K., Ramaswamy, A. Comparative Study on Flexural Response of Full and Partial Depth Fiber-Reinforced High-Strength Concrete. Journal of Materials in Civil Engineering 2002; 14 (2), 130-136.

[41] Aoude, H., Cook, W. D., Mitchell, D. (2009). Behavior of Columns Constructed with Fibers and Self-Consolidating Concrete. ACI Structural Journal 2009; 106 (3), 349-357.

Chapter 6

Materials and Processes for Ion Permeable Separating Membranes by Electro-Spinning

Rocío del A. Cardona and Jorge J. Santiago-Avilés

Additional information is available at the end of the chapter

http://dx.doi.org/10.5772/57094

1. Introduction

This chapter describes the generation of polymeric and composite materials, and their pertinent processing sequence for the fabrication of ion permeable membranes utilized in super-capacitors and other bipolar charge storage devices. Energy storage devices are conspicuous and ubiquitous these days. Mostly, because we are utterly dependent on electric energy for so many facets of our life, from the trendy and somewhat common electric or hybrid car, to the more rare, but no less useful pacemaker that keeps the heart pumping periodically for those in need for such device. Electric energy is so useful, because its versatility. Electric energy can be used to activate actuators to generate forces or torque, to sense mechanical, thermal, optical and chemical variables, to generate radiation fields for wireless communications, and in many other tasks. The problem with electrical energy is that in contrast with the chemical energy stored in liquid fossil fuels such as gasoline, the amount of energy per unit volume or mass stored in batteries or capacitors is less than a tenth [1, 2] of that of gasoline. This low energy density means that large volumes and masses are required to store reasonable amounts of energy resulting in reduce range for electric vehicles and short intervals between charging for "smart" phones.

2. Batteries and super-capacitors

The desire to increase the energy density of electrical cells or batteries (collection of cells) is what drives research in electrical energy storage systems. From the $Zn/ZnCl_2$ Leclanché cell to the modern Li-ion or Li-polymer batteries, what the scientist and engineers have been seeking are larger capacities (Coulombs, or Ampere-Hours delivered) [3]. All batteries consist of two

electrodes, a salt-bridge (permeable membrane that allows for the transport of ions), and electrically conductive liquid called the electrolyte. Batteries are very low impedance current sources, meaning that they have a small series resistance, this series resistance is kept small by design in order to reduce the time it takes to discharge the battery or charge the battery in the case of rechargeables [3]. Multiple challenges remain, such as better electrode materials (the density of Li ions "stored" in an electrode can be enhanced by intercalation, a phenomenon occurring in layered materials such as graphite, where the ions penetrate between the material layers), better electrolytes, the use of environmentally friendly materials (such as substituting Li for Mg as the active ion), and the use of inexpensive materials. Although electrical storage systems, such as batteries, are incapable of storing as much energy as liquid fossil fuels, for portable room temperature operations they avoid the burden that fossil fuels imposed as one try to extract the energy content stored in the chemical bonds, which require their oxidation or "burning" at high temperatures. Is evident that for this to happen at room temperature the combustion process must be thermally isolated, not a particularly inexpensive proposition, so under these circumstances batteries are a very good option.

Batteries are not the only charge storage device currently utilized or being researched. A relatively new breed of capacitors, called electrochemical capacitors, or depending on its formulation and operation, also called super-capacitors or pseudo-capacitors are been explored as potential energy storage devices [4]. The difference between these and the usual capacitors utilized in electronics / electrical applications is the capacitance or amount of charge stored per volt. The definition of a capacitor is therefore,

$$C = \frac{Q}{V} \tag{1}$$

Where C is the capacitance value, Q the stored charge in Coulombs, and V the electric potential in Volts. In terms of materials parameters and dimensions, another simple version of this relation is given by:

$$C = \frac{kA}{d} \tag{2}$$

In this case k is a material parameter, namely the product of ε the relative permittivity, and ε_0, the permittivity of free space, A, the effective capacitor area and d, the distance between the positive and negative charges. This last relation is fundamental in the understanding of these electrochemical super-capacitors functioning, as it is described in page 3 of this chapter.

3. Electrical double layer and pseudo-capacitors

There are two distinct types of electrochemical super-capacitors with different phenomena utilized as a charge storage mechanism. The first type is called an electrical double layer (EDL)

http://dx.doi.org/10.5772/57094

super-capacitor, and the second is called a redox pseudo-capacitor [4]. The first type, store charges utilizing the physical phenomenon of a double layer, where in the first layer lies negative charges (electrons) placed in the electrodes by a voltage bias, and the second layer is formed by mobile ions in an electrolyte. An EDL is formed when you immerse a conductor in an electrolyte, and proceed to bias the conductor. In that case, electrons are injected into the conductor, producing an attractive electric field to the positive ions in the electrolyte. These ions move to the surface of the conductor in order to minimize the distance between opposite polarity charges, forming the so-called inner Helmholtz layer. Since one can place more electrons in the conductor than there are ions in the electrolyte, not all the electric field from the conductor is cancelled, and more ions are accommodated increasingly farther away from the surface and the inner Helmholtz layer, forming the outer Helmholtz layer and the diffuse layer. The average distance from the conductor, where the diffuse layer ends, is called the Debye Length. See figure 1 for a schematic of the EDL.

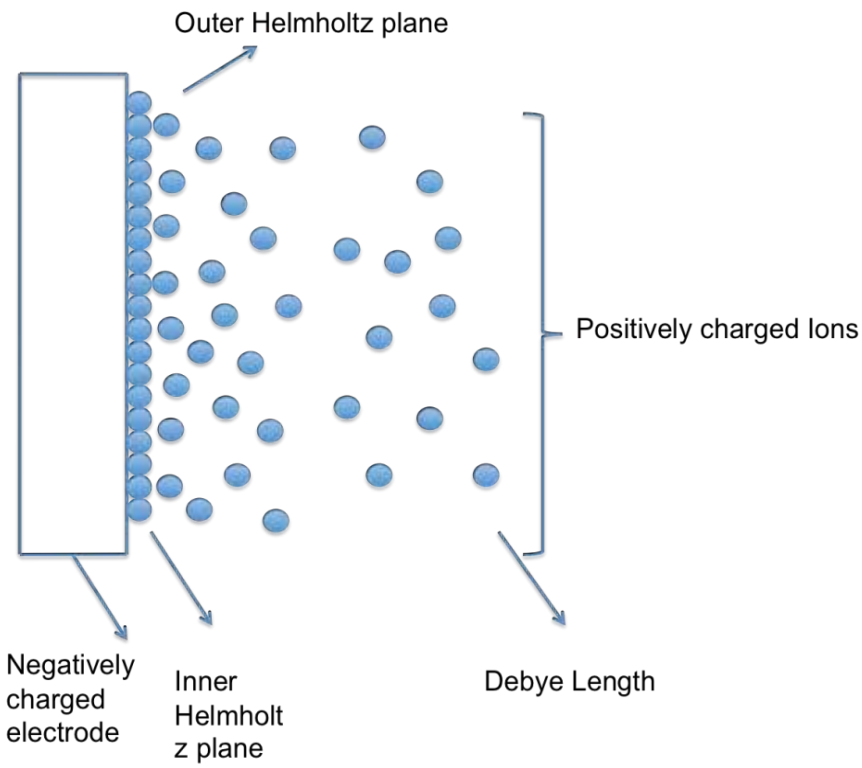

Figure 1. Simplified graphical description of the Electrical Double Layer (EDL).

For the second type, one has one or two electro active polymers (EAP) electro-deposited onto a metallic current collector and bathed by a suitable electrolyte. When you place opposite polarity voltage bias in the two electrodes, the built-on electric field attracts ions from the electrolyte, which undergo redox reactions placing charges in the peripheral chemical groups

of the EAP. If you find that this second type looks a lot like a battery, you are completely correct, it is a battery that can be charged and discharged quickly and for the electric circuit, if it behaves as a capacitor, it must be a capacitor. Since the phenomena mediating in the charge storage for this type of capacitor is chemical, they are generally addressed as pseudo-capacitors. From equation 2, one may note that capacitance increases with the effective area, which in the case of a DLC device, the area can be enhanced by using a high specific surface area (SSA) conductor such as activated carbon or any of a multiplicity of carbon allotropes [5] such as Graphene, carbon nano-tubes, carbide derived carbons, carbon onions and perhaps others.

4. Materials and models

Some of these materials possess SSA as large as 3,000 m^2 /g. The other geometrical parameter in equation 2 is d, the separation between oppositely charged particles, in this case, electrons in the electrode and ions in the electrolyte. As electrostatics demands, the mobile ions will lie on the surface of the carbon electrode pores, making d of nanoscopic dimensions. This combination of large numerator and small denominator leads to a large value of the capacitance, as large as several hundred Farads [4]. Super-capacitor in general consists of two capacitors in series, the one electrode biased negatively will attract the positive ions and the other, biased positively, will attract the counter-ions. For this reason, relation 3 gives the total capacitance, namely:

$$\frac{1}{C_T} = \frac{1}{C_1} + \frac{1}{C_2} \tag{3}$$

Note that some electrolytes are of the aqueous type (a salt dissociated in water) and other use more sophisticated organic liquids or ionic liquids, these last two, organic in origin and capable of sustaining larger voltages before degrading [4] as implied in the following relation (equation 4):

$$E = \frac{1}{2} CV^2 \tag{4}$$

Where, E is energy in Joules, C capacitance in Farads and V electrical potential in volts. Both types of super-capacitors have the distinct characteristic that they can be charged and discharged very quickly (the DLC more than the redox). Since you are doing work in order to load energy into these devices, and how quickly you do work (or use energy) is power, these super-capacitors possess large power densities (power per unit weight, or gravimetric power density, or power per unit volume, or volumetric power density). Most super-capacitors share a common configuration. If we look at one of those devices edgewise, they possess the packaging (usually metallic or polymeric), a metallization as a current collector for one of the electrodes, the electrode material (usually a carbon allotrope or a EAP / composite), the

http://dx.doi.org/10.5772/57094

electrolyte, and the separating membrane. The structure is symmetric, so the other side is pretty much the same sequence in reverse order. Figure 2 shows a schematic of a super-capacitor configuration and the inner details of its working. The simplest way of modeling a super-capacitor is by an ideal capacitor with a resistor in series. This resistor is a lump parameter, and includes all possible phenomena offering resistance (or impedance) to the flow of current, including the electrolyte, the electrodes, the current collectors, the external contacts, etc. One key aspect in the construction and improvement of EDLC is the ion permeable separator that prevents electrical contact between the conducting electrodes (shorting), but still allows ions from the electrolyte to pass through. Most of the membranes currently used, are made from polypropylene [6], a thermoplastic polymer that among other characteristics, can stand the chemical environment to which they are exposed. However, its use is limited due to UV-Vis degradation and low biocompatibility.

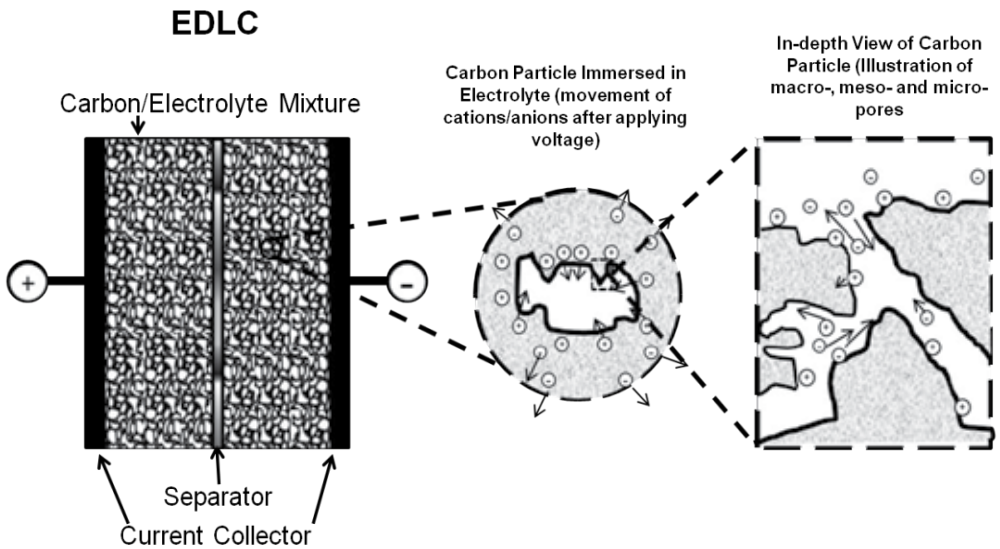

Figure 2. Schematic of the super-capacitor configuration and inner working details (not to scale).

5. Separating membranes

Ideally a good separating membrane will be thin (10-15 μm), mechanically strong (1-4 GPa), chemically inert to the electrolyte utilized, electrically insulating ($R>10^8$ Ω), and thermally stable. The high resistivity of the composite membrane might be counter intuitive, as the filler are highly conductive carbon nano-tubes (CNT's). Remember that in order for the composite to conduct an electric current effectively (with low resistance), the CNT's must be touching each other making a conductive path from one electrode to the other, in a process called percolation. The amount of CNT's as filler added to a given amount of binder in the composite

as to provoke this change in resistance is called the percolation threshold (PT). Although the PT for most polymers is small, for PLA at the highest concentration used in this study, the membrane resistance exceeded tens of MegOhms.

Besides polypropylene another common separating membrane is a composite layer of poly-tetra-fluoro-ethylene (PTFE or Teflon) between nylon or polyester layers. Polypropylene is a low-density linear polymer often used for its reasonable mechanical properties and low cost. The PTFE composite (GoreTex™) [7] relies on the properties of PTFE whose mechanical properties are defined by the rate of the strain applied during its manufacture. If high enough, it produces billions of slit shaped nanoscopic pores per square inch, allowing the flow of ions but impeding the passage of particles or colloids. The polypropylene membranes are often weaved mechanically, but they can be electro-statically deposited by electro-spinning, a process that will be described shortly. Polypropylene is also notorious for its sensitivity to sunlight, in particular the UV part of the solar spectrum as mentioned above, where carbon bonds in their chain structures are attacked by the UV photons. The ultra-violet rays modify the affected bonds to form highly reactive free radicals, which then further react with atmospheric oxygen forming carbonyl groups in the main chain. These chemical transformations modify the polymer properties, in particular mechanical properties. The device might lose color and surface cracks will appear often leading to device failure. There are other types of membranes being explored for the particular application of electrochemical super-capacitors. Some work on bipolar membranes constructed using ion-exchange membranes (anions) and a cation exchange solution to form the bipolar structure. This proto-membrane is then coated with a NAFION layer. NAFION has been utilized using other formulations [8]. Sulfonated poly (ether ether ketone, SPEEK) has been used, as a proton conducting polymer membrane in similar applications [9].

6. Polylactic acid

In our laboratory we have been exploring materials for ion permeable separating membranes showing ease of fabrication (primarily electro-spinning), chemical and mechanical stability, and low cost.

Poly lactic acid, an alpha polyester discovered in 1932 by Carothers in DuPont [10] has been the polymer of choice. There are two main routes for the synthesis of PLA, direct condensation of lactic acid, which produce low molecular weight polymers (2,000-10,000). This procedure can be followed by de-polymerization to form a cyclic dimmer intermediate followed by a ring opening polymerization to produce high molecular weight PLA (>100,000). The process is solvent free which represent a synthetic advantages for the scaling up, minimizing waste disposal. An alternative approach to obtain high molecular weight PLA is using chain coupling agents or azeotropic dehydrative condensation (figure 3) [11].

One of the principal advantages of PLA is that the precursor monomer, lactic acid, can be obtained from renewable sources including the fermentation of molasses, potato starch, or of the dextrose from corn. It can also obtained from petrochemical sources, however, due to the

http://dx.doi.org/10.5772/57094

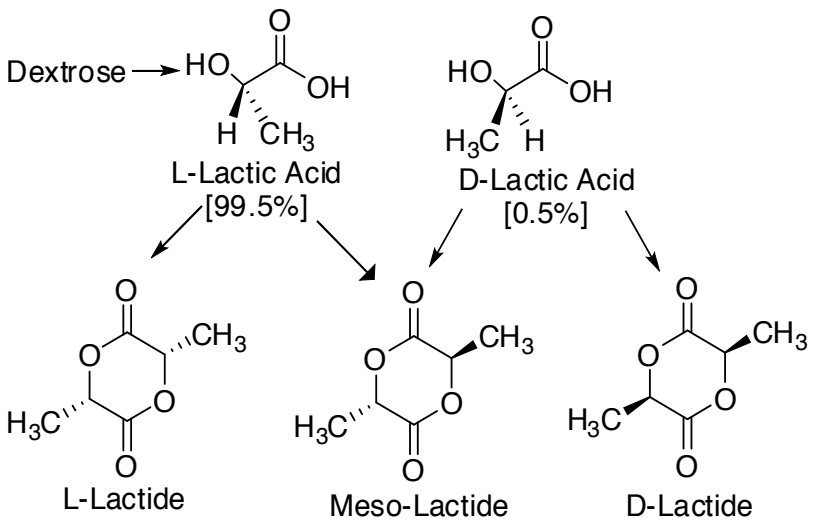

Figure 3. Synthetic routes for the production of Poly lactic acid

optimization of cornstarch bacterial fermentation using a Lactobacillus strain, this is now a days the most often employed method to obtained the monomer. Poly-L-lactic acid (PLLA), the principal product of the reaction under controlled synthetic conditions, is chiral, that is, it rotates the polarization plane of light, that is why the L, for levo-rotation. PLLA has a crystallinity of around 37%, a glass transition temperature between 60-65 °C, a melting temperature between 173-178 °C and a tensile modulus between 2.7-16 GPa. Interestingly, heat resistant PLLA can withstand temperatures of 110 °C (230F) [12]. These relatively high temperatures represent an adequate factor of safety for automotive and other traction applications of supercapacitors.

Besides its synthetic and physical properties advantages, PLLA is a biodegradable and biocompatible polymer approved by the FDA for food packaging and implantable medical devices, allowing it use in EDL applications as for example pacemakers.

There are several examples in the literature of PLA and other polymers [13] been combined with other materials to form composites. In a composite, one mixes (or react) two or more materials (phases) with diverse properties, to combine the effect of those properties in the product material or phase. In our continual study of materials for permeable membranes, we have combined the ease of fabrication by electro-spinning fibers formation of polymeric materials, with the enhanced mechanical and electrical properties of carbonaceous allotropes materials, and some metallic colloids such as silver. Although diamond and graphite are the most commonly mentioned allotropic phases of carbon, there are multiple members in this family, from graphene through various types of carbon nano-tubes and bucky-balls, to carbon onions, they span a gamma of physical and chemical characteristics of substantial relevance to super / pseudo- capacitor technology [14]. More on polymer based composites will be presented latter in the chapter.

7. Electro-spinning of polymers

Electro-spinning or electrostatic deposition is one of the easiest and most inexpensive methods of generating nanoscopic polymer / composite fibers of macroscopic lengths. In other words, the ease of processing, the low learning curve and inexpensive instrumentation render this technique extremely popular and versatile. One electro-spin viscous liquids, so having the right resin / solvent ratio, or in the case of composites, the right filler / binder / solvent proportions (and perhaps access to a good rheometer in order to characterize the polymer solution) is of some importance.

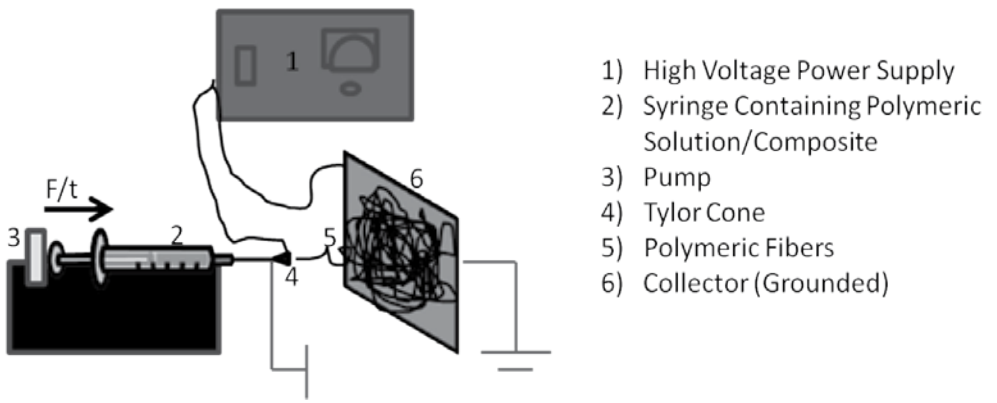

Figure 4. Details of a simple "home brew" electro-spinning apparatus.

The "home brew" configuration utilized in electro-spinning usually consists of a small (low power), high voltage power supply capable of voltage outputs in the range to several tens of kilovolts at very low current levels (below μA is desirable, see figure 4). A syringe pump, (to controlled the rate of fluid outcome from the syringe), syringe (containing the polymer solution), and an electrically grounded collector, complete the "home brew" set-up as shown above.

The morphology of the out coming fibers or mats will depend of several experimental conditions including: viscosity of the solution, applied electric field (applied voltage/needle to collector distance), the pump rate, temperature and pressure, solvent vapor pressure (evaporation rate), and collection time. Another method employed to control the fibers morphology (alignment) during electro-spinning is using a rotating collector or an oscillating needle [15]. These make electro-spinning a good tool to produce mats with a better-controlled morphology. A common morphological feature in electro-statically deposited fiber and mats is the formation of beads or beading. This particular feature involve the formation of random beads, preferentially where fibers cross each other, often due to the visco-elastic nature of the electro-spinned

http://dx.doi.org/10.5772/57094

precursor fluids or fluctuations in the deposition parameters. The mats permeability is a function of the pores dimensions distribution. These dimensions are statistically distributed and they tend to correlate inversely with the mat thickness or electro-spinning deposition time. The dimensions of most pores for reasonable deposition times (a few hours or less) lie in the range between micro and nano-meters, as evidenced by SEM micrographs.

8. Composites and characterization

In our studies, solutions of PLLA and PLLA- multi walled carbon nano-tubes (MWCNTS) composites were used. It is know that the addition of carbon nano-tubes to a polymeric solution can improved the mechanical properties of the resulting fibers and/or mat [16]. The PLLA was dissolved in 1:3 acetone/chloroform to prepare solutions of 13, 15 and 17 % w/v concentrations. The viscosity of the solutions were measured in a Bolin Rheometer with the following results, namely (1.1 +/_ 0.1, 2.8 +/_ 0.4 and 3.2 +/_0.6) Pa.s, respectively. As expected, viscosity increased as the content of polymer in solution is increased. These initial solutions were spun using the standard electro-spinning set-up, where the resulting fibers were collected in silicon wafers for subsequent structural analysis. The applied electric field during deposition was 2.3 kV/ cm, with a collection time of 10 s and a pump rate of 0.5 mL/hr. Usually for large anode-cathode distance, in excess of let's say 5 cm and a homogeneous solution, fibers diameters are randomly distributed usually following a log-normal distribution.

One problem when working with very small fibers, with diameters comparable to the wavelength of the visible light, is you inability to see or clearly image structural details such as diameters, asperities, and general morphological features. It is in such cases that scanning electron microscopy (SEM) can be a formidable characterization tool. Even when one ignores the differences in magnification between optical and SEM instruments (500,000 x, that is 250 times better magnification than a good optical microscope), the depth of field is what makes SEM such a versatile instrument. In optical microscopy, you can see the top of a micrometric diameter fiber, but not its sides or bottom, unless you move the focus. In SEM one sees around the complete fiber in focus, that is the top, sides and bottom. Of course, SEM requires a vacuum for the electron optics, and liquid samples, or samples involving liquids present serious imaging challenges. In our experimental work, SEM has been the instrument of choice for imaging and measure.

Analysis of SEM data for the fiber diameter reveals that as the solution viscosity increased, the diameter of the obtained fibers was smaller. One can see the effect by examining the distribution with a higher mean value of the fiber diameter (4 μm) for the 13 % w/v solution, and compare it to those with smaller mean diameters, i.e. (1 μm), for the 17 % w/v solution. Figure 5, show the SEM images of deposited fibers from different solutions and a histogram with the diameters frequency.

These experimental results on fibers diameter distribution suggested continuing further experimentation using the 15 % w/v solution. This particular solution produced fiber with an average diameter of (2.2±0.5) μm. It also, have no beading and more uniform morphology than

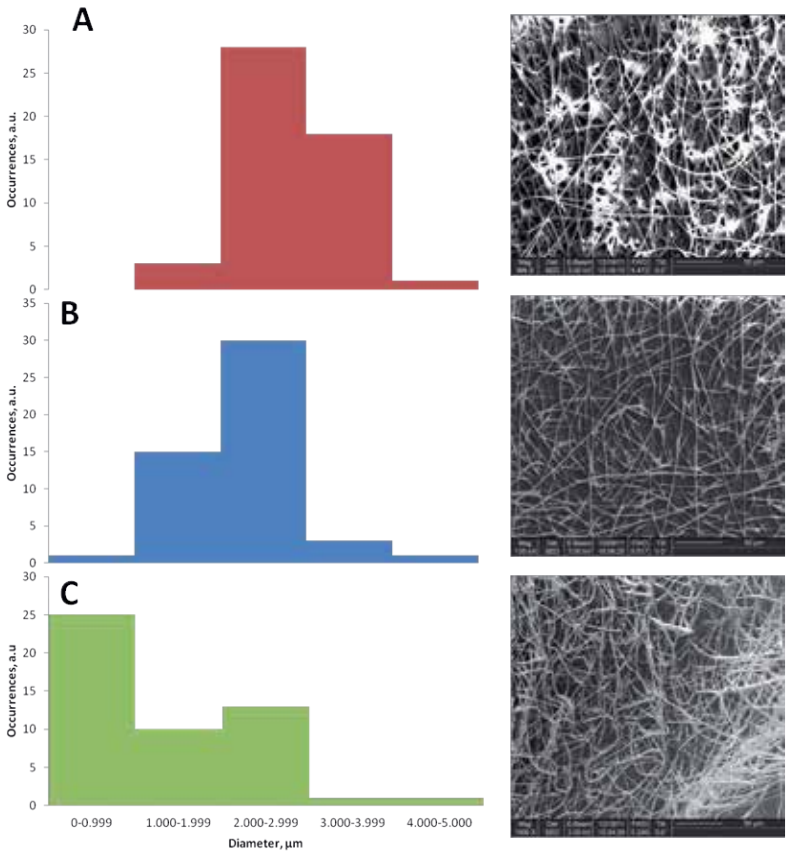

Figure 5. SEM images and data analysis for sample A) 13 % w/v PLLA, B) 15 % w/v PLLA, and C) 17 % w/v PLLA. All in 1:3 acetone/chloroform

the fibers collected from the other two solutions. These sets of facts are important, as later on they can be helpful in controlling the membranes morphology. As we proceed further, (0.2 mg/mL and 1.0 mg/mL) utilizing multi-walled carbon nano-tubes of different sizes, small (s), or large (l) (s-MWCNTs, 30-50 nm diameter, 0.5-2 μm length, and l-MWCNTs 60-100 nm diameter, 5-15 μm length), were added to the solution (15 % w/v PLLA). The viscosity of these solutions is lower than that of the pure PLLA solutions as expected, since the CNT's can only chemically interact through atoms lying in the prismatic planes (both ends of the tube) and defects, not through atoms in cylinder surface (the non-bonding π bands). Table 1 shows the viscosity data for all the solutions studied.

Figure 6 shows the SEM images and histograms for fiber diameter size distribution of 15 % w/v PLLA/ MWCNTs composites. From the SEM images we can observe that even when the viscosities of these solutions are similar, the morphology of the obtained fibers is affected by the size of the carbon nano-tubes.

Viscosity, Pa.s						
13%w/v PLLA	15% w/v PLLA	17% w/v PLLA	15% w/v PLLA (0.2 mg/mL s-MWCNT)	15% w/v PLLA (0.2 mg/mL l-MWCNT)	15% w/v PLLA (1.0 mg/mL s-MWCNT	15% w/v PLLA (1.0 mg/mL l-MWCNT
1.1 ± 0.1	2.8 ± 0.4	3.2 ± 0.6	1.6 ± 0.2	1.3 ± 0.1	1.5 ± 0.3	2.1 ± 0.6

Table 1. Viscosity as a function of composition for PLLA / MWCNT composites.

Note, how the diameters distribution shift to nano-metric size fibers for the solutions containing s-MWCNTs (figure 6, a-b) in comparison to the solutions containing l-MWCNTs (figure 6, c-d). From SEM images it can also be observed that the addition of l-MWCNTs seems to promote the formation of beads within the fibers. In order to study the suitability of PLLA/ MWCNTs composites in the production of membranes, the electro-spinning set-up was modified, using as a collector a rotating cylinder. The electro-spinning conditions were kept as before (applied electric field was 2.3 kV/ cm, and a pump rate of 0.5 mL/hr), with the exception of an extended collection time of 1 hr, while the cylinder angular speed was kept at 69 rpm.

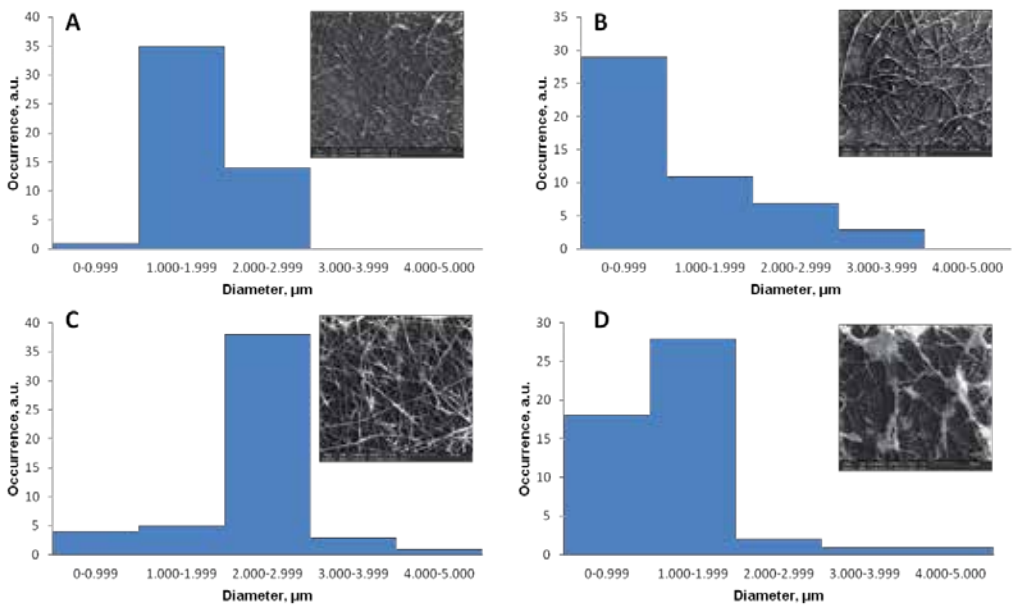

Figure 6. SEM images and histograms for A) 15 % w/v PLLA with 0.2 mg/mL s-MWCNTS B) 15 % w/v PLLA with 1.0 mg/mL s-MWCNTS, C) 15 % w/v PLLA 0.2 mg/mL l-MWCNTS, and D) 15 % w/v PLLA 1.0 mg/mL l-MWCNTS. All in a solution of 1:3 acetone/chloroform.

Other significant characterization techniques, of particular importance in the compositional and structural characterization of carbon allotropes and polymers are infrared (IR) and Raman spectroscopy. In the case of IR spectroscopy (see figure 7), the electric field associated with the photon; excite vibrations of existing dipoles in the material. If the material is crystalline, phonons of differing modes will propagate carrying part of the degenerated energy as heat (motion). In the case of Raman, a laser, with the intense electric field associated to its photons, induce a dipole in the material, and excite dipole oscillations with similar consequences as in IR. Of course, the light emitted by the vibrating charges in both cases (IR and Raman) is used as a signature of the material under study, collected by suitable optics, send to a photo-detector and transduced as a voltage to the processing unit and displayed. Most polymers are IR active, that is, they possess the pertinent dipoles in their structure. For these materials IR spectroscopy is a useful characterization tool, as most spectra are tabulated and indexed. In the case of carbonaceous materials, Raman spectroscopy is the technique of choice, as their spectrum, shows two prominent peaks around 1350 and 1600 cm^{-1}. (see figure 8) The peak at ~ 1350 wave numbers is a disorder induced response, and the other, ~1600 cm^{-1}, is a Raman-allowed mode found in highly oriented pyrolytic graphite (HOPG). The ratio of the intensity of both peaks often correlates with order and crystallinity [17]. In order to have a large SSA material, its crystallinity (order) is compromised and these spectroscopic tools become excellent local structural characterization instruments.

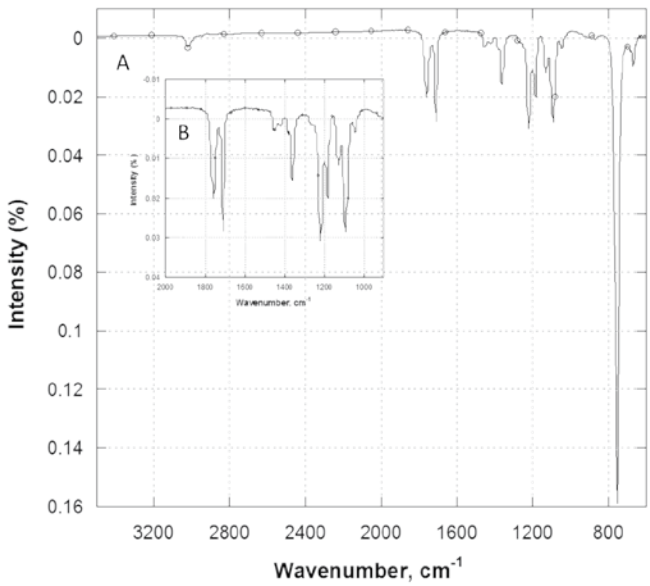

Figure 7. IR spectra for A) PLLA in 1:3 acetone/chloroform B) insert: bands at 1763 cm^{-1} and 1714 cm^{-1} assigned to the ester carbonyl and carboxylic acid carbonyl functional group respectively can be observed together to the OH bend at 1361 cm^{-1} and 1093 cm^{-1}, the C-O stretch can be observed at 1223 cm^{-1}. The strong band at 750 cm^{-1} is due to the S-C stretch because the samples were mounted in silicon wafers.

http://dx.doi.org/10.5772/57094

The interaction between mathematical modeling and experiments often can be mutually beneficial. A theoretical framework can provide experiments with the "backbone" of predictability. Clear correlations by fitting experimental results to a suitable theory helps the scientist decide how and where to do the next experiment, and to "understand" results, errors and fluctuations. The problem is that at times, analytical results are difficult or impossible to obtain. In that case the scientist often utilize numerical methods with the aid of a plethora of commercially available software packages of ease implementation in a personal computer. The software of our choice is COMSOL™. We like this software for its versatility, friendliness, and economy [18]. This software is capable of coupling the PDE's for mechanics, heat, E&M, acoustic, electro-chemistry and others. We have used it for about a decade now, and really benefited from it.

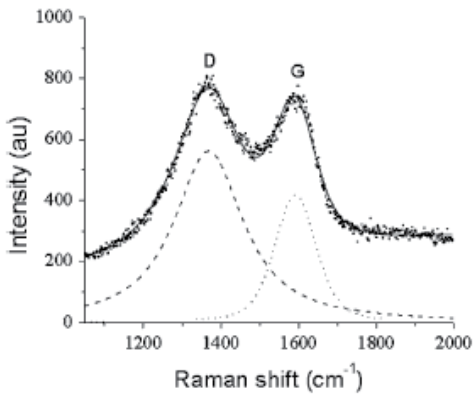

Figure 8. Raman spectrum for a carbonized electro-spun PAN fiber. The first peak, labeled D, correlates with disorder while the second, labeled G correlates with crystallinity.

9. Mechanical properties

The relevance of mechanical properties to the performance of super-capacitors separating membranes stem from the forces and stresses these membranes are exposed during capacitor fabrication, when the material is cut and aligned, as well as during service, when Joule heating generated thermal stresses load the fibers. Since the fibers forming the matt are randomly deposited, they are fluctuating in both on its spatial distributions in the deposition plane, and in fiber diameter. The possibility of having simultaneously a particular spatial location with a particular concentration of small diameter fibers, generating a "soft spot" mechanically and easily deformed by the transported fluid, is finite. Ongoing analytical and simulations research testing this hypothesis is expected to soon yield a predictive model.

The relation between stresses and deformation, at least for small deformations or strain are linear and they have been systematized by solutions to Hookes' Law that, for an anisotropic substance, linearly relates the strain tensor to the stress tensor with the elastic moduli as the

proportionality constant. For a homogeneous isotropic substance, the stress, strain and elastic constants are all scalars with the value of the elastic constants known as the Young's modulus as depicted in equations 5.

$$\sigma_{ij} = c_{ijkl}\varepsilon_{kl} \tag{5}$$

Equations 5, $\sigma_{ij} = c_{ijkl}\varepsilon_{kl}$ (anisotropic media), $\sigma = Y\varepsilon$ (isotropic media), where σ is the symbol for stress, c for elastic constants, Y for Youngs' modulus, and ε for strain.

Sample ID	Thickness, inches	Cross Section Length, inches	Area, inches^2	UTS, PSI	Breaking Point, PSI	Speed, inches/min	Breaking Time, min	Breaking Time, min/inch^2	Young's Modulus, PSI
GoreTex™	0.0011	0.197	0.00022	3508.97	2787.64	0.5	0.84	3818.18	653.73
15% PLA	0.0018	0.236	0.00042	889.37	728.93	0.3	1.56	3714.29	20.07
(1 mg/mL) s-MWCNT	0.0006	0.236	0.00013	1186.90	957.78	0.1	0.74	5692.31	12.27
(1 mg/mL) l-MWCNT	0.0007	0.236	0.00017	1711.86	1482.08	0.3	0.36	2117.65	29.73

Table 2. Mechanical properties of the mats studied.

There are multiple approximate solutions to Hooke's law for different experimental circumstances. Since the thickness of these permeable separating mats is small compared to the diameter when utilized in super-capacitors, they are bona-fide membranes. There are two types of membranes often encountered in practice [19] namely, the thick and thin membranes. The first type received its name when the maximum deflection at its center (in this case of a circular membrane as often used in super-capacitors) under load, w_o is far smaller than the membrane thickness d_m. The membrane is thin when the deflection is larger than the membrane thickness. The approximations are such that a thick membrane maybe treated as thin as the pressure head increases, and so the deflection. The deflection shape for a thick membrane relates to the torques acting along the circumference where the membrane is clamped. The deflection of a circular thick membrane w, with radius of R_m is described by equation 6. The membranes thickness range between 50 and 150 μm, while the estimated deflections are much smaller (nano-metric), so equation 6 for a thick membrane model the behavior of our separating membranes reasonably well.

$$w(r) = w_0\left(1 - \frac{r^2}{R_m{}^2}\right)^2 \tag{6}$$

Various fibers and mats were prepared for mechanical test as well as for morphological analysis. The mechanical strength was measured using the INSTRON (Model 4206), the sample were cut it with "doggy bone" configuration [20]. During the experiment, both ends of the

http://dx.doi.org/10.5772/57094

sample are clamped. The upper end is vertically pulled up at a constant force and velocity, until the samples fracture. From the geometry and strain rate information one can infer the value of the composite Young's modulus. Table 2 summarize the results for mechanical test for mats obtained from the electro-spinning of 15 % w/v PLLA solutions in 1:3 acetone/ chloroform with MWCNTs in comparison with currently use membrane in our laboratory, GoreTex™.

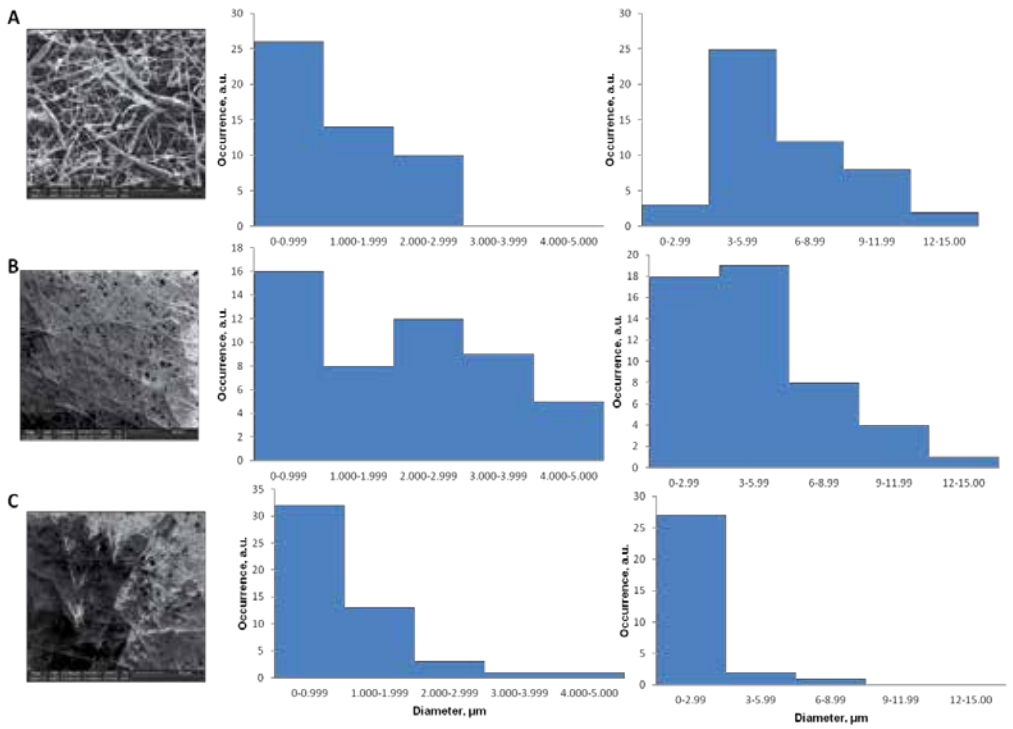

Figure 9. SEM with corresponding histogram analysis for fibers diameter and pores diameter for A) 15 % w/v PLLA B) 15 % w/v PLLA with 1.0 mg/mL s-MWCNTS, C) 15 % w/v PLLA 1.0 mg/mL l-MWCNTS in 1:3 acetone/chloroform.

It can be observed from our results that the Young's modulus decreases from l-MWCNTs (29.73 PSI) > 15 % PLA (20.07 PSI) > s-MWCNTs (12.27 PSI), this can be correlated with the mats fiber diameters distribution, where the number of nanometric diameter fibers increases in the same order: l-MWCNTs > 15 % PLA > s-MWCNTs. However, the number and dimensions of pores, decreases in the following order, 15 % PLA > s-MWCNTs > l-MWCNTs (figure 9). It has been reported previously that the Young's modulus in nonwoven fabrics is affected by porosity, fiber diameter, radius of curvature, and the distance between the junctions where fibers cross [21]. Therefore, not a single factor is responsible for the mechanical properties, but we can see a trend in our results that smaller fiber composition, together with bigger pores seems to somewhat enhance the Young's modulus. In comparison, the GorTex™ membrane has a higher Young's modulus, as it is expected for woven fabrics. We test the performance of the membrane

produced from the 15% w/v PLA solution to that of the GorTex for one of our devices. The decision to use the 15% w/v PLA membrane was done under the bases that this membrane posses more uniformity in the average pores' size than the others.

10. Concluding remarks

The device utilized to test the suitability of the PLLA based composite membrane was a pseudo-capacitor device, using as electrode material the oxidized and neutralized species of poly-3,4-propylenedioxythiophene (the process for the construction of this device have been previously reported by our group) [22,23]. The results indicated (figure 10) that over slow charging-discharging rates our membrane performed better than the bench mark membrane, but as we moved from moderate to fast charge-discharge rates, the performance of both membranes are comparable.

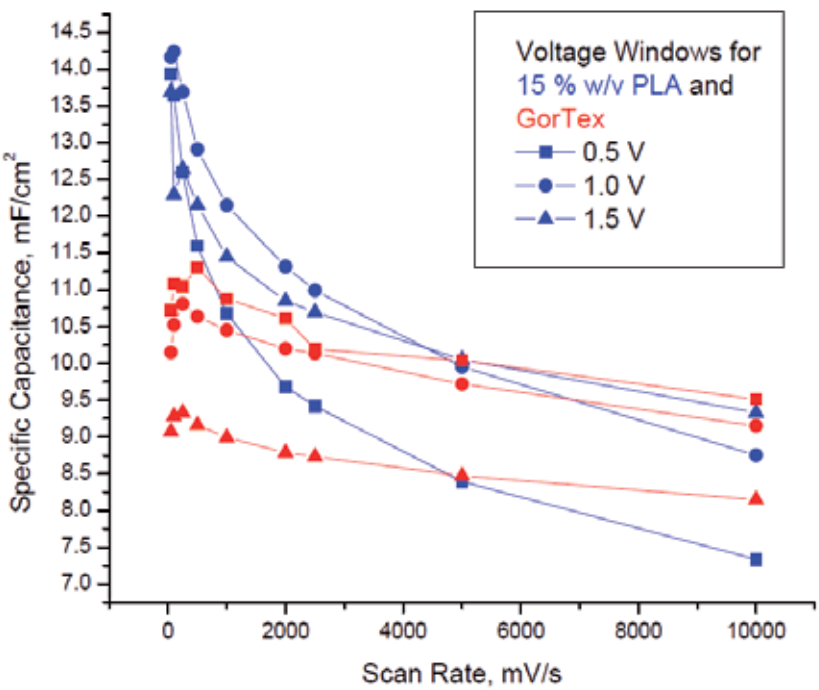

Figure 10. Specific capacitance as a function of scan rate and voltage window for poly-3,4-propylenedioxythiophene pseudo-capacitor using GorTex™ and PLLA separator membranes.

http://dx.doi.org/10.5772/57094

Acknowledgements

We would like to acknowledge support from the following sources:

The Penn's Nano-Bio Interface Center (NBIC) through the NSF sponsored grant NSEC DM R08-32802.

R. Cardona would like to acknowledge the University of Pennsylvania Provost Office and the Laboratory for the Research on the Structure of Matter (LRSM) through the NSF grant DMR11-20901 for her support as a postdoctoral fellow.

We like to acknowledge the SEM microscopy work of our collaborator Prof. Eva Campo from Penn' s LRSM.

We acknowledge the help offered by our graduate students Mr. Timothy Jones, and Hitesh Sahoo, as well as the NSF – REU sponsored undergraduates Mr. Matt Biggers, Mr. Esteban Villareal, Mr. Raymond Xu, Mr. Melvin Berrios and the two H.S. interns, Mr. Adam Flecher and the ACS-Seed fellow, Ms. Rebecca Irizarry.

Author details

Rocío del A. Cardona and Jorge J. Santiago-Avilés*

*Address all correspondence to: santiago@seas.upenn.edu

Electrical and Systems Engineering, University of Pennsylvania, Philadelphia, USA

References

[1] R.Kotz, M.Carlen, *Principles and Applications of Electrochemical Capacitors*, Electrochemica Acta, 2000; 45, 2483-2498

[2] H.D. Abruña, Y.Kiya, J.C.Henderson *Batteries and electrochemical capacitors*. Physics Today. 2008, 43-47

[3] C.A. Vincent, and B. Scrosati. Modern Batteries. In: Butterworth, Oxford; 1997.

[4] B.E. Conway. Electrochemical Supercapacitors. In: Plenum Publishers, N.Y. ;1999.

[5] Yury Gogotsi. Carbon Nanomaterials. In: CRC Press; 2006.

[6] E. P. Moore. Polypropylene Handbook. Polymerization, Characterization, Properties, Processing, Applications. In: Hanser Publishers, N.Y.; 1996.

[7] Gore Text. http://en.wikipedia.org/wiki/Gore-Tex (accessed August 2 2012)

[8] Mauritz, K. A., Moore, R. B. State of Understanding of Nafion. Chemical Reviews 2004; 104 (10) 4535–4585.

[9] Burger, C., Hsiao, B.S., Chu, B. Nano-fibrous Materials and Their Applications. Annual Reviews of Material Research. 2006; 36, 333–368.

[10] Mehta, R., Kumar, V., Bhunia, H., Upadhyay, S.N. Synthesis of Poly(Lactic Acid): A Review. Journal of Macromolecular Science. 2005; 45, 325-349.

[11] Gupta, B., Revagade, N., Hilborn, J. Poly(lactic acid) fiber: An overview. Progress in Polymer Science. 2007; 32, 455-482.

[12] Södergård, A., Stolt, M. Properties of lactic acid based polymers and their correlation with composition. Progress in Polymer Science. 2002; 27 (6), 1123–1163.

[13] Harris, A. M., Lee, E.C. Injection molded Polylactide(PLA) composites for automotive applications. Material Research and Advanced Engineering, Ford Company. http://speautomotive.com/SPEA_CD/SPEA2006/PDF/c/c1.pdf (Accessed August 2 2012).

[14] Rosario-Canales, M., Derias, P., Therien, M.J., Santiago-Aviles, J.J., Composite Electronic Materials Based on Poly(3,4-propylenedioxythiophene) and Highly Charged Poly(aryleneethynylene)-Wrapped Carbon Nanotubes for Supercapacitors, ACS Applied Materials and Interfaces. 2012; 4 (1), 102–109.

[15] Li, D., Xia, Y. Electrospinning of Nanofibers: Reinventing the Wheel?. Advanced Materials. 2004; 16, 1151-1170.

[16] Bal, S., Samal, S.S. Carbon nanotube reinforced polymer composite-A state of the art. Bulletin of Material Science. 2007; 30(4), 379-386.

[17] Fung, A.W.P., Rao, A.M., Kuriyama, K., Dresselhaus, G., Endo, M., Shindo, N. Raman scattering and electrical conductivity of highly disordered activated carbon fibers. Journal of Material Research. 1993; 8 (3), 489-500.

[18] Wang, Y., Ramos, I., Santiago-Aviles, J.J. Nanofibers "Diversity of Nano-fibers from Electro-spinning: from Graphitic Carbons to Ternary Oxides". In: INTECH publishers, Croatia; 2010. P89-120.

[19] Szegö, G. On Membranes and Plates. Proceedings of the Natural Academy of Science of the United States of America. 1950; 36(3), 210–216.

[20] Herrmann, A.M. Instrumentation for multiaxial mechanical testing of inhomogeneous elastic membranes. http://hdl.handle.net/1721.1/35671 (accessed August 2 2012).

[21] Pai, C-L., Boyce, M.C., Rutledge, G.C. On the importance of fiber curvature to the elastic moduli of electrospun nonwoven fiber meshes. Polymer. 2011; 52, 6126-6133.

http://dx.doi.org/10.5772/57094

[22] Rosario-Canales, M., Deria, P., Gopu, P., Therien, M., Santiago-Aviles,J.J. Composite Electronic Materials for Super-capacitor Applications, ECS Transactions. 2009; 23(1), 3-10.

[23] Partial content of this work was presented by the author (R. delA Cardona) at 2nd International Conference on Electrospinning, Jeju, S. Korea, 2012, Poly-l-Lactic Acid Membranes Produced by Electrospinning for Applications in Electrical Double Layer Capacitors.

Chapter 7

Nanofibers Reinforced Polymer Composite Microstructures

A. Alubaidy, K. Venkatakrishnan and B. Tan

Additional information is available at the end of the chapter

http://dx.doi.org/10.5772/57101

1. Introduction

In general, nanocomposites are defined as the combination of multiphase materials in which at least one of the constituents has one dimension in the nanometer range [1]– [3]. The nanoscale constituent could be one dimensional likenanofibres and nanowires, two-dimensional like nanoclay or three-dimensional like spherical particles in nanoscale range. Nanofibers reinforced polymermultifunctionalitycan be attributed to the combination of the constituent materials. Desired properties of nanofibers reinforced polymercan be obtained by the selection of the constituent materials and the size of the nanofibress based on the required application. Current research has focused in the areas of manufacturing techniques and material combination for the fabrication of the nanostructured reinforced polymers [4], [5].

Nanofibers reinforced polymer are progressing with the use of a combination of atomic scale characterization and detailed modeling. In the early 1990s, Toyota Central Research Laboratories in Japan reported working on a Nylon-6 nanocomposite [6], in which a small amount of nano filler resulted in a considerable improvement of thermal and mechanical properties. The properties of nanofibers reinforced polymer materials depend on their morphology and interfacial characteristics as well as on the properties of their individual parents (nanofillers and polymer, in this case).

Dramatic changes in physical properties will be the result of the transition from microparticles to nanoparticles. Nanoscale materials have a large surface area for a given volume [7]. A nanostructured material can have substantially different properties from a larger-dimensional material of the same composition because many important chemical and physical interactions are governed by surfaces and surface properties. In the case of nanoparticles and nanofibers, the surface area per unit volume is inversely proportional to the material's diameter. So, the smaller the diameter, the greater is the surface area per unit volume [7]. Figure 1 shows

common particle geometries and their respective surface area-to-volume ratios. For the nanofiber and layered material, the surface area to volume ratio is dominated by the first term in the equation, especially for nanomaterials. The second term (2/l and 4/l) has a very small influence and is often omitted compared to the first term. Therefore, a changefrom the micrometer to nanometer in particle diameter, layer thickness, or fibrous material diameter range, will affect the surface area to volume ratio by three orders of magnitude [8].

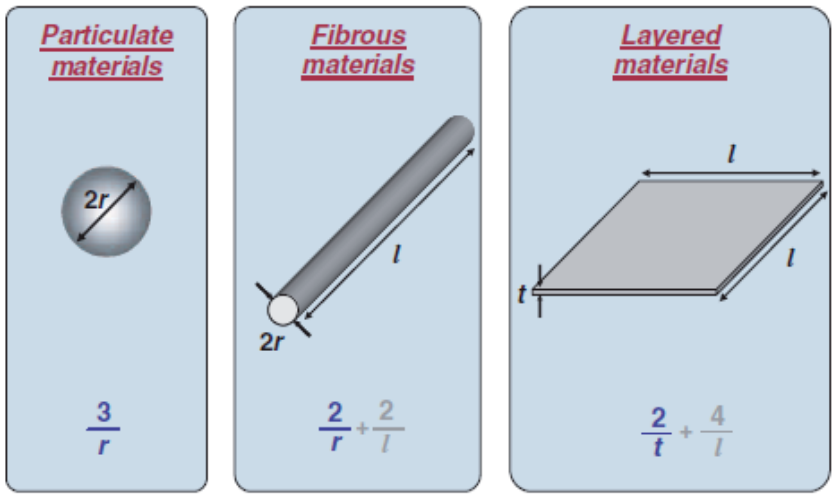

Figure 1. Common particle reinforcements/geometries and their respective surface areatovolume ratios. [8].

Typical nanomaterials currently under investigation include nanoparticles, nanotubes, nanofibers, fullerenes, and nanowires. In general, these materials are broadly classified by their geometries [9]: particle, layered, and fibrous nanomaterials [8], [9]. Carbon black, silica nanoparticle, polyhedral oligomericsislesquioxanes, can be classified as nanoparticle reinforcing agents, while nanofibers and carbon nanotubes are examples of fibrous materials [9]. When the filler has a nanometer thickness and a high aspect ratio (30–1000) plate-like structure, it is classified as a layered nanomaterial such as an organosilicate [10].

In general, the high aspect ratio of nanomaterials provides the necessary reinforcement properties. The properties of reinforced polymers are greatly influenced by the size of its nanomaterial and the quality of the interfacing between the matrix material and the filler material. Significant differences in composite properties may be obtained depending on the nature of the filler material used whether its layered silicate or nanofiber, cation exchange capacity, or polymer matrix and the method of preparation [11]. As an example, when the polymer is unable to intercalate (or penetrate) between the silicate sheets, a phase-separated composite is obtained, and the properties stay in the same range as those for traditional microcomposites [10]. In an intercalated structure, where a single extended polymer chain can penetrate between the silicate layers, a well-ordered multilayer morphology results with alternating polymeric and inorganic layers. An exfoliated or delaminated structure is obtained

when the silicate layers are completely and uniformly dispersed in a continuous polymer matrix. In any case, the physical properties of the resultant nanofibers reinforced polymer will be significantly different, as discussed in the following sections. Similarly, in fibrous or particle-reinforced polymer nanofibers reinforced polymer (PNCs), dispersion of the nanoparticle and adhesion at the particle–matrix interface play crucial roles in determining the mechanical properties of the nanofibers reinforced polymer. The nanomaterial will not offer improved mechanical properties without proper dispersion. A poorly dispersed nanomaterial may degrade the mechanical properties of the produced reinforced polymers [12]. Additionally, optimizing the interfacial bond between the nanostructures and the matrix, one can tailor the properties of the overall nanofibers reinforced polymer in a similar manner to what is done in macrocomposites. As an example, good adhesion at the interface will improve properties such as interlaminar shear strength, fatigue, delamination resistance,and corrosion resistance. Finally, it is important to recognize that snanofibers reinforced polymer researches are extremely broad,encompassing areas such as communications, electronics and computing, data storage, aerospace and sporting materials, health and medicine, transportation, energy, environmental, and many other applications. The focus of this chapter is to highlight the state of knowledge in processing, fabrication, characterization, properties, and potential applications of the nanofibrous reinforced polymer microstructures.

2. Fabrication techniques

The advancement in the technology of MicroElectroMechanical Systems (MEMS) has demand for the fabrication of 3D micro/nanostructures and devices. The excitement surrounding the nanoscale science and technology gives us unique opportunities to develop and examine revolutionary processes and materials. Nanofibers reinforced polymer embedded with 2D and 3D micro/nano materials find many applications in the field of medicine, tissue engineering, drug delivery, antibacterial implants or catheters, modification of textiles, and modification of polymers. Many optical, electrical and magnetic applications, have opened up new areas of research for manufacturing nanofibers reinforced polymer with engineered nanoparticles materials.

Researchers have been working on different micro/nano manufacturing techniques. LIGA (German acronym for Lithographie, Galvanoformung, Abformung) [7], [8], Photolithography (6), Electrochemical Fabrication (EFAB) [9], localize electrochemical deposition [10] and laser sintering [13] are some of the techniques used for micro/nano fabrication. Some of these techniques have been used for the fabrication of nanofibers reinforced polymer by dispersing nanofibers in polymer resins.

The LIGA technique was invented approximately 20 years ago. It is a powerful method that facilitates the high volume production of nanofibers reinforced polymer components for many fields of applications [14]. Researchers presented designs, fabrication and experimental results of high power electrostatic microactuators, using LIGA process. This process is capable of producing high aspect ratio microstructures of nanofibers reinforced polymer, as shown in Figure 3 [15].

The LIGA process uses the simple shadow printing process onto a resist on an electrically conducting substrate. After development of the irradiated resist, an electroforming step fills the holes of the relief with metal. This more stable body is used as a mold insert for further molding or embossing steps [8]. The deep lithography step, performed by the use of highly parallel and collimated synchrotron radiation, is the basic step, thus not only defining the shape but also the structural accuracy of the final product. [16].

Typically LIGA structures allow for the free choice of the lateral 2D pattern that is projected into the third dimension to form prismatic or cylindrical geometries. Generally, this technique has been used to produce structures with straight walls. However, for all major LIGA process steps, variations have been developed to increase the fabrication flexibility. Geometrical variations in the third dimension (vertical) are possible and can be obtained in different ways by modifying or combining process steps, in particular for producing shapes with increased dimensionality. The consecutive process steps of deep UV lithography, electroforming, and plastic molding can be used to fabricate three dimensional (3D) microstructures with almost no restrictions in their lateral shape in a large variety of snanofibers reinforced polymer.

Photolithography is one of the widely used techniques for fabrication of nanofibers reinforced polymers. Two photolithography-based approaches has been presented to directly micromachinephotopatternablesuperhydrophobicmicropatterns with excellent adaptability and flexibility to a wide variety of substrates, employing the nanomorphology and hydrophobicity of polytetrafluoroethylene (PTFE) nanoparticles and the photopatternability and transparency of an SU-8 photoresist [17].

A light source such as UV light is used in photolithography to polymerize the photo-responsive resin with suspended nanoparticles through a mask [6]. Depending upon the requirement of the feature, a mask is prepared and the feature is transferred using a UV source light. The removal of the unaffected part by the light source is performed using the secondary process of chemical etching. UV light has been used primarily for transferring the mask, but various other alternatives such as X-ray lithography,lithography, nanoimprint and ion projection lithography are being explored [6], [18]. For several decades, this technique has been researched and developed, but the resolution of the fabricated feature using photolithography is limited due to the optical diffraction limitation. Photolithography also requires the use of expensive masks and molds for the fabrication process. These techniques are effective for the mass fabrication of high resolution microfeatures, but they are limited to 2D geometries [18]. Nanofibers reinforced polymer microstructures can be fabricated by dispersing the photosensitive resin with naomateirals [14]. Figure 2 shows SEM photographs of the photolithographic patterns for photosensitive polyimide with montmorillonitenanofibers reinforced polymers [19].

Electrochemical Fabrication (EFAB) was originally invited to addresses the long development time for Optical MEMS, which can go up to few weeks. This method has also been used for the fabrication of nanofibers reinforced polymer microstrucutres. The fabrication of nanofibers reinforced polymer film of polypyrrole (PPY) and TiO_2 nanotube (TNT) arrays via electrochemical methods was reported in several articles. A novel dual-layered photore-

http://dx.doi.org/10.5772/57101

ceptor based on the reinforced polymer film as a charge generation layer (CGL) was designed and fabricated [20].

EFAB is a solid free-form fabrication technology that creates complex, miniature three-dimensional shapes based on 3-D computer aided design CAD data [8]. Inspired by rapid prototyping methods, EFAB can fabricate complex shapes by stacking multiple patterned layers. Unlike rapid prototyping,EFAB is a batch process that is suitable for volume production of fully functional devices in engineering materials, not only models and prototypes [9]. EFAB has some limitations and shortcomings. EFAB is a technique that requires the use of masks to build two-dimensional (2D) planar structures. High aspect ratio microstructures are thus a result of multiple steps of material deposition or removal through the use of several masks, that requires increased fabrication time and cost.

A conducting microelectrode is untilizedin a localized electrochemical deposition (LECD) technique to fabricate high aspect ratio structures. During fabrication, a localized deposition is produced by placing an electrode tip that has micrometre-scale dimensions, near a substrate in an electrolyte and applying an electric potential between them. Confined deposition is produced due to the highly localized electric field in the region between themicroelectrode and the substrate. High aspect ratio microstructures result from the displacement of the end of the electrode along the trajectory of the desired geometry while maintaining continuity with the deposited materials. However, nanocompositemicrostructures fabricated by this method are usually porous and have feature sizes in the tens of micrometers due to the limitation in fabricating and maintaining a sharp conductive probe, and in confining the electric field down to the nanoscale dimensions [10].

Laser sintering is another technique that has been widely used for the microfabrication of nanofibers reinforced polymers. In this method, a high intensity laser is used to ablate the material and form nanoparticles. Chen et al, reported a new technique for conductive nanofibers reinforced polymer microfabrication and they were able to lower the percolation threshold of the nanofibers reinforced polymer [21]. This process takes place inside a liquid polymer resin which is then polymerized using UV light to form nanofibers reinforced polymers layers. The main advantage of this technique is that metals, non-metals, glass, polymers can be utilized to fabricate nanofibers reinforced polymer s with various properties. The main drawback of this technique is its limitation to planar geometries. Stacking of different layers has been tried, but the alignment and handling of the layers contributes to the limitation of higher aspect ratio of the micro device [13].

The nonlinear optical process of multiphoton absorption (MPA) was first predicted in 1931 by the Nobel laureate physicist Marie Goeppert-Mayer in her doctoral dissertation [22]. The technique was not verified experimentally until the advent of laser. An intuitive explanation of MPA is the transition from the ground electronic state to an excited electronic state which is usually achieved by the absorption of a high-energy photon or instead reached by simultaneous absorption of multiple low energy photons. The most common implementation of this method is degenerate two-photon absorption (TPA) where both photons have the same energy. The spatial confinement of MPA excitation is used to induce a chemical reaction at the laser focal point. This polymerization reaction occurs by radical reaction mechanisms that

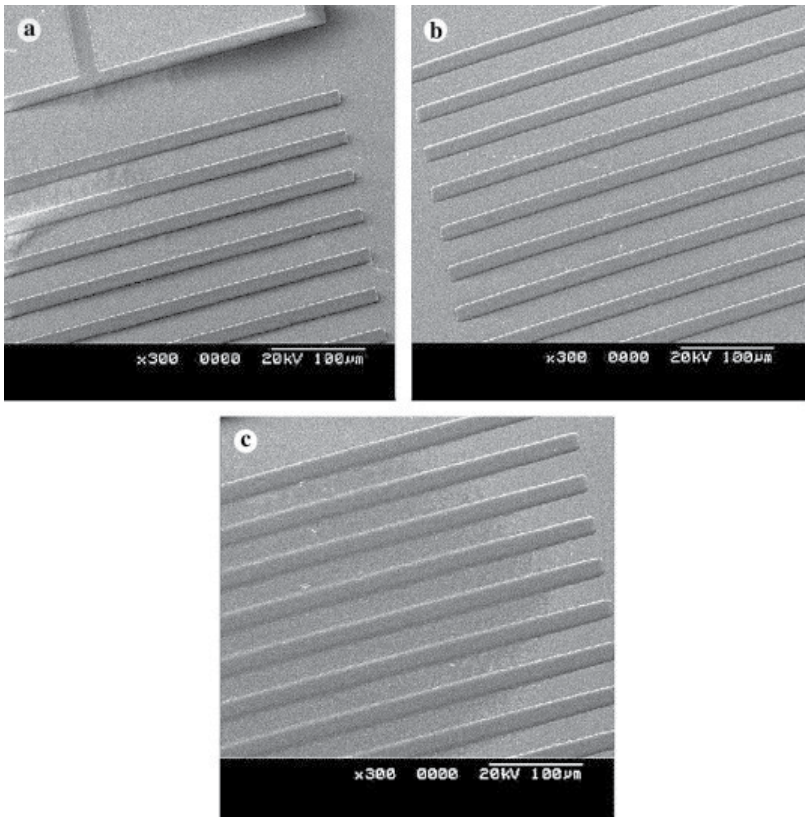

Figure 2. SEM photographs of the photolithographic patterns of (a) pure PSPI, PSPI/MMT nanofibers reinforced polymers with (b) 2 wt. % and (c) 3 wt. % MMT contents. [19].

depend on the photoinitiator and monomer being used. The photoinitiators used for radical MPA vary from small molecules to large conjugated molecules. A number of groups have reported the successful application of radical MPA using a different kind of resins, homemade and commercial, and different excitation sources. Custom photoinitiators have been designed by several groups and have been shown to be effective both for low threshold powers and for the ability to use less expensive laser systems. While the benefits of custom initiators are clear, their availability is limited. Commercial resins or resins made of commercial components have the advantage of accessibility but suffer from a slightly higher power threshold for fabrication. However, for the entire laser systems used, the threshold for these resins is always well below the available power and therefore their use is completely practical.

MPA can achieve resolution that is considerably better than that predicted by the diffraction limit due to a combination of optical nonlinearity. The probability for MPA is proportional to I_n,where I is the light intensity and n is the number of absorbed photons. This effectively narrows the point-spread function (PSF) of the beam near the focal point so that it is smaller than the diffraction limit at the excitation wavelength. The real benefit of the optical nonlinearity of MPA lies in the negligible absorption away from the focal point. Photoinitiator

http://dx.doi.org/10.5772/57101

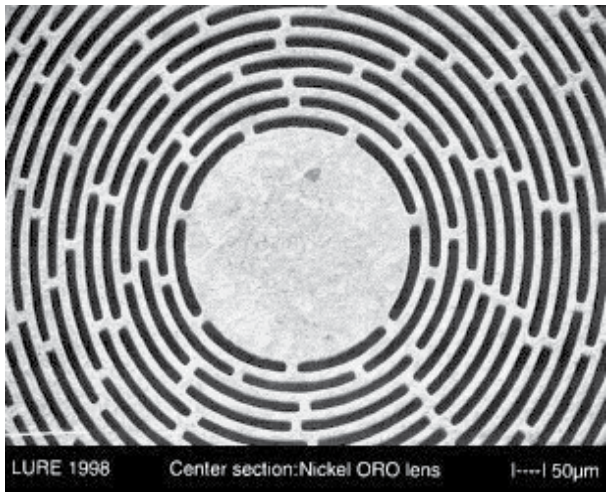

Figure 3. Center section of a fabricated ORO lens. Nickel matrix with 20 µm wide and 600 µm deep holes. Measured aspect ratios (sidewall inclination) >400 [15].

concentrations can be employed that are about ten times more than would be feasible for single-photon excitation without any fear of out-of-plane polymerization.

Multi Photon Absorption (MPA) is a relatively new and evolving method for the manufacturing of micro/nano structures. Unlike other methods, this technique does not involve any secondary operations or processes for nanofibers reinforced polymer fabrication. Micro/nano structures and devices are fabricated with higher accuracy and complexity using MPA than other prevailing methods of fabrication for various applications. When an ultrashort laser pulse is focused in a photo responsive polymer resin, a solid voxel (volumetric pixel) is generated. The voxel size defines the minimum resolution of the polymer which is converted into solid form. Complex 2D and 3D microstructures can be fabricated by scanning the laser in the photo responsive resin [23]. Research on fabrication of micro/nano structures from different types of polymers using MPA has been conducted in the past decades. In certain applications there is a real need of complex nanofibers reinforced polymer structures fabrication [24]. The prevailing methods for nanofibers reinforced polymer manufacturing are good for planar or 2D device fabrication. For maskless manufacturing 2D and 3D nanofibers reinforced polymer devices with accuracy and precision there is a need of identifying or performance research towards the development of new maskless fabrication techniques using MPP due to its advantages over other methods.

3. Nanofibers reinforced polymers enhanced properties

The samples that presented in this section are polymer microstructures fabricated with MPA using laser ablative synthesis generated nanofibers as reinforcement [25] [26].

3.1. Mechanical properties

NanoIndentation Tester (Figure 4) uses an already established method where an indenter tip with a known geometry is driven into a specific site of the material to be tested, by applying an increasing normal load. When reaching a pre-set maximum value, the normal load is reduced until partial or complete relaxation occurs. At each stage of the experiment, the position of the indenter relative to the sample surface is precisely monitored with a differential capacitive sensor. For each loading/unloading cycle, the applied load value is plotted with respect to the corresponding position of the indenter. The resulting load/displacement curves provide data specific to the mechanical nature of the material under examination. Established models are used to calculatequantitative hardness and elastic modulus values for such data [27]. Hardness and elastic modulus can be determined using the method developed by Oliver and Pharr [28]. The hardness represents the resistance of a material to local surface deformation. The Indentation Testing Hardness, H, is determined from the maximum load, F_{max}, divided by the projected contact area A_p at the contact depth h_c [29];

Figure 4. NanoIndentationtester (CSM Instruments)

$$H = \frac{F_{max}}{A_p(h_c)} \tag{1}$$

Where A_p (h_c) is the projected area of indenter contact at distance, h_c from the tip and h_c is the depth of the contact of the indenter with the test piece at F_{max}. Which can be expressed by $h_c = h_{max} - \varepsilon (h_{max} - h_r)$, where h_{max} is the maximum indentation depth at F_{max}, h_r is the point of intersection of the tangent to the unloading curve with the depth axis, and ε is a constant depending on the nonlinearity of the unloading curve (Figure 5). For modified Berkovich indenter, $A_p(h_c) = 24.5\, h_c^2$ [30]. The elastic modulus represents the overall stiffness of the reinforced polymer network and the reduced modulus of the indentation contact, E_r, is given by [29];

http://dx.doi.org/10.5772/57101

$$E_r = \frac{\sqrt{\pi}.S}{2\sqrt{A_p(h_c)}} \tag{2}$$

where S is the contact stiffness or the slope of the unloading curve shown in Figure 5 at the point of maximum load which can be found by [31];

$$S = \frac{F_{max}}{h_{max} - h_r} \tag{3}$$

The relationship between Indentation Modulus, E, and the reduced modulus, E_r, of the sample is given by [29];

$$\frac{1}{E_r} = \frac{1 - \upsilon_s^2}{E} + \frac{1 - \upsilon_i^2}{E_i} \tag{4}$$

Where ν_i is the Poisson's ratio of the indenter, ν_s is the Poisson's ratio of the sample and E_i is the modulus of the indenter. The elastic stress–strain characteristics of a randomly nanofibers dispersed polymer are expressed by three elastic constants, namely, Young's modulus E, Poisson's ratio n νs, and shear modulus G. Only two of these three elastic constants are independent since they can be related by the following equation [32];

$$G = \frac{E}{2(1 + \nu_s)} \tag{5}$$

By substituting the values of E, and ν_s, the shear modulus can be calculated. A thin layer containing randomly oriented discontinuous nanofibers exhibits planar isotropic behavior. The properties are ideally the same in all directions in the plane of the layer. For such a layer, the tensile modulus and shear modulus are calculated from [32];

$$E = \frac{3}{8}E_{11} + \frac{5}{8}E_{22} \tag{6}$$

$$G = \frac{1}{8}E_{11} + \frac{1}{4}E_{22} \tag{7}$$

where E_{11} and E_{22} are the longitudinal and transverse tensile moduli for a unidirectional discontinuous nanofiber lamina of the same nanofiber aspect ratio, and same nanofiber volume fraction as the randomly oriented discontinuous nanofiber composite. Rearrange Eqn 7 and subtract Eqn 6 from Eqn 7, then using transverse modulus $E_{22} = \frac{1 + 2\eta_t \upsilon_f}{1 - \eta_t \upsilon_f} E_m$, $\eta_t = \frac{(E_f / E_m) - 1}{(E_f / E_m) + 2}$, Poisson's ration $\nu_s = \upsilon_f \nu_f + \upsilon_m \nu_m$ and $\upsilon_f + \upsilon_m = 1$, the volume fraction ratio of the nanofibers in the polymer matrix can be obtained by [31];

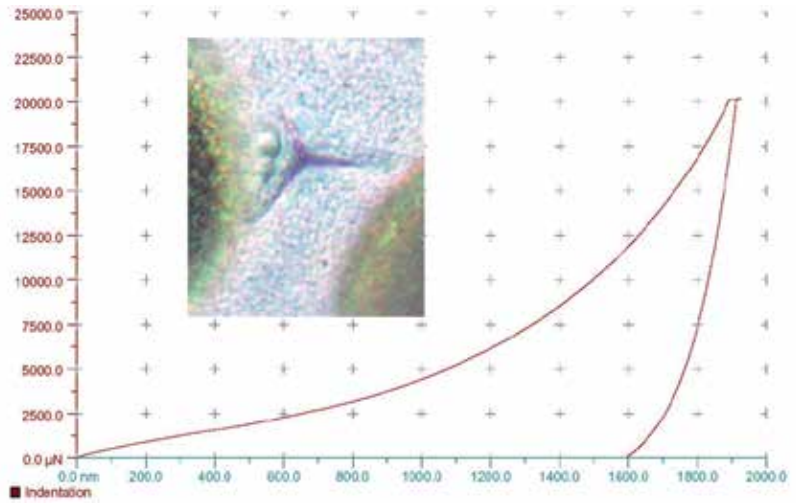

Figure 5. Typical indentation load–displacement curves for the reinforced polymer

$$v_f = \frac{\frac{8(3G - E)}{E_m} - 1}{\left(\frac{(E_f / E_m) - 1}{(E_f / E_m) + 2}\right)\left(2 + \frac{8(3G - E)}{E_m}\right)} \tag{8}$$

Where v_m is the volume fraction of the polymer matrix,ν_f and ν_m are Poisson's rations of nanofibers and polymer matrix respectively, E_f and E_m are Young's moduli for nanofibers and polymer matrix respectively. By substituting the appropriate values in Eqn 8, the volume fraction of the nanofibers in the polymer matrix can be calculated. An important function of the matrix in a nanofiber-reinforced composite material is to provide lateral support and stability for nanofibers under longitudinal compressive loading like the one applied by the indenter head. In polymer matrix composites with which the matrix modulus is relatively low compared to the nanofiber modulus, failure in longitudinal compression is usually initiated by localized buckling of nanofibers. In general, the shear mode of failure is more important than the extensional mode of failure and the shear mode is usually controlled by the matrix shear modulus as well as nanofiber volume fraction.

A viscoelastic polymer has both elastic component and a viscous component. Applying stress to a polymer causes molecular rearrangement due to changing positions by parts of the long polymer chain (creep). Polymers remain solid even when these parts of their chains are rearranging in order to accompany the stress which creates a back stress in the material. The material no longer creeps when the back stress is of the same magnitude as the applied stress. If the original stress is taken away, the accumulated back stresses will cause the polymer to get back to its original form with the help of its elastic component. The polymer loses energy when a load is applied then removed with the area between loading and unloading curves (Figure 5) being equal to the energy lost during the loading cycle. Thus permanent plastic deformation of the polymer occurs even when the applied load is removed.

http://dx.doi.org/10.5772/57101

The large surface area of nanofibers provides better interaction between the polymer chains and nanofibers. The nanofibrous structures act as a preferential nucleation site for crystalline phases which cause an increase in the modulus and hardness. Hardness, which is directly related to the flow strength of a material, depends on the effective load transfer between the matrix and the reinforcement phase in the nanofibers reinforced polymer. Strong interfacial bonding between the matrix and the nanofibers is essential for efficient load transfer to obtain high strength. Plastic deformation in polymers occurs by nucleation and propagation of shear bands which in the unreinforced polymer matrix propagate unhindered as there are no barriers for their movement. Thus, the presence of nanofibers in the nanofibers reinforced polymers could offer resistance for the propagation of shear bands. A good mechanical interlocking and the presence of obstacles to the motion of shear bands are the reasons for the enhancement of hardness and elastic modulus in polymer dispersed nanofibers.

3.1.1. Electrical conductivity

Many techniques for the synthesis of conductive polymers have been developed. Most conductive polymers are prepared by oxidative coupling of monocyclic precursors. One challenge is usually the low solubility of the polymer. An important property of the electrically conductive reinforced polymer is the positive temperature coefficient (PTC) effect. PTC reflects the increase in electrical resistivity of the composites during the heating process, and hence decreasing the electrical conductivity of the reinforced polymer. PTC materials have so many potential applications, including sensors, self-regulating heaters, and switching materials. The PTC behavioroccurs as a result of the difference in the coefficients of thermal expansion between the fillers and the matrix.

Electrical properties of compositions made of nanofibers, dispersed in polymers, are mainly characterized by the formation of a conduction network by contact conditions between neighboring nanofibers in the network. Carbon nanofibers (CFN's) dispersed in the developed resin was used as a conductive composition materials in several applications. The conductivity of the nanofibers reinforced polymer films can be measured using two points probe testing device from SVSLabsInc as shown in Figure 6. Four probe systems can also be used. The voltage passing through the nanofibers reinforced polymer film can be recorded, as well as the current and the value of the resistance (and hence the conductivity) can be obtained using Ohm's law.

Figure 6. Two points probe testing device (SVSLabsInc).

Electrical conductivity in CNF's reinforced polymer is generated as a result of the direct contact between CNF's and tunneling resistance determined by the width of the insulating resin around the CNF's. Thermal expansion caused by heat gradient increases gap width between contiguous CNF's and reduces the number of conductive pathways which results in a decrease in electrical conductivity. The temperature dependence of the electrical conductivity can be explained by the general theory of the thermal fluctuations. The resistivity of the junction is given by;

$$\rho = \rho_o e^{-T_1/(T+T_o)} \tag{9}$$

Where the constants ϱ_0, T_1, and T_0 depend essentially on the characteristics of the tunnel junctions, which are supposed to be functions of various parameters such as filling factor, filler size and shape, sample processing. The relative resistivity (ϱ_r) can be used to characterize the intensity of the PTC effect:

$$\rho_r = \log\left(\frac{\rho_{140}}{\rho_{20}}\right) \tag{10}$$

Where ϱ_{140} and ϱ_{20} are the resistances of the composites at two different temperatures, for example, 140 and 20°C. Thus the relative conductivity can be expressed as;

$$S_r = \log\left(\frac{\rho_{20}}{\rho_{140}}\right) \tag{11}$$

This represents how sensitive and to what extent the reinforced polymer resistance responds after being stimulated by the temperature change. The electrical sensitivity of a reinforced polymer fabricated by femtosecond laser material processing can be expressed by;

$$K_s = \frac{\Delta S_r}{\Delta \omega_r} \tag{12}$$

Where $K_s$is the electrical sensitivity, ΔS_r is the change in relative conductivity and $\Delta\omega_r$ is the change in relative repetition rate of the femtosecond laser that can be expressed by;

$$\omega_r = \frac{\omega}{\omega_{min}} \tag{13}$$

Where ω_{min} is the minimum repetition rate used for the generation of nanofibers. For example, The equation of the straight line obtained from Figure 7 is S_r=0. 17 ω_r - 10. 61 17 which indicate that the electrical sensitivity K_s is about 0. 17. The higher the value of the electrical sensitivity, the more sensitive is the reinforced polymer to change in temperature and thus less conductivity at higher temperatures. Also, the PTC effect of nanofibers reinforced polymers fabricated with higher laser repetition rate is weaker than that of nanofibers reinforced polymer s

fabricated with lower repetition rate. This is a direct result of the matrix volumetric expansionwhich cause more contiguous CFN's to get disconnected and reduce number of electrical pathways.

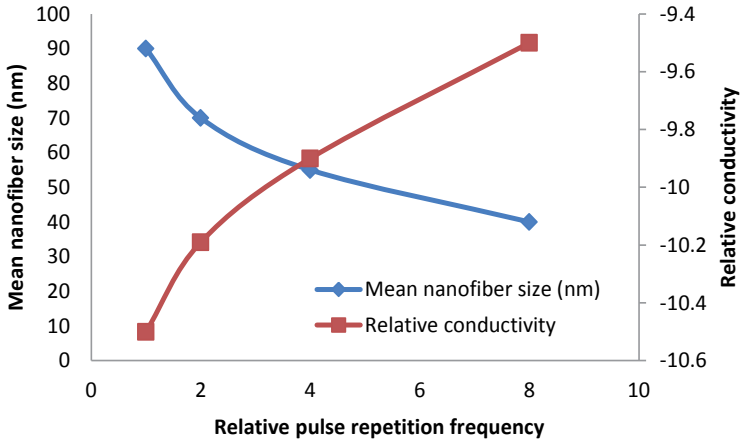

Figure 7. Pulse repetition frequency effect on the relative conductivity of the nanofibers reinforced polymer microstructures.

3.1.2. Magnetic enhancement

Magnetic neodymium-iron-boron (NdFeB) nanofibers and nanoparticles, have become one of the most important spot in the research field of magnetic nanomaterials to meet the demand for miniaturization of electronic components recently. They have been successfully prepared by various techniques like the sol-gel auto-combustion method [33], co-precipitation [34], hydrothermal method [35], reverse micelles [36], microemulsion method [37], alternate sputtering [38], pulsed laser deposition [39], and many others.

The total magnetization of a nanofiber is given by the vectorial sum of all single magnetic moments of the atoms. As for the atomic magnetic moments in nanofibers, the average magnetization will be zero in the absence of magnetic field since all magnetic moments are randomly directed in space. When a magnetic field is applied by the substrate, the magnetic moments orient in the direction of the field and give rise to a net magnetization of the nanofibers [40].

In ferromagnetic materials (Figure 8 (a)), the saturation magnetization MS of the magnetic nanofibers reinforced polymer microstructures at room temperature is higher than that of the pure polymer. The larger coercivitiesHC that we see could be as a result of the oxide Fe. Figure 8 (b) shows the room temperature M-H curves for the polymer (Ormocer). It has a weak diamagnetic response to the applied field, but appears to have a small amount of unknown impurity which contributes to a very weak non- linear deviation near zero fields that could be a paramagnetic effect. Small traces of paramagnetic impurities can be found in almost all

materials and hence, it is not surprising in these polymers. However, these trace impurities do not affect the quality of our ferromagnetic composites. Figure 8 (c) shows the magnetic measurements of the nanofibers reinforced polymers which has a coercive field HC of approximately 260 Oe at room temperature. This large coercivity suggests that oxide nanofibrers are present on the microstructure.

It can be seen that the magnetization of the generated nanofibers reinforced polymer increases compared to pure polymer. This increase in magnetization is expected below the superparamagnetic- ferromagnetic transition temperature, which is above 300K for the magnetic nanofibers of 20 nm average size due to reduced thermal activation energy. Nanoparticle interactions, which depend on the iron concentration in the polymer matrix, strongly influence the remnant magnetization. Since agglomeration of nanoparticles into nanofibers is observed in all our polymer nanofibers reinforced polymer samples, interactions are expected to play a significant role in the magnetic response. These interactions lead to a non- linear increase in MR as the concentration of iron is increased. The magnetic interactions are generally expected to be dipolar in nature, although in strongly coupled clusters, exchange interactions are also possible.

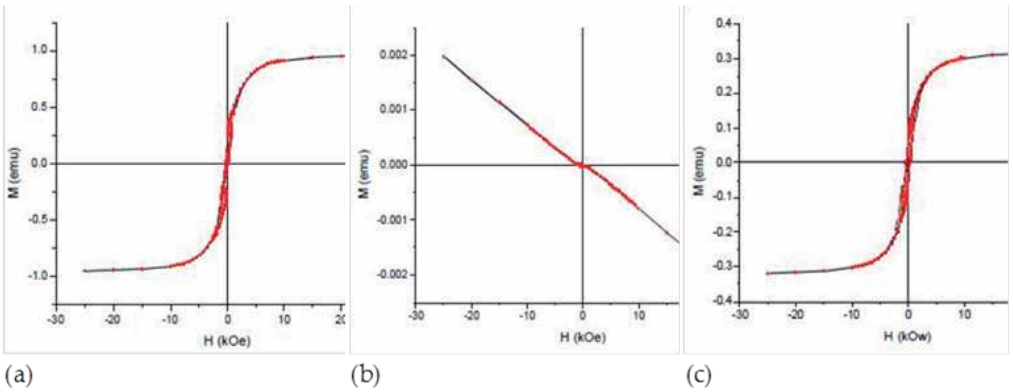

Figure 8. Room temperature M-H curves (a) Magnetic nanofiberous structures, (b) Ormocer, and (c) magnetic nanofibers reinforced polymer.

4. Applications

4.1. Bioapplications

There are unlimited applications of reinforced polymer microstructures. One of the most recent application is DNA sensing based on reinforced polymer microstructuring. A conducting polymer containing nanofibrous structure can be very sensitive even to small perturbations at the interface, thanks to its high electrical conductivity and electron transfer capabilities when the interface is covered by its film. Biocompatible conducting polymers can be variably

http://dx.doi.org/10.5772/57101

modified for immobilization of probe DNA via covalent linking or electrostatic interactions. The conductivity of the conducting polymer electrochemically deposited on the electrode surface can be modulated by changing the pH of the medium, the electrochemical potential, and/or the electrolyte. Because of these characteristics and other advantages, conducting polymers could be utilized extensively for the construction of biosensors including DNA sensors which, to the best of our knowledge, is reported for the first time.

Noble metals are known to create strong chemical bonds with compounds terminating with a thiol (-SH) group. In order to achieve immobilization of nucleic acids on solid substrates, researchers have developed techniques by which DNA molecules can be linked to a thiol group. In this case, the thiolated terminal of molecules is chemisorbed on the substrate, while the DNA portion of the molecules are standing parallel to each other and away from the substrate. Since they are formed quickly, resulting in a well-defined and reproducible surface, and are stable under normal laboratory conditions, gold electrodes are fabricated using femtosecond laser material processing or other techniques [41].

4.2. Energy applications

Reinfoced polymer microstructuring can be utilized in neomerous application. Researchers prepared dye-sensitized solar cells using micro/nanofibers reinforced polymer $Ti0_2$ porous films [42]. This result in cells with enhanced light collection. They applied a technique which opens an alternative way for manufacturing solar cells on an industrial scale. $Ti0_2$ micro/nano-composite structured electrodes for quasi-solid-state dye-sensitized solar cells [43]. These revolutionary nano-structured ultra thin film solar PV products will provide affordable clean renewable energy for everyone. Another unique technology has been developed that absorbs and converts more sunlight throughout the day by utilizing special kind of nanofibers reinforced polymers. This result in a dramatic increase in total power output. Each nanofiber increases the total PV surface area by an incredible 6-12 times over current other thin film products on the market today. Figure 9 shows luminescent solar concentrators (LSCs) comprising CdSe core/multishell quantum dots (QDs) developed by Bomm et al [44].

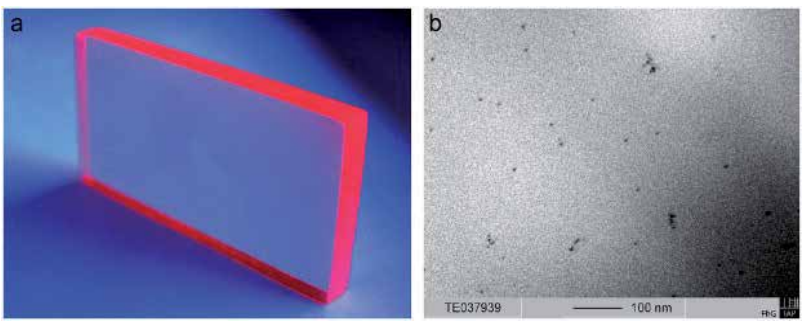

Figure 9. (a) Photograph of a P (LMA-co-EGDM) plate containing CdSe core/multishell QDs (illuminated by a UV-lamp) illustrating the concentrator effect and (b) TEM image of a QD-LSC/P (LMA-co-EGDM) nanofibers reinforced polymer showing single QDs and a few small QD aggregates [44].

5. Summary

In conclusion, this chapter focused on nanofibers reinforced polymer microstructures, including fundamental properties, manufacturing techniques, and applications. The chapter also discussed the scientific principles and mechanisms in relation to the methods of processing, manufacturing and commercial applications. The mechanical, electrical, and magnetic properties of nanofibers reinforced polymers has been discussed in details and it offers insight studies on technology, modeling, characterization, processing, manufacturing, and applications for nanofibers reinforced polymer nanocomposites.

Author details

A. Alubaidy[1], K. Venkatakrishnan[2] and B. Tan[3*]

*Address all correspondence to: tanbo@ryerson. ca

1 School of Mechanical and Electrical Engineering, Sheridan Institute of Technology & Advanced Learning, Brampton, Canada

2 Department of Mechanical Engineering, Ryerson University, Toronto, Ontario, Canada

3 Department of Aerospace Engineering, Ryerson University, Toronto, Ontario, Canada

This chapter is designed to be a comprehensive source for nanofibers reinforced polymer studies. The fundamental properties, manufacturing techniques, and applications of nanofibers reinforced polymer materials are discussed. In addition, this chapter introduce an in depth scientific framework for the advances in nanofibers reinforced polymer researches as well as scientific principles and mechanisms in relation to the methods of fabrication of reinforced microstructuring with a discussion on potential commercial applications. The mechanical, electrical, and magnetic properties of nanofibers reinforced polymer microstructures will be the focus of this chapter. It also offers an in depth discussion on methodology, modeling, characterization, fabrication, and applications for nanofibers reinforced polymers.

References

[1] T. Rogers-Hayden and N. Pidgeon, “Moving engagement ‘upstream’? Nanotechnologies and the Royal Society and Royal Academy of Engineering’s inquiry,” *Public Understanding of Science*, vol. 16, no. 3, pp. 345–364, Jul. 2007.

[2] A. Pomogailo, "Synthesis and intercalation chemistry of hybrid organo-inorganic nanocomposites," *Polymer Science Series C*, vol. 48, no. 1, pp. 85–111, 2006.

[3] J. -J. Luo and I. M. Daniel, "Characterization and modeling of mechanical behavior of polymer/clay nanocomposites," *Composites Science and Technology*, vol. 63, no. 11, pp. 1607–1616, Aug. 2003.

[4] E. Thostenson, C. Li, and T. Chou, "Nanocomposites in context," *Composites Science and Technology*, vol. 65, no. 3–4, pp. 491–516, Mar. 2005.

[5] M. Alexandre and P. Dubois, "Polymer-layered silicate nanocomposites: preparation, properties and uses of a new class of materials," *Materials Science and Engineering: R: Reports*, vol. 28, no. 1–2, pp. 1–63, Jun. 2000.

[6] J. Li and L. S. Melvin, "Sub-resolution Assist Feature Modeling for Modern Photolithography Process Simulation," *Japanese Journal of Applied Physics*, vol. 47, p. 4862, 2008.

[7] A. Bertsch, H. Lorenz, and P. Renaud, "Combining microstereolithography and thick resist UV lithography for 3D microfabrication," in *Micro Electro Mechanical Systems, 1998. MEMS 98. Proceedings., The Eleventh Annual International Workshop on*, 1998, pp. 18–23.

[8] A. Schmidt and W. Ehrfeld, "Recent developments in deep x-ray lithography," *Journal of Vacuum Science&Technology B: Microelectronics and Nanometer Structures*, vol. 16, no. 6, pp. 3526–3534, Jan. 1998.

[9] A. Cohen, G. Zhang, F. G. Tseng, U. Frodis, F. Mansfeld, and P. Will, "EFAB: rapid, low-cost desktop micromachining of high aspect ratio true 3-D MEMS," in *Micro Electro Mechanical Systems, 1999. MEMS'99. Twelfth IEEE International Conference on*, 1999, pp. 244–251.

[10] J. D. Madden and I. W. Hunter, "Three-dimensional microfabrication by localized electrochemical deposition," *Microelectromechanical Systems, Journal of*, vol. 5, no. 1, pp. 24–32, 1996.

[11] S. Barcikowski, M. HUSTEDT, and B. CHICHKOV, "Nanocomposite manufacturing using ultrashort-pulsed laser ablation in solvents and monomers," *Polimery*, vol. 53, no. 9, pp. 657–662, 2008.

[12] Z. B. Sun, X. Z. Dong, S. Nakanishi, W. Q. Chen, X. M. Duan, and S. Kawata, "Log-pile photonic crystal of CdS–polymer nanocomposites fabricated by combination of two-photon polymerization and in situ synthesis," *Applied Physics A: Materials Science & Processing*, vol. 86, no. 4, pp. 427–431, 2007.

[13] X. -Z. D. Z. -B. Sun, "Log-pile photonic crystal of CdS–polymer nanocomposites fabricated by combination of two-photon polymerization and in situ synthesis," vol. 86, no. 4, pp. 427–431, 2007.

[14] C. K. Malek and V. Saile, "Applications of LIGA technology to precision manufacturing of high-aspect-ratio micro-components and-systems: a review," *Microelectronics Journal*, vol. 35, no. 2, pp. 131–143, 2004.

[15] R. K. Kupka, F. Bouamrane, C. Cremers, and S. Megtert, "Microfabrication: LIGA-X and applications," *Applied Surface Science*, vol. 164, no. 1–4, pp. 97–110, Sep. 2000.

[16] R. Kondo, S. Takimoto, K. Suzuki, and S. Sugiyama, "High aspect ratio electrostatic micro actuators using LIGA process," *Microsystem technologies*, vol. 6, no. 6, pp. 218–221, 2000.

[17] L. Hong and T. Pan, "PhotopatternableSuperhydrophobicNanocomposites for Microfabrication," *Journal of Microelectromechanical Systems*, vol. 19, no. 2, pp. 246–253, Apr. 2010.

[18] X. Zhang and C. Sun, "Experimental and numerical investigations on microstereolithography of ceramics," *Journal of Applied Physics*, vol. 92, no. 8, p. 4796, Jan. 2002.

[19] J. Marqués-Hueso, R. Abargues, J. L. Valdés, and J. P. Martínez-Pastor, "Ag and Au/DNQ-novolacnanocompositespatternable by ultraviolet lithography: a fast route to plasmonic sensor microfabrication," *J. Mater. Chem.*, vol. 20, no. 35, pp. 7436–7443, 2010.

[20] M. Ouyang, R. Bai, Y. Xu, C. Zhang, C. A. Ma, M. Wang, and H. Z. Chen, "Fabrication of polypyrrole/TiO2 nanocomposite via electrochemical process and its photoconductivity," *Transactions of Nonferrous Metals Society of China*, vol. 19, no. 6, pp. 1572–1577, 2009.

[21] D. Z. Chen, S. Lao, J. H. Koo, M. Londa, and Z. Alabdullatif, "Powder Processing and Properties Characterization of Polyamide 11-Graphene anocomposites for Selective Laser Sintering," in *Proc. 2010 solid freeform fabrication symposium, Austin, TX, August*, 2010, pp. 2–4.

[22] M. Goeppert-Mayer, "ON ELEMENTARY ACTS WITH TWO QUANTUM JUMPS.," May 1967.

[23] T. Baldacchini, "Acrylic-based resin with favorable properties for three-dimensional two-photon polymerization," *Journal of Applied Physics*, vol. 95, no. 11, p. 6072, Jan. 2004.

[24] K. -S. Lee, D. -Y. Yang, S. H. Park, and R. H. Kim, "Recent developments in the use of two-photon polymerization in precise 2D and 3D microfabrications," *Polymers for Advanced Technologies*, vol. 17, no. 2, pp. 72–82, 2006.

[25] M. Alubaidy, K. Venkatakrishnan, and B. Tan, "Fabrication of a reinforced polymer microstructure using femtosecond laser material processing," *J. Micromech. Microeng.*, vol. 20, no. 5, p. 055012, May 2010.

[26] M. Alubaidy, B. Tan, A. Mahmood, and K. Venkatakrishnan, "Nanofiber Plasmon Enhancement of Two-Photon Polymerization Induced by Femtosecond Laser," *J. Nanotechnol. Eng. Med.*, vol. 1, no. 4, pp. 041015–041015, Nov. 2010.

[27] B. Gu and W. Ji, "Two-step four-photon absorption," *Opt Express*, vol. 16, no. 14, pp. 10208–10213, Jul. 2008.

[28] W. c. Oliver and G. m. Pharr, "An improved technique for determining hardness and elastic modulus using load and displacement sensing indentation experiments," *Journal of Materials Research*, vol. 7, no. 06, pp. 1564–1583, 1992.

[29] B. Bhushan and X. Li, "Micromechanical and tribological characterization of doped single-crystal silicon and polysilicon films for microelectromechanical systems devices," *Journal of Materials Research*, vol. 12, no. 01, pp. 54–63, 1997.

[30] S. Carusotto, G. Fornaca, and E. Polacco, "Multiphoton Absorption and Coherence," *Phys. Rev.*, vol. 165, no. 5, pp. 1391–1398, Jan. 1968.

[31] M. Alubaidy, B. Tan, A. Mahmood, and K. Venkatakrishnan, "Mechanical Property Enhancement of Nanocomposite Microstructures Generated by Two Photon Polymerization," *J. Nanotechnol. Eng. Med.*, vol. 1, no. 4, pp. 041016–041016, Nov. 2010.

[32] P. K. Mallick, *Fiber-Reinforced Composites: Materials, Manufacturing, and Design*. M. Dekker, 1993.

[33] N. T. K. Thanh, *Magnetic Nanoparticles: From Fabrication to Clinical Applications*. CRC Press, 2012.

[34] P. Kruus, M. O'Neill, and D. Robertson, "Ultrasonic initiation of polymerization," *Ultrasonics*, vol. 28, no. 5, pp. 304–309, Sep. 1990.

[35] G. J. Lee, S. H. Lee, K. S. Ahn, and K. H. Kim, "Synthesis and characterization of soluble polypyrrole with improved electrical conductivity," *Journal of Applied Polymer Science*, vol. 84, no. 14, pp. 2583–2590, 2002.

[36] J. R. Li, J. R. Xu, M. Q. Zhang, and M. Z. Rong, "Carbon black/polystyrene composites as candidates for gas sensing materials," *Carbon*, vol. 41, no. 12, pp. 2353–2360, 2003.

[37] J. X. Li, M. Silverstein, A. Hiltner, and E. Baer, "The ductile-to-quasi-brittle transition of particulate-filled thermoplastic polyester," *Journal of Applied Polymer Science*, vol. 52, no. 2, pp. 255–267, 1994.

[38] S. Loshaek, "Crosslinked polymers. II. Glass temperatures of copolymers of methyl methacrylate and glycol dimethacrylates," *Journal of Polymer Science*, vol. 15, no. 80, pp. 391–404, Feb. 1955.

[39] K. Matyjaszewski, *Cationic Polymerizations: Mechanisms, Synthesis & Applications*. Taylor & Francis, 1996.

[40] M. -A. Alubaidy, K. Venkatakrishnan, and B. Tan, "Synthesis of magnetic nanofibers using femtosecond laser material processing in air," *Nanoscale Research Letters*, vol. 6, no. 1, p. 375, May 2011.

[41] M. Alubaidy, L. Soleymani, K. Venkatakrishnan, and B. Tan, "Femtosecond laser nanostructuring for femtosensitive DNA detection," *Biosensors and Bioelectronics*, vol. 33, no. 1, pp. 82–87, Mar. 2012.

[42] A. S. Mahmood, K. Venkatakrishnan, B. Tan, and M. Alubiady, "Effect of laser parameters and assist gas on spectral response of silicon fibrous nanostructure," *Journal of Applied Physics*, vol. 108, no. 9, pp. 094327–094327–6, 2010.

[43] Y. Zhao, J. Zhai, S. Tan, L. Wang, L. Jiang, and D. Zhu, "TiO2 micro/nano-composite structured electrodes for quasi-solid-state dye-sensitized solar cells," *Nanotechnology*, vol. 17, p. 2090, 2006.

[44] J. Bomm, A. Büchtemann, A. J. Chatten, R. Bose, D. J. Farrell, N. L. A. Chan, Y. Xiao, L. H. Slooff, T. Meyer, A. Meyer, W. G. J. H. M. van Sark, and R. Koole, "Fabrication and full characterization of state-of-the-art quantum dot luminescent solar concentrators," *Solar Energy Materials and Solar Cells*, vol. 95, no. 8, pp. 2087–2094, Aug. 2011.

Chapter 8

Use of Self-Assembly Nanofibre Biomaterials for Neural Repair After Injury

Mingyong Gao, Jiasong Guo,
Gilberto K. K. Leung and Wutian Wu

Additional information is available at the end of the chapter

http://dx.doi.org/10.5772/57098

1. Introduction

1.1. Central nervous system injury

Traumatic brain injury (TBI) and spinal cord injury (SCI) are serious health problems in society. It is estimated that approximately 1.7 million TBI (Ghajar, 2000) and 12,000 new cases of SCI (https://www.nscisc.uab.edu, 2011) occur each year in the U.S. TBI is the leading cause of death and permanent severe neurological disabilities in individuals aged below 45 years in the western world. Similarly, SCI affects young adults with an average age of 40.7 years, and is predominantly caused by motor vehicle accidents. Both types of central nervous system (CNS) injuries commonly result in significant sensorimotor deficits as well as psychological and cognitive impairments. The associated social-economic burden is significant.

1.2. Peripheral nervous system injury

Peripheral nervous injuries (PNI) are most primarily caused by traffic accident, bone fractures and joint dislocations (Millesi et al., 1998). Additionally, complications of regional anesthesia and some neuropathic or metabolic disorders may also cause PNI. The incidence is around 2.8% of trauma patients per year. Injuries to the peripheral nerves may lead to partial or complete loss of sensory, motor or autonomic functions that can seriously compromise the life quality of the patients and result in significant socioeconomic loss (Noble et al., 1998; Taylor et al., 2008).

1.3. current neural tissue engineering

1.3.1. Tissue engineering for the repair of central nerve injury

CNS injuries are characterized by the permanent loss of neural tissues as the result of apoptosis, axonal damage, as well as acute and chronic neural degeneration. These primary and secondary neuropathological cascades lead to severe destruction of neuronal circuitry. Subsequent significant astrogliosis may also constitute a microenvironment that is inhibitory to regeneration. The capacity for self-repair within the adult CNS after injury is poor, and numerous reparative strategies have been developed to enhance axonal regrowth, reactivate the plasticity of the spared neural tissue, and replace lost tissue by means of cell transplantation (Kim et al., 2012). Of these, neural bioengineering adopts a multifaceted approach in providing both a permissive microenvironment and a suitable three-dimensional scaffold that integrates transplantable cells with bioactive factors. By modifying the components, morphology, and architecture of biodegradable and biocompatible materials, a number of scaffolds have been developed to tailor to the desired physical and chemical properties required for neural repair. Both natural and artificial polymers such as collagen, chitosan, PLGA (poly lactic-co-glycolic acid), and nanofiberous scaffold have been tested in TBI and SCI models (Peter et al.,2009; Wang et al.,2011). When combined with engrafted stem cells and surface modification, these bioengineered scaffolds represent some of the most promising materials in neuro-regenerative therapy. A wide range of transplantable cells have been used in combination with these scaffolds, including embryonic stem cells, neural stem cells, mesenchymal stem cells, Schwann cells and a variety of adult multipotent stem cell types. The underlying principle is that these engrafted cells may promote neural repair and regeneration by means of growth factor production, neuronal replacement and remyelination. Similarly, enhancement with integrated bioactive factor or oligopeptide motifs may provide a more conducive environment for the survival of the engrafted cells and their integration with the host tissue-scaffold. More importantly, novel controllable release techniques can potentially facilitate the delivery of embedded tissue factors that counteract or neutralize the local inhibitory signals, and degrade glioscar. Given the complexity in anatomical organization and functional communication within the CNS, bioengineered scaffold-based is an reparative strategy of significant potential.

1.3.2. Tissue engineering for repair of peripheral nerve injury

When compared with the CNS, the PNS has a much greater capacity for regeneration after traumatic injury. For lesion gaps of over 5cm in length, autologous nerve grafting is a treatment of choice. However, the recovery of sensory and motor function is often slow and incomplete. Nerve grafting is limited by the availability of the donor nerve, the loss of donor nerve function, and the additional surgical trauma and complications (Gordon et al., 2003). Peripheral nerve is mainly constituted by fascicles of myelinated and unmyelinated nerve fibers as well as multiple layers of connective tissue and blood vessels. PNS bioengineering approaches therefore require longitudinally orientated conduits to provide the physical support and contact guidance for neurite regrowth, while maintaining the biological and functional viability of the distal denervated targets during the regenerative process. The ultimate goal of

http://dx.doi.org/10.5772/57098

PNS bioengineering is to develop bioengineered nerve implant that could match or exceed the performance of autograft. Currently, various conduits made of diverse synthetic or natural biomaterials have been exploited to bridge experimental nerve transection gaps of between 10mm and 80mm in experimental rodent and primate models. The most commonly used biomaterials are biodegradable polymers such as PLGA, type I Collagen and chitosan. The engrafted cells may include Schwann cells, neural stem cells and olfactory ensheathing cells (OECs). However, the degree of axonal regeneration and functional recovery has so far been found to be limited, and inferior to nerve grafting control. Further studies are required to explore the applications of other novel materials. (Battiston et al., 2009).

1.4. Biomaterials developed in the field of Neural Tissue Engineering

Various promising biomaterials have been exploited to meet the diverse needs for specific bioengineering applications. The fundamental requirements of biomaterials utilized in neural tissue engineering include biodegradability, neural bioactivity and neural tissue-matched mechanical module.

1.4.1. Biological biomaterials

These are mainly natural polymers such as collagen, laminin, fibronection, fibin, hyaluronic acid. agarose, alginate, and chitosan. The majority of them are derived directly from ECM and have been extensively studied due to their inherent merits including the presentation of biological receptor-binding ligands, the susceptibility to proteolytic degradation and remodeling in vivo (Ma et al., 2008). These natural macromolecules can be hydrated, and serve as bioscaffolds for various cells *in vivo* and *in vitro*. For example, collagen is the most abundant protein from natural ECM in connective tissue. In mammalian tissues, the primary structural collagen is type I collagen. The collagen conduit made of type 1 collagen such as NeuraGen conduit has been approved by the United States Food and Drug Administration (FDA) and is commercially available for clinical use practice, whereas limited in field of the peripheral nerve repair (Kehoe et al., 2012). Major concerns regarding the clinical application of biologically derived materials, include the problems with sustainable production, immunogenicity, and pathogen transmission as well as weak mechanical *in vivo* strength.

1.4.2. Artificial biomaterials

Compared to the natural polymers, artificial biomaterials or biomimetic materials, could be designed and synthesized to mimic one or multiple desired characteristics of the natural ECM for specific purposes. For reparative applications, artificial polymers have the advantages of having great flexibility for design and modification so as to allow for the control of orientation and development of new-born tissue for better functional outcomes.

1.4.2.1. Degradable materials

Biodegradability is an important property of biomaterials in tissue engineering. Due to the well-accepted biodegradability and biocompatibility, linear aliphatic polyesters including

poly(lactic acid) (PLA), poly(glycolic acid) (PGA), and their copolymers poly(lactic acid-co-glycolic acid) (PLGA) have been widely utilized to reconstruct bioscaffold in diverse conditions of neural repair. To facilitate host-material integration, biomaterial candidates must also possess the appropriate elastic module. For instance, hydrogel made of poly(2-hydroxyethyl methacrylate-co-methyl methacrylate) (p(HEMA-co-MMA)) has similar mechanical properties to the mammalian spinal cord (elastic modulus of 200 to 600 kPa), and could be customized by altering the ratio of co-monomers (Dalton et al.,2002). The hydrophobic surface properties in most of the synthetic biodegradable materials such as PLGA, PCL and PHB, may be modified by coating them with ECM proteins components like laminin, fibronectin, collagen. Specific adhesion oligopeptide such as RGD and IKVAV, YIGSR may also be added to improve their adhesion properties for seeded cells. Several studies showed that the cellular adhesion performance of these artificial biomaterials including methyl cellulose, alginate, poly (hydroxyethyl methacrylate) (PHEMA), poly (hydroxybutyrate) (PHB) (Samadikuchaksaraei, 2007), could be significantly improved by surface modifications. Another category of synthetic biomaterial is related to the nanofibre scaffold which will be discussed in later sections.

1.4.2.2. Nondegradable materials

The use of synthetic nondegradable materials in neural repair is limited by their nondegradablilty and unbioabsorbility. The majority of reported studies involved PNI. For example, poly (2-hydroxyethyl methacrylate) has been demonstrated to support regeneration of injured axons in a rat SCI model (Tsai et al. 2006). Recently, electroactive polymer like polypyrole or hybrid conduct materials showed neuronal attachment and growth. The major concerns regarding these materials are related to immunorejection, chronic inflammatory responses, fibrous scarring, and the associated problems of neural compression and need for re-operation. These render nondegradable materials unsuitable for CNS repair (Cullen et al., 2008).

2. Nanofibrous scaffolds applied in CNS regeneration

2.1. Current fabrication of nanofiber-based bioscaffolds used in CNS regeneration

The aim of biomedical engineering is the design and development of novel biomaterials that can recapitulate the key characteristics of natural ECM with the associated topographical cues, cellular adhesion sites, biochemical signals and physiological viscoelastic modules. In general, extracellular proteins such as collagen, fibrin and glycosaminoglycans, possess fibrous structures with diameters on the nanometer or sub-micrometer scales. Several bioengineering approaches have been developed for the fabrication of artificial nanofibre constructs with diameters that range from 10 to 100nm.

2.1.1. Self-assembling peptide nanofiber scaffolds (SAPNS)

Many biological macromolecules such as like phospholipids can readily self-assemble to form highly ordered bio-structures through van der Waals forces, hydrogen bonds, ionic bonds, and

http://dx.doi.org/10.5772/57098

hydrophobic interactions. To recapitulate the bioactive motif of laminin, Stupp and coworkers designed a self-assembling peptide amphiphile (PA) that consisted of the laminin-derived peptide IKVAV (Ile-Lys-Val-Ala-Val). The self-assembly of IKVAV could be initiated spontaneously upon the introduction of physiological buffer which leads to the formation of nanofibers with diameter ranging from 6 to 8 nm (Tysseling-Mattiace, 2008).

2.1.2. Eletrospun nanofiber scaffolds

Electrospinning was a traditional industrial fabrication technique used widely in 1930s. Due to its effectiveness of producing microfibers with diameters of sub-micron or nanometer scale, it has been utilized to process a number of natural and synthetic polymers such as collagen, fibroin, PLLA, PLGA, and PCL. The electrospun nanofiber matrices resemble the structural morphology of ECM with a high surface area–to-volume ratio, which has been shown to greatly facilitate cellular attachment, proliferation and differentiation. Recent studies continue to report the development of novel electrospun nanofibers, and the introduction of bioactive molecules such as growth factors during the fabrication process of nanofibers for peripheral nerve regeneration (Prabhakaran et al., 2008). The intrinsic limitations of this technique include the degradation of bioactive factors during procedure, the inability to fabricate complex 3D structures or specific microstructure with designed internal pore size.

2.1.3. Phase separation

Phase separation, or thermally induced liquid–liquid phase separation, was developed by Ma and Zhang to produce a nanofibrous foam materials. Polymer scaffolds generated by phase separation normally have a sponge-like porous morphology with spherical pores 50–500 nm in diameter. Phase separation system consists of a polymer-rich component and a polymer-lean/solvent-rich component, by which the polymer morphology can solidify by quenching under low temperature. A few nanofibre scaffold from artificial biodegradable polymers have been produced with phase separation including PLLA, which was studied as a suitable matrices in which NSCs can grow and differentiate (Yang et al., 2004). Compared with other techniques previously discussed phase separation has simpler and the need for specialized equipment is minimal. However, due to the small number of candidate polymers suitable for *in vivo* study, reports on nanofiber scaffold generated by phase separation in neural tissue engineering are limited.

2.2. Current application of SAPNS for the repair of injured CNS

2.2.1. Traumatic brain injury

The applications of RADA16-I, a representative SAPNS, in 3D cell culturing, wound hemostasis and healing has been well described in a series of studies. The initial research of RADA16-I in experimental TBI was conducted by Ellis-Behnke et al. (Ellis-Behnke et al. 2006). Using an acute TBI model in which the midbrain of P2 hamsters was injured surgically with a knife wound (1.5 mm deep and 2.0 mm wide), 10μl of 1% SAPNS was applied to bridge the injury gap. The central traumatic lesion showed restoration in all SAPNS-treated animal subjects

within the first 24-hour and at all other timepoints up to 30 days post-injury. Compared with saline-treatment, SAPNS created a seamless connection across lesion site and appropriate host-scaffold interfaces which led to significantly improved repair. Further studies were conducted by Guo et al. using a rodent TBI model (Guo et al., 2009). Immediately after the infliction of severe mechanical injury to the sensory-motor cortex, 20 μL of 1% RADA16-I SAPNS was implanted at the lesion sites to bridge the injury gap. Histological, immunohistochemical and apoptosis studies were performed at 2 days, 2 weeks, and 6 weeks after injury. The SAPNS-treated lesion sites had no cyst formation after injury and showed integrated host-scaffold interfaces; saline-treatment resulted in significant cyst formation. Moreover, SAPNS significantly reduced apoptosis in the perilesional area and effectively mitigated reactive gliosis and inflammation. Currently, a few integrative strategies of SAPNS incorporated with bioactive factors have been conducted with an aim to improve functional recovery after severe TBI.

2.2.2. Spinal cord injury

A variety of biodegradable hydrogel have been extensively studied in the treatment of experimental SCI. IKVAV peptide amphiphile, which consists of neuroactive pentapeptide epitope from laminin, has been applied in a moderate spinal cord contusion model in which 1% aqueous solution of IKVAV-SAPNS was injected into the lesion sites 24h after injury. IKVAV-SAPNS significantly reduced the degree of oligodendroglial apoptosis perilesion and enhanced their survival rate with cleaved caspase-3 immunohistochemistry at 10 d after SCI. Additionally, astrogliosis was reduced significantly and the regeneration of motor-sensory axons were improved remarkably on BDA-labeling 11 week after treatment. Moreover, at 9wks after treatment, the mean locomotor score of IKVAV-SAPNS group was significantly better than that of the control group on BBB score measurement, and dorsal stepping was observed with IKVAV-treatment, indicating functional return in hindlimb movement (Tysseling-Mattiace, 2008).

One of the most important advantages of SAPNS is its ability to provide a 3-D matrice in which neural cells can survive and differentiate. Guo and coworkers incorporated neural stem cells (NSCs) and Schwann cells in SAPNS, and transplanted them into dorsal column lesion of the cervical spinal cord. At 6 wks after implantation, there was excellent integration between the implant and the host tissue. Moreover, extensive axonal regrowth was observed with immunohistochemistry staining with NF, 5-HT, and CGRP (Guo et al., 2007). Recent reports highlighted the further applications of controlled release of bioactive factors incorporated into the SAPNS *in vitro* and *in vivo*. For instance, CT04, a cell permeable RhoA inhibitor, was incorporated into RADA16-I-SAPNS and implanted in a complete transection lesion at T9 level of the spinal cord. This novel integrative SAPNS not only reconstructed the injured nerve gap, but also elicited significant axonal regeneration and motor functional recovery. Additionally it also effectively reduced the infiltration and apoptosis of activated macrophages within the injured spinal cord. The SAPNS-based delivery of RhoA inhibitor is a potentially effective therapeutic strategy by reknitting lesion gap, attenuating secondary injury and improving axonal regeneration (Fig.1). Moreover, Gelain and Zhang's group has developed functionalized SAPNS that can improve the engraftment and neural differentiation of seeding neural

progenitor cells *in vitro,* and enhance neural regeneration *in vivo*. With the aid of phage display technology, a functionalized SAPNS was found to demonstrate high *in vitro* stem cell viability and neural differentiation, as well as significantly promoted axonal regrowth and locomotor functional recovery in acute spinal cord injury (Gelain et al., 2006; 2012).

Collectively, these in vivo studies with various SCI models evidenced the significant potential of SAPNS in the repair of SCI from different aspects that SAPNS provide. Based on the current advances of fabrication and biochemistry techniques, future directions would consider introduction of updated topographical cues and more bioactive motifs or growth factors into the scaffold design to induce more robust and organized regeneration for injured central neural system, achieving more significant functional recovery.

3. Nanofibrous scaffolds applied in PNS repair

3.1. Development of nanofiber biomaterials used for PNS regeneration

A variety of biodegradable materials have been processed into nanofibrous scaffold using eletrospining technique for PNI repair (Xie et al., 2010). In an early study, a bilayer chitosan conduit with inner layer of nano/microfibrous structure modified with oligopeptide was generated to repair a 15mm sciatic nerve gap in rats (Wang et al., 2008). This novel integrative chitosan conduit effectively promoted the axonal regeneration that was comparable to that of autologous nerve grafting? on histological assessment. Recently, a blend of biodegradable polymers PLGA/PCL was used to produce electrospun tubes to bridge a 10mm long sciatic nerve lesion gap in rat. Four months after surgery, most of the electrospin conduit-treated animals showed neural regeneration and functional restoration on immunohistochemial studies and electrophysiological assessment (Panseri et al., 2008). More interestingly, a novel bi-layer nanofibrous nerve conduit made of poly (L-lactide-co-caprolactone) and poly(propylene glycol) has been fabricated with electrospinning technique for PNI repair. The electrospin nerve conduit was designed as the luminal layer composed of longitudinally aligned nanofibers to promote axon regeneration, while the outer layer was equipped with random- organized nanofibers for mechanical support. After being implanted to bridge a 10mm gap of sciatic nerve, the nanofibrous nerve conduit significantly improved the regeneration of injured peripheral axons and motor functional recovery at 2 and 12 month post-surgery (Zhu et al., 2011). More recently, the effects of fibre diameter of electrospun conduits on peripheral nerve regeneration was analyzed with a 15mm sciatic nerve injury model. These fibrous conduits consisted of aligned electrospun poly (ε-caprolactone) (PCL) nanofibers (251±32 nm) and microfibers (981±83 nm). The nanofiber-treated group showed significantly greater total number of myelinated fibers and thicker myelin sheaths when compared with groups that received Microfiber and Film conduits at 3 month post-treatment. The number of regenerated dorsal root ganglion neurons in animals that received nanofiber conduits was increased significantly by retrograde labeling with fluorogold. On electrophysiological testing including compound

muscle action potential and distal motor latency, the nanofibre-group showed greater improvement than the microfiber group (Jiang et al., 2012). These positive observations provide useful insights for the applications of electrospun nanofibrous nerve conduits with designed nanostructure in the development of peripheral nerve guide conduits.

3.2. Reconstruction of injured PNS with SAPNS

SAPNS has a well-defined sequence of L-amino acids that self-assemble under physiological conditions to form a fibrous scaffold within the nanoscale (~10 nm in diameter). In the recent decades, SAPNS has been shown to facilitate the survival and growth of various neural cells within a 3D matrice, and effectively improved the axonal regeneration and tissue repair in context of CNS injuries. It also has significant potential for PNI repair. For example, a novel SAPNS-based nerve conduit was generated by RAD-I SAPNS ensheathed with a segment of aortic wall. With a sciatic nerve transection model of rat, the SAPNS-nerve conduit was used to bridge a 10mm nerve gap. Neural histomorphology, retrograde-labeling and locomotor functional assessments demonstrated significant therapeutic effects of SAPNS-based nanofiber conduit implant on axonal regeneration, remyelination and target reinnervation (Fig.2,). Additionally, SAPNS acts as a designer peptide backbone and provides the opportunity to integrate various growth factor, or functional motifs for cell adhesion, differentiation and homing, and to define and direct biological commitment of seeding cells; furthermore, functional SAPNS will provide better support for viability, migration and differentiation of engrafted stem cells in vivo and lead to better performance of neural repair in vivo.

4. Conclusion

The functional repair of peripheral and central nervous system injuries is a major challenge. Based on the advances of development of novel biomaterials, biochemistry and fabrication techniques, bioengineered scaffold enhanced with bioactive motifs and engrafted cells can provide a regeneration-facilitating environment for injured nervous tissues, and effectively promote the host's capacity of neural regeneration and plasticity. Numerous *in vitro* models have demonstrated that 3-D bioscaffold, in particular the nanofibre scaffold, can greatly support the attachment, proliferation, migration and neural differentiation of various neural cells. Moreover, significant neuroprotection and axonal regeneration have been achieved in *in vivo* neural injury models after treatment with these novel scaffolds. More importantly, the recovery of injured sensory and locomotor function has been shown to occur in a number of peripheral and central injury models using different animal species. However, critical issues such as functional integration of host-implant, organized regeneration pattern with updated bioengineering scaffolds and further restoration of useful neurology function, remain to be addressed in future researches.

Immunohistochemistry with Neurofilament(NF) staining showed a number of NF-positive axons (Green)penetrated into the lesion sites with SAPNS+CT04 treatment(A). Counterstained

http://dx.doi.org/10.5772/57098

DAPI area (blue) indicated the gross structure of the injured spinal cord. (B) is the high power magnification corresponding to the boxed area of (A) demonstrated the NF-positive axons in the center of lesion area. Quantification analysis of the NF-positive axons in the center of the lesion area indicated that axonal regeneration was significantly improved by the SAPNS+CT04 implants compared to the only SAPNS group (Student t test, *p<0.05).

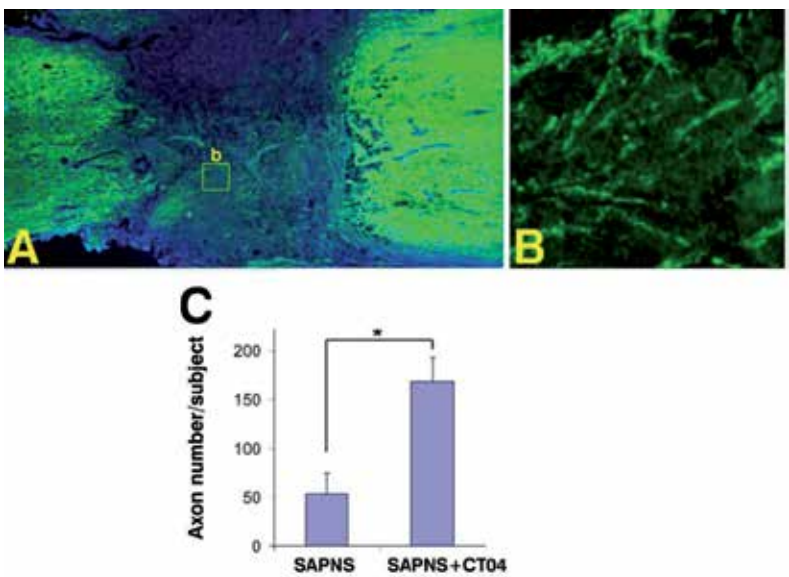

Figure 1. Axonal regeneration in the SAPNS-treated groups.

With NF/MBP-double immunofluoresent labeling, in sharp contrast to that of Empty Nerve Conduit (ENC) group (A-C), significant remyelination of regenerated axons was detected throughout the entire Nanofiber Nerve Conduit (NNC) 16 weeks after treatment (D-F). Representative transverse sections of proximal, middle and distal parts of Nerve Conduit (NC) were demonstrated at panel (A, D), (B, E), and (C, F) in ENC and NNC group, respectively. (G) is the higher magnification of boxed area of (E) with arrows indicating the representative remyelinated fibers. Furthermore, with electron microscopy, typical remyelinated fibers (arrowheads) could be found in both NC groups, while the diameter of the fiber and the thickness of the myelin are greater in NNC (H) compared with ENC (I). (J,K) showed the quantification analysis of the myelinated fiber caliber and the G-ratio (an index of myelin thickness) separately. Both comparisons using student's t test indicated significantly statistical differences (*p<0.05;**p<0.01).

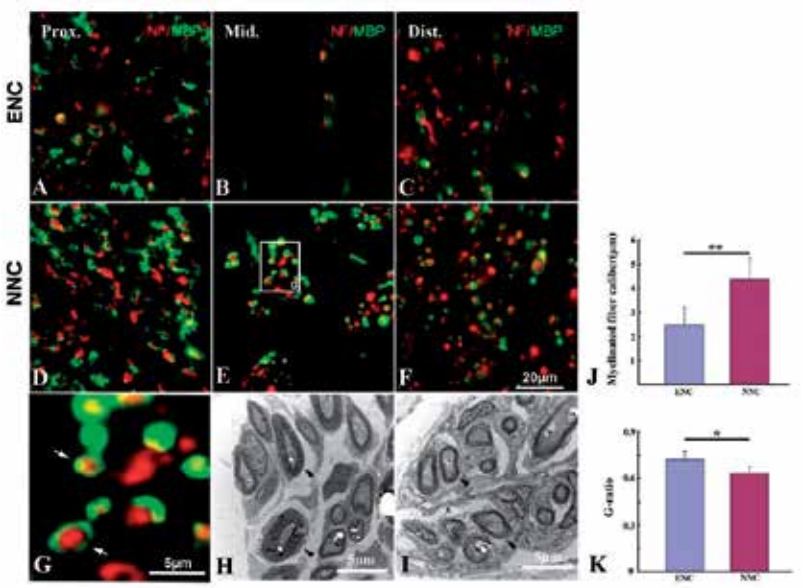

Figure 2. Remyelination of regenerated axons in the peripheral nerve conduits

Author details

Mingyong Gao[1,7], Jiasong Guo[5], Gilberto K. K. Leung[6] and Wutian Wu[1,2,3,4]

1 Department of Anatomy, Li Ka Shing Faculty of Medicine, The University of Hong Kong, Hong Kong SAR, China

2 State Key Laboratory of Brain and Cognitive Sciences, China

3 Research Center of Reproduction, Development and Growth, Li Ka Shing Faculty of Medicine, The University of Hong Kong, Pokfulam, Hong Kong SAR, China

4 Joint Laboratory for Brain Function and Health (BFAH), Jinan University and The University of Hong Kong, Guangzhou, China

5 Department of Histology and Embryology, Southern Medical University, Guangzhou, China

6 Department of Surgery, Li Ka Shing Faculty of Medicine, The University of Hong Kong, Pokfulam, Hong Kong SAR, China

7 Department of Orthopeadics, Renmin hospital of Wuhan University, Wuhan, China

References

[1] Battiston B, Raimondo S, Tos P, Gaidano V, Audisio C, Scevola A, Perroteau I, Geuna S. Tissue engineering of peripheral nerves. Int Rev Neurobiol. 2009; 87: 227–49.

[2] Chen VJ, Wei G, Ma PX, Nanostructured scaffolds for tissue engineering and regeneration, in: H.S. Nalwa (Ed.), Handbook of Nanostructured Biomaterials and Their Applications in Nanobiotechnology,vol. II, American Scientific Publishers, Stevenson Ranch, California, 2005; 415–35.

[3] Cullen DK, R Patel A, Doorish JF, Smith DH, Pfister BJ. Developing a tissue-engineered neural-electrical relay using encapsulated neuronal constructs on conducting polymer fibers. J Neural Eng. 2008;5(4):374-84.

[4] Cunha C, Panseri S, Antonini S.Emerging nanotechnology approaches in tissue engineering for peripheral nerve regeneration. Nanomedicine. 2011; 7(1):50-9.

[5] Dalton PD, Flynn L, Shoichet MS. Manufacture of poly(2-hydroxyethyl methacrylate-co-methyl methacrylate)hydrogel tubes for use as nerve guidance channels. Biomaterials. 2002; 23(18):, 3843-51.

[6] Deumens R, Bozkurt A, Meek MF, Marcus MA, Joosten EA, Weis J, Brook GA. Repairing injured peripheral nerves: Bridging the gap. Prog Neurobiol. 2010; 92(3): 245-76.

[7] Ellis-Behnke RG, Liang YX, You SW, Tay DK, Zhang S, So KF, Schneider GE.. Nano neuro knitting: peptide nanofi ber scaffold for brain repair and axon regeneration with functional return of vision. Proc. Natl. Acad.Sci. USA. 2006; 103(13): 5054–9.

[8] Gelain F, Bottai D, Vescovi A, Zhang S. Designer self-assembling peptide nanofiber scaffolds for adult mouse neural stem cell 3-dimensional cultures. PLoS ONE. 2006; e119:1.

[9] Gelain F, Cigognini D, Caprini A, Silva D, Colleoni B, Donegá M, Antonini S, Cohen BE, Vescovi A.New bioactive motifs and their use in functionalized self-assembling peptides for NSC differentiation and neural tissue engineering. Nanoscale. 2012;4(9): 2946-57.

[10] Ghajar J. Traumatic brain injury. Lancet. 2000; 356(9233):923-9.

[11] Gordon T, Sulaiman O, Boyd JG., Experimental strategies to promote functional recovery after peripheral nerve injuries. J Peripher Nerv Syst. 2003; 8(4): 236-50.

[12] Guo J, Leung KKG, Su H, Yuan QJ, Wang L, Chu TH, Zhang W, Pu JKS, Ng GKP, Wong WM, Dai X, Wu WT.. Self-assembling peptide nanofi ber scaffold promotes the reconstruction of acutely injured brain.Nanomedicine. 2009; 5(3): 345–51.

[13] Guo J, Su H, Zeng Y, Liang YX, Ellis-Behnke RG, So KF, Wu W. Reknitting the injured spinal cord by self-assembling peptide nanofi ber scaffold. Nanomedicine 2007; 3(4): 311–21.

[14] Jiang X, Mi R, Hoke A, Chew SY. Nanofibrous nerve conduit-enhanced peripheral nerve regeneration. J Tissue Eng Regen Med. 2012 Jun 15. [Epub ahead of print]

[15] Keeley RD, Nguyen KD, Stephanides MJ, Padilla J, Rosen JM. The artificial nerve graft: a comparison of blended elastomer-hydrogel with polyglycolic acid conduits. J Reconstr Microsurg 1991;7(2):93-100.

[16] Kehoe S, Zhang XF, Boyd D. FDA approved guidance conduits and wraps for peripheral nerve injury: a review of materials and efficacy. Injury. 2012; 43 (5):553-72.

[17] Kim H, Cooke MJ, Shoichet MS. Creating permissive microenvironments for stem cell transplantation into the central nervous system. Trends Biotechnol. 2012; 30(1): 55-63.

[18] Ma PX. Biomimetic materials for tissue engineering. Adv Drug Deliv Rev. 2008; 60(2): 184–98.

[19] Millesi H. Trauma involving the brachial plexus. In: Omer GE, Spinner M, Van Beek AL, eds. Management of Peripheral Nerve Problems. Philadelphia: Saunders; 1998;433–44.

[20] Noble J, Munro CA, Prasad VSSV, Midha R. Analysis of upper and lower extremity peripheral nerve injuries in a population of patients with multiple injuries. J Trauma. 1998; 45(1): 116-22.

[21] Panseri S, Cunha C, Lowery J, Del Carro U, Taraballi F, Amadio S, Vescovi A, Gelain F. Electrospun micro- and nanofiber tubes for functional nervous regeneration in sciatic nerve transections. BMC Biotechnol. 2008; 8:39.

[22] Prabhakaran MP, Venugopal JR, Chyan TT, Hai LB, Chan CK, Lim AY, Ramakrishna S. Electrospun biocomposite nanofibrous scaffolds for neural tissue engineering. Tissue Eng Part A. 2008;14(11):1787-97.

[23] Raimondo S, Fornaro M, Tos P, Battiston B, Giacobini-Robecchi MG, Geuna S. Perspectives in regeneration and tissue engineering of peripheral nerves. Ann Anat. 2011,193(4):334-40.

[24] Samadikuchaksaraei A. An overview of tissue engineering approaches for management of spinal cord injuries. J Neuroeng Rehabil. 2007; 4: 15.

[25] Toba T, Nakamura T, Lynn AK, Matsumoto K, Fukuda S, Yoshitani M, Hori Y, Shimizu Y. Evaluation of peripheral nerve regeneration across an 80-mm gap using a polyglycolic acid (PGA)--collagen nerve conduit filled with laminin-soaked collagen sponge in dogs. Int J Artif Organs. 2002; 25(3):230-7.

[26] Taylor CA, Braza D, Rice JB, Dillingham T. The incidence of peripheral nerve injury in extremity trauma. Am J Phys Med Rehabil, 2008; 87(5): 381-85

[27] Tsai EC, Dalton PD, Shoichet MS, Tator CH. Matrix inclusion within synthetic hydrogel guidance channels improves specific supraspinal and local axonal regeneration after complete spinal cord transection. Biomaterials. 2006; 27(3):519-33.

[28] Tysseling-Mattiace VM, Sahni V, Niece KL, Birch D, Czeisler C, Fehlings MG, Stupp SI, Kessler JA.

[29] Self-assembling nanofibers inhibit glial scar formation and promote axon elongation after spinal cord injury. J Neurosci. 2008;28(13):3814-23.

[30] Walker PA, Aroom KR, Jimenez F, Shah SK, Harting MT, Gill BS, Cox CS Jr.. Advances in progenitor cell therapy using scaffolding constructs for central nervous system injury. Stem Cell Rev. 2009; 5(3): 283–300.

[31] Wang M, Zhai P, Chen X, Schreyer DJ, Sun X, Cui F. Bioengineered scaffolds for spinal cord repair. Tissue Eng Part B. 2011;17(3):177-94.

[32] Wang W, Itoh S, Matsuda A, Aizawa T, Demura M, Ichinose S, Shinomiya K, Tanaka J.Enhanced nerve regeneration through a bilayered chitosan tube: the effect of introduction of glycine spacer into the CYIGSR sequence. J Biomed Mater Res A. 2008; 85(4): 919-28.

[33] Xie J, MacEwan MR, Schwartz AG, Xia Y. Electrospun nanofibers for neural tissue engineering. Nanoscale. 2010; 2(1):35-44.

[34] Yang F, Murugan R, Ramakrishna S, Wang X, Ma YX, Wang S. Fabrication of nanostructured porous PLLA scaffold intended for nerve tissue engineering. Biomaterials 2004; 25(10):1891-900.

[35] Zhu Y, Wang A, Patel S, Kurpinski K, Diao E, Bao X, Kwong G, Young W, Li S. Engineering Bi-layer Nanofibrous Conduits for Peripheral Nerve Regeneration. Tissue Eng Part C Methods. 2011; 17(7):705-15.

Edited by Russell Maguire

Book Advances in Nanofibers is a research publication that covers original research on developments within the Nanofibers field of study. The book is a collection of reviewed scholarly contributions written by different authors. Each scholarly contribution represents a chapter and each chapter is complete in itself but related to the major topics and objectives. The target audience comprises scholars and specialists in the field.

ISBN 978-953-51-5726-7

Photo by tofumax / iStock

IntechOpen